Study and development of an *in situ* acoustic absorption measurement method

E.H.G. Tijs

Study and Development of an *In Situ* Acoustic Absorption Measurement Method

Emiel Tijs

Promotiecommissie

Voorzitter:	prof. dr. ir. A.J. Mouthaan	
Secretaris:	prof. dr. ir. A.J. Mouthaan	
Promotoren:	prof. dr. ir. W.F. Druyvesteyn	Universiteit Twente
	prof. dr. ir. G.J.M. Krijnen	Universiteit Twente
Leden:	prof. dr. M.C. Elwenspoek	Universiteit Twente
	prof. dr. ir. C.H. Slump	Universiteit Twente
	prof. dr. rer. nat. M. Vorländer	RWTH Aachen
	prof. W. Desmet	KU Leuven
Referent:	dr. ir. H.E. de Bree	Microflown Technologies

The research described in this thesis is enabled by Microflown Technologies

E.H.G. Tijs, Study and development of an *in situ* acoustic absorption measurement method, PhD thesis, University of Twente, Enschede, The Netherlands, 2013

STUDY AND DEVELOPMENT OF AN *IN SITU* ACOUSTIC ABSORPTION MEASUREMENT METHOD

PROEFSCHRIFT

ter verkrijging van
de graad van doctor aan de Universiteit Twente,
op gezag van de rector magnificus,
prof. dr. H. Brinksma,
volgens besluit van het College voor Promoties
in het openbaar te verdedigen
op 19 april 2013 om 12:45 uur

door

Emiel Henricus Gerardus Tijs
geboren op 6 september 1983
te Deventer

Dit proefschrift is goedgekeurd door de promotoren:
Prof. dr. ir. G.J.M. Krijnen
Prof. dr. ir. W.F. Druyvesteyn

ISBN 978-90-365-3521-2

Contents

1. Introduction

1.1. *Background*

There are many unwanted noise sources in our industrialised society. Acoustic noise pollution can be reduced by lowering the radiation of the sound source itself, by reflecting sound towards different directions, by dispersing it, or by absorbing sound energy. Absorbing material packages are used in many applications to attenuate sound because it is sometimes impossible to reduce acoustic emission. Although these samples are extensively used, determination of their absorption properties remains a topic of interest due to the lack of appropriate characterisation techniques. A group of a restricted number of absorbing material package types is analysed theoretically well, but proper examination of the properties of many commonly used package types is too complex. Even though some methods are standardised, available measurement techniques have limitations. At times, their outcomes are inconsistent and conflicting, and do incorrectly reflect the characteristics of the material package after installation. Other measurement methods are unsuitable for certain frequency ranges, for certain material package types or for the way in which they are installed.

As existing methods leave room for improvement, there is a demand for a convenient and reliable method to measure sound absorption. This work focuses on the development of a method to determine the acoustic absorption of materials *in situ* (at the position at which they are used), taking advantage of a combined sound pressure - particle velocity measurement method.

1.2. *Acoustic absorbers*

Although numerous sound-absorbing structures exist, there are three basic forms; i.e. porous absorbers, cavity resonators, and membrane resonators (fig. 1-1) [1]. Porous absorbing materials consist of a network of pores. Acoustic energy is partially dissipated and converted into heat due to viscous and thermal effects. Examples are mineral wool, felt or high porosity foams. Porous materials are most effective at high frequencies because sufficiently large thicknesses compared to the sound wavelength are required. Cavity absorbers often use the principle of Helmholtz or quarter-lambda resonators.

They consist of a perforated surface, behind which there are certain cavities. Their principle is based on conversion into heat by viscous losses to some degree, and on fractional conversion into reactive energy[1] caused by interference effects. Although classic versions are most efficient in a narrow band around the resonance frequency, some resonators are tuned to operate in a wider frequency band. The degree of absorption depends on the number of cavities and the geometry of their opening, neck and cavity volume. Cavity absorbers are for example applied for noise attenuation of jet engines or in piping systems. Membrane absorbers consist of flexible impervious sheets. Sound is dissipated into heat due to thermo-elastic damping. Membrane absorbers can be effective at low frequencies. Many acoustic absorbing packages consist of multiple layers of several material types and are a combination of the above-mentioned absorber types.

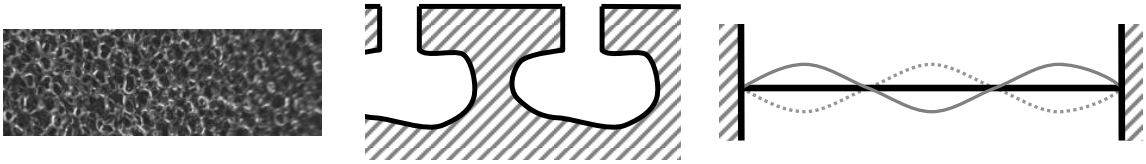

Fig. 1-1. Three basic types of absorbers.

For reasons of simplicity absorbing boundaries are often assumed locally reacting, which means that the normal particle velocity at a particular point depends only on the sound wave incident on that portion and is independent on the motion of other areas. This implies that waves inside such a sample propagate in the direction normal to the surface for all angles of incidence [2]. Several sound field models in this dissertation are also based on this assumption. Local reaction can be expected for near normal angles of incidence, for samples with a high propagation loss, or for samples with a high refraction index (i.e. a low speed of sound inside the sample compared to the speed of sound in air) [3]. Sometimes, this assumption is violated and extended reaction has to be taken into account for samples that are more complex.

[1] Reactive energy is non-propagating energy; only in an active sound field there is net energy flow. Net energy flow is obtained when sound pressure and particle velocity are in phase, e.g. as in a free field situation. When sound pressure and particle velocity are in anti-phase, e.g. as in the situation of standing waves, there is no net energy flow.

1.3. *Reflection, absorption, and transmission*

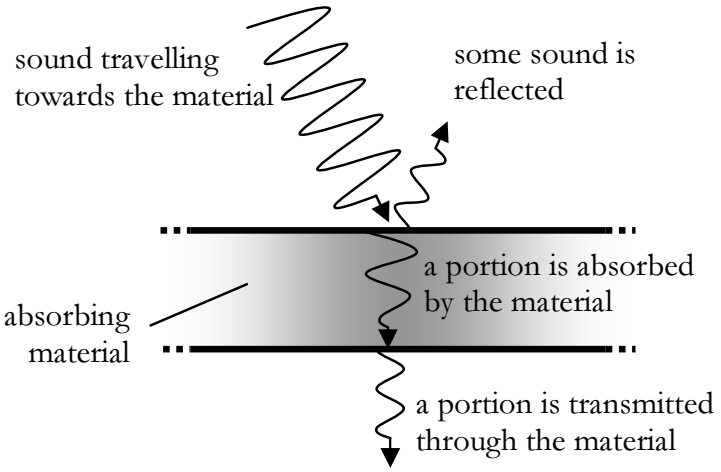

Fig. 1-2. Plane waves above an infinitely large sample.

Sound reflects if there is an impedance difference between two media; for example air and an acoustic sample [4, p. 149]. In addition, incident sound is partially absorbed by or transmitted through a sample (fig. 1-2). The frequency dependent rates of reflection, absorption, and transmission are usually represented as follows:

- The complex (sound pressure) *reflection* coefficient is the ratio of reflected to incoming sound pressures. Its absolute part is expressed as a value between zero and one, which corresponds to zero and full reflection, respectively.
- The acoustic *absorption* coefficient is also expressed in a range from zero to one, but instead of using the ratio of sound pressures, the ratio of absorbed to incoming sound intensities is used; which is equal to the squared sound pressure for a wave in the free field [5].
- The *transmission* loss is the ratio of transmitted to ingoing sound intensities in a decibel scale. Transmission loss should be distinguished from insertion loss. The latter is defined as the difference in sound pressure level at the receiver with and without a sample.

Whereas reflection is a complex angle dependent quantity, absorption and transmission values are usually integrated over all angles of incidence. In particular cases the sound field can be modelled, and reflection, absorption, or transmission can be calculated. Such cases require a good sound source description (for example, is there a single point source or are there plane waves), the sample type (local or extended reaction), the geometries, and the angle of incidence.

1.4. *Acoustic impedance and sound intensity*

Acoustic impedance and intensity are often used for sound absorption tests. In a given direction and a single-frequency sound field, the specific acoustic impedance Z_s in a medium is the complex ratio of sound pressure p to particle velocity u_{dir} in the specified direction at the same point [4, p. 126], [6]:

$$Z_s = \frac{p}{u_{\mathrm{dir}}} \quad \left[Ns/m^3\right] \tag{1-1}$$

where $\boldsymbol{u} = u_{\mathrm{dir}} \cdot \hat{e}$ with $\boldsymbol{u}$ being the full particle velocity vector and $\hat{e}$ a unit vector in the direction of interest. The impedance ratio, which is the specific impedance Z_s normalised with the characteristic impedance of the medium, is sometimes used instead; $\xi = \frac{Z_s}{Z_c} = \frac{Z_s}{\rho c}$ (ρ is the density and c is the speed of sound) [5]. Real and imaginary parts of the acoustic impedance are also called acoustic resistance and reactance, respectively [7]. In some cases, usage of acoustic admittance Y is preferred which is $1/Z$.

Sound intensity is the area averaged rate at which sound energy is transmitted through a unit area perpendicular to the specified direction, and is used for localising, quantifying, and ranking sound sources. The instantaneous sound intensity $\boldsymbol{I}_c$ is a vector quantity that is the product of sound pressure and its associated particle velocity at the same position [8-10]:

$$\boldsymbol{I}_c(t) = p(t)\boldsymbol{u}(t) \quad \left[W/m^2\right] \tag{1-2}$$

Usually, the averaged intensity of stationary sources is of interest (commonly simply called 'sound intensity'). Following Euler's Identity, a harmonic sound wave's pressure and particle velocity can be written as $p = re\left(\hat{p}e^{iwt}\right)$ and $\boldsymbol{u} = re\left(\hat{\boldsymbol{u}}e^{iwt}\right)$ respectively, where $\hat{p}$ and $\hat{\boldsymbol{u}}$ are the complex amplitudes of pressure and velocity. It can be shown that by integrating the instantaneous intensity over time the active intensity becomes [8-10]:

$$\boldsymbol{I}(\omega) = \tfrac{1}{2}\mathrm{Re}\left\{\hat{p}(\omega)\hat{\boldsymbol{u}}^{*}(\omega)\right\} \quad \left[W/m^{2}\right] \qquad (1\text{-}3)$$

here the asterisk * denotes complex conjugation. Whereas active intensity describes the net flow of sound energy, reactive intensity $\boldsymbol{J}$ describes the non-propagating part of energy that is merely flowing back and forth, which is expressed as:

$$\boldsymbol{J}(\omega) = \tfrac{1}{2}\mathrm{Im}\left\{\hat{p}(\omega)\hat{\boldsymbol{u}}^{*}(\omega)\right\} \quad \left[W/m^{2}\right] \qquad (1\text{-}4)$$

Examples of reactive sound fields are a standing wave tube with low damping, where the magnitude of the reflected wave is nearly equal to that of the ingoing wave, or the acoustic near field of a sound source, where air is essentially moving back and forth as if it were incompressible. The phase between sound pressure and particle velocity approaches 90 degrees in these cases.

Intensity has been measured for many years with so-called PP probes. In this method, particle velocity is derived from the pressure difference between two microphones positioned at a certain distance with respect to each other. Sound pressure is obtained by averaging both microphone signals. With a Microflown particle velocity sensor and a microphone, the intensity can be measured at one spot, thus avoiding spacing problems encountered with PP probes. This sensor can be used in environments with high levels of background noise or reflections where PP probes cannot be used [11, 12]. The error of intensity measurements with a microphone and Microflown is unaffected by the height of the pressure-intensity index (the ratio of sound pressure squared to active intensity), and mainly depends on the reactivity of the sound field (the ratio of reactive to active intensity in logarithmic form).

If the reactivity is high, as for example in the near field of a source, even a small phase mismatch error between the two transducers may lead to a considerable error, as can be seen from:

$$\begin{aligned} \boldsymbol{I}_{\text{measured}} &= \tfrac{1}{2}\,\text{Re}\left\{p(\omega)\boldsymbol{u}^*(\omega)e^{i\varphi_e}\right\} = \boldsymbol{I}\cos\varphi_e - \boldsymbol{J}\sin\varphi_e \\ \boldsymbol{I}_{\text{measured}} &= \boldsymbol{I}\left(\cos\varphi_e - \sin\varphi_e\tan\varphi_{\text{field}}\right) \approx \boldsymbol{I}\left(1-\varphi_e\tan\varphi_{\text{field}}\right) \end{aligned} \qquad (1\text{-}5)$$

where $\boldsymbol{I}_{\text{measured}}$ is the measured real intensity, φ_e is a small phase error between the measured and 'true' particle velocity, $\boldsymbol{J}$ and $\boldsymbol{I}$ are the 'true' (re-)active intensities, and φ_{field} is the phase between the sound pressure and the particle velocity of the sound field. The approximation is only valid if $\varphi_e << 1$. Accurate phase calibration is critical for tests carried out in strong reactive conditions, but typically not for far field tests. Reactivity is therefore an indication to whether this source of error is of concern [11]. In [13] it was mentioned that, in practical situations, the imaginary part of intensity should not exceed the real part with more than 5 dB, which corresponds to a φ_{field} of ± 72 degrees.

1.5. *Aim of the investigation*

For optimal material selection the performance of acoustic samples should be known. There are many methods to measure the acoustic absorption of samples, but they all have their specific weaknesses. Most of them are laboratory-based methods. The few *in situ* techniques that do exist have problems with reflections and have limitations in terms of bandwidth, sample size and signal to (background) noise ratio.

An *in situ* test would uncover the true behaviour of the material package, depending upon how and where it is installed. However, several issues complicate such measurements. Methods incorporating plane waves can be uncomplicated, but such sound waves are hardly encountered *in situ*. Therefore, more sophisticated methods are often required. Tests are also affected by air-flows, background noise, reflections from other surfaces, finite sample sizes and sound source distances. Up to date, no good sensors or measurement methods exist to determine the absorption of a range of samples in a convenient manner.

Although the history of sound pressure microphones goes back to 1876, it was not until 1994 before a convenient particle velocity sensor called the Microflown was invented [14, 15]. It provides a direct measurement of the acoustic particle velocity and it can be regarded as a point sensor, due to its sub-millimetre dimensions; much smaller than the wavelength of most frequencies of interest [15]. Microflowns are usually combined with a conventional microphone in a so-called PU probe; where P stands for sound pressure and U for acoustic particle velocity. PU probes have demonstrated to have advantages because of their small size, wide operational frequency range and the direct measurement of particle velocity.

In 2003, this particle velocity sensor has been used successfully for the first time to determine the acoustic absorption coefficient *in situ*. A sound source was positioned at some distance at normal incidence, and the impedance was measured near the sample [16]. Later a point source was used in semi-anechoic conditions at different angles of incidence [17].

As the Microflown sensor is relatively new, its features for *in situ* absorption tests are still largely unexplored. Development of an *in situ* absorption measurement method is therefore continued. The subject of this thesis is the development of a method that can be used conveniently in environments that are not necessarily anechoic. The characteristics and the limitations of such methods are examined, and several new applications are explored for the first time. Acoustic absorbing samples are tested under more realistic conditions than could be done before with other techniques.

The topic of absorption measurements is a rich field, and therefore it is not exhaustingly investigated in this thesis. In this work, the topic of sound absorption of separate acoustic samples is considered, but not the overall absorption in a room, which is also depending on the arrangement and interaction of all surfaces and sources relative to a certain observer's position.

1.6. *Outline*

Several renowned and widely-used acoustic absorption methods will be reviewed in the next chapter. A range of techniques will be discussed as well as their advantages and drawbacks. In addition, several models that are described are used to calculate the *in situ* absorption coefficient from an impedance or intensity measured above an acoustic absorbing sample. Particle velocity sensors and their unique properties will be introduced.

The determination of the distinct frequency dependent characteristic of Microflown sensors is the topic of chapter three. A broadband calibration technique is presented that involves two steps; one for middle and high frequencies, and one for low frequencies. Absolute sensor responsivity values are not always required for absorption measurements. A reference test without the sample that is performed just before or just after the test with the sample is often more practical to use.

An easy to use absorption method is developed, which involves a handheld measurement set-up. The different set-ups designed throughout the years are shown in chapter four. Subjects such as sound source selection and suppression of vibrations are treated.

Although anechoic conditions are assumed in most sound field models, there will be reflections from surrounding surfaces that affect the *in situ* tests. In chapter five, several techniques to cancel reflections are presented, and their effectiveness is evaluated using simulations and measurements.

Most acoustic absorption models assume only one reflection at the front side of the sample. However, sound also partially penetrates through its surface, and standing waves are formed between the front and backside of the sample. The topic of chapter six is to compensate for these spherical sound waves inside the sample, and two techniques that combine several measurements to calculate absorption are presented. Acoustic samples with and without a backplate are considered.

In chapter seven possibilities and limitations of the PU *in situ* method are analysed. Tests are done with relatively small samples (<0.1 m^2) and with a resolution of approximately a millimetre. A comparative study revealed that the outcome of measurements in Kundt's tubes are incorrect in certain cases. The influence of background noise on the *in situ* method is evaluated and is found small because of the small probe-sensor-sample distance. The effect of varying set-up geometries, different models, probe stability, sensor dynamic range and disturbance of wind are also investigated.

The acoustic response of samples could change after installation. Up to now, measurements were impossible in certain environments. In chapter eight, some applications which could not be measured before are explored. Results are shown of tests done in non-anechoic conditions (cars and concert halls), on jet engine liner samples (with and without flow) and on asphalt roads whilst driving. Finally, a fast, high-resolution sound mapping method called Scan and Paint is presented. Surfaces are scanned with a compact probe and the results are visualised as a colour-map.

In Chapter 9, two alternative principles to characterise sound absorption are described. Using three-dimensional probes the full intensity and energy vectors can be determined. The ratio of these quantities is used as a parameter for diffusion at a particular position. Multiple intensity measurements are used to visualise the sound field flow around objects.

In chapter 10 and 11 (the latter in Dutch) contain a summary of what has been accomplished and to which extent the research goals have been achieved. Finally, in chapter 12 the potential implications for material testing are discussed and a brief outlook for future development of (*in situ* absorption) measurements using PU probes is presented.

The author has contributed to publications referenced throughout this document with an italic font; i.e.: *[…]*.

2. Overview of existing absorption measurement methods

2.1. *Introduction*

Throughout the years, many methods have been developed to measure sound absorption. These techniques all have their specific strengths and weaknesses. Often, results of several approaches are combined. However, even for acoustic engineers, interpretation of these results can be challenging when various methods yield conflicting or inconclusive results. Some well-known techniques will be discussed in this section.

The two most popular methods are the Kundt's tube and the reverberant method. Both methods are suited for laboratory use and are restricted in frequency range, specimen composition, and sound field type. Samples can be analysed as installed using *in situ* techniques based on microphones only. However, apart from the aforementioned problems, they require large samples and are susceptible to background noise and reflections. In this thesis, it will be shown that *in situ* tests with PU probes are affected little by such issues. These probes are able to capture sound pressure as well as particle velocity in a convenient manner. Their measurement principle is introduced, and existing methods to calculate absorption properties with such probes are presented.

Amongst other quantities, the aforementioned methods are used to determine the frequency dependent sound intensity absorption coefficient. The absorption coefficient is a dimensionless quantity that is the ratio of the absorbed to the ingoing intensities, which ranges from zero to one (or from 0% to 100%). It is sometimes represented in one-third octave bands for the ease of interpretation. With many methods actually reflection is measured instead of absorption. The absorption is then usually calculated by assuming that there is no transmission and that the absorbed intensity is equal to that part of the intensity that is not reflected.

Depending on the properties and the geometry of the sample, and on the applied sound field, absorption could be defined in a number of ways. The goal of this thesis is to obtain the absorption coefficient of an entire sample in

the way it is installed, taking into account its mounting conditions (with and without a backplate or with an air gap behind the sample), without influence from surrounding objects. The absorption should represent the statistical or random incidence absorption coefficient; as if there would be plane sound waves arriving from all directions. In the application or during tests there might be different sound fields, but corrections are applied which allow for convenient interpretation and comparison to results from other (measurement) techniques. Sometimes, the absorption coefficient is estimated from measurements at a limited number of angles only (thus effectively assuming the sample to be locally reacting). The absorption coefficient as is studied in this work does not refer to the energy attenuation coefficient (units m^{-1}) of waves propagating through the medium, which is sometimes also called the absorption coefficient. The latter is a material property rather than a whole sample characteristic.

2.2. *Kundt's method*

2.2.1. Kundt's tubes

The standing wave tube, or Kundt's tube, is one of the oldest and most well-known instruments to measure impedance, reflection, absorption, and transmission of a sample at normal incidence. Kundt's tube methods are comprehensible because only plane waves propagating in the direction of the tube are considered. The maximum frequency for a cylindrical tube for the sound propagation to be uni-directional (i.e. plane wave front) is related to its inner diameter d and the speed of sound c; $f_{\max} = 0.586\frac{c}{d}$. Above this frequency sound also propagates in transverse directions. For a tube with a square cross-section $f_{\max} = 0.5\frac{c}{L}$, where L is its inner width [18].

Since compact particle velocity sensors are available only recently, microphones were used. Early tubes comprised a single microphone [3, 18]. A sound source is placed at on one side of the tube, and the acoustic sample that is cut out is installed at the other end (fig. 2-1). The standing wave ratio is used to calculate the absorption coefficient. This is the ratio of the sound pressure maximum to the sound pressure minimum, which is measured by moving the microphone along the axis of the tube.

The sample mounting conditions, and thus the determined absorption values, can be changed. An air gap can be left between the sample and the reflecting backplate shown in fig. 2-1, or the backplate can be replaced by an anechoic termination. The one microphone method is standardised in ISO 10534-1 and ASTM C384-04.

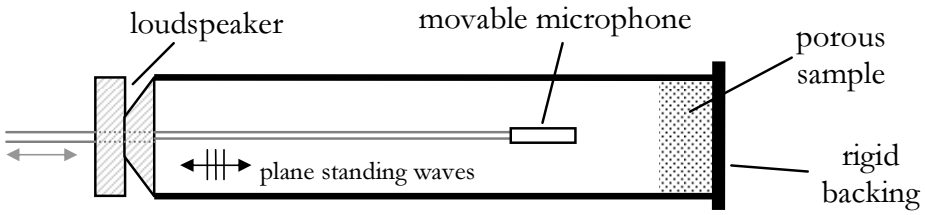

Fig. 2-1. Single microphone Kundt's tube.

In ISO 10534-2 and ASTM E1050-98 the use of the transfer function method as developed by Chung&Blaser in 1980 is specified [19]. The set-up is similar to the one microphone method, but instead, two microphones at fixed positions x_1 and x_2 are used (fig. 2-2). Contrary to the single microphone method, the reflection coefficient R and absorption coefficient a can be calculated at multiple frequencies simultaneously [3, 20, 21]:

$$R = \frac{H_{12}e^{ikx_2} - e^{ikx_1}}{H_{12}e^{-ikx_2} - e^{-ikx_1}} \qquad (2\text{-}1)$$

$$a = 1 - R \cdot R^* \qquad (2\text{-}2)$$

where the transfer function H_{12} is the ratio of the cross-spectrum G_{12} of the two microphones to the auto-spectrum G_{22} of the second microphone; $H_{12} = G_{12}/G_{22}$. The frequency range mainly depends on the microphone spacing and the inner tube diameter. The accuracy decreases if the microphone's separation is close to half a wavelength, or if the distance between one of the microphones and the backplate approximates a quarter wavelength. Typically, several tube diameters are available; for example the company Brüel&Kjær provides tubes with an inner diameter of 100mm with a specified frequency range of 50Hz to 1.6kHz, a 62.5mm diameter with a range of 100Hz to 3.2kHz, and a 29mm diameter tube with a range of 500Hz to 6.4kHz [22]. Tubes are often equipped with a third microphone mounting for accurate calibration [23]. Tube extensions and two additional microphones are used for transmission loss tests. The impedance is then measured at both sides of the sample, with four microphones in total.

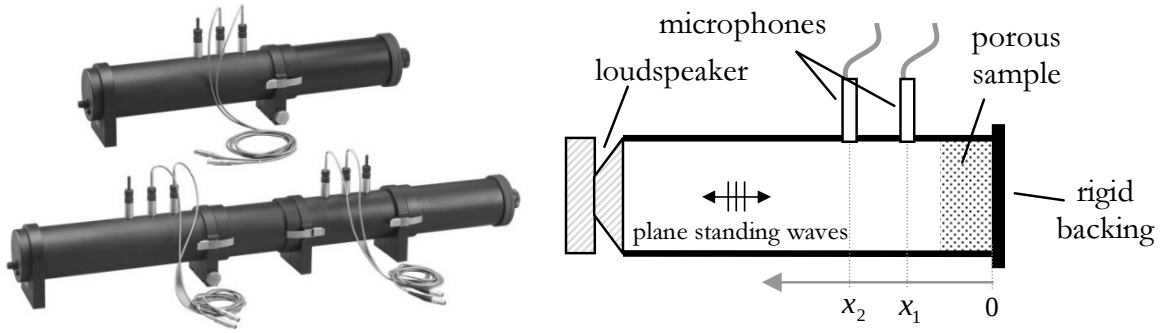

Fig. 2-2. Double microphone Kundt's tube. Left: picture, source [22]. Right: sketch.

Instead of using two microphones, the impedance in the tube can also be measured using a PU probe [24-26]. With such probes frequencies as low as 20Hz have been accessed by de Bree et al. *[27]*. The PU Kundt's method is scarcely used up to now because the procedure is not standardised yet. In this work, the PU Kundt's tube method is used as a reference for *in situ* tests.

Compared to other methods, Kundt's tubes are cost friendly, easy to use, and, because the tube is closed, the influence of background noise is low. However, there are concerns using Kundt's tubes:

- Acoustic samples can only be determined at normal incidence, thus non-locally reacting samples cannot be measured properly.
- Sample cut-out is destructive and time intensive, and is problematic for hard or fragile materials such as concrete or light foams.
- There are sample installation problems. Air gaps behind the sample and at the specimen side are difficult to avoid because at the same time mechanical contact with the tube itself should be prevented. This non-clamping condition is usually not achieved, and this proves a problem for samples with a high flow resistivity and a low Young's modulus. Many double layer samples have such characteristics. When the top layer of the sample is clamped against the sidewalls of the tube, effectively a membrane with a certain diameter is created, which alters the properties of the sample [28, 29].
- Sample size is restricted by the tube's inner diameter. Depending on the sample properties, the measured absorption can be different to that of an infinitely large sample *[30]*.

Variations in for example mounting, equipment, measurement details, cause (inter-laboratory) inconsistencies. Based on round-robin tests, a dispersion of the impedance and absorption values larger than 20% was reported in [31].

2.2.2. Open Kundt's tubes

Some samples are difficult to mount inside a tube. In 1963, Berendt and Schmidt were the first to develop an open tube [32]. The principles are similar to that of closed Kundt's tubes, only the open side is placed on the sample. However, strong sound leakage occur through porous samples, which results in an incorrect high measured absorption, mainly at low frequencies. Flanges that cover parts of the sample can be applied to reduce this leakage, together with sealants to the surface like modelling clay (fig. 2-3). This method is often called the Guard tube or spot method, and is standardised in ISO 13472-2 [33]. The flange does not prevent all sound leakage through the sample, and can introduce resonances between the flange and the bottom of the sample (see *[34]* Tijs et al. and section 8.3).

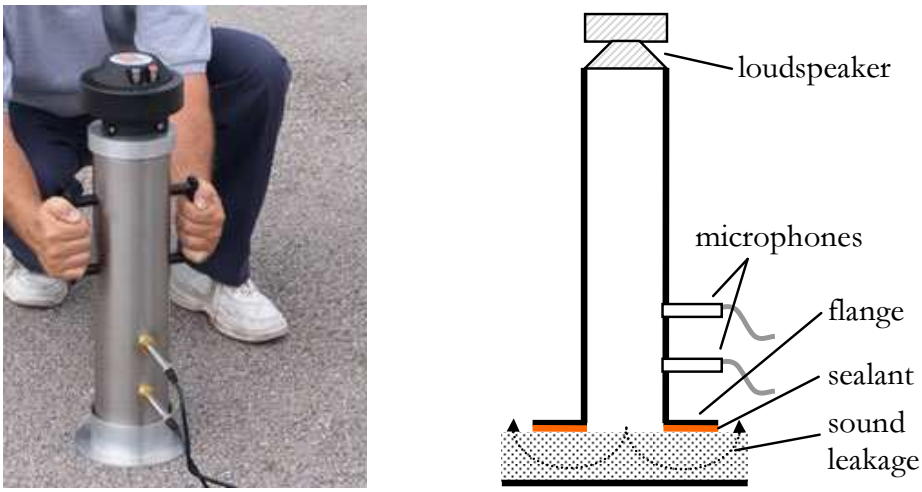

Fig. 2-3. Open Kundt's tube with flange. Left: picture, source [35]. Right: sketch.

Alternatively, to reduce leakage, impulse subtraction techniques or an inner and outer tube are used. The latter method is based on the principle that the actual test is done in the inner tube (fig. 2-4). Leakage in the inner tube is partially compensated by leakage from the outer tube into the inner tube. Despite of the abovementioned measures, leakage still occurs, and can cause substantial deviations. Furthermore, open Kundt's tubes suffer from many aforementioned problems of closed tubes.

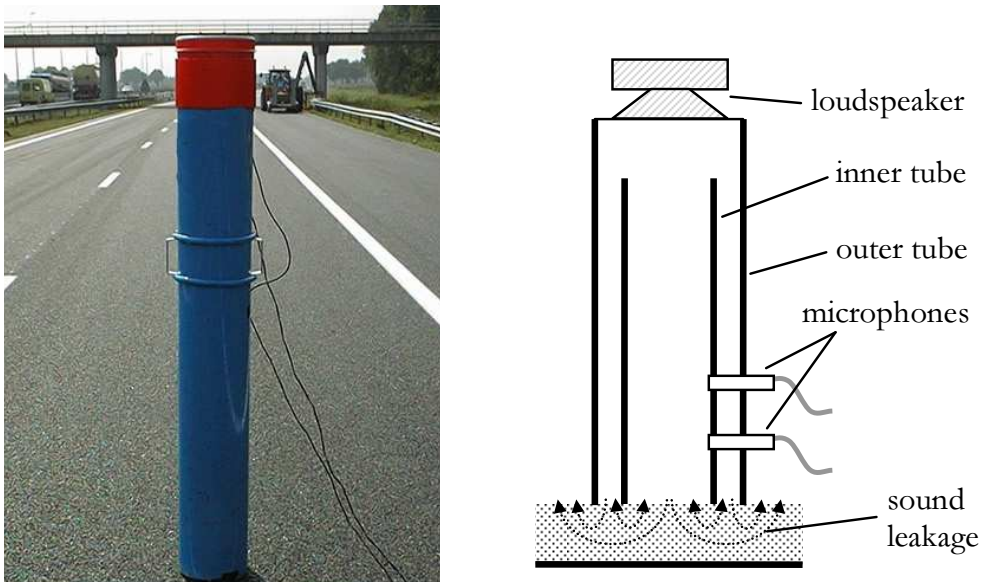

Fig. 2-4. Open Kundt's tube with inner and outer tube.
Left: picture, source [36]. Right: sketch.

2.3. *Reverberant method*

Absorption measurements in a reverberant room are based on the principle that an acoustic absorbing sample reduces the sound pressure over time. Usually, the T_{60} reverberation time is used to determine the sound pressure decay, which is the time that would be required for it to decrease 60 dB after the sound source has stopped.

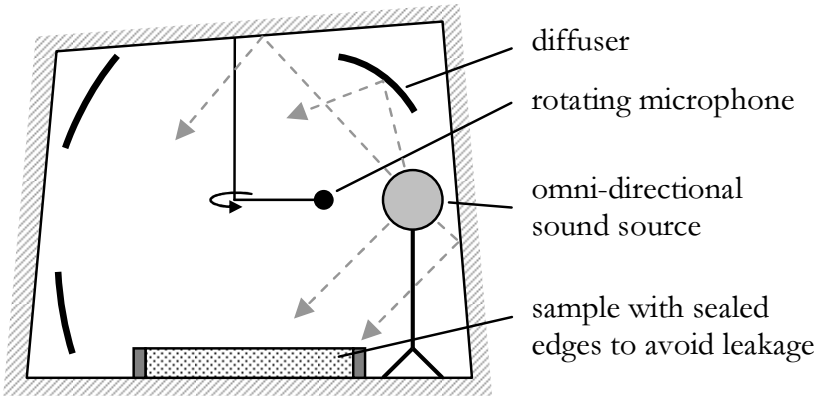

Fig. 2-5. Reverberant room with a rotating microphone.

The sound field in a reverberant room is supposed perfectly diffuse, meaning that there are uncorrelated random noise sources from all possible directions and that the sound pressure level is equal at all positions. To achieve this, random sound is generated inside a room that has strongly reflecting walls, which preferably are shaped irregularly to avoid standing waves (fig. 2-5).

The effect of room modes can further be reduced by rotating or moving diffusers, sound sources, or (multiple) measurement microphones. The well-known Sabine equation relates the reverberation time of a room, to its volume V and its total sound absorption A_{sabine} [4, pp. 333-339], [7]:

$$T_{60} = \ln(10^6)\frac{4V}{cA_{\text{sabine}}} \approx C\frac{V}{A_{\text{sabine}}} \qquad (2\text{-}3)$$

where constant C is 0.161 s/m. The total sound absorption A_{sabine}, which is expressed in m^2 or sabins, can be seen as the area that would fully absorb at that particular frequency. The reverberation time is measured with and without a sample installed. The Sabine absorption coefficient is then defined as [5]:

$$\alpha_s = \frac{A_{\text{sabine},1} - A_{\text{sabine},0}}{S_{\text{test}}} + \frac{A_{\text{sabine},0}}{S_{\text{tot}}} \qquad (2\text{-}4)$$

here $A_{\text{sabine},1}$ and $A_{\text{sabine},0}$ are the total sound absorption with and without the sample installed, respectively. S_{test} and S_{tot} are the surface area of the test sample and the total area of the room, respectively.

The reverberant room method is standardised in ISO 354 and ASTM C423. There are differences between these standards in terms of sample size and room volumes required, differences in sample mounting, and calculation methods [37]. ASTM C423 [38] uses the sound pressure decay rate of an interrupted random noise source over time. ISO 354 [39] on the other hand uses the reverberant time, which can also be obtained by integrating the impulse response of the microphone. Both standards define an equivalent sound absorption A_{ASTM} and A_{ISO}:

$$A_{\text{ASTM}} = 0.9210\frac{Vd}{c} \qquad (2\text{-}5) \qquad A_{\text{ISO}} = \frac{55.3V}{cT_{60}} - 4Vm \qquad (2\text{-}6)$$

where c is the speed of sound and d is the decay rate in dB/s. Parameter m is the power attenuation coefficient calculated according to ISO 9613-1.

The sound absorption is determined for the empty room ($A_{\mathrm{ASTM},0}$, $A_{\mathrm{ISO},0}$) and a room with a sample ($A_{\mathrm{ASTM},1}$, $A_{\mathrm{ISO},1}$). The absorption coefficient α is then obtained by:

$$\alpha_{\mathrm{ASTM}} = \frac{A_{\mathrm{ASTM},1} - A_{\mathrm{ASTM},0}}{S_{\mathrm{test}}} + \alpha_0 \qquad (2\text{-}7) \qquad \alpha_{\mathrm{ISO}} = \frac{A_{\mathrm{ISO},1} - A_{\mathrm{ISO},0}}{S_{\mathrm{test}}} \qquad (2\text{-}8)$$

in which α_0 is the absorption coefficient of the surface covered by the specimen when it is not installed.

Large and expensive facilities are required for these standardised methods. The sample size should be $\geq 6.69\,\mathrm{m}^2$ according to ASTM C423, and between $10\,\mathrm{m}^2$ and $12\,\mathrm{m}^2$ according to ISO 354. Typically, values are calculated in a 100 Hz - 5 kHz range using averaged values in one-third octave bands. A smaller reverberant room called the alpha cabin was developed for the automotive industry (fig. 2-6 right). Its volume is reduced to $6.44\,\mathrm{m}^3$ and the sample size to $1.2\,\mathrm{m}^2$ [40]. However, to achieve reverberant conditions at low frequencies large rooms are required [41].

Fig. 2-6. Two examples of reverberant rooms. Left: large room with omni-directional sound source and deflectors, source [42]. Right: Alpha cabin, source [40].

Reverberant room methods have several disadvantages:

- Large samples are not always obtained and installed easily.
- The position of the sample in the room can influence the results [4, p. 355].
- Significant differences are experienced from one room to another [41].
- Only the absolute absorption value is measured, and not the complex surface impedance or reflection which can be required for simulations.
- Absorption values are often overestimated; values higher than one are not uncommon. These deviations are usually contributed to the finite sample size and edge diffractions. However, up to date the effect of these effects has been characterised insufficiently.
- The sound field is not perfectly diffuse anymore after the large acoustic absorber is introduced [8].
- Even though large facilities and samples are used, deviations are found compared to theoretical infinitely large samples.

2.4. *Material models using micro-structural properties*

Rather than a direct measurement of the sound field around the sample, there are a number of methods involving the measurement of separate material properties of the solid frame and the fluid in the pores. These quantities are used to describe viscous and thermal interactions [4, p. 210]. Some important micro-structural characteristics are [42, 43]:

- Flow resistivity: the resistance offered by a material to a static airflow. It can be determined by measuring the pressure drop over the material due to an air flow.
- Porosity: the ratio of fluid volume to total volume. One measurement method is to fill the sample with a liquid, and to determine the additional weight due to that volume.
- Tortuosity: a degree for the 'non-straightness' of the pore structure. It shows how well the porous material blocks direct flow. It can be determined by applying a pulse with an ultrasonic transducer on one side of the sample, and by measuring the time delay with another transducer on the other side.
- The viscous and thermal characteristic lengths, which are related to the viscous and thermal losses.

With exact or (semi-)empirical models the so-called bulk properties of materials can be obtained which are independent of the sample geometries and mounting conditions. They are often expressed by the complex characteristic impedance Z_1 and wavenumber k_1. The degree of reflection at the impedance boundary is determined by the ratio of impedances of the two media. Sound waves are attenuated as they propagate through the material because k_1 is complex; sound pressure and particle velocity of a plane propagating wave in a specified direction x decay with distance by $e^{-i(\omega t - kx)}$ [5]. The models involve one or more material parameters. Biot was one of the earlier pioneers [28, 44]. Other well-known models are developed by Zwikker and Kosten (which requires 3 parameters), the Attenborough (4 parameters), and Johnson / Allard / Lafarge (6 parameters) [43]. Perhaps the most popular model is the empirical formula of Delany and Bazley from 1969 for locally reacting fibrous anisotropic materials, which requires only the flow resistivity σ [32]. For plane waves, the complex characteristic material impedance Z_1 and wave number k_1 of the sample are calculated by:

$$\begin{aligned} Z_1 &= \rho_0 c_0 \left(1 + 0.057 \left(\frac{\rho_0 f}{\sigma} \right)^{-0.754} - 0.087 i \left(\frac{\rho_0 f}{\sigma} \right)^{-0.732} \right) \\ k_1 &= \frac{2\pi f}{c_0} \left(1 + 0.0978 \left(\frac{\rho_0 f}{\sigma} \right)^{-0.700} - 0.189 i \left(\frac{\rho_0 f}{\sigma} \right)^{-0.595} \right) \end{aligned} \qquad (2\text{-}9)$$

These expressions are valid when:

$$0.01 < \frac{f}{\sigma} < 1 \qquad (2\text{-}10)$$

Later also different solutions based on similar expressions have been introduced, like the Miki or Komatsu model [46]. These mainly improve the low frequency accuracy.

Whereas most other absorption methods involve a direct measurement of sound reflection or absorption, with these models, the sample absorption is predicted indirectly using separate material properties. Usually, results from these models are used as reference for Kundt's tubes and reverberant room tests. The drawbacks are that many material parameters are difficult to measure and that assumptions of the material type have to be made for selecting the appropriate model. Also, these methods are not *in situ* and they disregard specific mounting conditions.

2.5. *Tamura method*

The Tamura method [3, 17, 18, 43] closely resembles near field holography [46-48], and involves the measurement of sound pressure in two planes above the sample surface. By a two dimensional spatial Fourier transform, the sound pressure distribution is decomposed into plane wave components of the incident and reflected sound, and the plane wave reflection coefficient is obtained. The reflection and absorption from all angles of incidence can be obtained. However, there are some drawbacks. A rather complicated test set-up has to be installed in a semi-anechoic room, and large samples (~10 m^2) are required (fig. 2-7). The method cannot be used *in situ* and the measurement time is long (several hours).

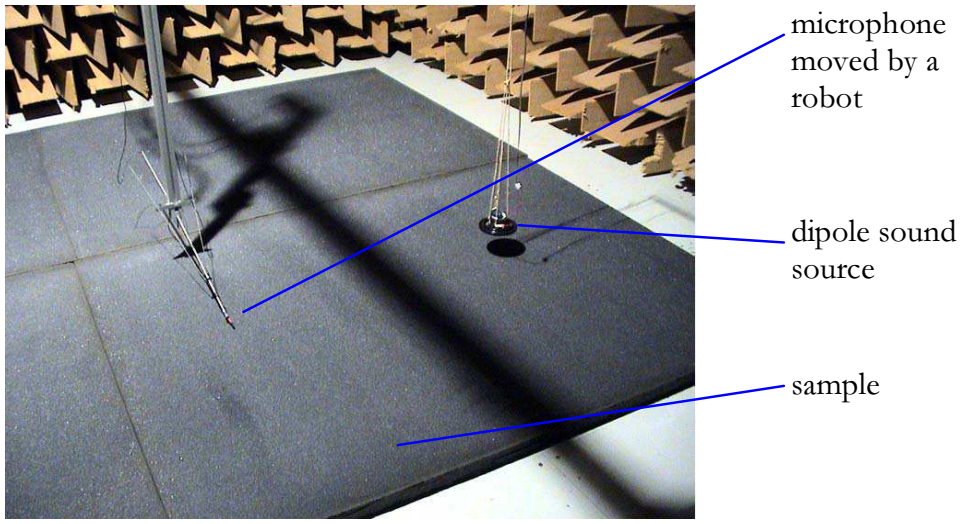

Fig. 2-7. Example of a test set-up for the Tamura method, source [44].

2.6. *In situ (microphone-based) techniques*

The main shortcoming of the aforementioned laboratory methods is that they do not represent the sample after installation. When samples are mounted they can be deformed which can change acoustic properties, but also nearby structures can influence the behaviour. For example, the absorption may be influenced by the presence of another damping material or by an air cavity behind the sample. Many attempts have been made to develop *in situ* measurement methods. Apart from the PU method that is investigated in this work, several other *in situ* methods are discussed. Compared to laboratory techniques, *in situ* methods are more influenced by external disturbances such as background noise and reflections from (nearby) objects.

2.6.1. Single microphone methods

A straightforward method involves a single microphone and a sound source near the acoustic sample. A pulse is generated, and the direct signal and its reflection are measured. Both signals can be separated using time windows. The reflection and absorption coefficient are then calculated from the ratio of the reflected to incident sound pressures [3, 23, 49]. The microphone is positioned at a certain distance from the sample to obtain sufficient time delay between direct and reflected signals. Alternatively, one can use other noise types that provide increased signal-to-noise ratios, such as random noise, MLS, and swept sines. Incident and reflected components can then be separated by calculating the microphone impulse response or by subtracting the incident pulse in the time domain using a free field calibration. The latter approach is susceptible to changes of surroundings such as room reflections and air impedance.

Single microphone techniques have been standardised in CEN/TS 1793-5 and AFNOR NF S 31-089 for measuring the absorption of (road) noise barriers at several angles of incidence [51], and in ISO 13472-1 for measuring road surfaces under normal incidence. These methods are called the "Adrienne method" and the "extended surface method", respectively. There is a spacing between the sound source, the microphone, and the sample to avoid strong near field effects and to ensure that the reflections from the sample do not overlap the direct sound in time. For example, in ISO 13472-1 a distance of

1.25m between the sound source and the sample, and 0.25m distance between the microphone and the sample are specified. The standards use time subtraction techniques and a so-called Adrienne window. The Adrienne window usually consists of a leading edge having a left-half Blackman-Harris shape (0.5ms), a flat portion (5.18ms) and a trailing edge having a right-half Blackman-Harris shape (2.22ms), see fig. 2-8. It is reported that this type of window has good time resolution and, at the same time, avoids leakage effects in the frequency domain as much as possible [52]. Frequencies below approximately 250Hz cannot be reached because the window length is limited. With most test set-ups, the maximum frequency is about 4kHz because the signal-to-noise ratio is limited [50]. Typical test set-ups for both methods are shown in fig. 2-9.

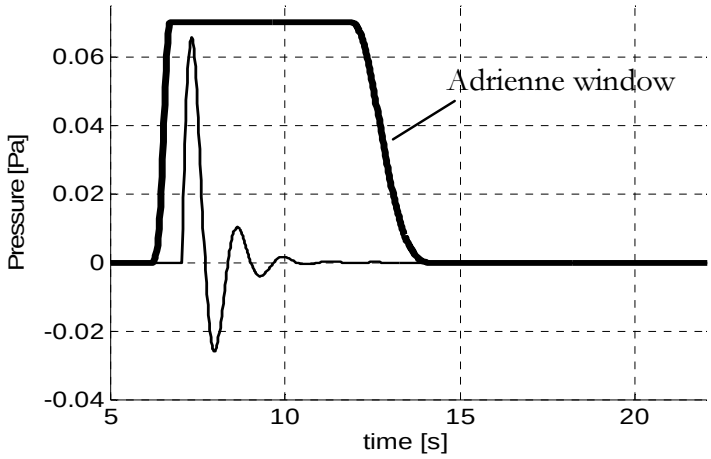

Fig. 2-8. Microphone impulse response.

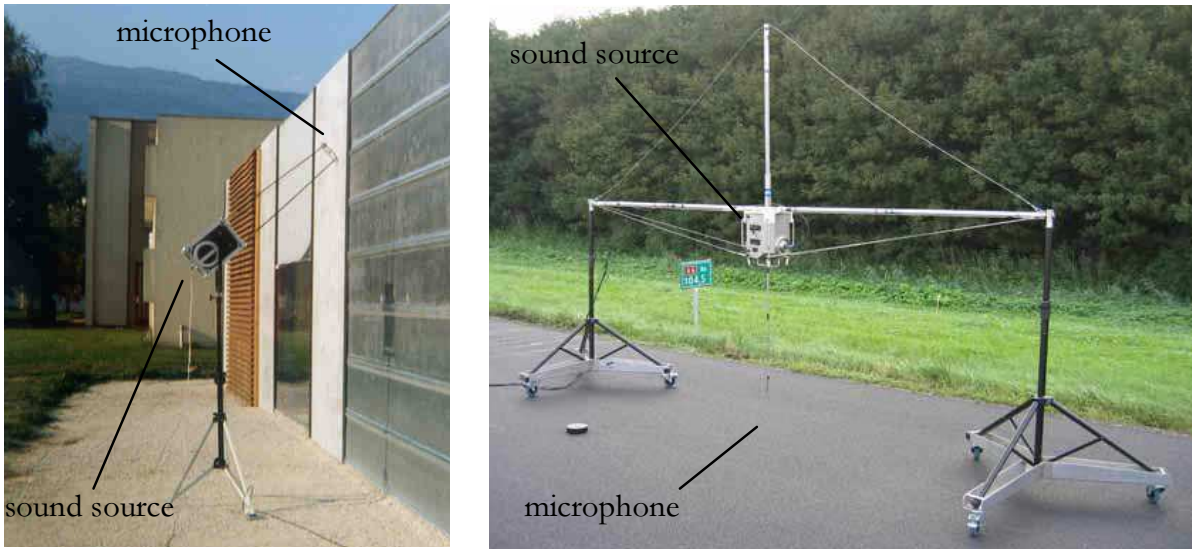

Fig. 2-9. Examples of two single microphone test set-ups. Left: The Adrienne method (source [53]). Right: The extended surface method (source [54]).

Advantages of these single microphone techniques are that they can be applied *in situ* and that their principle is easy to comprehend. However, there are downsides. Large sample sizes are required; in the range of $1\,m^2$ for the extended surface method, and $3\,m^2$ for the Adrienne method at normal incidence [50]. The sample size required for the Adrienne method is even larger for smaller angles of incidence. The active surface area and the minimum frequency that can be accessed depend on the length of the time window and on the distance between source, microphone and surface. Background noise can severely deteriorate the measurement quality. Difficulties are experienced with high absorbing samples, because the reflected signal is low [55].

2.6.2. Two microphone method

Impedance can be determined *in situ* using two closely spaced microphones [3, 18, 55-58], [59, p. 945]; the same configuration as used for intensity measurements. There are similarities between absorption measurement methods that incorporate PP probes and methods that incorporate PU probes, which are examined in this study. In most cases, a point source is involved at a certain distance from the sample, and the microphone pair is positioned near its surface. Using spherical sound field models, the absorption of the sample is obtained from the sound pressure and the particle velocity, which are measured above the sample. With PP probes, the sound pressure is obtained by averaging both microphone signals and the particle velocity is obtained from the sound pressure gradient.

In principle, the two-microphone method can also be used at oblique incidence. However, the phase difference between the two microphones decreases with increasing angle of incidence, and therefore the remaining phase error between the microphones makes it difficult to obtain good results beyond 60 degrees [23].

There are differences between the use of PP- and PU probes. Whereas the error of intensity measurements with on PU probes depends on the reactivity of the sound field, the error of impedance or intensity measurements with PP probes depends on the ratio of sound pressure squared to active intensity [11, 12]. In addition, the frequency range of PP probes is limited by the microphone separation distance. Moreover, standardized calibration procedures exist for PP probes. Furthermore, the size of PU probes is an advantage for absorption tests. With PP probes the spacing needs to be large for low frequencies due to (background) noise, which means that the measurement centre of the PP probe is further from the sample surface. Larger samples are then required to avoid edge effects [62], and typically larger set-ups are used which are prone to reflections from surrounding surfaces. The measurement quality deteriorates for larger source-surface distances because the reflection becomes weaker compared to the direct source.

2.7. *PU in situ absorption measurement methods*

2.7.1. Microflown particle velocity sensors

Sound pressure and particle velocity are of interest for many acoustic problems. Whereas sound pressure is related to the acoustic potential energy, particle velocity on the other hand can be related to acoustic kinetic energy. Norwegian Electronics manufactured an probe that contains a microphone, which measures the sound pressure, and ultrasonic transducers, with which the particle velocity is obtained [14]. However, this probe is rather large, it is susceptible to wind, and there are limitations at high frequencies. In 1994, a sensor called the Microflown was invented, which can directly measure acoustic particle velocity in a small spot (approximately 3mmx1mmx0.5mm) compared to the wavelength of audible frequencies [14, 15]. This sensor was commercialised in 1997.

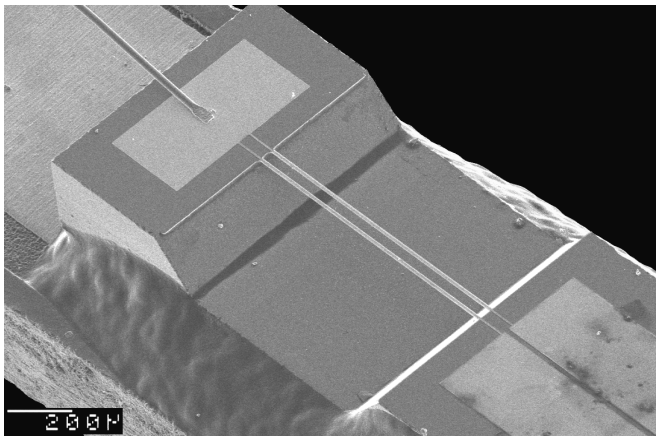

Fig. 2-10. A microscope picture of an example Microflown particle velocity sensor

The sensor principle is based on the measurement of the temperature difference between closely spaced wires. Two 200 nm thick platinum wires are heated to about 300°C. The operation principle involves intriguing physics [62-64] but can be understood using hand waving arguments as follows; if there is particle velocity, the temperature distribution asymmetrically alters, and therefore cause a temperature difference between both wires. Due to the thermal resistance effect, the heat flux also induces a resistance difference between the wires, which is measured. Since the thermal effects are frequency dependent, the sensor responsivity is too. However, the sensor output voltage is to good approximation and to high acoustic intensities proportional to the acoustic particle velocity.

Fig. 2-11. Three main probe types that contain Microflown sensors. Left: scanning probe (1D particle velocity). Middle: PU probe (sound pressure and 1D particle velocity). Right: USP probe (sound pressure and 3D particle velocity).

Several probe types that contain Microflown sensors are available. Each of them is designed for a specific purpose. Fig. 2-11 shows the three main probe versions. A scanning probe consists of a single Microflown sensor, and it is used for near field vibration tests. For sound intensity, energy or impedance

tests, a particle velocity sensor is combined with a microphone. PU probes are used for 1D measurements, and contain one particle velocity and one sound pressure sensor. USP probes use three orthogonally placed particle velocity sensors and one sound pressure sensor, and can be used for 3D tests.

In recent years, the number of applications and of users of Microflown probes has grown rapidly. Nowadays, they are used in industries such as automotive, aerospace, surveillance, and military. Applications vary from sound source localisation (in the acoustic near field or far field), intensity measurements, vibration tests, absorption measurements, and many more. Appendix A contains a summary of some important applications of PU probes.

2.7.2. Methods involving particle velocity sensors

PU probes were first applied for acoustic impedance measurements in the throat of a horn loudspeaker [67]. Later, a PU probe and UU probe (a probe that contains two particle velocity sensors) where used in a Kundt's tube and compared to the standardised transfer function method based on two microphones. These tests showed that particle velocity sensors can also be used to determine acoustic characteristics of acoustic samples.

The absorption of a sample depends on its geometry and properties, on its mounting conditions (for example a rigid backplate behind the sample with or without air gap), and on the sound field around the sample. Samples can therefore be measured best as mounted and with the sound field present in the application. In 2003, Iwase and Yoshihisa were the first to use PU probes for measuring impedance *in situ* to obtain the absorption coefficient [16]. They used a single sound source at normal incidence above a layer of asphalt. Sound pressure and particle velocity were both measured, and therefore impedance, which is the ratio of the two, could directly be obtained. Lanoye et al. independently developed a similar method, and in 2004 they showed that the acoustic reflection coefficient could be determined in a wide frequency range for oblique and normal angles of incidence [17]. In 2005, Takahasi et al. used ambient noise assuming random incidence instead of normal incident sound [68]. These studies were a reason for Microflown Technologies to start research on acoustic absorption measurement methods using PU probes.

With a microphone and a Microflown combined in one probe, the sound pressure and particle velocity can conveniently be measured in virtually one spot. Sound pressure and particle velocity can be measured close to the sample because such PU probes can be small. When a known sound source is used, the sound field can be described by a model and the absorption at the sample surface can be calculated from the measured impedance or intensity. Absorption tests with PU probes have particularities, which are discussed in more detail throughout the next chapters. With these probes, the complex impedance, intensity, reflection or absorption can be measured. In general, the most important advantages of such tests are that they can be performed:

- *in situ*;
- fast;
- in a wide frequency range;
- with high spatial resolution and a small sample size compared to most other *in situ* methods;
- under relatively high levels of background noise and reflections.

In situ absorption measurement methods based on PU probes have not yet been standardised.

2.7.3. Principle of measuring reflection and absorption

A probe near an acoustic sample measures the direct field and its reflection simultaneously. With a sound field model, the degree of reflection can be calculated from the sound pressure and the particle velocity. The distribution of sound sources for samples as they are installed can be unknown. The sound field is also influenced by reflections from other surfaces. For simplicity, and to allow for comparison of different samples, a constant geometry and the same type of sound source are assumed. A convenient approximation is to consider plane waves above an infinitely large impedance plane, without reflections from other surfaces.

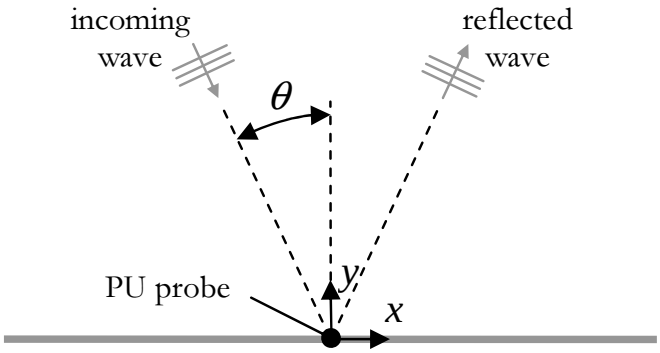

Fig. 2-12. Plane waves above an infinitely large impedance plane.

In anechoic conditions and far from the sound source where there is no divergence and where sound waves are approximately plane, particle velocity u in a given direction can be calculated by sound pressure p divided by the impedance of air (i.e. ρc). Two conditions must be satisfied at the boundary of two media, 1) continuity of sound pressure, and 2) continuity of normal particle velocity; which is equivalent to requiring continuity of normal specific impedance. The first condition implies that there is no net force on the boundary separating the two media. The second condition guaranties that both media remain in contact. Complex sound pressure and normal particle velocity u_{n} (in direction y) near the reflecting surface are:

$$p(\theta) = p_0 + p_0 R(\theta) = p_0 \{1 + R(\theta)\} \qquad (2\text{-}11)$$

$$u_{\mathrm{n}}(\theta) = p_0 \frac{\cos\theta}{\rho c} - p_0 R(\theta) \frac{\cos\theta}{\rho c} = p_0 \{1 - R(\theta)\} \frac{\cos\theta}{\rho c} \qquad (2\text{-}12)$$

where p_0 is the sound pressure of the incoming acoustic wave and R is the angle dependent complex reflection coefficient. For harmonic waves, a normal surface impedance Z_{n} above the sample can then be obtained:

$$Z_{\mathrm{n}}(\theta) = \frac{p(\theta)}{u_{\mathrm{n}}(\theta)} = \frac{1 + R(\theta)}{1 - R(\theta)} \cdot \frac{\rho c}{\cos\theta} \qquad (2\text{-}13)$$

The reflection coefficient R is obtained from the impedance:

$$R(\theta) = \frac{Z_{\mathrm{n}}(\theta)\cos\theta - \rho c}{Z_{\mathrm{n}}(\theta)\cos\theta + \rho c} \qquad (2\text{-}14)$$

Whereas the reflection coefficient R is defined as the ratio of reflected to incoming sound pressures, the absorption coefficient is an absolute value that is determined by the ratio of absorbed to ingoing sound intensities normal to the surface; I_a and I_{in}, respectively. In most cases, the angle independent absorption is of interest, which is either obtained by performing a test in a diffuse field or by integrating measurements at different angles of incidence. In the special case of a locally reacting material, the surface impedance at any angle is related to the normal surface impedance; $Z_n(\theta) = Z_n/\cos(\theta)$.

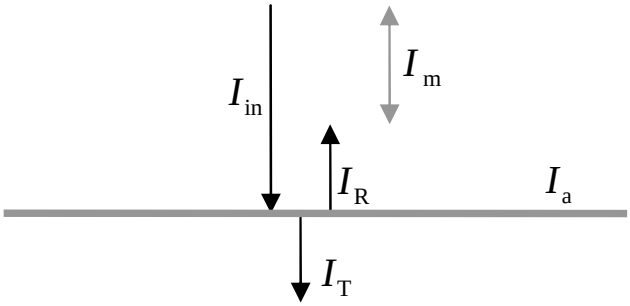

Fig. 2-13. Intensities near an absorbing surface.

The incoming sound wave is not only reflected or absorbed by the sample, but might partially go through it as well. Therefore, the transmitted intensity I_T should also be considered. The reflected and measured intensity I_R and I_m above the sample are:

$$I_R = I_{in} \cdot R \cdot R* \qquad (2\text{-}15) \qquad\qquad I_m = I_{in} - I_R \qquad (2\text{-}16)$$

The absorption coefficient can be defined as the ratio of absorbed to ingoing intensity:

$$a = \frac{I_a}{I_{in}} = \frac{I_{in} - I_R - I_T}{I_{in}} = (1 - R \cdot R*) \cdot \left(1 - \frac{I_T}{I_m}\right) \qquad (2\text{-}17)$$

Often, a reflecting rigid surface is present behind the sample. Without transmission through the sample, absorption can directly be calculated from the reflection coefficient. Equation 2-17 then simplifies to:

$$a = 1 - R \cdot R* \qquad (2\text{-}18)$$

2.8. *Absorption models for a point source above an impedance plane*

Plane sound waves are difficult to generate in a broad frequency range. The distance between the sample and the sound source should be large to avoid near field effects, especially at low frequencies. Also, if the wave front is not plane there can be complicated interference patterns. Arrays of loudspeakers could generate planar wave fronts, but again at lower frequencies there are difficulties because the array would need to be large to avoid diffraction.

Diffuse sound fields would theoretically involve an infinite number of sound sources (or reflections thereof) from all directions, as for example approximately present in a reverberant room. Several tests have been done by Otsuru et al. [67-69] where reverberant conditions were assumed, using initially ambient noise only, and later also loudspeakers at different positions to improve the signal-to-noise ratio [71]. However, reverberant room measurements are not *in situ*, and in most situations diffuse conditions are hard to create.

A point source is often used instead of plane or diffuse sound sources. Corrections have to be made for near field effects and spherical wave fronts in order to obtain the plane wave impedance, reflection or absorption that most people are familiar with. To extract the plane wave absorption properties, there are many models describing the sound field above a sample due to a point source [72]. Some of these will be discussed here. Most models assume that the sample is infinite and bonded on a rigid impervious backplate. Plane wave models are easiest to understand and implement, but do not correct for the spherical geometry of sound fields. Especially at low frequencies, near field effects are strong and errors are introduced. When point sources are far away ($kr >> 1$), the spherical behaviour is negligible, and plane wave models (for example equation 2-14 and 2-18) can be used to good approximation. The first spherical model that is introduced, the mirror source model, corrects for the elevation of particle velocity relative to the sound pressure in the near field, but not for the spherical wave front. The second model, called the Q-term model, also considers the spherical wave front for an infinitely thin locally reacting sample. The surface impedance of the sample can be obtained through a complicated iterative approach.

The aforementioned models are based on measured impedances. The last model presented is based on the intensity. Pro's and con's of the models will be discussed in more detail in chapter six.

2.8.1. Mirror source model

The acoustic impedance in the close proximity of a sound source is different from the plane wave impedance of air. Compared to the far field, particle velocity in the near field is elevated more than sound pressure. Also, the phase between them, instead of being 0 degrees as in the far field, increases towards 90 degrees. For a harmonic wave with time dependence $e^{i\omega t}$, the complex sound pressure and particle velocity at distance r from a monopole are written [4, p. 127], [72, p. 36]:

$$p = p_0 \frac{e^{-ik_0 r}}{r} \qquad (2\text{-}19) \qquad \boldsymbol{u} = \frac{p}{\rho c}\left(1 + \frac{1}{ik_0 r}\right) \qquad (2\text{-}20)$$

where p_0 is the amplitude related to the strength of the monopole.

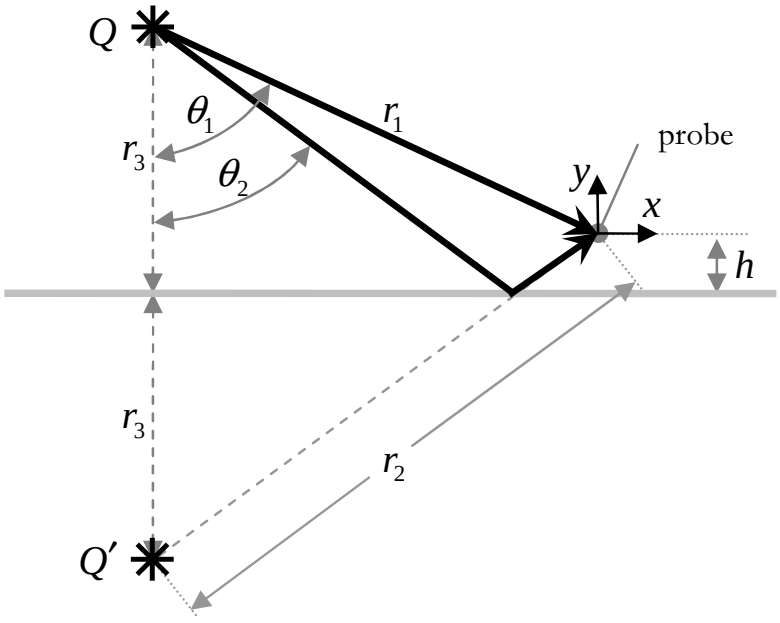

Fig. 2-14. Direct source Q above an impedance plane and its mirror source Q'.

A near field correction can be applied for impedance as measured close to the sample. The model that incorporates this is often referred to as the mirror source or image source model. The reflected sound wave from the surface is represented as a 'mirror source' at distance r_3 below the impedance boundary (fig. 2-14). A correction is made for the shorter path r_1 from the direct source to the probe relative to the distance r_2 of the reflection to the probe. The measured impedance Z_m normal to the surface of a locally reacting material is [27, 75, 76], [73, 74]:

$$Z_{\mathrm{m}}(r_1,\theta_1,h)=\frac{p_{\mathrm{direct}}(r_1)+p_{\mathrm{reflected}}(r_2)}{u_{n,\mathrm{direct}}(r_1,\theta_1)+u_{n,\mathrm{reflected}}(r_2,\theta_2)}$$
$$=\frac{e^{-ik_0r_1}r_2+R\cdot e^{-ik_0r_2}r_1}{\frac{ik_0r_1+1}{ik_0r_1}e^{-ik_0r_1}r_2\cos\theta_1-R\frac{ik_0r_2+1}{ik_0r_2}e^{-ik_0r_2}r_1\cos\theta_2}\rho c \qquad (2\text{-}21)$$

where u_{n} is the particle velocity normal to the surface and:

$$r_2=\sqrt{r_1^{\,2}+4h\left(r_1\cos\theta_1+h\right)} \quad \text{, and:} \quad \cos\theta_2=\left(r_1\cos\theta_1+2h\right)/r_2 \qquad (2\text{-}22)$$

Note that when the probe-surface distance becomes small, or when the sound source is assumed far away ($r_1\approx r_2$ and $\theta_1\approx\theta_2\approx 0$), the mirror source model approximates the plane wave model (equation 2-13).

2.8.2. Q-term model

The mirror source model takes into account the change in amplitude and in phase caused by near field effects of the point source. However, no correction is made for the spherical wave front [32]. There have been many publications concerning the description of the spherical wave front above an impedance boundary [3, 18, 58, 74, 77, 78]. Some use the solution of Sommerfeld or that of Wehl. In [80] an historical overview of such models is presented. Their formulations were originally intended for electromagnetic wave propagation, but can also be applied for an acoustic point source above an impedance plane. The sound field is represented by superposition of equivalent mirror sources along a line. Nobile and Hayek found an approximate solution for infinitely

thin locally reacting samples, which they presented as an "F-term", a "Q-term", and a Hankel form solution [81]. The Q-term solution describes the sound field as the sum of the direct wave and a wave originating from a mirror source using the spherical reflection coefficient Q. The F-term solution [3, 74, 80] allows for a better comparison with plane wave reflection theory. Sometimes only the first order solution of the F-term is used, which can be confusing. In this thesis the Q-term solution is used. The full derivation of the formulas goes beyond the scope of this work and is not shown here. In [73, 81] the Q-term solution was presented in a comprehensive way, which is also used in this thesis.

2.8.3. Solving the Q-term model

Procedures to obtain the surface impedance of the sample from the measured impedance above the sample with the Q-term model are rather intricate. Usually, an iterative procedure is implemented where the impedance above the sample is calculated with an initial guess of the surface impedance. The surface impedance is then varied until the difference between the calculated, and the measured impedance above the sample vanishes. In [82] the Secant method [83] was used to converge to the minimum difference, although end results can depend on the initial guessed value.

There are special cases; if the sound source is positioned far from the surface and at normal or grazing incidence, or if the reflection coefficient of the sample is equal to either zero or to one, the Q-term values and those of the mirror source method are identical [81].

Interestingly, the mirror source model and Q-term model are often in good agreement if a point source is positioned close to the sample at normal incidence and if the distance between the probe and the sample is kept small, see *[77]*, [82], and section 6.2 of this thesis. In some cases, the easier and less computation intensive mirror source model is therefore preferred instead of the Q-term model.

2.8.4. Intensity model

Instead of impedance, also the real part of intensity can be used to calculate absorption. Intensity normal to the sample should be integrated over a closed surface to avoid local deviations and to obtain the absorption coefficient integrated over all angles of incidence. This means that the surface should be scanned or that multiple points of a larger surface area should be measured while keeping the probe orientated towards the surface and the sound source position fixed. Without sound transmission the absorption coefficient α is:

$$\alpha = \frac{\mathrm{Re}\int_S I_{\mathrm{incident}}\,dS - \mathrm{Re}\int_S I_{\mathrm{reflected}}\,dS}{\mathrm{Re}\int_S I_{\mathrm{incident}}\,dS} \qquad (2\text{-}23)$$

The intensity I_{m} is the sum of the normal incident and reflected intensity (the latter with a negative sign because it is directed in the opposite direction of I_{incident}). Sometimes, a limited number of positions are measured instead of a larger area because of practical reasons. Often, only the position is measured where the sound source is at normal incidence. In that case, the absorption coefficient is approximated by $\alpha \approx \frac{\mathrm{Re}(I_{\mathrm{incident}})-\mathrm{Re}(I_{\mathrm{reflected}})}{\mathrm{Re}(I_{\mathrm{incident}})}$. However, spherical waves complicate the matter, and corrections that can be applied are discussed in more detail in chapter six.

2.9. *Conclusion*

Up to date determination of a sample's absorption is complicated. Material selection is still based on the combination of multiple results of different measurement and simulation techniques. The choice for optimal materials depends to large extents on the 'experience' of the acoustic engineer because results of separate tests are often conflicting.

Some well-known and frequently used methods have been described. There are many shortcomings, even with standardised techniques. The main weakness of laboratory tests is that they do not represent the sample after installation. Although *in situ* microphone-based techniques exist, there are limitations in frequency range, sample size and they are susceptible to background noise and reflections. An easy to use *in situ* technique is therefore desirable.

Since 2003, *in situ* absorption measurements with PU probes have been attempted. PU probes offer interesting opportunities because; they are small, they allow for frequency independent execution, the susceptibility to background noise and to reflections is low in various situations, and they can easily be extended to full 3D probes. Although plane wave relations between impedance or intensity and absorption are easy to comprehend, they are inadequate for situations with a point source near the sample surface. The reflection from the sample might be represented by a mirror source behind the surface at the same distance as the physical source is placed from the surface. The mirror source model corrects for near field effects occurring because of the longer path from the mirror source to the receiver than that of the direct path from the source. More accurate descriptions are available that also consider spatial interferences. One particular model, called the Q-term model, is used in this thesis. Apart from methods based on impedance, also a rather intuitive method based on active intensity integrated over the surface is presented. However, near field corrections have to be applied in case at one position is measured only. Such corrections and differences between the different models are discussed in more detail in chapter six.

3. Characterisation of the PU probe responsivity

3.1. *Introduction*

(Sensor) calibration is an important part of a measurement procedure, and it involves checking or adjusting (by comparison with a standard) the accuracy of the involved test equipment and the used method. Standard calibration procedures for microphones exist [84], and their response can be checked easily using for example a pistonphone [85], or with another microphone that has already been calibrated [86]. Currently, no standards are specified for calibration of particle velocity sensors like the Microflown. Moreover, calibration of a Microflown is not straightforward because no other convenient reference particle velocity sensors are available.

The main purpose of calibrating acoustic sensors is to determine their responsivities[2]. Calibration is done by measuring the voltage output of the sensor when a certain acoustic signal is applied. Whereas the responsivity of a microphone is expressed in V/Pa, the responsivity of a Microflown is expressed in V/(m/s). Broadband calibration of a Microflown is essential because, unlike many instrumentation microphones, its responsivity is rather frequency dependent.

Several solutions have been found in the past to calibrate Microflown sensors. In [87] de Bree et al. showed that the particle velocity is equal to the velocity of a vibrating surface if the distance between the sensors and the object is smaller than the structural size of the object divided by 2π, and if the acoustic wavelength is larger than the structural size. In the very near field of a sufficiently large surface, the outcome of the Microflown can be compared to for example laser Doppler vibrometers, accelerometers or optical sensors [14], which measure structural velocity. However, very near field conditions are increasingly difficult to meet at higher frequencies because it is impossible to measure sufficiently close to the surface.

[2] Responsivity is the output gain of the sensor to a given input. Sometimes the term sensitivity is used as a synonym for responsivity. However, sensitivity is the minimum magnitude of input signal to produce a specified output with a specified signal-to-noise ratio [102].

Particle velocity sensors can also be calibrated in environments where the acoustic impedance is known. Laser Doppler anemometers [88] and microphones can be used as reference, of which the latter are more often used because they are generally available in acoustic labs. An example of such an environment is a standing wave tube where plane waves propagate in one dimension below the tube's cut-off frequency [88, 89].

Also free field calibration methods have been attempted. However, plane waves are hard to generate under free field conditions at low frequencies because of near field effects and because there can be diffraction at the edges of a sound source when its size is small compared to the wavelength. To avoid diffraction, one may use an acoustic monopole instead. In [14] and [89], a sound source was used that generates a spherical sound field in half-space. The sound source consists of a small circular hole in a large plane baffle behind which a loudspeaker was mounted. However, still diffraction effects were experienced. Attempts have also been made with omni-directional sound sources, which usually consist of a tube that is connected to a loudspeaker inside an enclosure. However, a broadband omni-directional sound source with sufficient sound power is complicated to manufacture because of their low radiation efficiency. A large tube opening is required to generate sufficient sound power at low frequencies, while the opening should be small compared to the wavelength to ensure onmi-directional radiation at high frequencies [91].

Instead of an omni-directional sound source in the free field, F. Jacobson proposed to use a piston-on-a-sphere [89]. The radiation impedance of this type of sound source is similar to that of a true monopole while its radiation efficiency is higher than that of typical omni-directional sound sources. A piston-on-a-sphere loudspeaker box is used here because of these broadband capabilities. The calibration procedure will be further described in the next sections, and the outcome is compared to several other calibration techniques. Tijs et al. investigated a procedure to check calibration values, which involves comparing sound intensity as measured with a PU probe to the sound intensity as derived from a (sound pressure) microphone measurement *[61]*. The latter is suitable as reference because the impedance is known, which relates the intensity to the sound pressure.

Although sound pressure and particle velocity sensors can be calibrated separately, a test without the sample used as reference is sufficient for most absorption measurements. Procedures will be presented which can be used to determine the free field response of a PU probe, which do not require an additional reference sensor [76, 91, 92].

3.2. *Microflown responsivity characteristics*

Most measurement microphones are designed to have constant responsivity in a broad frequency range. The amplitude and phase responsivity of a Microflown particle velocity sensor varies over frequency. The sensor is most responsive at about 250Hz, and less responsive at lower and higher frequencies. Typical examples of responsivity curves of a microphone and a particle velocity sensor from a PU probe are shown in fig. 3-1. Their responsivities are expressed in mV/Pa, in case of a microphone, and in V/(m/s), in case of a Microflown.

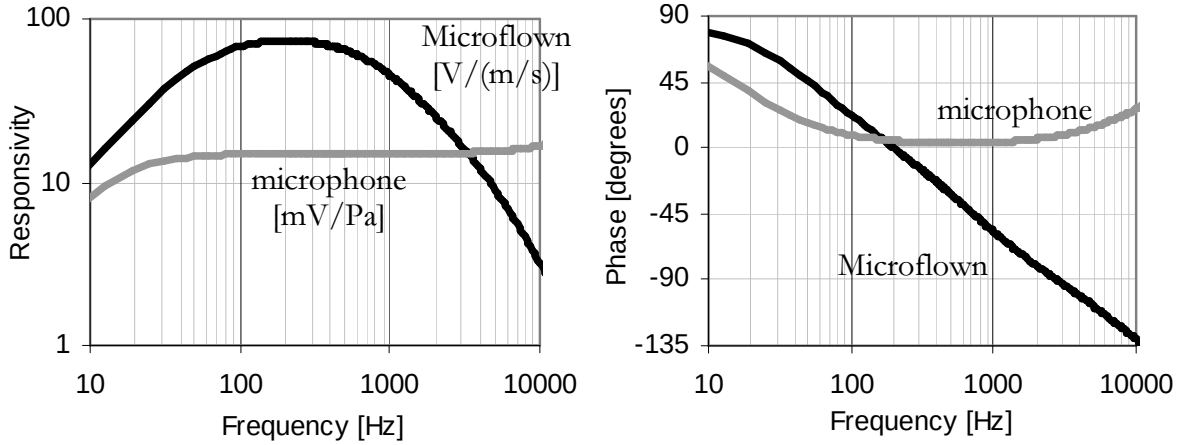

Fig. 3-1. Typical responsivity of a microphone and a Microflown. Left: amplitude. Right: phase.

Several studies were dedicated to this frequency dependent behaviour. Two main reasons are given for the decreasing responsivity at high frequencies; heat diffusion effects (it takes time for heat to travel between the wires), and the thermal mass of the wires [62-64, 93]. Up to date, an undisputable explanation for the reduced responsivity at low frequencies is lacking; although in [14] thermal boundary layer effects are suggested as the cause.

As part of the calibration process, the frequency dependent amplitude and phase responsivity curve are approximated by the cascade of one first order high pass filter and two first order low pass filters [14]:

$$|S_u| = \frac{S_{u,250}}{\sqrt{1+\frac{f_1^2}{f^2}}\sqrt{1+\frac{f^2}{f_2^2}}\sqrt{1+\frac{f^2}{f_3^2}}}\left(\frac{V}{m/s}\right) \quad (3\text{-}1)$$

$$\varphi_{Su} = \arctan\frac{C_1}{f} - \arctan\frac{f}{C_2} - \arctan\frac{f}{C_3} \quad (3\text{-}2)$$

where $|S_u|$ and φ_{Su} are the amplitude and phase responsivity defined by the constants $S_{u,250}$, f_1, f_2, f_3 and C_1, C_2, C_3. Theoretically the values of f_1 and C_1, of f_2 and C_2, and of f_3 and C_3 should be equal, but in reality the sensor responsivity is often better approximated using slightly different values. Additional first order high pass filters can be added to describe the behaviour of certain wind caps or electronic high pass filters.

3.3. *Piston-on-a-sphere calibration*

Calibration methods such as standing wave tubes or methods based on vibration measurements are limited at high frequencies (typically 4kHz and 1kHz, respectively). In [89] a broadband method is proposed that uses a so-called piston-on-a-sphere sound source and a reference microphone in the free field. The radiation characteristics of this type of sound source are discussed in section 3.3.1. These results are based on those reported by Tijs et al. in *[95]*. The principles of the broadband calibration method itself will be explained in section 3.3.2. With this method, the sound pressure microphone of the PU probe can be calibrated from 20Hz to 20kHz. The signals from the Microflown and those of the reference microphone are uncorrelated because the sound pressure level due the background noise exceeds the sound pressure level of the loudspeaker below typically 100 Hz, and because this is not so much the case for the particle velocity level. Calibration of the Microflown is therefore difficult at low frequencies. In [96] another method that uses the same sound source was developed for particle velocity calibration at low

frequencies (see section 3.3.3). Usually, the frequency range of this method is 20 Hz to 1 kHz. In section 3.3.4, both methods are combined in order to cover the full audible frequency range. The results obtained with the two piston-on-a-sphere methods are compared with those of three other calibration methods. It will be shown that the low frequency piston-on-a-sphere method can even be used at frequencies as low as 4 Hz.

3.3.1. Piston-on-a-sphere sound source

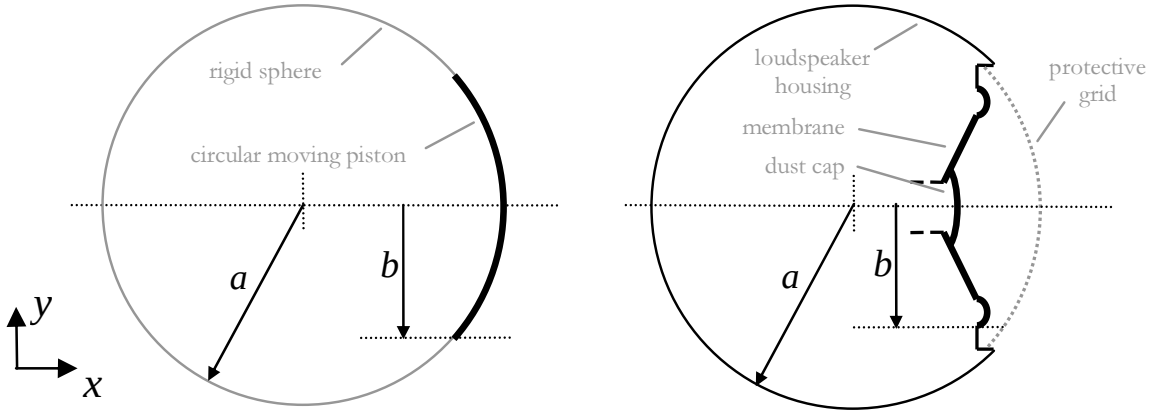

Fig. 3-2. Left: cross-section of a piston-on-a-sphere. Right: loudspeaker box that resembles a piston-on-a-sphere.

The radiation characteristics of a piston-on-a-sphere are investigated. This axis-symmetrical type of sound source consists of a circular (spherical cap) moving piston with radius b on a rigid sphere with radius a (fig. 3-2 left). In reality, such a sound source is difficult to construct. A loudspeaker with a hollow membrane inside a spherical housing is used instead (fig. 3-2 right). Several tests have been performed with a piston-on-a-sphere loudspeaker box in order to determine the radiation characteristics of such sound sources. It will be shown that its directivity at low frequencies is similar to that of a point source and that there are no noticeable side lobes. Furthermore, the position of the acoustic centre varies little throughout the measurement bandwidth and the broadband radiation efficiency is high compared to that of typical omni-directional sound sources.

In most experiments as they are reported in this thesis a piston-on-a-sphere loudspeaker box was used with $a = 50.5\,\text{mm}$ and $b = 37.5\,\text{mm}$. The directivity and the position of the acoustic centre of this sound source have been determined. For the purpose, the sound pressure is measured at many points in a plane around the loudspeaker box (fig. 3-3).

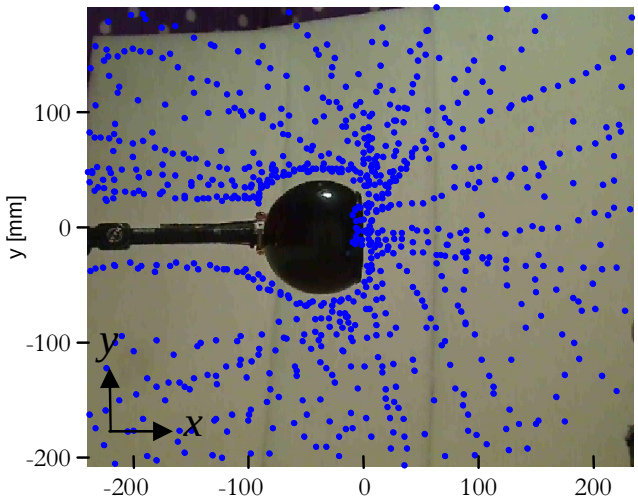

Fig. 3-3. Irregular distribution of measurement points around the loudspeaker box.

Fig. 3-4 left shows the measured sound pressure level on the acoustic axis, which is normalised to be 0 dB at $x = 100\,\text{mm}$. It can be seen that the sound pressure decays approximately with $1/r$ if distance to the membrane is larger than 70 mm.

Fig. 3-4 to 3-6 show the sound pressure distribution around the loudspeaker box. It can be seen that the directivity in the region of interest, i.e. in front of the sound source around its acoustic axis, is similar to that of a monopole in a broad frequency range. Although the source becomes more directive, no substantial spatial interferences occur at higher frequencies. For square loudspeaker housings, interferences caused by edge diffractions are common.

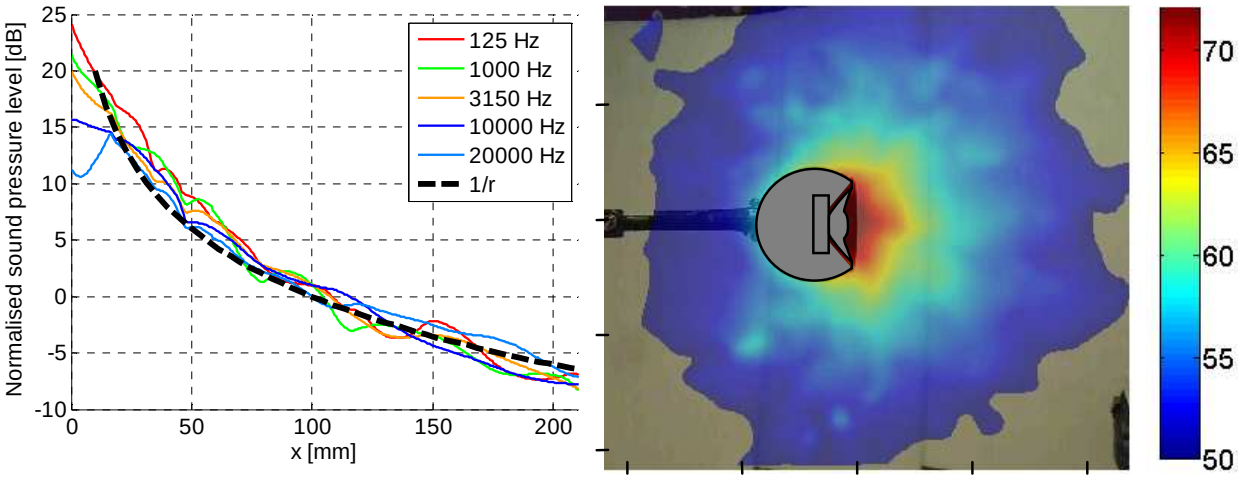

Fig. 3-4. Left: Decay of sound pressure versus r for several frequencies. Right: Sound pressure distribution at 125 Hz, scale in dB.

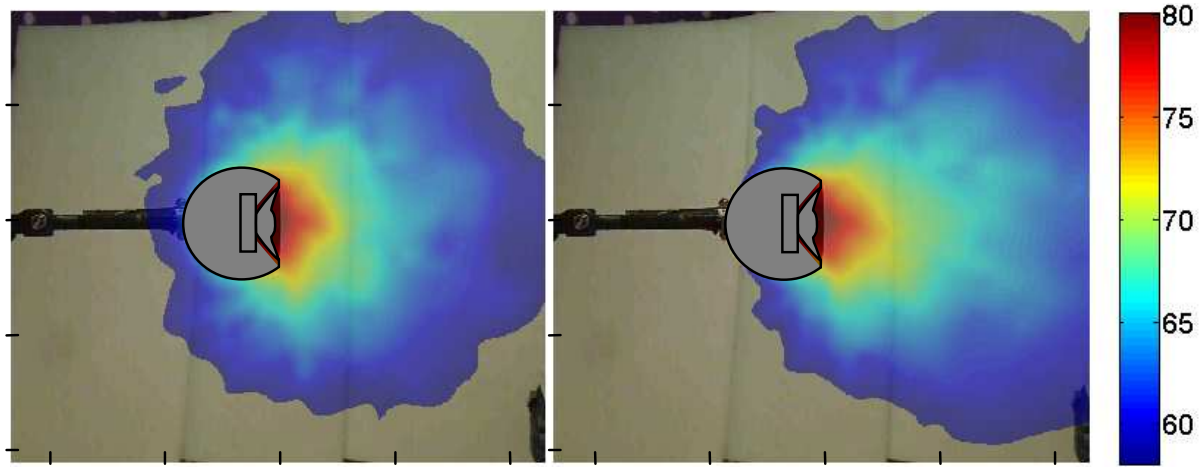

Fig. 3-5. Sound pressure distribution at 1 kHz (left) and 3.15 kHz (right), scale in dB.

The microphone becomes directive at high frequencies. During the test it was orientated at an angle of about 20 degrees compared to the axis of the sound source (see fig. 3-7 right), which could be the reason for the slightly asymmetrical radiation pattern that is measured at 20 kHz (fig. 3-6 right).

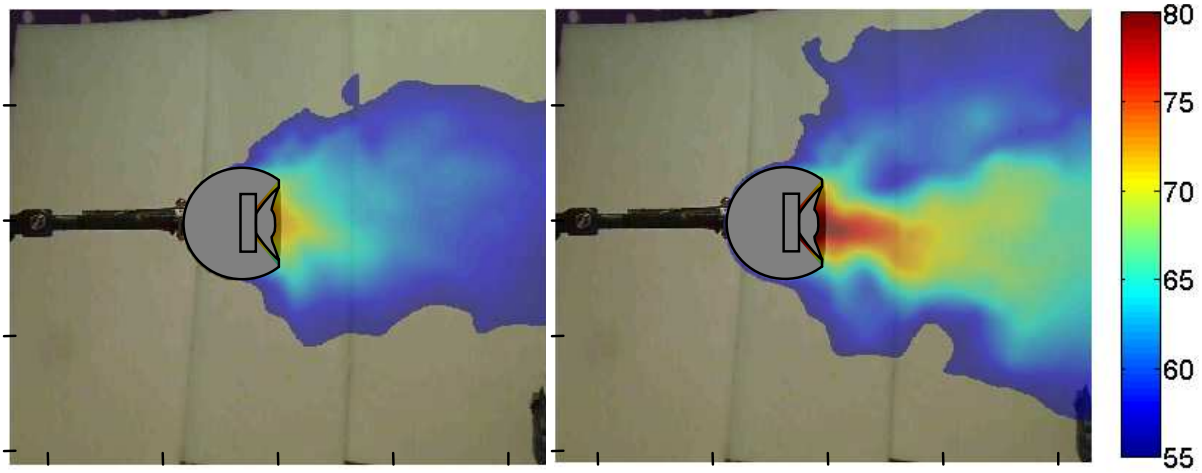

Fig. 3-6. Sound pressure distribution at 10 kHz (left) and 20 kHz (right), scale in dB.

The location of the acoustic centre varies with frequency. The same tests are also used to determine the position of the acoustic centre of the piston-on-a-sphere loudspeaker box. The position is determined using the sound pressure maps, such as the ones shown in fig. 3-4 to 3-6. For each one-third octave band the distance between the acoustic centre and the front of the sound source is determined. First, a low pass filter was applied to the colour maps to reduce local variations. Next, the position of the sound pressure maximum was determined. Fig. 3-7 shows the estimated acoustic position in a 40 Hz - 20 kHz band and a straight line fitted through these values.

The acoustic centre appears inside the source at low frequencies. For example, at 100Hz its position is x =-15mm (just behind the dust cap). The centre moves in positive x-direction as the frequency increases. The maximum variation in the position is ±5mm in a 100Hz-20kHz frequency range, which can be considered small compared to the source-probe distances usually used. Therefore, this small distance variation can be ignored in most cases.

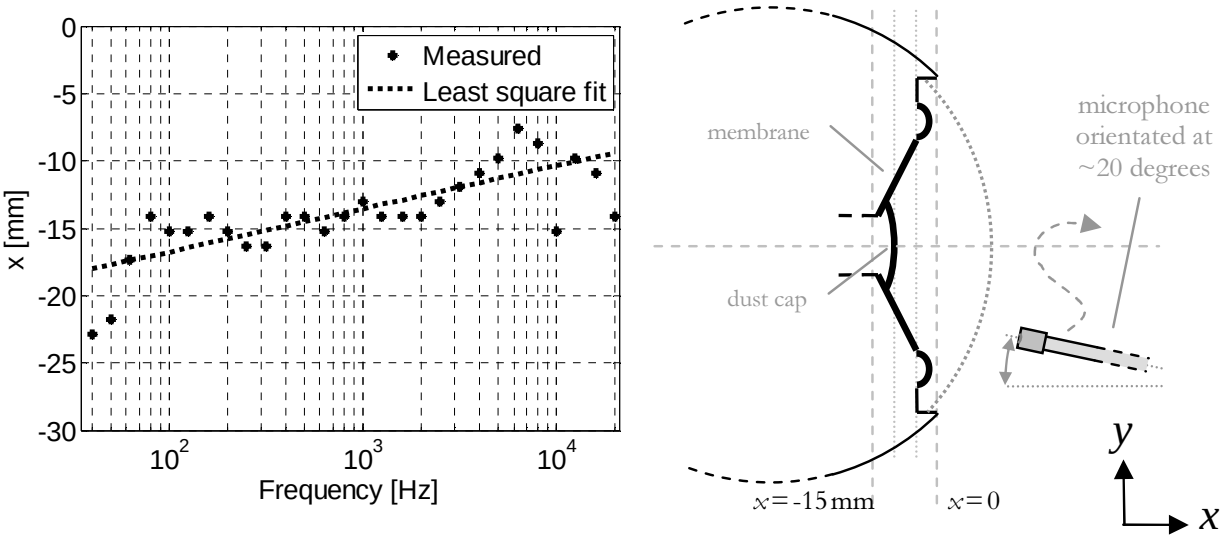

Fig. 3-7. Left: Estimated distance between the acoustic centre and the front of the loudspeaker box (x=0). Right: A detailed cross-section of the loudspeaker box and the microphone that is moved around.

As was mentioned earlier, the broadband radiation efficiency of a piston-on-a-sphere is higher than that of typical onmi-directional sound sources. This is verified with tests that were performed using the same piston-on-a-sphere loudspeaker box and a commercially available "Mid-High frequency onmi-directional loudspeaker" from Microflown Technologies, which is shown in fig. 3-8 left. The sound pressure level at 27cm distance from both sound sources was measured. The electric input level was kept the same. As can be seen in fig. 3-8 right, the output of the piston-on-a-sphere exceeds that of the omni-directional sound source below 500Hz and above 3kHz. Their output is similar in between these frequencies.

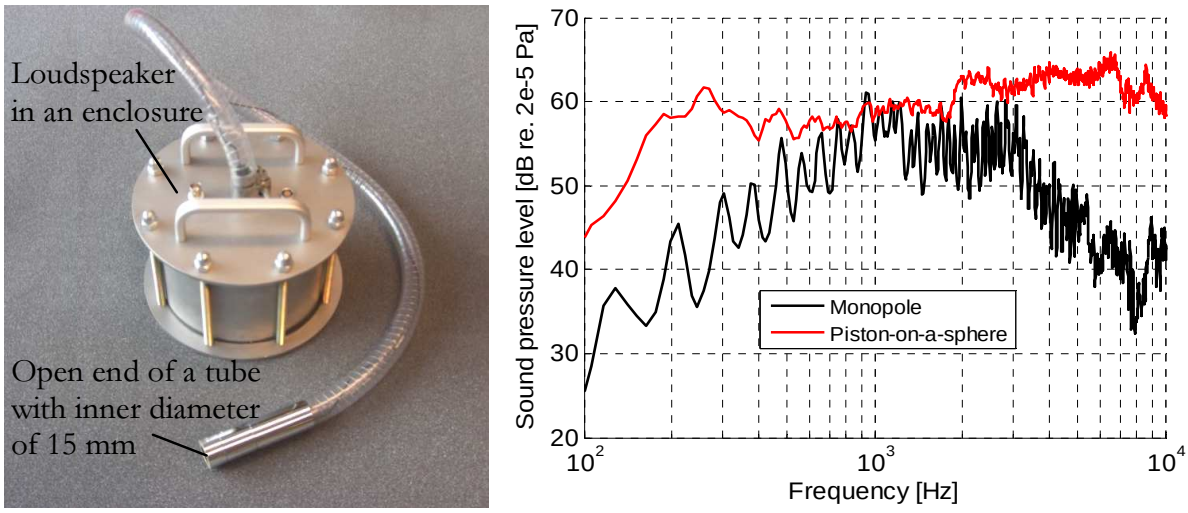

Fig. 3-8. Left: omni-directional sound source [97]. Right: SPL at 27 cm from the omni-directional sound source and the piston-on-a-sphere loudspeaker box.

3.3.2. Broadband calibration

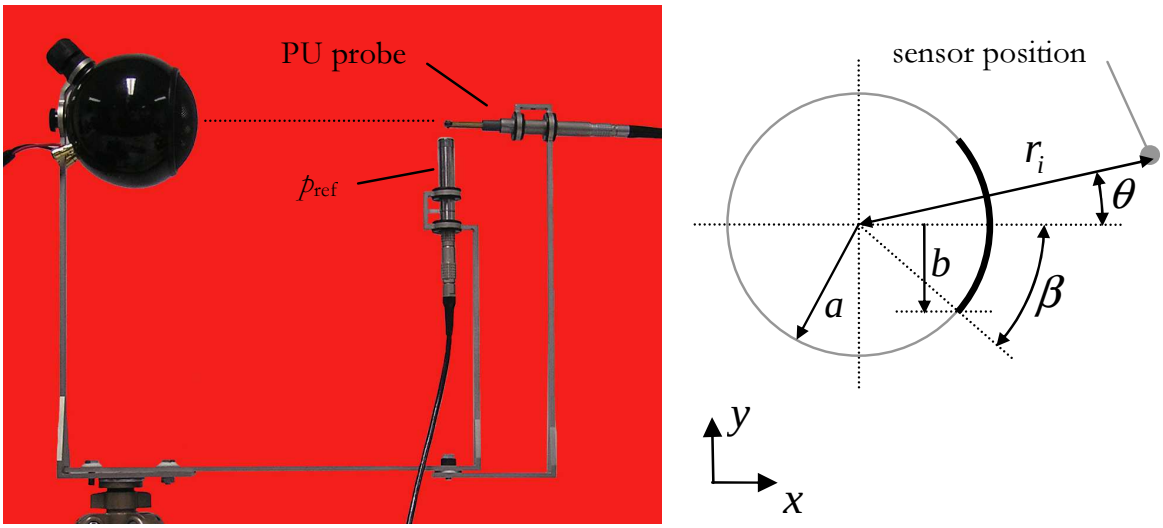

Fig. 3-9. Piston-on-a-sphere; a PU probe and reference microphone p_{ref} are positioned at 23 cm from the membrane.

As was proposed in [89], the piston-on-a-sphere can be used to calibrate sound pressure and particle velocity sensors. The PU probe that is calibrated is then placed near a reference microphone at the same distance from the loudspeaker. The signals of the PU probe microphone and the reference microphone can be compared directly because they measure the same quantity (i.e. sound pressure). If the impedance in front of the sound source is known, the particle velocity can also be calculated from the sound pressure measured by the reference microphone. In this section, an expression for the impedance of a piston-on-a-sphere will be presented and the outcome is compared to that of an omni-directional sound source.

The frequency range for calibrating sound pressure or particle velocity with this method is considered. Compared to the far field, the particle velocity level in the near field of the sound source is elevated more than the sound pressure level. The signal to (background) noise ratio (SNR) of the particle velocity signal is therefore high, even though the sound source efficiency decreases at low frequencies. Unfortunately, the sound pressure is dominated by background noise at low frequencies. Generally, the impedance cannot be determined accurately anymore below 100Hz. Instead, another method is used to calibrate below 100Hz (see section 3.3.3). The method uses a reference microphone that is placed inside the sphere where the SNR is high.

Even though the sound pressure in front of the sphere at low frequencies is dominated by background noise, the microphone of the PU probe can be calibrated in the whole audible 20Hz-20kHz frequency range, provided that the distance to the reference microphone is small compared to the wavelength *[61]*. Background noise consists of sound waves that may arrive from different directions. The sound pressure varies depending on the position in the room because of these (interfering) waves. However, the wavelength is long at low frequencies and the sound pressure varies little per unit distance. The sound pressure at the positions of the two closely spaced microphones is therefore nearly the same. The assumption is invalid at higher frequencies because the wavelength is smaller, but then the signal from the sound source is dominant.

In order to calibrate the particle velocity sensor, a relation between the particle velocity and the sound pressure as measured by the reference microphone is needed. The impedance of a piston-on-a-sphere is given by [48, 88]:

$$Z(r_i) = \frac{p(r_i)}{u_{\mathrm{n}}(r_i)} = -i\rho c \frac{\sum_{m=0}^{\infty} \left(P_{m-1}(\cos\beta) - P_{m+1}(\cos\beta)\right) \frac{h_m(k_0 r_i)}{h_m'(k_0 a)} P_m(\cos\theta)}{\sum_{m=0}^{\infty} \left(P_{m-1}(\cos\beta) - P_{m+1}(\cos\beta)\right) \frac{h_m'(k_0 r_i)}{h_m'(k_0 a)} P_m(\cos\theta)} \qquad (3\text{-}3)$$

here k_0 is the wavenumber in air, r_i is the distance from the centre of the sphere, $\beta = \sin^{-1}(b/a)$, θ is the angle with the axis of the piston. P_m is the Legendre function of the order m, h_m is the spherical Hankel function of the

second kind and order m, and $h_m^{'}$ is its derivative over m. For the sake of clarity, it must be noted that the numerator holds the terms $h_m(k_0 r_i)$ while the denominator holds the derivatives $h_m^{'}(k_0 r_i)$. Although the description of the impedance of the spherical sound source is rather complicated, quantitatively, the outcome is similar to that of a monopole. The impedance Z at distance r from a monopole can be described by [4, p. 128], [89]:

$$Z(r) = \rho c \frac{ik_0 r}{ik_0 r + 1} \qquad (3\text{-}4)$$

The difference in impedance in front of a monopole and a piston-on-a-sphere are compared for a piston-on-a-sphere loudspeaker box with radius $a = 50.5\,\text{mm}$ and piston radius $b = 37.5\,\text{mm}$. Fig. 3-10 shows the calculated difference between the two source types as a function of frequency and for several values of r (where for the piston-on-a-sphere $r = r_i - a$ and $\theta = 0$).

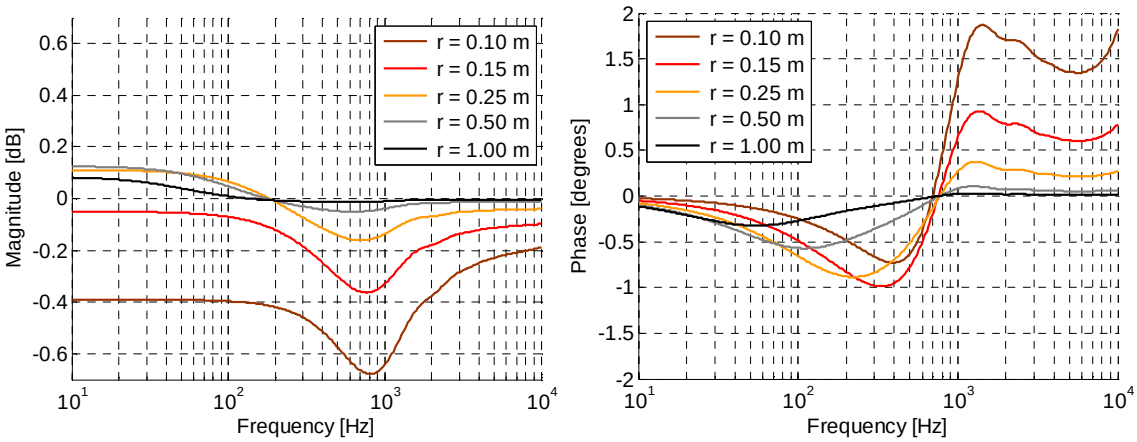

Fig. 3-10. Ratio of the impedance of a monopole to the impedance of a piston-on-a-sphere (Source code for the figure from T. Basten).

As can be seen in fig. 3-10, the maximum difference between the monopole and piston-on-a-sphere impedance in a 10Hz-10kHz bandwidth is ± 0.68 dB in amplitude and ± 1.9 degrees in phase for a range of realistic probe distances. As discrepancies are small, monopole equations are often used instead because they are easier to implement. However, the degree of discrepancies varies depending on the combination of the sphere- and piston radii, and therefore the difference should be re-calculated for each geometry. For the current geometry, the maximum deviation in amplitude occurs between 600Hz and

1kHz, and between 200Hz and 2kHz for phase. The point of maximum deviation occurs at higher frequencies for larger sphere dimensions.

Positioning errors of the particle velocity sensor and the reference microphone can lead to discrepancies during calibration. Equation 3-3 can be used to estimate such discrepancies. These are small if the same positioning error is made with both sensors. For example, if r is 0.25m or larger, and if the positioning error is ± 2cm, the impedance deviates with maximally ± 0.3dB in amplitude and ± 2 degrees in phase in a 10Hz-10kHz frequency band. Higher deviations are found for smaller values of r. For example, when $r = 0.1$m the maximum deviation is ± 0.7dB and ± 5.1degrees. However, there can be higher discrepancies if the positions of both sensors are different. If $r > 0.15$m and the sensor separation in direction x or y is ± 1cm, an amplitude deviation of maximal ± 0.3dB is found, depending on frequency. Phase errors are mostly related to the separation distance between the sensors, instead of distance r. At 10kHz, a 1cm separation in direction x causes a substantial phase mismatch of approximately $360\frac{f\Delta r}{c} = 360\frac{10000 \cdot 0.01}{343} =$ 105 degrees. It must therefore be noted that for accurate phase calibration the distances of both sensors to the sound source should be the same.

3.3.3. Low frequency calibration

In [96] a method to calibrate particle velocity sensors at low frequencies has been developed for which the same piston-on-a-sphere can be used. The particle velocity level in front of the sound source is high at low frequencies because of near field effects. Especially if the probe is placed close to the loudspeaker, the influence from background noise is usually small. This is not the case for sound pressure. The sound pressure level from the loudspeaker is often exceeded by background noise in non-anechoic environments. However, the SNR of sound pressure inside the loudspeaker box is high. The low frequency piston-on-a-sphere calibration method uses these principles. The particle velocity sensor is positioned near the loudspeaker and the reference microphone is put inside the sphere (fig. 3-11).

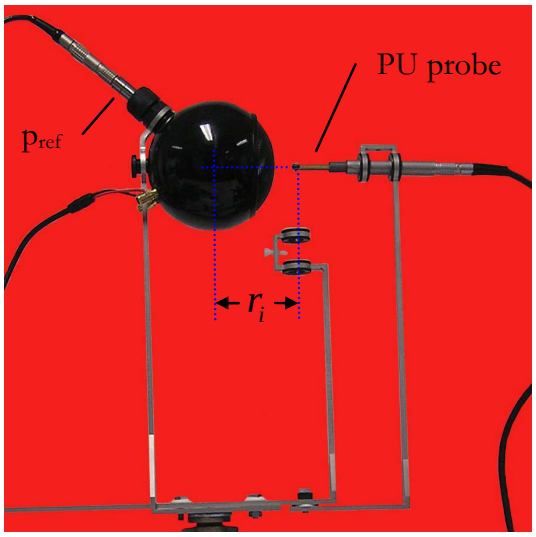

Fig. 3-11. Piston-on-a-sphere; the PU probe is positioned near the loudspeaker and the reference microphone is put inside the sphere.

The particle velocity in front of the piston-on-a-sphere can be related to the sound pressure inside the sphere. First, a relation between the particle velocity in front of the piston-on-a-sphere and the velocity of its membrane is established. Subsequently, a relation is found between the velocity of the membrane and the sound pressure as measured by the reference microphone inside the sphere, taking into account that there are standing waves.

Due to the movement of the membrane, there is a particle velocity in front of it. The particle velocity at distance r_i from the centre of the sphere is a function of the normal velocity of the membrane (u_{piston}) [96]:

$$u_{\mathrm{n}}(r_i) = -\frac{u_{\mathrm{piston}}}{2}\sum_{m=0}^{\infty}\left(P_{m-1}(\cos\beta) - P_{m+1}(\cos\beta)\right)\frac{h_m'(k_0 r_i)}{h_m'(k_0 a)} \qquad (3\text{-}5)$$

This expression is familiar with equation 3-3 that describes the impedance in front of the piston-on-a-sphere. According to the momentum equation, a variation in the interior pressure causes acceleration. When the process of sound in the cavity is adiabatic (no heat transfer), and when the diameter of the sphere is small compared to the wavelength, the movement of the membrane causes the sound pressure inside the sphere to vary by [95, 97, 98]:

$$u_{\mathrm{piston}} = -\frac{i\omega V_0}{\gamma A_0 p_{static}}\, p \qquad (3\text{-}6)$$

in which ω is the angular frequency, V_0 is the interior volume of the sphere, A_0 the surface area of the moving piston, p_{static} is the static ambient pressure and γ is the ratio of specific heat of gas at a constant pressure to the specific heat of that gas at constant volume (1.4 for standard air). The sound field inside the sphere is only uniform if the wavelength is large. Therefore, a correction for standing waves is applied to measure at higher frequencies. The correction is a cosine function if the membrane of the reference microphone is flush mounted, and equation 3-6 is then modified to:

$$u_{\text{piston}} = -\frac{i\omega V_0}{\gamma A_0 p_{static}} \frac{1}{\cos\left(\frac{\pi}{2 f_{\text{d}}} f\right)} p \qquad (3\text{-}7)$$

where parameter f_{d} is the frequency of the first sound pressure amplitude minimum which can be obtained from the transfer function $u_{\text{n}} / p_{\text{ref}}$ of the low frequency calibration (fig. 3-12, thin black line, 1.4kHz). The error that is made if the reference microphone is placed too deep into the sphere usually is negligible. For example, at 1kHz the sound pressure due to an eventual misalignment of $\Delta x = 0.02\text{m}$ varies by a factor of only $\cos(\frac{\pi}{2}\frac{\Delta x}{c} f) = 0.9958$.

This equation cannot be solved in absolute sense because parameters V_0, A_0 and r_i are not known exactly. However, only an amplitude error is made which is constant over frequency. The phase on the other hand is precisely known because it is independent of these parameters. The maximum frequency of this procedure depends on geometries of the sphere and on objects inside the sphere such as the loudspeaker and the reference probe. Frequencies above the first internal mode of the sphere are typically unusable because of reflections from objects inside the sphere.

3.3.4. Combining both calibration methods

Together, both piston-on-a-sphere methods cover a wide frequency range. The broadband approach is mostly used in a 100Hz-20kHz bandwidth, and the low frequency approach from 20Hz to 1kHz, so usually the results of both methods overlap between 100Hz and 1kHz. The amplitude response can be determined with the low frequency approach, except for some frequency independent constants. Therefore, a certain value is chosen for this constant until it fits the curve of the broadband approach in the mid frequency range. Two steps are done to correct the low frequency measurement (fig. 3-12):

1. Equation 3-5 and 3-7 are applied to the uncorrected measurement (green line) except for the unknown constants; and the blue line is obtained.
2. This curve is then multiplied by a constant until it optimally matches that of the broadband method (black line) and the corrected low frequency curve is obtained (red curve).

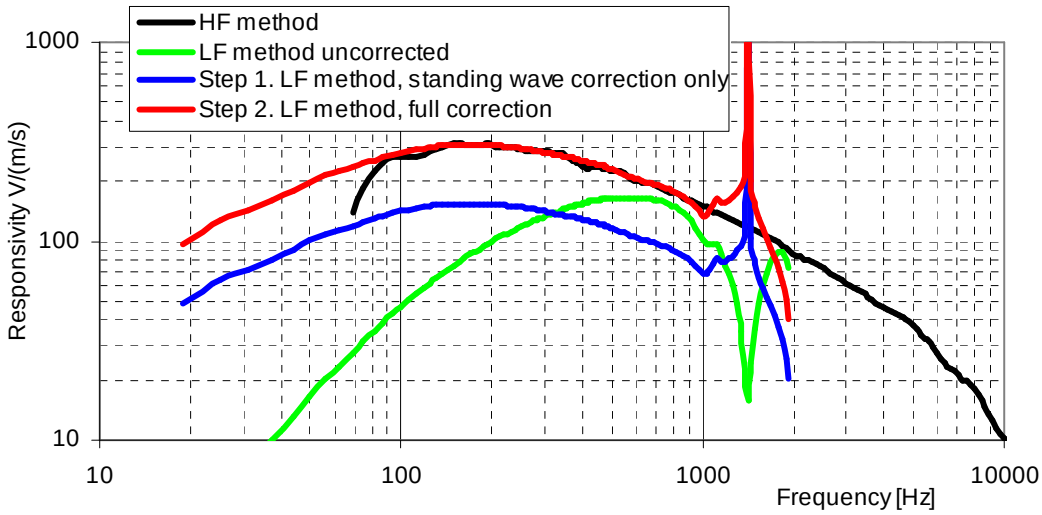

Fig. 3-12. Correction of particle velocity amplitude of the low frequency calibration.

In [96] the results of the combined low frequency procedure were compared to those of a standing wave tube calibration. Up to 400Hz the difference was found to be less than 0.5 dB in amplitude and smaller than 4 degrees in phase. To validate the calibration of the particle velocity sensor with the piston-on-a-sphere, the results are compared here to that of three other calibration methods (fig. 3-13 and 3-14). The first alternative calibration method involves a set-up were the sensor is placed in between two large loudspeakers driven with opposite phase. At low frequencies the air is

considered incompressible and the particle velocity equal to the velocity of the membranes. The particle velocity can be measured by an accelerometer that is mounted on one of the membranes.

The second alternative calibration method is called the 'long' standing wave tube method [90]. Standing waves occur inside a tube that is closed at one end and has a loudspeaker at the other. As a result, there are minima and maxima of the particle velocity depending on the wavelength and the distance to the endplate. The standing wave pattern is visible in fig. 3-13 left (red line). In this case, the particle velocity sensor was placed 60cm from the endplate and the reference microphone was mounted inside the endplate. The cross-section of the tube was circular and had an inner diameter of 5cm, so the cut-off frequency was 4kHz. At the maxima, which are indicated by the red circles in fig. 3-13 left, the amplitude of the particle velocity sensor and the reference microphone can be compared. Throughout the frequency range, the phase between sound pressure and particle velocity is ± 90 degrees. Therefore, 90 degrees has been added or subtracted to the phase response. Measurement inaccuracies occur at frequencies where the particle velocity is low, and results around these frequencies have therefore been omitted in fig. 3-14 left.

The third method, called the 'short' standing wave tube [89], is similar to the long method, but instead a tube is used in which the particle velocity sensor is placed at only 5cm from the endplate. Again, the measured phase response has been adjusted with ± 90 degrees. There are only two maxima below the 3.2kHz cut-off frequency of the tube because the spacing between the sensor and the endplate is small. Instead of using only the maxima, a correction for the standing waves is applied so that also other frequencies can be assessed. The corrected particle velocity and sound pressure are calculated by:

$$u_{\text{corrected}} = \frac{u_{\text{measured}}}{\sin\left(\frac{\pi}{f_{\text{u}}} f\right)} \qquad (3\text{-}8)$$

$$p_{\text{corrected}} = \frac{p_{\text{measured}}}{\cos\left(\frac{\pi}{2 f_{\text{p}}} f\right)} \qquad (3\text{-}9)$$

where f_{u} and f_{p} are the frequencies of the first particle velocity and sound pressure minima, which can be obtained from the measured responses.

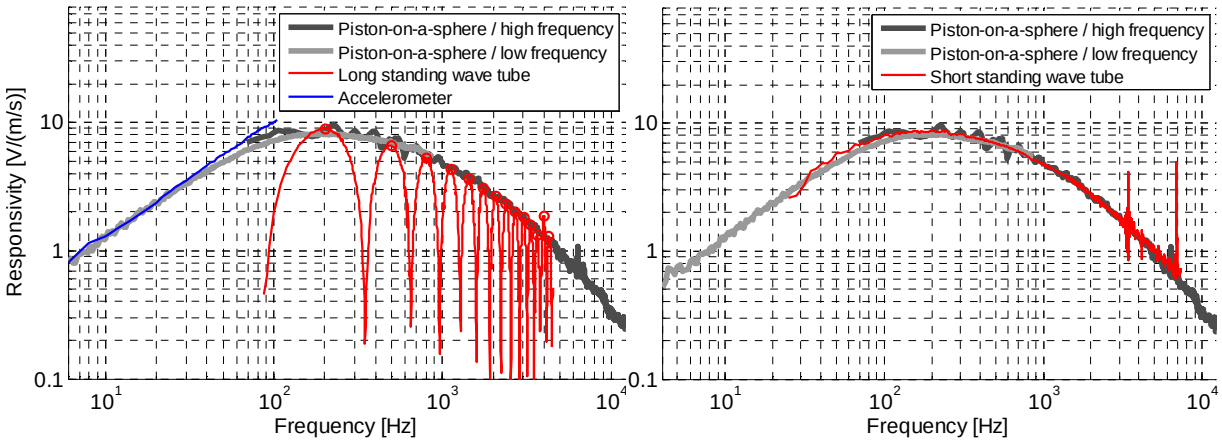

Fig. 3-13. Piston-on-a-sphere amplitude calibration compared to other methods. Left: long standing wave tube and accelerometer. Right: short standing wave tube.

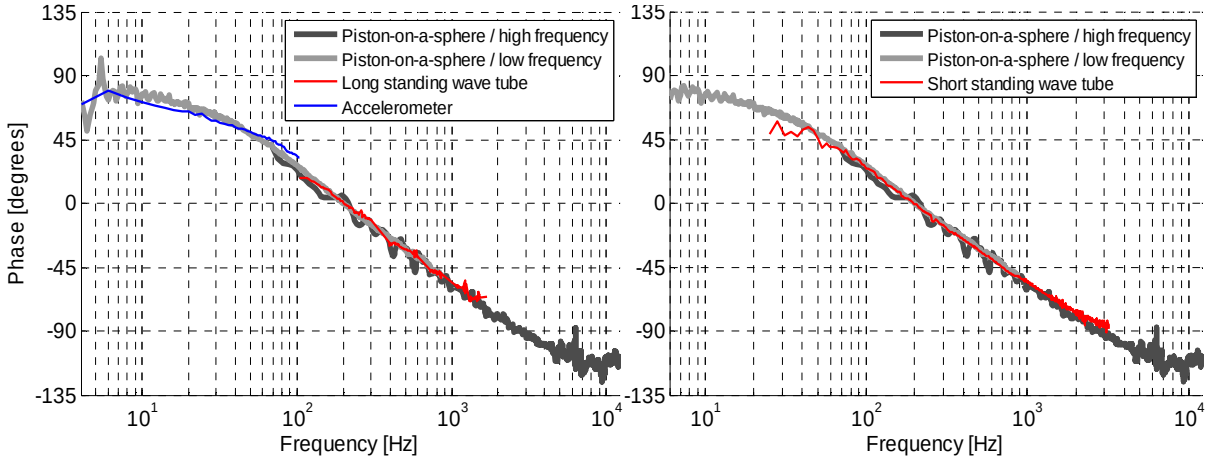

Fig. 3-14. Piston-on-a-sphere phase calibration compared to other methods. Left: long standing wave tube and accelerometer. Right: short standing wave tube.

Proper results were obtained with the piston-on-a-sphere method. As can be seen in fig. 3-13 and 3-14, the results of the two piston-on-a-sphere methods match well in a 4Hz-7.3kHz frequency band with those of three independent calibration methods. The piston-on-a-sphere calibration procedure has advantages compared to other calibration techniques; with one sound source and by combining two tests a broad frequency range can be assessed, and mounting of probes that have different sizes and different directivities is simple.

3.4. *Calibration verification with sound intensity*

To check the calibration accuracy, and to certify that the probe signals are corrected appropriately, active sound intensity is compared to sound pressure under conditions for which the acoustic impedance is well-known. Such a comparison is convenient because sound pressure measurements involve little calculation, are well-defined, and reference microphones are generally available. A study was carried out by Tijs et al. to make a comparative assessment of a microphone and a PU intensity probe *[61]*.

Sound pressure and particle velocity in a given direction are linked through the specific acoustic impedance, which is the ratio of both quantities. Sound intensity in the direction of the particle velocity can be determined by the product of sound pressure and particle velocity. Therefore, sound intensity and sound pressure are also related through acoustic impedance. The relation between (active) sound intensity and acoustic impedance on the acoustic axis of the sound source is given by *[61]*:

$$\frac{I_x(r)}{p(r)\cdot p^*(r)/\rho c}=\frac{\mathrm{Re}\left\{p(r)\cdot u_x^*(r)\right\}}{p(r)\cdot p^*(r)/\rho c}=\frac{\mathrm{Re}\left\{p^2(r)/Z_x^*(r)\right\}}{p(r)\cdot p^*(r)/\rho c}=\mathrm{Re}\left\{\frac{\rho c}{Z_x^*(r)}\right\} \tag{3-10}$$

where: $$u_x(r)=\frac{p(r)}{Z(r)}$$

One specific case is that of a monopole source, where the real part of one over the impedance is equal to $1/\rho c$, [4, p. 129]:

$$\frac{1}{Z_x^*(r)}=\frac{1}{\rho c}\left(1-\frac{1}{ik_0 r}\right) \tag{3-11}$$

hence: $$\frac{I_x(r)}{p(r)\cdot p^*(r)/\rho c}=\mathrm{Re}\left\{\frac{\rho c}{Z_x^*}\right\}=1 \tag{3-12}$$

For a monopole, the active intensity can easily be derived from sound pressure. Active intensity expressed in dB is equal to sound pressure in dB because there are different reference values (re. 20 μPa and re. 1 pW/m^2, respectively).

Tests with five PU probes were performed to study the variations among them. A piston-on-a-sphere source was used because the acoustic impedance is known from equation 3-3, and because its sound power output is higher in a broad frequency range than that of typical omni-directional sound sources. The active intensity as measured by the PU-probes can be compared directly to sound pressure because the radiation impedance of the spherical source is known. Measurements at two distances r from the membrane of the piston-on-a-sphere source were performed (fig. 3-15). The loudspeaker has been powered with random noise during these tests.

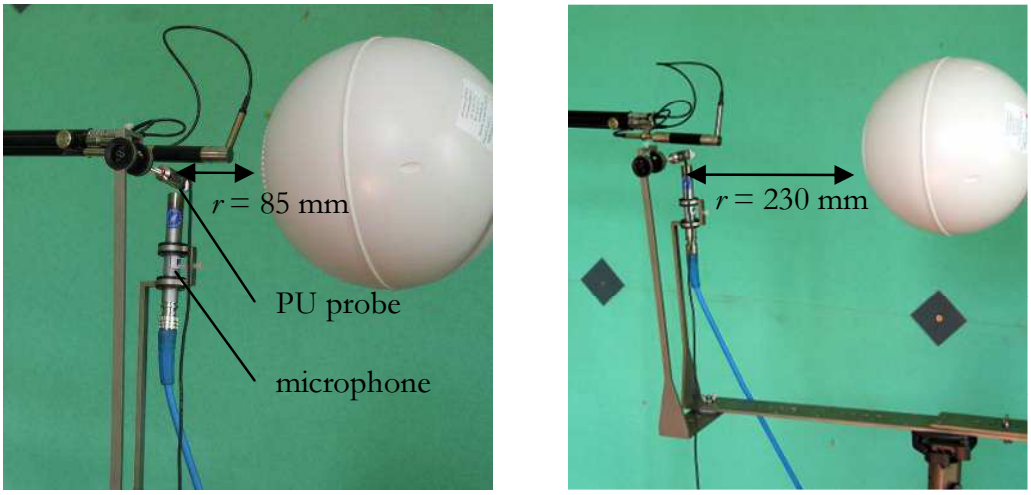

Fig. 3-15. A microphone and a PU probe in front of a piston-on-a-sphere source.

Fig. 3-16 and 3-17 show the active intensity as measured by the PU probes divided by the active intensity that is derived from the signal of the microphone by applying a correction for the specific acoustic impedance. Discrepancies between the intensity derived from the sound pressure microphone and the intensity derived from the PU probes are small in the middle frequency range. The deviations at high frequencies are caused by small inaccuracies in alignment amongst the probes and by reflections against the housings of the probes. At low frequencies, deviations are found because the field is reactive at small measurement distances. The error associated with the PU method grows as the field becomes more reactive, for example like in the acoustic near field of a source. In other words, the error increases as the phase

between sound pressure and particle velocity approaches ±90 degrees [11, 13]. Although in active sound fields accurate phase calibration is not so important, a small phase inaccuracy can lead to a high error in reactive fields. Therefore the error below 150 Hz is higher for the 85 mm source-probe distance compared to the 230 mm distance in these tests.

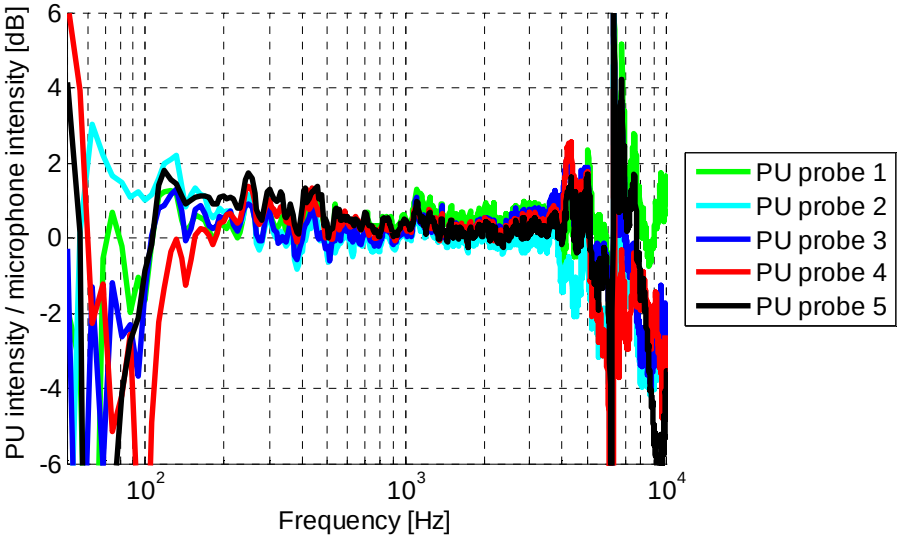

Fig. 3-16. The ratio of the active intensity that is obtained with a PU probe to the active intensity that is derived from the microphone signal; for five PU probes and r=85 mm.

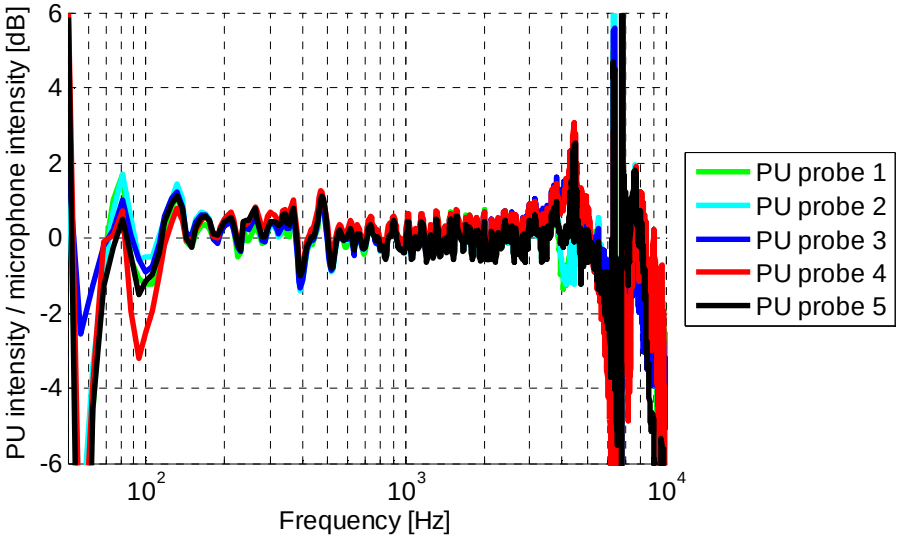

Fig. 3-17. The ratio of the active intensity that is obtained with a PU probe to the active intensity that is derived from the microphone signal; for five PU probes and r=230 mm.

The routine presented in this section is easier than a full calibration, especially in case a monopole sound source is used, and can be used to verify if the sensor signals are still corrected appropriately.

3.5. *Reference measurement without sample and reference sensor*

With the high and low frequency piston-on-a-sphere calibration method combined, the absolute responsivity of sound pressure and particle velocity sensors can be determined in a broad band. However, for most absorption measurements it is sufficient to determine the relative sensor responsivities in a well-defined situation. Simply the ratio (for impedance), or the real part of the product (for active intensity) of sound pressure and particle velocity is used; thus no reference microphone is required. The reference test can therefore be done just before the test of the sample. No correction is required for measurement conditions such as data acquisition settings, software settings, and impedance of air (which depends on for example temperature), because these are assumed to remain constant [76, 91, 92]. The procedures for the reference test without a sample as they are described in section 3.5 are applied to all measurements in this thesis, unless mentioned otherwise.

A disadvantage of measuring without a reference microphone is that the low frequency piston-on-a-sphere calibration method cannot be used anymore. The broadband calibration method is limited at low frequencies because only low sound pressure levels can be obtained from the loudspeaker compared to background noise in practical situations. However, in a similar way also the measurement above an acoustic sample is affected. One could argue that a calibration at low frequencies is of little interest anyhow if a sound source without sufficient radiation efficiency at low frequencies is used during the sample measurement. The low frequency piston-on-a-sphere calibration method is rarely used for absorption measurements because of the aforementioned reasons, and because a reference test without a sample is easier to perform than a full calibration.

3.5.1. Mirror source model

The mirror source model corrects for elevated particle velocity relative to the sound pressure in the near field above a locally reacting impedance layer, but not for the spherical wave front. A reference test that is performed in an environment where the specific impedance is known can be used instead of a separate calibration of the probe. If a monopole source is used during the reference test without the sample and the test with the sample, if distance r_1

between the probe and the sound source remains constant, and if the measurement is performed at normal incidence, equation 2-21 and 3-4 can be combined and simplified to:

$$Z_n = \frac{Z_{\text{sample}}}{Z_{\text{ff}}} = \frac{e^{-ik_0 r_1} r_2 + e^{-ik_0 r_2} r_1 R}{e^{-ik_0 r_1} r_2 - R \dfrac{ik_0 r_1}{ik_0 r_1 + 1} \dfrac{ik_0 r_2 + 1}{ik_0 r_2} e^{-ik_0 r_2} r_1} \qquad (3\text{-}13)$$

where r_1 is the distance between the probe and the sound source, h is the distance between the probe and the sample surface, $r_2 = r_1 + 2h$, and Z_n is the impedance at distance h normal to the sample surface, which is the ratio of the un-calibrated measured impedance Z_{sample} normal to the sample to the un-calibrated reference impedance Z_{ff} without a sample. The reflection coefficient R then becomes:

$$R = \frac{Z_n - 1}{Z_n \dfrac{r_1}{r_2} \dfrac{ik_0 r_2 + 1}{ik_0 r_1 + 1} + 1} \frac{e^{-ik_0 r_1} r_2}{e^{-ik_0 r_2} r_1} \qquad (3\text{-}14)$$

3.5.2. Intensity model

Also for the intensity method, a reference test performed in a defined situation can be used instead of a calibration measurement. The measured complex intensity without the sample can also be used to determine the relative responsivities of the sensors if the free field impedance is known. The intensity method can be simplified if the same source-sensor configuration is used during the reference test without the sample and the test with the sample.

The true complex intensity I_{true} is the measured intensity I_{m} corrected for responsivity of the sound pressure and the particle velocity sensor, which are respectively S_{p} and S_{u} for the amplitude and φ_{Sp} and φ_{Su} for the phase. These are replaced by an amplitude correction G_{corr} and phase correction φ_{corr} for simplicity.

$$I_{\text{true}} = \frac{|I_{\text{m}}| e^{i\varphi_{I_{\text{m}}}}}{S_{\text{p}} e^{i\varphi_{\text{Sp}}} S_{\text{u}} e^{i\varphi_{\text{Su}}}} = |I_{\text{m}}| e^{i\varphi_{I_{\text{m}}}} G_{\text{corr}} e^{-i\varphi_{\text{corr}}} \qquad (3\text{-}15)$$

In section 2.8.4, the absorption coefficient was defined as the ratio of the absorbed to ingoing intensities. If the source strength is kept the same during the tests, the amplitude correction G_{corr} can be omitted because it appears on both sides of this fraction. The phase correction φ_{corr} can be determined if the phase φ_{field} between sound pressure and particle velocity in the particular sound field during the test without a sample is known. For example, equation 3-4 for a point source in the free field can be used and rewritten so that the phase $\varphi_{\text{field}} = \arctan(\frac{1}{kr})$. The relative phase $\varphi_{I_{\text{ff}}}$ between the two signals measured without a sample consists of the phase responsivity φ_{corr} of both sensors plus the phase of the sound field φ_{field}. Hence, φ_{corr} can be obtained by subtracting the phase of the sound field from the measured phase:

$$\varphi_{\text{corr}} = \varphi_{I_{\text{ff}}} - \varphi_{\text{field}} \qquad (3\text{-}16)$$

3.6. *Conclusion*

Several techniques exist to calibrate particle velocity sensors. The advantage of using a piston-on-a-sphere sound source in the free field is that sound pressure and particle velocity can be calibrated in a broad frequency range. The calibration results can be checked with the same sound source by comparing the calculated intensity to the squared sound pressure. The responsivities of the sound pressure and particle velocity sensor are often easier to determine relative to each other, than with a full calibration. For a relative test, no reference microphone is required, and measurement conditions such as air impedance and system settings can be kept constant if the test with and without a sample are performed in the same period of time and under the same conditions. The mirror source model can be simplified if the distance and orientation of the sensor to the sound source are equal during the reference test without the sample and the test with the sample. The method based on the ratio of absorbed to incoming intensities can also be simplified if both measurements are performed with the same configuration.

4. Development of a handheld measurement set-up

4.1. *Introduction*

The goal for this research is to develop an *in situ* method to determine the absorption coefficient. The system used for such tests should be convenient to operate, suitable for a broad frequency range (i.e. 500Hz or lower, to 4kHz or higher), and suitable for environments which are not necessarily anechoic, such as regular offices, cars, and concert halls. In addition, the responsivities of the sensors need to be characterised with the same system just before or after the absorption measurement is performed, because then the functionality of the probe can be checked, and because many environmental conditions and system settings can be disregarded as they are assumed to remain constant. A handheld set-up that enables such tests has been created. The set-up will be presented in this chapter, and the considerations that have been made during its design are described.

The absorption coefficient can be calculated with one of the models that were introduced in the previous sections. These absorption models require a sound source above a probe that, depending on the model used, measures the impedance or intensity near the sample. However, measurement errors can occur if the position and orientation of the probe or sound source vary. With a fixed configuration, positioning errors between the probe and the sound source can be avoided. A set-up was therefore developed that contains the sound source and the probe.

The following section concerns the choice of the sound source. Its characteristics affect the size and shape of the set-up and the sound levels that can be generated, thus the manageability and performance of the measurement system. The particularities of several sound source types are evaluated.

Subsequently, the way in which vibrations that may be caused by the sound source can be cancelled is discussed. Measurement errors can occur if these vibrations pass through the frame of the set-up to the probe. The conditions under which vibrations affect the tests, and the solutions which have been found to reduce them, are described.

Thereafter, several set-ups that have been constructed are presented. The difficulties that were faced with early versions and the improvements that have been made before the final set-up could be build are discussed. Test results are presented, which demonstrate the effectiveness of the suspension systems that dampen the vibrations of the sound source.

Finally, the software and hardware that have been developed especially for these absorption measurements are briefly described.

4.2. *Sound source selection*

Although sound can be generated in various ways, a loudspeaker is chosen for the handheld set-up because such a sound source can be small, broadband and easy to power. The size, shape, and performance of the set-up, and the sound levels that can be generated, depend on the size, shape and type of loudspeaker box. This defines the sound field above the sample (thus the absorption model that should be used), the operating frequency range, and the degree to which measurements are affected by background noise and reflections.

An uncomplicated absorption model would suffice if plane waves would be generated by the loudspeaker box. However, plane waves are difficult to generate *in situ*. Usually, sound diffracts at the edge of the loudspeaker box, which causes near field effects. The distance to the sample should be small compared to the size of the sound source to minimise the influence of divergence. In order to avoid the relative increase of particle velocity in the near field, the distance to the loudspeaker should be large compared to the wavelength. A large (array of) loudspeaker(s) would be required that is positioned far from the probe to meet both requirements. Yet, in that case, a set-up consisting of a probe and a loudspeaker would not be small and handheld any more. Alternatively, a diffuse sound field with plane waves in all directions could be generated by multiple loudspeakers or many reflecting panels around the test set-up. Unfortunately, such conditions are difficult to create in most measurement environments.

Another option would be to use a monopole sound source. Ideally, such a sound source needs to radiate uniformly in each direction. Actual sound sources that radiate in a similar way as monopoles generally consists of a tube that is open on one end, and is connected to a loudspeaker in an enclosure on the other end. If the diameter of the open end of the tube is sufficiently small compared to the wavelength the sound radiates omni-directionally like a true monopole [91]. However, the broadband radiation efficiency of such sound sources is rather low. More than one sound source is needed to cover a broad band; a larger tube diameter should be used at low frequencies for sufficient output, whereas the wavelength is shorter at high frequencies and the tube's diameter should be small for omni-directional radiation.

In this study, a piston-on-a-sphere loudspeaker box is used for most absorption measurements. It comprises a loudspeaker that is mounted in a rigid spherical housing. The piston-on-a-sphere is chosen mainly because:

- its broadband radiation efficiency is higher than that of typical omni-directional sound sources (section 3.3.1),
- no significant diffraction effects are present (section 3.3.1),
- its frequency response is smooth relative to most omni-directional sound sources (section 3.3.1 and 5.3),
- the impedance on the acoustic axis of sound source is similar to that of a monopole (section 3.3.2),
- the same sound source can be used for the reference test without the sample and the test with the sample.

4.3. *Suppression of loudspeaker vibrations*

Positioning errors between the probe and the sound source can be avoided with a fixed set-up. However, in that case loudspeaker vibrations can pass through the frame of the set-up to the probe, which may disrupt the tests. These vibrations should therefore be damped. Structural vibrations mostly affect the signal of the particle velocity sensor for samples with a high reflection coefficient. In that case, the loudspeaker membrane is moving in the direction were the particle velocity sensor is most sensitive. Even the slightest vibration through the frame has a profound effect because the particle velocity level due to airborne sound is low near a reflective surface. A broadband damping system is required because a wide frequency range can be affected by

these structural vibrations. The solution to dampen vibrations that was ultimately found comprises a probe suspension and a sound source suspension. These suspension systems, and results from tests that demonstrate their effectiveness, will be presented in the next section.

4.4. *Final measurement set-up*

Several set-ups have been created throughout the years. Some are shown in chronological order in fig. 4-1 to 4-4. The first handheld set-up was created in 2005 (fig. 4-1). The probe is attached to a housing that contains a loudspeaker box, a signal conditioner, and a sound card [100]. Absorption tests can be performed quickly and easily with the set-up. However, measurement errors were found and the probe needed to be calibrated with a separate set-up.

Fig. 4-1. First handheld absorption measurement set-up.

The second version contains a piston-on-a-sphere loudspeaker box, which allows characterization of the responsivities of the sensors with the same set-up (fig. 4-2) *[76]*. Again, measurement errors occurred because loudspeaker vibrations passed through the steel rod that holds the probe, and the set-up was large and heavy. The electronics were moved outside the loudspeaker housing in following versions to reduce size and weight, and a small piston-on-a-sphere was used.

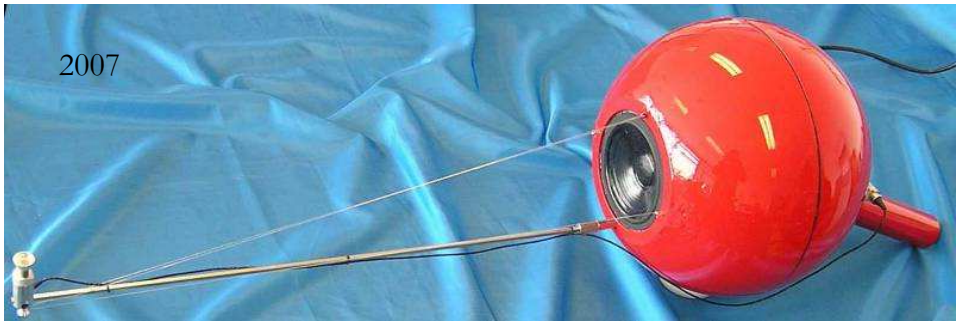

Fig. 4-2. First version with a piston-on-a-sphere.

The next set-up functioned well for middle and high frequencies (fig. 4-3 left). Deviations were found at low frequencies because loudspeaker vibrations through the frame were insufficiently damped. Subsequently, a version that successfully suppressed the vibrations was constructed (fig. 4-3 right) *[30]*. The position of the probe could vary amongst tests because the probe suspension, which consisted merely of plastics and glue, was weak. Nevertheless, promising measurement results were obtained. Therefore, more robust versions made from steel were created.

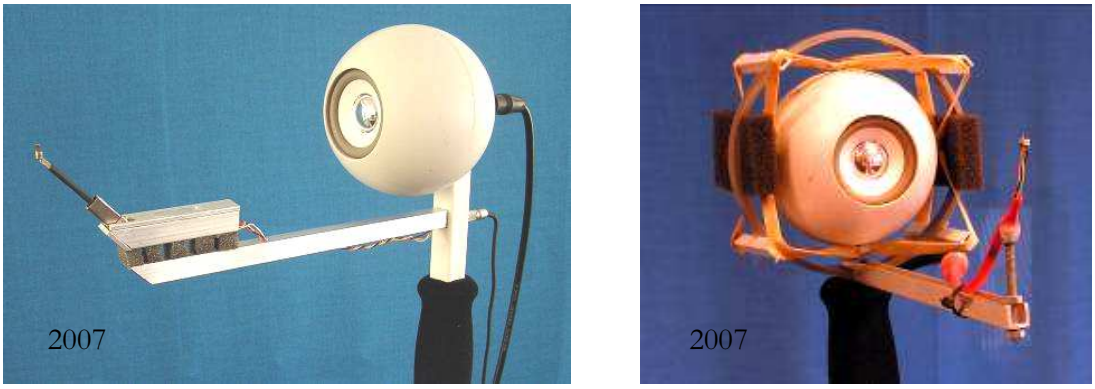

Fig. 4-3. Left: First version with a small piston-on-a-sphere. Right: First successful vibration suspension.

Vibrations from the loudspeaker passed easily through the frame of the first set-up made from steel because steel has little damping (fig. 4-4 left) *[101]*. The elastic bands that were used also began to sag over time due to the weight of the sound source. Similar problems were experienced with the following version (fig. 4-4 middle).

Fig. 4-4. Several versions with a steel grid. Right: The version used up to date.

In 2008, the set-up that is now mostly used was designed (fig. 4-4 right) *[92]*. Two suspensions with different resonant frequencies are used to reduce vibrations in a broad band; i.e. a suspension of the probe in elastic bands, and a suspension of the sound source in springs. The used piston-on-a-sphere source has a radius of 50.5 mm, and its membrane has a 37.5 mm radius. The distance between the probe and the loudspeaker membrane is 260 mm. A high signal-to-noise ratio can be obtained from 100 Hz to 20 kHz with the set-up during the reference test without the sample. Lower frequencies might even be reached with a larger sound source, but this would also mean the set-up would become large and therefore impractical to use.

As was mentioned before, loudspeaker vibrations can cause measurement errors, which mainly affect the particle velocity at low frequencies for high reflecting materials Several tests have been performed with and without the suspensions systems of the probe and the sound source to demonstrate the functionality of the suspension systems that were incorporated in the final set-up. During these tests, the sound pressure and particle velocity were measured 1 cm from an aluminium plate for the following configurations:

- a free suspension were the probe was held by a separate tripod,
- a rigid suspension (no springs and elastic bands),
- only the sound source suspension with springs,
- only the probe suspension with elastic bands,
- the sound source and probe suspension.

The results obtained are shown in fig. 4-5. It can be seen that the sound pressure is similar for all mounting conditions. Only at high frequencies slight variations are found, which are caused by small variations in the position of the probe. For particle velocity, discrepancies occur at low frequencies if one of the suspension systems is not used. With both suspension systems, frequencies above 100 Hz are sufficiently damped.

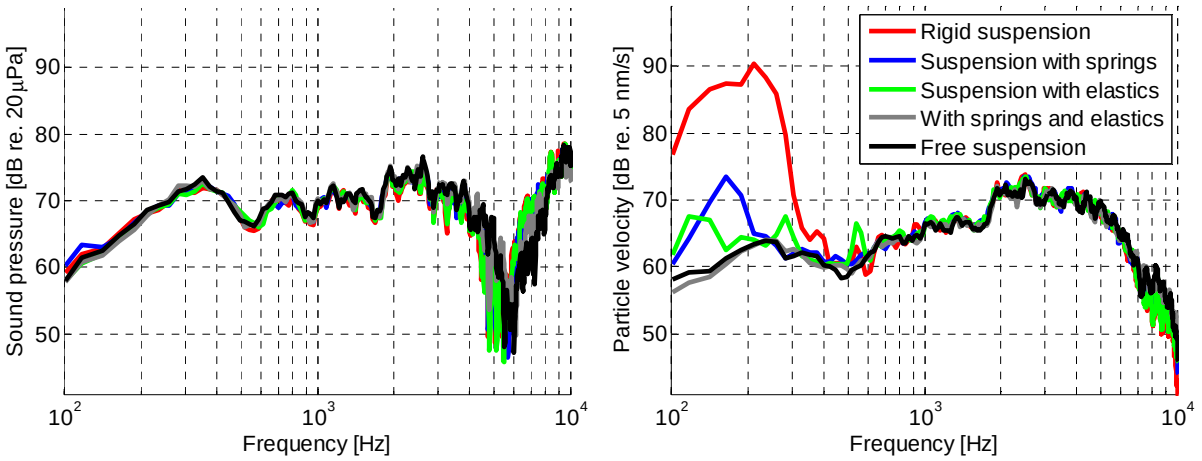

Fig. 4-5. The measured sound pressure and particle velocity for different suspensions.

4.5. *Data acquisition and software*

PU probes come standard with a dedicated power supply and signal conditioning. For measuring absorption an additional data acquisition module has been developed, which consists of two recording channels and one amplified loudspeaker output. The output signal can be correlated to the inputs in order to calculate the impulse response. In addition, dedicated software has been written that incorporates a test procedure for the handheld set-up. The measurement signals from the data acquisition module can be acquired with the software, and reflections from surrounding surfaces can be removed by applying a moving average in the frequency domain or by windowing the impulse response (see chapter five). The plane wave model, the mirror source model, and the Q-term model have been implemented. Quantities such as sound pressure, particle velocity, impedance, reflection, and absorption can be visualised. With a special feature the absorption coefficient that is calculated by the mirror source model can be visualised real-time.

4.6. *Conclusion*

A handheld, broadband measurement set-up is created that contains a PU probe and the same piston-on-a-sphere that was introduced in the previous chapter. With the set-up, high signal-to-noise ratios can be achieved from 100Hz to 20kHz, and both the reference test without a sample and the test with a sample can be performed. Positioning inconsistencies in between both measurements are avoided because of the fixed orientation and distance of the probe relative to the loudspeaker. Vibrations through the frame of the set-up are reduced using multiple springs and elastic bands.

5. Removing room reflections

5.1. *Introduction*

During the measurements, there are reflections from objects surrounding the test set-up. Even anechoic rooms cannot be considered fully anechoic at low frequencies. Depending on frequency, objects may attenuate and change the phase of reflected waves; this affects the degree to which reflections distort the tests. In general, reflections become more dominant if the source-probe distance is larger compared to the distance of other surfaces, and when these surfaces have strong reflections. In this chapter, several techniques will be investigated to remove reflections, and the effect of reflections with measurements on several samples is studied.

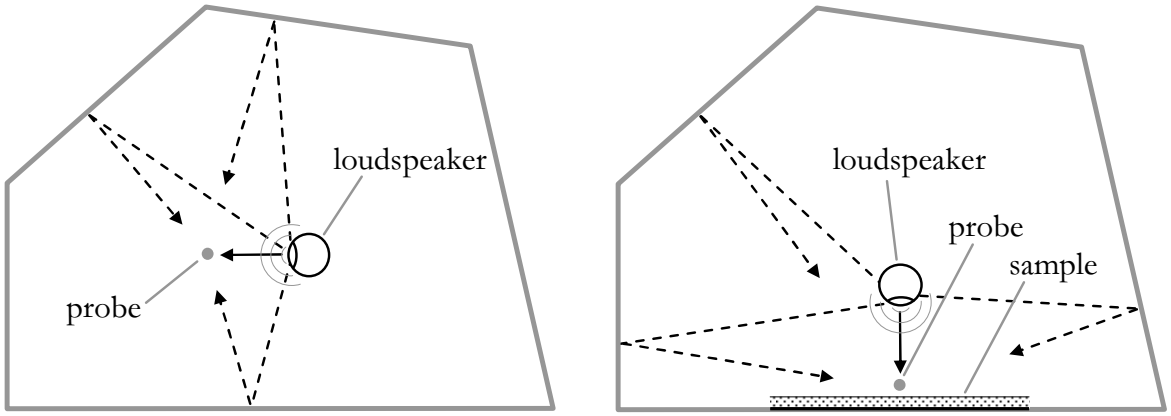

Fig. 5-1. Reflections are present during the measurements.

A measured signal $y(t)$ contains the direct signal and its reflection, and might be modelled by [102]:

$$y(t) = x(t) + ax(t - t_0) \qquad (5\text{-}1)$$

here $x(t)$ is the direct signal, $ax(t - t_0)$ is the reflection, a is the amplitude of the reflection, and t_0 is the time delay between the reflection and the direct signal. a is frequency dependent and complex because the reflected sound is attenuated and delayed by surrounding surfaces.

The Fourier transform of $y(t)$ is [102]:

$$Y(f) = \left(1 + ae^{-i2\pi f t_0}\right) X(f) \qquad (5\text{-}2)$$

The term $\left(1 + ae^{-i2\pi f t_0}\right)$ is a function of frequency, and has an oscillatory effect in magnitude and in phase. At low frequencies, particle velocity is less affected by reflections because particle velocity is elevated compared to sound pressure in the acoustic near field of the source.

A single reflection causes 'ripples' on the spectrum. Additional reflections and dispersions cause more interference. A comb filter can be applied to cancel reflections if the time delay and the amplitude of individual reflections are known. However, even small erroneous estimates of the time delay cause deviations at high frequencies. In practice, the time delay and amplitude of (multiple) reflections are difficult to estimate, especially because the complex reflection coefficients of surrounding surfaces are unknown.

The cancellation of reflections present during reference test without a sample is a rich field, which is not discussed exhaustively in this thesis. For example, there are several acoustic echo cancellation techniques involving filters such as a Wiener filter or adaptive filters, see [59, pp. 883-895], [103]. However, these techniques are unsuitable or impractical for measurements with the sample where reflections from surrounding objects should be cancelled, but not those from the sample.

In the following subsections, three methods are described that can be applied to remove reflections during the reference test without a sample and the test with a sample. No single cancellation technique can be applied under all circumstances. The choice of the most optimal method depends on the number of surrounding surfaces, on their attenuation, and on their distance to the measurement set-up. Particularly at low frequencies, these methods have their limitations while the strength of reflected waves can be considerable because the damping of surrounding surfaces usually is poor at low frequencies.

5.2. *Windowing the impulse response*

An impulse response describes the reaction of a system in time to a delta pulse [59, p. 65]. The impulse response contains the direct wave and its reflections. Reflections are delayed in time compared to the direct wave due to the longer path length. Therefore, reflections from surrounding objects can be isolated from the direct contribution and the reflections from the sample using time selective techniques.

The impulse response can be obtained by applying a short pulse and by recording the time signals. However, a short pulse with sufficient energy at all frequencies is difficult to generate in practice because of the high crest factor (the ratio of the peak signal divided by its rms. value). For jointly stationary random processes, the impulse response can also be obtained by de-convolution. Unfortunately, this process requires high computational power for long signals [104]. Instead, the impulse response is obtained via a procedure involving converting measured time signals to the frequency domain, and then back again using (inverse) Fast Fourier Transforms [43, 99, 104]. The procedure consists of the following steps (see also fig. 5-2):

1. A continuous broadband signal $s(t)$ is applied to the loudspeaker input (for example random noise or a sine sweep). This signal and the sensor response $y(t)$ are recorded for certain duration Δt. If Δt is too short, parts of the direct sound and the reflections from the sample are not measured. However, the reflections from a surrounding object are also be included in the sensor signal if $\Delta t > \frac{c}{\Delta L}$, where c is the speed of sound and ΔL is the difference in path length between the direct sound and the reflections. The measured signal therefore contains the signal from the direct source and its reflections.
2. The time signal $s(t)$ and sensor response $y(t)$ are converted to the frequency domain.
3. The sensor spectrum is divided by the loudspeaker spectrum in order to obtain the transfer function H between the loudspeaker and the transducer; an operation equivalent to de-convolution in the time domain [105, 106].
4. The impulse response h of the sensor is obtained with an inverse Fourier transform.

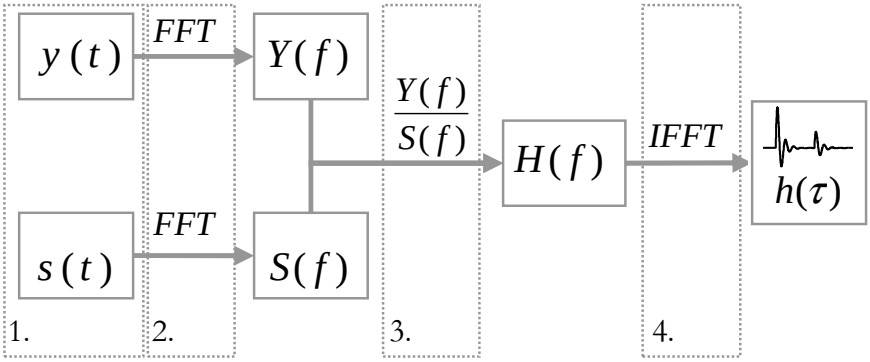

Fig. 5-2. Flow-chart for calculating the impulse response.

Subsequently, unwanted reflections can be removed from the impulse response with a procedure that is also used in standards such as CEN/TS 1793-5, AFNOR NF S 31-089, and ISO 13472-1, which were described in section 2.6.1. The direct signal and early reflections from surrounding objects can be recognised by the user in the impulse response, which is convenient because the exact path length of the reflected sound wave is usually unknown. The reflections are removed from the impulse response of both sensors, and the impedance that is free from the unwanted reflections is calculated. The procedure consists of a number of steps (see also fig. 5-3):

5. The reflections are cancelled by multiplying the impulse with a certain window function w. This window function should be one for the duration of the direct signal, and low or zero for sections of the impulse response that contain reflections.
6. The transfer function between the loudspeaker and the sensor that is free from the unwanted reflections is obtained by converting the windowed impulse response h_{win} to the frequency domain. The procedure is repeated for both sensors in order to acquire the transfer functions between sound pressure and the loudspeaker $H_{\text{ps,win}}$, and between particle velocity and the loudspeaker $H_{\text{us,win}}$.
7. Finally, the estimated impedance $\tilde{Z}$ is calculated by the ratio of $H_{\text{ps,win}}$ to $H_{\text{us,win}}$, and hence the loudspeaker response is eliminated.

The same window size should be used for both transfer functions to ensure the energies are equal. Also, nonlinearities of for example the loudspeaker or the sensor should be avoided because they can deteriorate the quality of the impulse calculation.

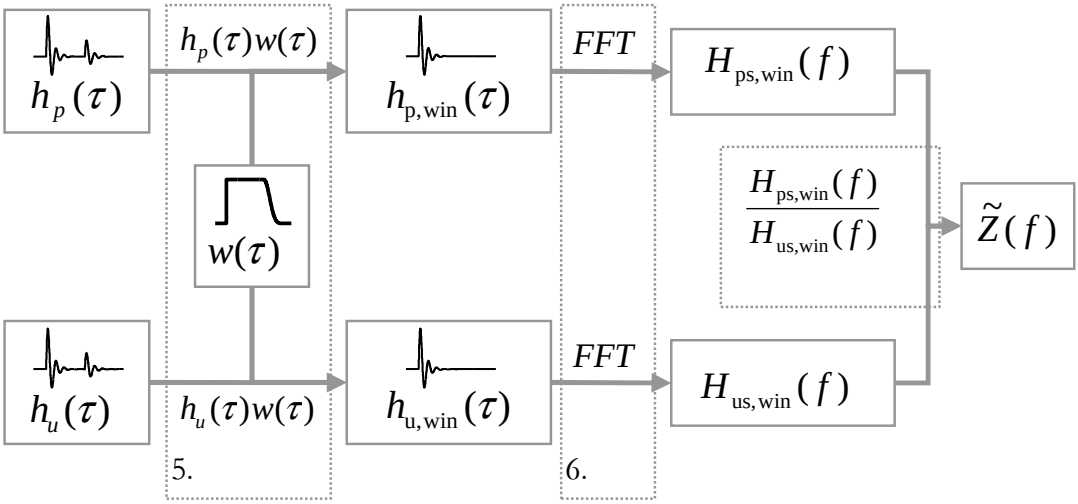

Fig. 5-3. Flow-chart for calculation of impedance free from reflections.

In step 7 the loudspeaker response was eliminated for the impedance using the ratio of the transfer functions free from unwanted reflections ($\tilde{Z} = H_{ps,win} / H_{us,win}$). A similar approach can be used to remove reflections for the intensity-based absorption model introduced in section 2.8.4. Intensity is defined as the sound pressure times the complex conjugate of the particle velocity. The estimated intensity without unwanted reflections can therefore be obtained by multiplying $H_{ps,win}$ and (the conjugate of) $H_{us,win}$. Although, this quantity is still proportional to the strength of the sound source, the sound source strength is finally eliminated because the intensity based absorption model uses the ratio of absorbed to incoming intensities, and because the input signal from the loudspeaker is kept constant during both tests.

In order to explore this impulse windowing procedure, measurements and simulations have been done for the situation without a sample. An anechoic room is considered with a PU probe at a distance $r = 0.3\,\mathrm{m}$ from the loudspeaker (fig. 5-4) which is driven with random noise. The first test yields the 'perfect' anechoic response. The second test involves an additional reflection from a reflecting plate at distance $y = 1\,\mathrm{m}$. The reflection from this $1\,\mathrm{m} \times 1\,\mathrm{m}$ large plate is $\frac{1}{c}(\sqrt{r^2 + (2y)^2} - r) \approx \sim 5\,\mathrm{ms}$ delayed in time compared to the direct sound. The recording time was sufficiently long (four seconds) to guarantee that the reflection is included in the measurement.

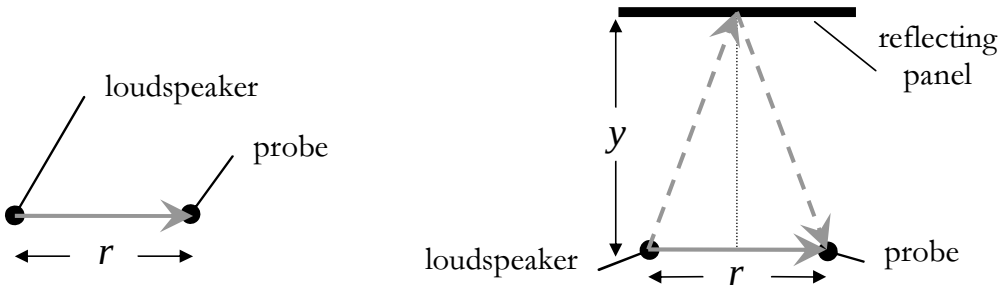

Fig. 5-4. Left: anechoic measurement with direct source only. Right: added reflection.

Additionally, a signal was simulated that contains the direct source and its reflected wave from a plate at distance $y = 2\,\text{m}$ ($\approx 11\,\text{ms}$ delay) and a strength that is half that of the direct sound. A trace of four seconds of random noise was generated, and weighted by the analytical Microflown model (equations 3-1 and 3-2). Corner frequency values used for this model were: $f_1 = C_1 = 100\,\text{Hz}$, $f_2 = C_2 = 1\,\text{kHz}$, $f_3 = C_3 = 10\,\text{kHz}$. An inverse Fourier transform was used to convert this weighted random noise to the time domain. Then, a first order Butterworth high-pass filter with a 100 Hz cut-off frequency was used to mimic the reduced sound source output at low frequencies. Fig. 5-5 shows the measured and simulated impulse responses, and the window that is applied to the impulse response with reflection. An Adrienne window was used, which, for a variable length l, is defined as a leading edge having a left-half Blackman-Harris shape ($\approx 0.0005\,l$), followed by a flat portion ($\approx 0.69965\,l$), and by a trailing edge having a right-half Blackman-Harris shape ($\approx 0.29985\,l$). Rectangular windows are rarely used because sharp edges can cause deviations at high frequencies [44]. The window begins just before the direct sound wave, and its length is selected in such a way that the reflection is not included. Low frequencies are affected when the window length is limited.

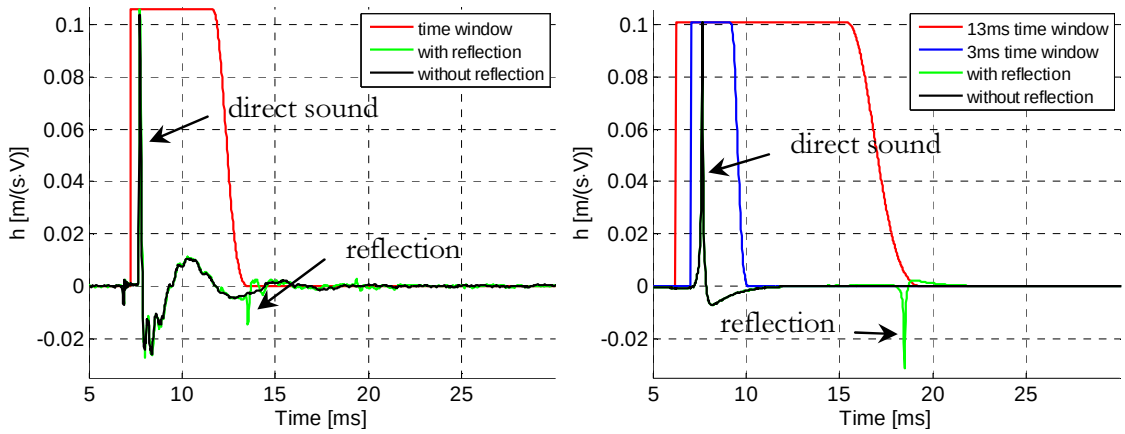

Fig. 5-5. Impulse responses and window; measurement (left), simulation (right).

Reflections can be removed successfully by windowing the impulse response of the transducers if the surrounding objects are sufficiently far away. The low frequency limit depends on the path length difference of the direct sound and its reflections. Fig. 5-6 shows calculated spectra of the measurement and the simulation. A relatively short 6.3ms window was applied for correcting the measurement that contains the reflected wave (green line). The time windowed response of this test (red line) deviates below ~400 Hz from that of the first test without plate (black line).

For the simulations, a longer window of 13ms and a shorter window of 3ms were used to study the effect of the window length. Little discrepancies occur between the time windowed signal with reflection and the signal without reflection above ~80Hz for the longer window and above ~400Hz for the shorter window. This is close to the theoretical limit of a rectangular window, which is $\frac{1}{0.013s} = 77\,\text{Hz}$ and $\frac{1}{0.003s} = 330\,\text{Hz}$, respectively [108].

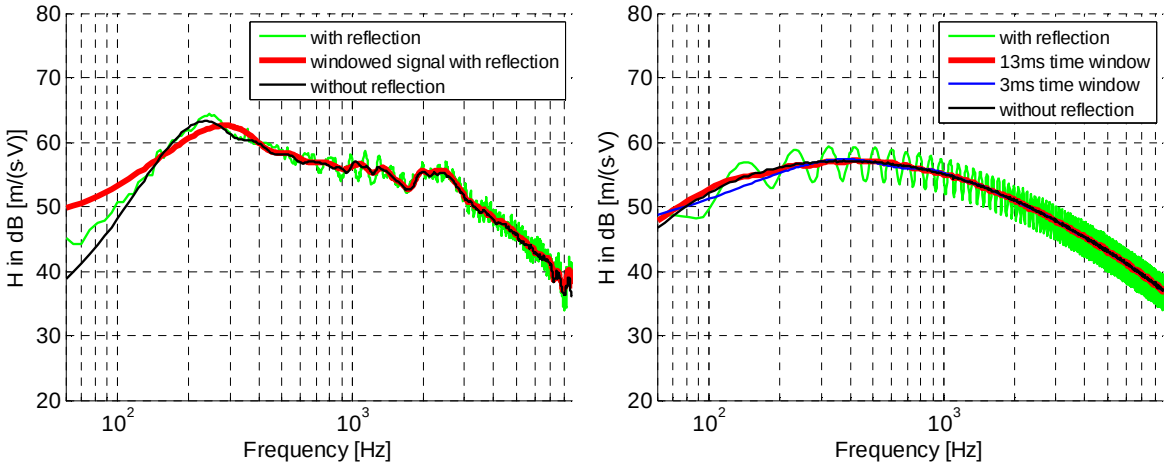

Fig. 5-6. Loudspeaker-sensor transfer function; measurement (left), simulation (right).

The beginning of the window can be selected from the impulse response of the transducer because the first peak of the direct sound wave is recognisable. The length of the window should be selected in such a way that reflections are not included. The time delay between direct sound and reflections can also be detected using auto-correlation [102]. The auto-correlation between the loudspeaker and the transducer signals is calculated for the measurement and simulation with reflecting plate, and is shown in fig. 5-7.

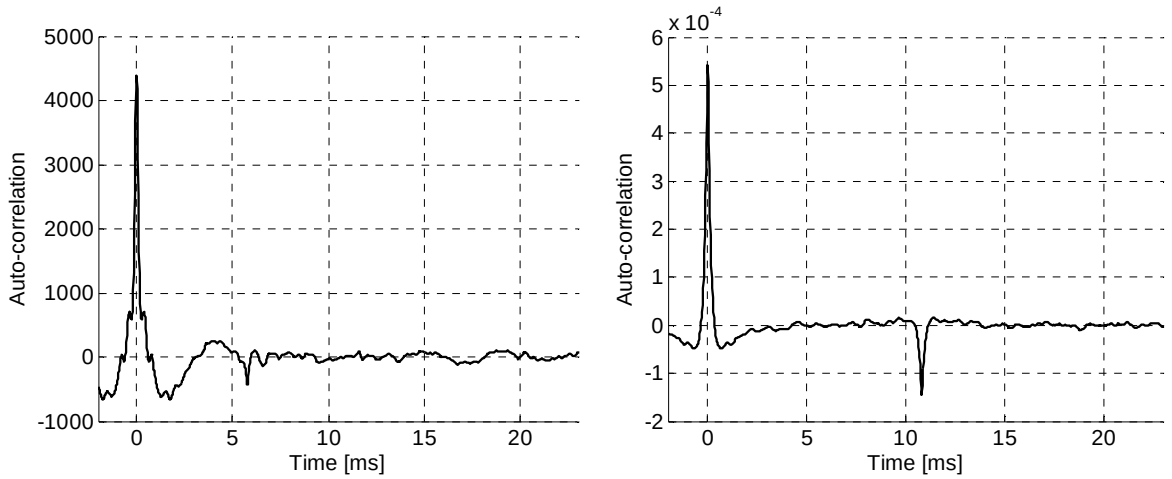

Fig. 5-7. Loudspeaker-sensor auto-correlation; measurement (left), simulation (right).

5.3. *Moving average in the frequency domain*

Two other approaches to cancel reflections are based on the assumption that the sound field is sufficiently diffuse and that there are many reflections from all directions. The first one is the 'moving average' technique. As was mentioned earlier, reflections have a harmonic modulation effect on sound pressure or particle velocity in the frequency domain. Their influence depends on the distance to the reflective surface and the strength of the reflected wave. There are many interfering reflecting waves when there are many surrounding surfaces at different distances and directions. Although a small frequency band can be strongly affected by reflections from a single direction, the average of multiple adjacent frequency bands are influenced less by individual acoustic modes. A moving average of the frequency response can therefore be applied to minimise the effect of reflections. A moving average filter smoothens the measured data X_{m} by replacing each data point with the average of neighbouring data points defined within a certain span n:

$$X_{\mathrm{averaged}}(f) = \frac{1}{2n} \sum_{f'=f-n}^{f'=f+n} X_{\mathrm{m}}(f')\phi(f') \qquad (5\text{-}3)$$

X could for example be impedance or intensity. The span can be a fixed or a frequency dependent value.

The moving average can be weighted with a certain weighting function $\phi(f')$, which might for example be one or a Gaussian weighting function [109]:

$$\phi(f') = \frac{1}{\mathrm{erf}\left(\sqrt{2}/2\sigma\right) n\sigma\sqrt{2\pi}} e^{0.5\left(\frac{f'-f}{n\sigma}\right)^2} \qquad (5\text{-}4)$$

where σ is the standard deviation and erf is the Gaussian error function. With the $\frac{1}{\ldots}$ initial part of this function, the exponential expression is normalised for the distribution of the Gaussian weighting function and for the limited range to which it is applied ($f' = f \pm n$ instead of $f' = f \pm \infty$). The density of frequency points in an octave band is lower at low frequencies because of the FFT algorithm. A logarithmic increment of n versus frequency has shown to give good results in many situations. Examples of measurements performed in a small office with and without a sample are shown in fig. 5-8.

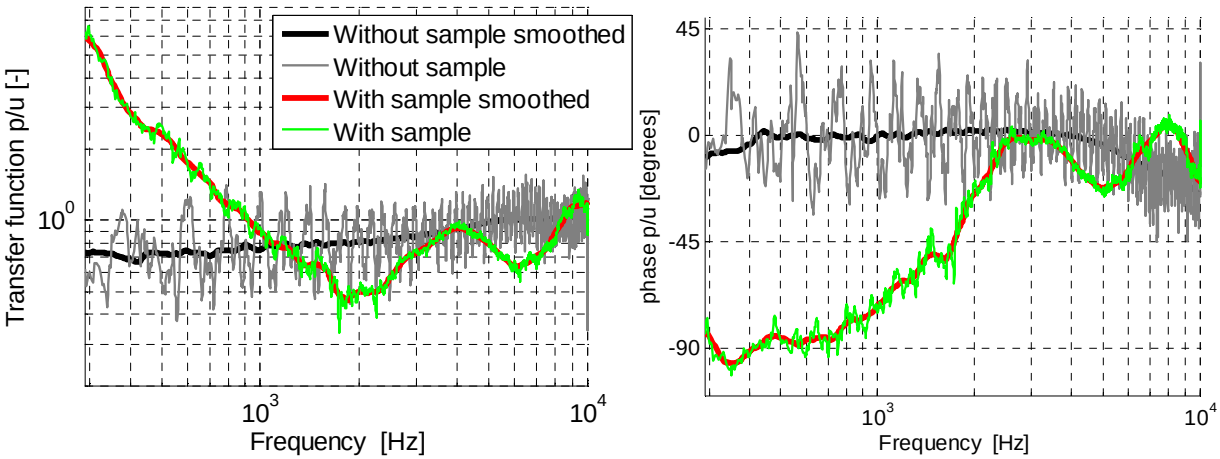

Fig. 5-8. p/u transfer function smoothed using a moving average.

There are considerations of using this moving average technique. Selection of an appropriate number of averages in a particular frequency range requires knowledge of the sensor response beforehand, and is subjective to the interpretation of the user. If the strength of reflections is considerable compared to that of the initial field from the source it becomes more complicated to apply the moving average approach. In addition, the moving average approach should not be used if there are sharp changes in impedance or the frequency response of the sensor; impedance changes and slight sensor imperfections could be smoothed as if they would not exist. Therefore, the

user should ensure that the absorption properties of the sample gradually change with frequency. It is uncertain if this moving average procedure would be integrated in a future standard because the latter condition may be violated unintentionally. Also, contrary to the impulse windowing technique, the results of the moving average are unaffected by loudspeaker nonlinearities because the loudspeaker signal is not used as reference. Finally, the effectiveness of this technique improves if there are more reflections with different time delays because these partially cancel each other. The frequency band of which the average is taken should be wide in order to include multiple reflections. Rooms typically have few standing waves per frequency band at lower frequencies, which makes it harder to remove individual reflections. A similar problem is experienced in typical reverberant room tests; only above the Schroeder frequency adjacent modal resonances have sufficient overlap [7, 109].

5.4. *Spatial average*

The moving average approach is intended for a fixed position of the probe and the sound source relative to surrounding reflective surfaces. In another approach, the distance to surrounding panels is varied over time by moving or rotating the sensor-source combination during the test. This causes a variation of the phase and amplitude of the reflected waves, and hence the degree to which they interfere. The measured diffusion effectively increases and the relative contribution of individual reflections reduces. However, vibrations and turbulences induced by movements should be avoided as much as possible. In addition, in most circumstances reflections cannot be cancelled sufficiently by spatially averaging alone. Usually, impulse windowing or moving averages in the frequency domain are more effective.

5.5. *Measurements with strong early reflections*

Anechoic conditions are ideal for *in situ* absorption tests because then all reflections come from the sample, which is the assumption for the absorption models that have been introduced. However, reflections from objects that surround the measurement set-up influence the results in reality. It has been shown that in most relevant environments the outcome of tests performed with the set-up that is presented in chapter 4 are usually affected little by reflections because the distances between the sample, the PU probe, and the sound source are small. For example, in the middle of a regular office the

measured absorption typically deviates less than 0.1 *[27, 110]*. Test results obtained successfully under reverberant conditions such as inside cars and concert halls will be shown in chapter eight. Although a PU probe is used for these tests, it may have been possible to use other types of intensity probes instead. However, other intensity probes are larger than PU probes, and the impact on the results of the larger separation between the sensors and the sample has not been investigated here.

Several measurements with six samples and a reflecting side plate have been performed to demonstrate the effect of strong early reflections. During these tests, an 800mmx800mm large steel plate with a reflection coefficient of nearly one was placed at several distances next to the set-up (fig. 5-9). Distance r between the sound source and the probe was 0.27m, and distance h between the probe and the sample was 0.005m. The mirror source model was used to calculate the absorption coefficient, and the measured impedance was smoothened with a moving average in the frequency domain.

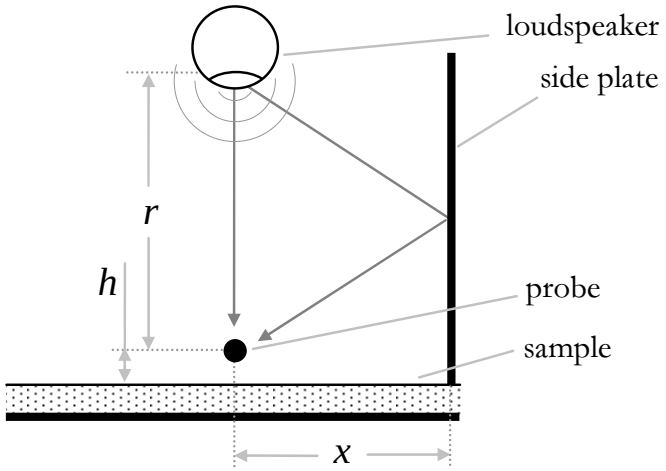

Fig. 5-9. The reflecting side plate was positioned at x=65, 200, 400, 600, and 1000mm.

Fig. 5-10 shows the measured absorption for a sample consisting of a homogeneous 20mm layer of polyurethane and for a 28mm thick sample, which consists of shredded pieces of recycled low-density polyurethane foam that are bonded together. The absorption coefficient that is obtained with reflecting side plate differs little from the situation without reflections. Strongest variations are found for x=200mm and 400mm in between 200Hz and 500Hz. Smaller deviations than expected are found for x=65mm were the side plate is close to the set-up. Similar findings were also reported in *[77]*.

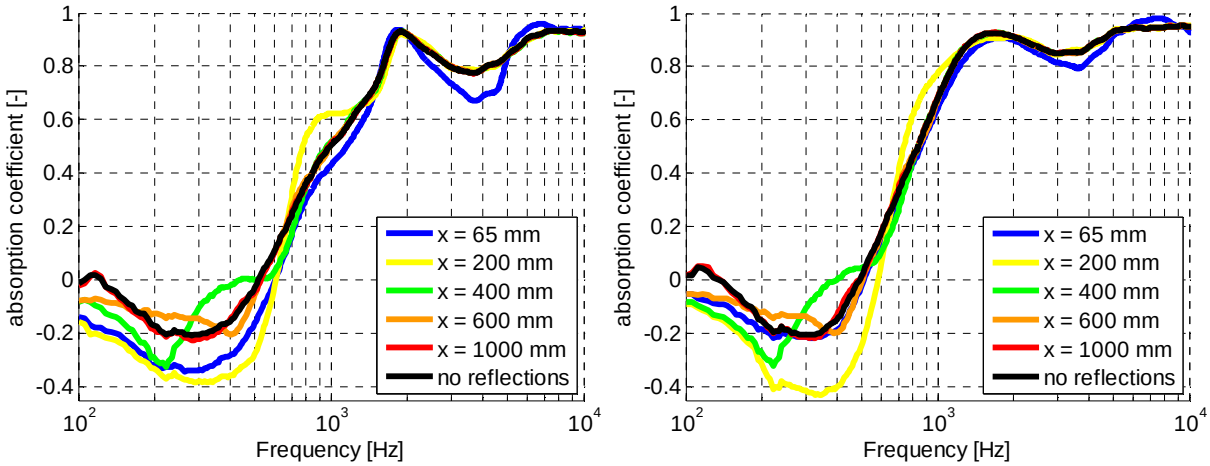

Fig. 5-10. Absorption measurements with a reflecting side plate: homogeneous polyurethane (left), and shredded pieces of polyurethane (right).

The four other samples that were measured are; melamine foam called Flamex with a thickness of 27 mm and 40 mm, and open polyester wool called Akotherm with a thickness of 22 mm and 50 mm. Fig. 5-11 shows the measured absorption coefficients. Larger deviations are found for these samples. The discrepancy is highest for $x = 65$ mm, 200 mm, and 400 mm. Similar discrepancies have also been reported in [112] and *[113]*.

The deviations are caused by interferences between the direct sound from the loudspeaker and its reflections from the sample, and the sound that has reflected against the side plate. During the reference measurement without a sample the effect of these interferences are strongest near frequencies were the direct path r from the source to the sensor, plus an odd multiple of half a wavelength, is equal to the path length $\sqrt{r^2+4x^2}$ of sound waves reflected against the side plate. The centre frequency at which the error occurs is $f_{error} = \frac{n-0.5}{\sqrt{r^2+4*x^2}-r}c$ (where $n = 1$, 2, 3, etc.). For the test with a sample the exact degree and frequency of the deviation is hard to predict because the phase and amplitude of the reflected sound waves are altered by the sample. Yet, it can be mentioned that small deviations are found if the reflecting side plate is positioned 600 mm or further from the set-up.

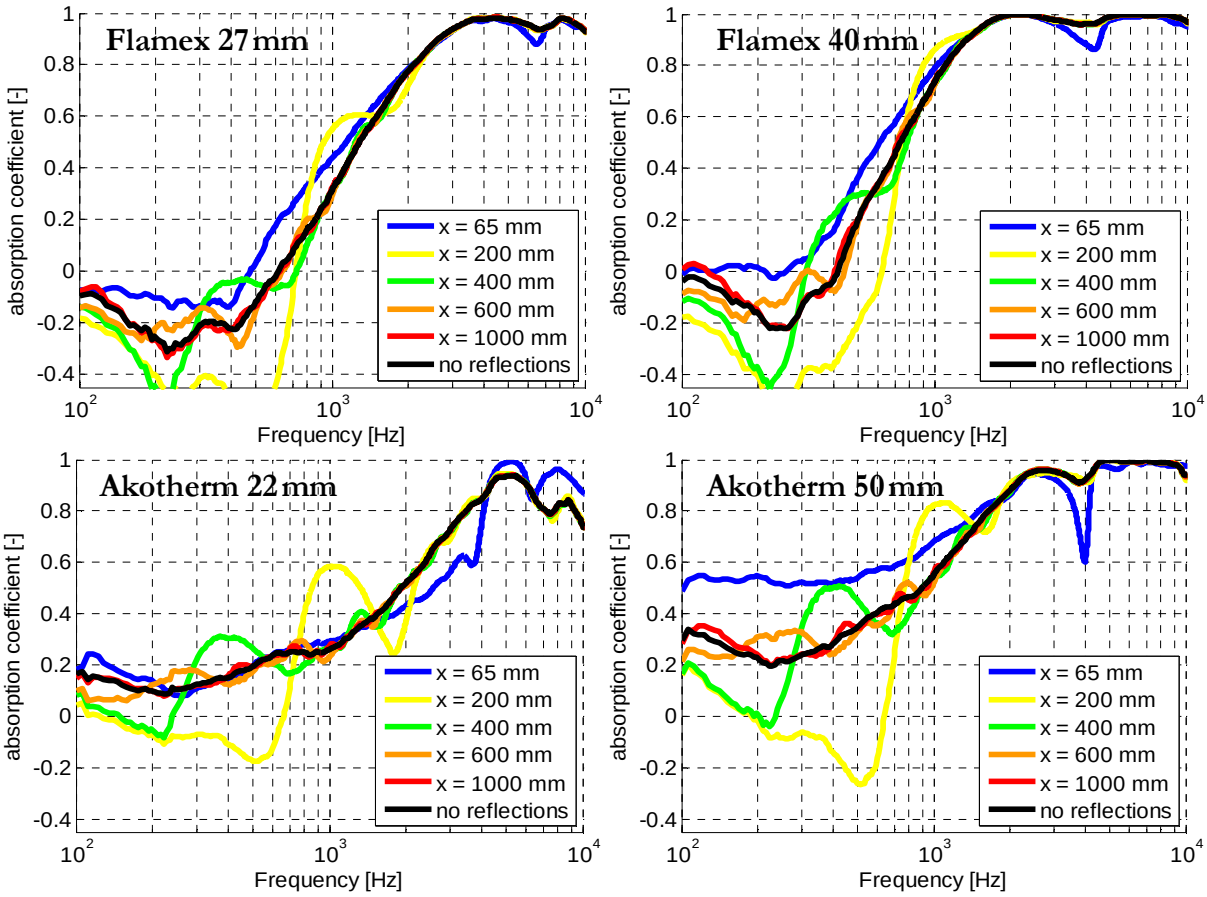

Fig. 5-11. Absorption measurements with a reflecting side plate for four samples.

5.6. *Conclusion*

Three approaches that cancel reflections have been presented. Firstly, if the surrounding objects are far from the setup, the direct sound and the reflections from the sample can be isolated from the impulse response of the sensors with a time window because they arrive earlier at the probe than reflections. Secondly, if there are multiple reflections, and if their amplitude is small compared to the direct signal, the rippling effect that reflections have on the measured frequency response can be smoothed with a moving average. Thirdly, the set-up can be moved or rotated to reduce the influence of individual reflections because of the position dependence of reflections.

These reflection-cancelling techniques may be used separately or combined. Compared to other *in situ* measurement techniques, the influence of reflections is low because the separations between the source, the probe, and the sample are kept small. However, if there are reflecting surfaces near the set-up, discrepancies can be found at frequencies where the direct sound waves and the waves that have reflected against these surfaces strongly interfere.

6. Improved models for standing waves inside acoustic samples

6.1. *Introduction*

Plane wave absorption models that use the impedance measured in a Kundt's tube are used for a long time. Modified models based on similar principles have been used frequently for tests without a tube. Usually, additional corrections for the sound field characteristics are implemented in such models. This is also the case for the previously introduced mirror source model and Q-term model. Their purpose is to correct for the spherical sound field existing because of the close proximity to a monopole sound source. However, depending on the measurement conditions, incorrect results are sometimes obtained. The discrepancies that can be found with the aforementioned models are discussed in this chapter. Results and conclusions are partially based on those reported in [73], *[114]*, and *[115]*.

As will be shown in more detail in the next sections, there are cases were artefacts of absorption models are observed because in these models only corrections for the spherical sound field above the sample are made, while plane propagation of sound waves inside the material is assumed. Consequently, even negative absorption values are found. Methods based on the combination of multiple tests are investigated to overcome this problem. An extrapolation technique is introduced to eliminate near field effects, which combines several absorption measurements using either intensity or impedance. Ultimately, the plane wave absorption coefficient can be obtained without prior knowledge of the material. The methods are examined theoretically and verified with experiments. Sections 6.3 to 6.8, and 6.10 are based on references *[116]* and *[117]* of Tijs et al.

6.2. *Negative absorption values with existing models*

Some of the problems experienced with the plane wave model, the mirror source model, and the Q-term model are investigated. Three sample types have been measured; an open melamine foam called Flamex, a dense PU foam and a linoleum floor (sample thickness 27mm, 28mm, and 2.5mm, respectively).

Measurements have been performed with a PU probe, which was positioned 5mm above the sample, and a sound source, which was placed 0.3m above the sample at normal incidence. The test results were smoothed using a moving average in the frequency domain to remove room reflections (see section 5.3). In all cases, the sample and the full reflective backplate can be considered large (>1.5m^2). The plane wave model, the mirror source model and the Q-term model are used to calculate the absorption from each test.

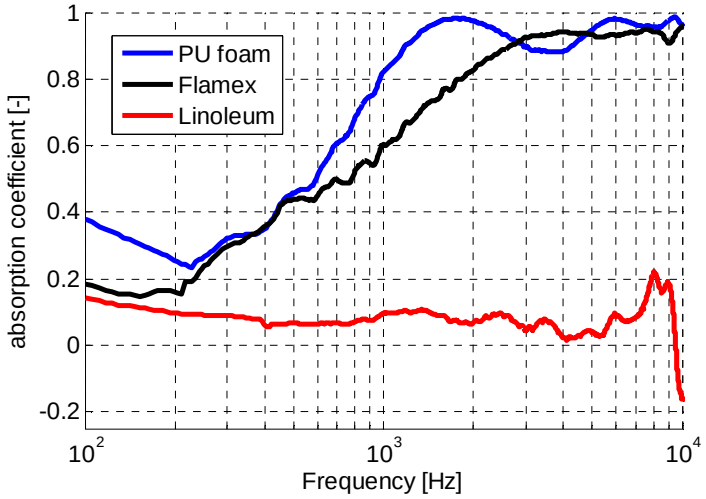

Fig. 6-1. Absorption values of three samples calculated using the plane wave model.

Fig. 6-1 shows the results obtained with the plane wave model. For most frequencies, an absorption coefficient near zero would be expected for the linoleum sample because such a thin non-porous material attenuates the sound little. Too high values are obtained (red line) because the plane wave model does not correct for the close proximity of the sound source emitting spherical waves. Also, the absorption coefficient of the PU foam and the Flamex sample (blue and black line) are expected to be near zero at low frequencies because these samples are thin compared to the wavelength, and because little damping occurs inside the material at those frequencies. Again, too high values are obtained with the plane wave model. Only at high frequencies, where there are fewer near field effects, the outcome of the plane wave model is valid. The absorption of such materials is expected to increase with frequency until a certain maximum is reached. The frequency at which this maximum occurs is related to the sample thickness. Subsequently, the absorption goes down and up in an oscillating manner because of interferences of sound waves inside the sample.

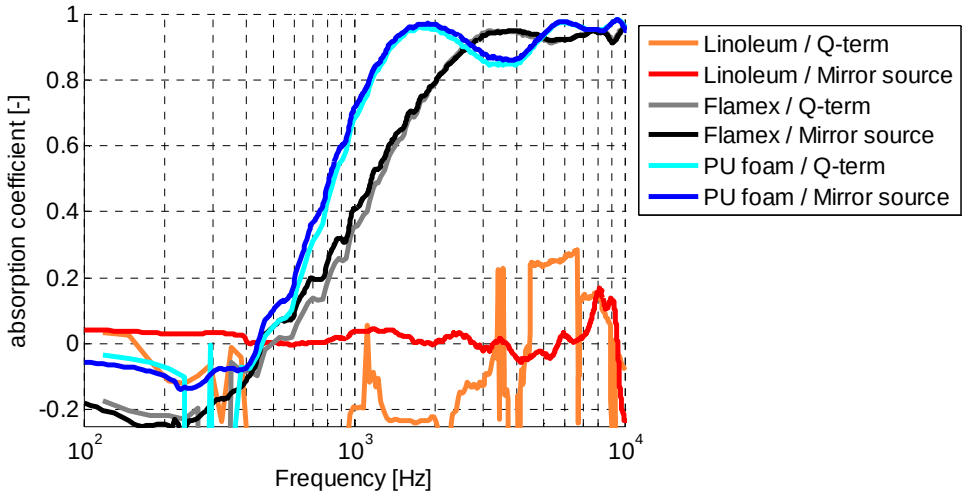

Fig. 6-2. Absorption values of three samples calculated with the mirror source model and the Q-term model.

Fig. 6-2 shows the absorption values obtained using the mirror source model and the Q-term model. The results from both methods are similar for the PU and Flamex sample. Such similarities of both models were also reported in [74], *[114]*, which is remarkable because the fundamentals of both models are rather different. However, discrepancies can be found as was also stated in *[115]*. This is apparent for the Linoleum sample for which the Q-term results are unreliable (orange line). These errors can partly be contributed to the poor signal-to-noise ratio above this low absorbing sample (the particle velocity is small), but mainly to high reactivity. In those cases, small phase inaccuracies between the sound pressure and the particle velocity signal can have profound effect. Although the Q-term model can be supposed theoretically more precise because spatial interferences effects are included, sometimes the simpler mirror source model is preferred, as it appears to be more robust. The Q-term model is based on involved integrals and an iterative procedure, which are sensitive to measurement inaccuracies.

Apart from these differences among the models, also negative absorption values are obtained below ~500Hz for the PU foam and the Flamex sample. Similar behaviour of samples was also simulated with a boundary element method by Hirosawa [62]. These negative absorption values at low frequencies are incorrect and this was one of the most interesting problems throughout the research period. Negative values have been measured on many different samples (but not all), and under many different conditions (different acoustic environments, different set-up geometries, etc.). Although magnitude and

frequency are somewhat influenced by the measurement conditions, the negative values are persistent. As will be explained in the next sections, this effect is caused by the spherical standing waves inside the sample. Similar negative values have also been found with simulations that involved a spherical sound field model, see sections 6.5 and 6.11.

6.3. *Intensity method*

6.3.1. Introduction

Another approach is used because the results from the previously mentioned absorption models were not completely convincing; from the sound pressure and particle velocity measurements the active intensity is calculated *[116]*. A measurement based on intensity seems sensible because the absorption coefficient is defined as the ratio of absorbed to incoming sound intensity. However, in practice difficulties are experienced [10]. Tests with traditional PP intensity probes [8, 117, 118] are often hampered by high pressure-intensity index ratios. Techniques combining intensity and sound energy have also been attempted [120]. None of these methods compensates for near field effects caused by a point source above a sample.

The procedure to interpret the measurements in terms of the real part of intensity seems straightforward, yet near field effects in the spherical waves complicate the matter and have to be considered. An extrapolation technique is introduced, which combines several intensity measurements with varying sound source - probe distances. The test procedure and the extrapolation method will be explained, and they are investigated theoretically and experimentally. Acoustic absorbing samples can be installed in several ways and this affects the eventual absorption coefficient measured by the set-up. Therefore, sample conditions with a backplate (a typical assumption for e.g. cars), and without a backplate (typical for e.g. office walls), are analysed.

6.3.2. Description of the experiments

A spherical piston-on-a-sphere sound source has been used to measure three arrangements (fig. 6-3). I_0 corresponds to the normal intensity measured from the sound source at distance r, and is used as the calibration of the sensors under free field conditions. I_1 is the intensity at a distance h above the sample

with a rigid full reflecting backplate. I_2 and I_3 are measured in front and behind a sample without a backplate, respectively.

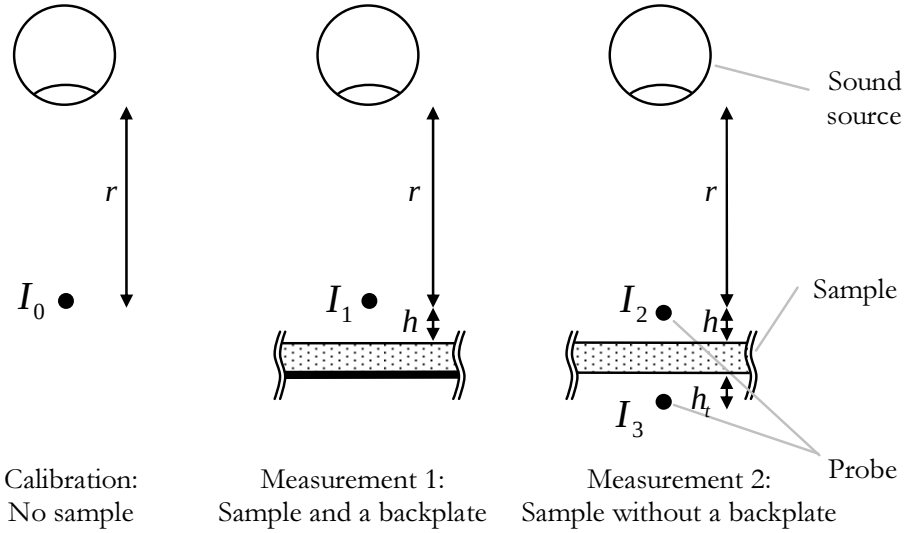

Fig. 6-3. Three measurement arrangements.

The sound field above a sample can be highly reactive, especially if the reflection is high, which affects the intensity measurement. The sound source distance r was varied from 25mm to 625mm in 25mm steps. Distance h and h_t were both 5mm. The same three samples were tested; the Flamex sample, the PU foam and the linoleum floor.

The impedance, which is the ratio of sound pressure to particle velocity, is unaffected by a changing source strength. With a method based on intensity the source strengths between measurement I_0 and I_1 could differ, especially if there are strong early reflections in measurement I_1. However, the effect of reflections is small because of the short source-probe distance.

6.3.3. Physical model

The absorption coefficient is defined as the ratio of the normal absorbed to normal incident sound intensity. The intensity should actually be integrated across a surface to avoid local deviations and to obtain the random incidence absorption coefficient. This means that a large surface area should be measured at multiple points for each probe-source distance while keeping the sound source at a fixed position and the probe orientated towards the surface. However, a scan across a large surface area can be impractical.

The probe was placed at a single position above the sample surface only during these experiments, while the sound source was placed at normal incidence. Hence, under these conditions near field effects have to be considered.

Here, $\alpha_{\mathrm{nf},I}$ is defined as the measured ratio of normal absorbed to normal incident intensity without correction for near field effects. In the measurement of I_1 (the test with a sample and a backplate), no transmission through the sample is assumed because of the impenetrable backplate behind the sample, and $\alpha_{\mathrm{nf},I1}$ can be calculated from *[117]*:

$$\alpha_{\mathrm{nf},I1} = \frac{\mathrm{Re}\left(I_{\mathrm{incident}} - I_{\mathrm{reflected}}\right)}{\mathrm{Re}\left(I_{\mathrm{incident}}\right)} = \frac{\mathrm{Re}\left(I_1\right)}{\mathrm{Re}\left(I_0\right)} \qquad (6\text{-}1)$$

Intensity I_1 is the sum of the incident and the reflected intensity normal to the sample surface (the latter with a negative sign because it is directed in the opposite direction of I_0). Because of the small size of the PU probe used during these experiments, h could be small compared to r and the wavelength, and for reasons of simplicity, h is assumed zero. If other types of intensity probes had been used for such a test, h would have been larger because such probes are larger. In that case h should be considered, although the impact of a larger value of h on the results is not investigated here.

The absorption coefficients of a sample with and without a backplate are different. With incident intensity I_0, and intensity I_3 behind the sample, the intensity transmission coefficient $T_{\mathrm{nf},I3}$ can be calculated:

$$T_{\mathrm{nf},I3} = \frac{\mathrm{Re}(I_{\mathrm{transmitted}})}{\mathrm{Re}\left(I_{\mathrm{incident}}\right)} = \frac{\mathrm{Re}\left(I_3\right)\left(\dfrac{r+d+h+h_t}{r}\right)^2}{\mathrm{Re}\left(I_0\right)} \qquad (6\text{-}2)$$

The transmitted intensity $I_{\mathrm{transmitted}}$ is determined from the measured intensity I_3 using a correction factor for the extra distance $d+h+h_t$ from the source because this extra distance cannot be assumed small compared to r.

With the intensity I_2 in front of the sample, and (corrected) intensity I_3 behind the sample, absorption $\alpha_{\mathrm{nf},I2}$ can be calculated:

$$\alpha_{\mathrm{nf},I2} = \frac{\mathrm{Re}(I_{\mathrm{incident}} - I_{\mathrm{reflected}}) - \mathrm{Re}(I_{\mathrm{transmitted}})}{\mathrm{Re}(I_{\mathrm{incident}})} = \frac{\mathrm{Re}(I_2) - \mathrm{Re}(I_3)\left(\frac{r+d+h+h_t}{r}\right)^2}{\mathrm{Re}(I_0)} \quad (6\text{-}3)$$

The measurement of I_0 can be used to calibrate the intensity probe if the specific impedance during this test is known. A loudspeaker inside a spherical housing is chosen because the impedance in front of the source can be described, and because it has a higher radiation efficiency than a point source. In [89] this type of sound source was modelled as a moving piston on a rigid sphere, and a description of the impedance in front of the sphere was given. With the existing source and set-up dimensions the phase between sound pressure and particle velocity as calculated with the piston-on-a-sphere model and with a monopole model are similar; a maximum ± 1.9 degree deviation occurs in a 10Hz-10kHz band ($r > 0.1$m). Therefore, the equations for a point source can be used instead of the piston-on-a-sphere expressions.

6.4. *Sound field reactivity*

In a similar way as for the impedance, the intensity, which is related to the energy flow, is also complex. Sound pressure and particle velocity are out of phase and there can be strong near field effects. Intensity measurements with PU probes become less accurate in reactive sound fields. In [13] it was mentioned that in practical situations the error would increase significantly if the imaginary part of the intensity exceeds the real part of the intensity with more than 5dB, which corresponds to a phase of ± 72 degrees between sound pressure and particle velocity. This 5dB or ± 72 degrees boundary is also used as limit here for the intensity measurements to be valid. Fig. 6-4 shows the free field phase and the measured phase for the three samples with a backplate.

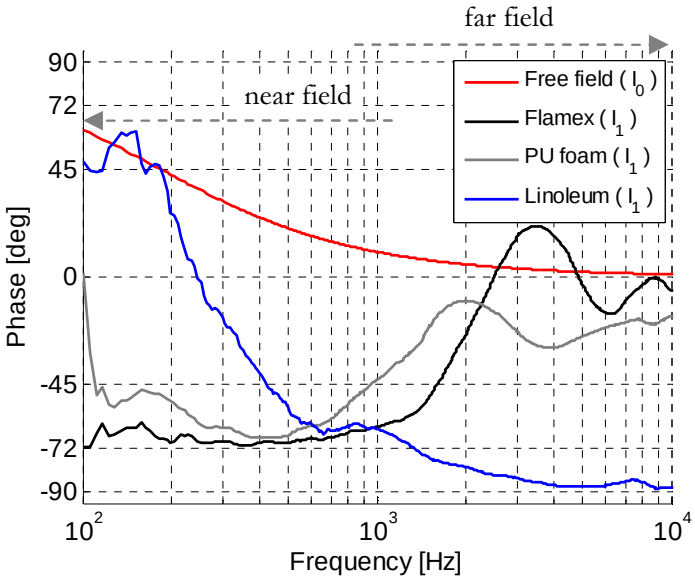

Fig. 6-4. Phase between sound pressure and particle velocity near three samples and under free field conditions (r=0.3m).

As can be seen in fig. 6-4 the reactivity is low during the calibration measurement I_0 (red line), and the phase remains between ± 72 degrees. The reactivity can be higher near the samples. The error of the intensity measurement increases in such situations. Fig. 6-5 shows the phase of the separate incoming wave (I_0) and the reflected waves ($I_{\text{sample}} - I_0$) for tests near three samples.

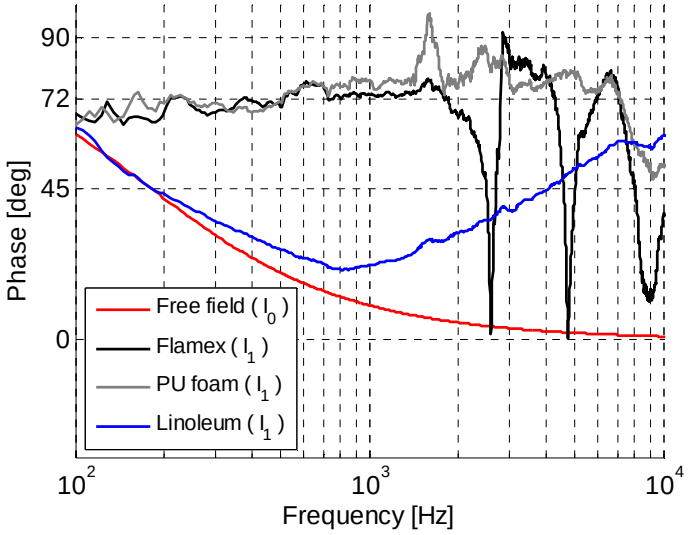

Fig. 6-5. Phase between sound pressure and particle velocity of the reflected intensity and under free field conditions (r=0.3m).

6.5. *Model incorporating travelling spherical waves inside the sample*

Apart from the tests, a spherical sound field model is used to simulate the pressures and velocities above and inside a sample to show that the measurement procedure that will be introduced does not produce negative absorption values. Contrary to a condition with plane waves a short elegant analytical expression is not found. Spherical waves complicate the matter and also the complex material impedance and wavenumer have to be taken into account. Instead, a model based on the summation of individual travelling waves, some reflected at the top surface and some travelling through the sample several times, is used. A near field correction is made for each successive travelling wave. As input for the simulations the complex material wavenumber and surface impedance are derived from the Delany and Bazley equations (section 2.4). Other, more sophisticated material models, might be used for such simulations as well.

Some sound reflects directly at the top surface of a sample due to the impedance change at the air-sample interface. A portion also penetrates through the surface. Inside the sample there is some degree of absorption. Depending on the medium behind the sample a part of the sound is reflected back towards the receiver. The portion that is not reflected at the air-sample interface contributes to the measured sound pressure and particle velocity. The reflected part might be absorbed, reflected against the back of the sample, and so forth... The result is a standing wave inside the sample of which the components that transmit through the top surface contribute to the sound pressure and particle velocity above the surface.

Let us concider fig. 6-6. Wave 1 travels from sound source S towards the sample. At the air-sample interface at $z = 0$ this wave is partly reflected as wave 2, and partly transmitted into the sample, i.e. wave 3. At the bottom of the sample, wave 3 is partly transmitted, i.e. wave 4, and partly reflected, i.e. wave 5. The fraction of transmitted and reflected portions of the waves depends on the impedance of the medium behind the sample. If a backplate is present there is no transmission and thus waves 4, 8, etc. are zero.

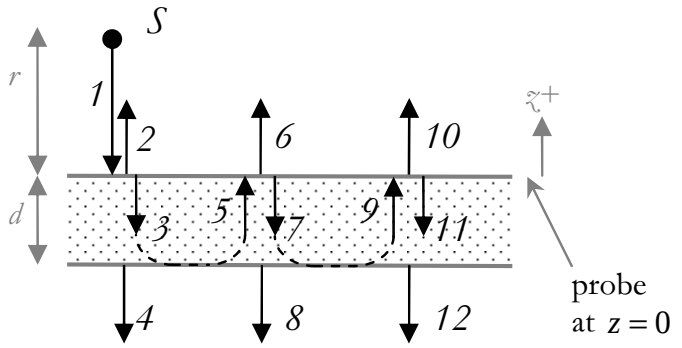

Fig. 6-6. Illustration of individual travelling waves in vertical direction.

Waves numbered 1, 2, 6, 10, etc. contribute to the measured sound pressure and particle velocity above the sample. Depending on whether a full reflecting backplate is present behind the sample, there is some degree of transmission through the sample as well.

An approximate interface model is made for the reflected and transmitted sound pressure and particle velocity at the air-sample impedance boundary, which involves a monopole source at position r and its reflection represented as a mirror source at $-r$. The equation for the continuity of sound pressure can then be written as [4, p. 127]:

$$\frac{p_{\text{in}}}{r}e^{-ik_0 r} + \frac{p_{\text{r}}}{r}e^{-ik_0 r} = \frac{p_{\text{t}}}{r}e^{-ik_1 r} \qquad (6\text{-}4)$$

where p_{in}, p_{r}, and p_{t} are respectively the incoming, the reflected, and the transmitted sound pressure, and k_1, k_0 are the complex wavenumber of the sample and the air respectivily. The continuity equation for particle velocity at the interface can be formulated in terms of sound pressures by involving a correction for the impedance of spherically propaging waves [4, p. 127]:

$$\frac{p_{\text{in}}}{Z_0 r}\left(1+\frac{1}{ik_0 r}\right)e^{-ik_0 r} - \frac{p_{\text{r}}}{Z_0 r}\left(1+\frac{1}{ik_0 r}\right)e^{-ik_0 r} = \frac{p_{\text{t}}}{Z_1 r}\left(1+\frac{1}{ik_1 r}\right)e^{-ik_1 r} \qquad (6\text{-}5)$$

where Z_1, Z_0 are the complex impedance of the sample and the air respectivily. Z_1, Z_0, k_1, and k_0 can for instance be obtained from material models like those from Delany and Bazley (see section 2.4).

Assuming that $p_r = R_{01} p_i$ and $p_t = T_{01} p_i$, the reflection R_{01} and transmission T_{01} for a sound wave propagating from the air towards the sample are obtained by combining equation 6-4 and 6-5:

$$R_{01} = \frac{x-1}{x+1} \quad (6\text{-}6) \qquad T_{01} = e^{-ir(k_0-k_1)} \frac{2x}{x+1} \quad (6\text{-}7)$$

with x being:

$$x = Z_1\left(1+\frac{1}{ik_0 r}\right) \Big/ Z_0\left(1+\frac{1}{ik_1 r}\right) \quad (6\text{-}8)$$

For a sound wave propagating from the sample towards the air the reflection R_{10} and transmission T_{10} are:

$$R_{10} = \frac{1-x}{1+x} \quad (6\text{-}9) \qquad T_{10} = e^{-ir(k_0-k_1)} \frac{2}{x+1} \quad (6\text{-}10)$$

The ingoing sound pressure p_1 and normal particle velocity u_1 at distance r from a monopole are [4, p. 127]:

$$p_1 = p_0 \frac{e^{-ik_0 r}}{r} \quad (6\text{-}11) \qquad u_1 = p_1\left(1+\frac{1}{ik_0 r}\right)/\rho c \quad (6\text{-}12)$$

where p_0 is the amplitude that is related to the strength of the monopole, ρ is the density of air and c is the speed of sound in air. Sound pressure p_2 and particle velocity u_2 of the first reflection at the sample surface are:

$$p_2 = p_1 R_{01} \quad (6\text{-}13) \qquad u_2 = -u_1 R_{01} \quad (6\text{-}14)$$

P and U above a sample

The contribution of a wave going a times through the sample to the sound pressure and the normal particle velocity above the sample are:

$$p_{(4a+2)} = p_0 \frac{e^{-ik_0 r}}{r+2ad} T_{01} R_{12}^{a} R_{10}^{a-1} e^{-2aik_1 d} T_{10} \qquad (6\text{-}15)$$

$$u_{(4a+2)} = -p_{(4a+2)} \left(1 + \frac{1}{ik_0 (r+2ad)} \right) / \rho c \qquad (6\text{-}16)$$

where R_{12} is the reflection coefficient at the backside of the sample, which is equal to one if there is a backplate, and equal to R_{10} if there is no backplate. The measured sound pressure p_{m} and particle velocity u_{m} just above the sample (probe height $h = 0$) is the summation of the ingoing wave, the initial reflection and all the contributions of the waves that went through the sample:

$$p_{\mathrm{m}} = p_1 + p_2 + \sum_{a=1}^{\infty} p_{(4a+2)} \qquad (6\text{-}17)$$

$$u_{\mathrm{m}} = u_1 + u_2 + \sum_{a=1}^{\infty} u_{(4a+2)} \qquad (6\text{-}18)$$

Simulations revealed that sound waves that are reflected more than 6 times between the backside of the sample and the top surface contribute little to the measured sound pressure and particle velocity above the sample. Twenty travelling waves are included for safety for the simulations as they are done in this thesis.

P and U behind a sample without a backplate

Behind the sample there are only sound waves that have travelled through it. The measured sound pressure and particle velocity are the summation of:

$$p_{4a} = p_0 \frac{e^{-ik_0 h}}{r+2ad-d} T_{01} \left(R_{10}^{a-1} \right)^2 e^{-ik_1 d(1+2a)} T_{10} \qquad (6\text{-}19)$$

$$u_{4a} = -p_{4a} \left(1 + \frac{1}{ik_0 (r+2ad-d)} \right) / \rho c \qquad (6\text{-}20)$$

Plane wave simplification

A different near field correction is applied for each sound wave that travels one or multiple times through the sample. An exact solution is therefore not easily found for spherical waves. Yet, an exact solution can be obtained for plane waves by treating each successive wave as part of an infinite series. If r approaches infinity, x can simply be replaced by the characteristic material impedance $Z_{\mathrm{c,n}}$ ($=\rho c \cdot Z_1 / Z_0$). The measured impedance Z_{m} in front of the sample with a backplate becomes:

$$Z_{\mathrm{m}} = Z_{\mathrm{c,n}} \frac{1+e^{-2ik_1 d}}{1-e^{-2ik_1 d}} = -iZ_{\mathrm{c,n}} \cot\left(k_1 d\right) \qquad (6\text{-}21)$$

The expression $-iZ_{\mathrm{c,n}} \cot\left(k_1 d\right)$ is often found in literature [18], [4, p. 273]. Without the backplate the impedance in front of the sample is:

$$Z_{\mathrm{m}} = Z_{\mathrm{c,n}} \frac{1+e^{-2ik_1 d}\,\dfrac{\rho c - Z_{\mathrm{c,n}}}{\rho c + Z_{\mathrm{c,n}}}}{1-e^{-2ik_1 d}\,\dfrac{\rho c - Z_{\mathrm{c,n}}}{\rho c + Z_{\mathrm{c,n}}}} = Z_{\mathrm{c,n}} \frac{iZ_{\mathrm{c,n}} \tan\left(k_1 d\right) + \rho c}{i \tan\left(k_1 d\right)\rho c + Z_{\mathrm{c,n}}} \qquad (6\text{-}22)$$

This is consistent to the solution found in [4, p. 153]. The ratio of the measured sound pressures $p_{\mathrm{m,2}}$ in front and $p_{\mathrm{m,3}}$ behind the sample depends on the characteristic impedance and wavenumber of the material:

$$\frac{p_{\mathrm{m,2}}}{p_{\mathrm{m,3}}} = \frac{Z_{\mathrm{c,n}} + \rho c}{2e^{-jk_1 d}} - e^{-jk_1 d}\,\frac{Z_{\mathrm{c,n}} - \rho c}{2} \qquad (6\text{-}23)$$

6.6. $a_{\mathrm{nf},I}$ and $T_{\mathrm{nf},I}$ at several distances

From the measurements of sound pressure and particle velocity, the real part of intensities I_1, I_2 and I_3 are calculated and divided by the real part of the intensity I_0, see equation 6-1 to 6-3. It vanishes from these equations if the source strength is kept constant. The intensity is measured in three arrangements (as shown in fig. 6-3) and the reflection-, absorption- and transmission coefficients are calculated. A moving average in the frequency domain is used

to cancel early room reflections (see section 5.3). Tests have been performed for several distances of r (fig 6-7). As is mentioned previously, there are near field effects during these individual measurements. Later, in section 6.8, a procedure will be presented which combines several of these tests in order to estimate the values of $\alpha_{\mathrm{nf},I}$ and $T_{\mathrm{nf},I}$ for $r \to \infty$.

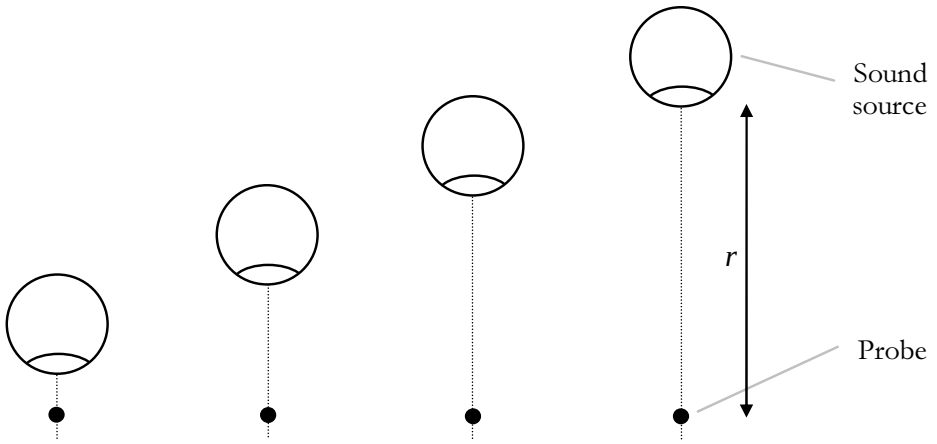

Fig. 6-7. For each configuration (i.e. with or without a sample and with or without a backplate), measurements have been performed for several values of r.

Simulated results from the spherical model described in section 6.5 are shown next to the figures with test results. It can be seen that the results from the measurements and the simulations are affected by near field effects in a similar way. The spherical model uses a summation of travelling waves inside the sample. The variables from the Delany and Bazley equations are used as input and a sample thickness of 27 mm (equal to that of the Flamex sample) and a flow resistivity of 25 kPa·s/m^2 are used. The valid frequency range of the Delany and Bazley model depends on the flow resistivity, which is in this case 250 Hz to 25 kHz. The results from the simulations can appear similar to the measured values on the Flamex sample, but this is merely a coincidence.

6.6.1. With backplate (I_0 and I_1)

Fig. 6-8 shows $\alpha_{\mathrm{nf},I1}$ of the Flamex sample with backplate and the simulations. The dotted parts of the lines are the frequencies where the phase exceeded ± 72 degrees. The reactivity is mainly high at low frequencies and increases for larger sound source distances.

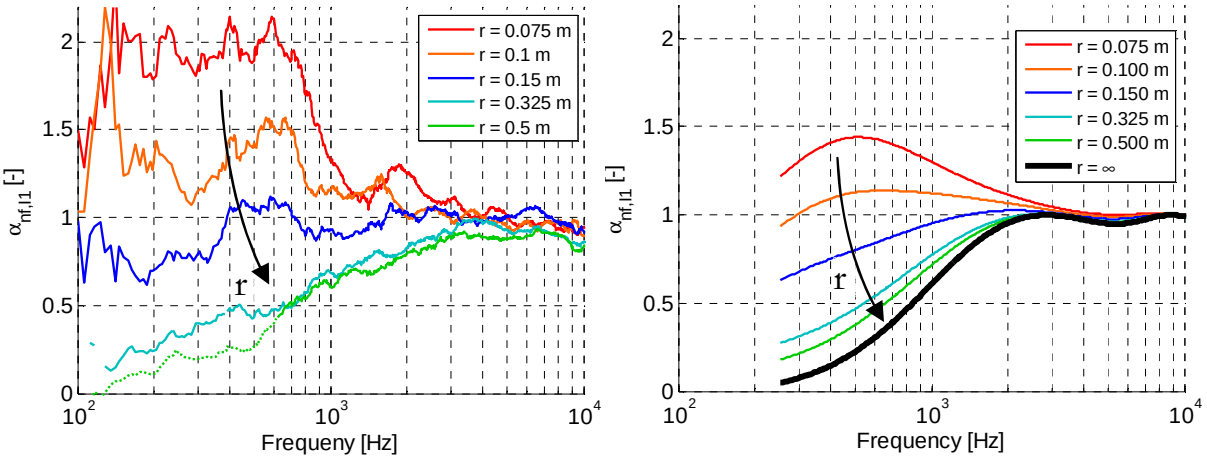

Fig. 6-8. $\alpha_{\mathrm{nf},I1}$ **in front of a sample with a backplate. Left: Flamex measured. Right: simulated.**

Strong near field effects occur, especially for small distances of r, and the measured 'absorption' $\alpha_{\mathrm{nf},I1}$ even exceeds one. Therefore, a correction for these near field effects needs to be applied.

6.6.2. Without backplate (I_0, I_2 and I_3)

The intensity transmission and absorption of the same sample without a backplate are calculated using measurement I_2 in front and I_3 behind the sample. The absorption is different from the situation with plate because the boundary conditions of the sample have changed. The results are shown in fig. 6-9 to 6-11.

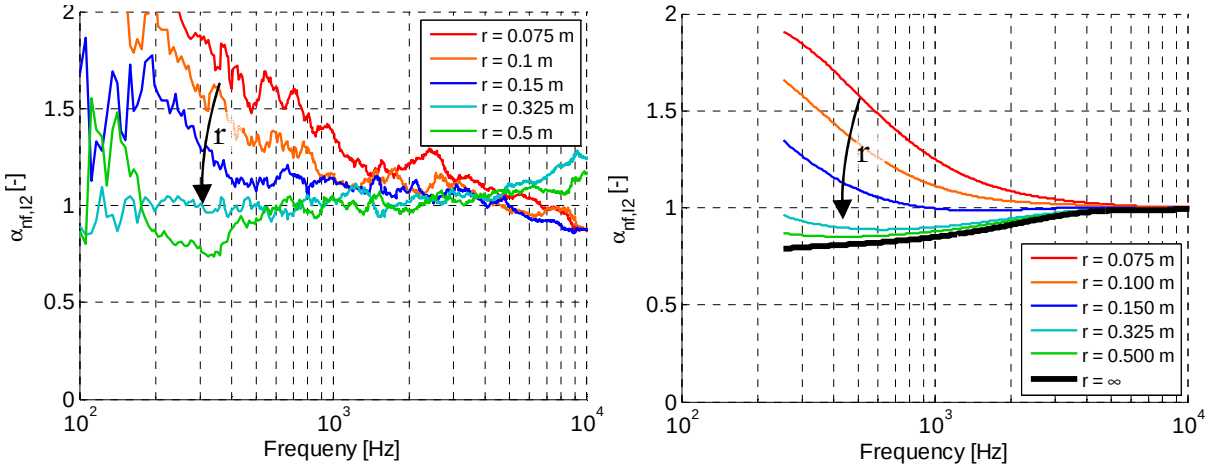

Fig. 6-9. $\alpha_{\mathrm{nf},I2}$ **for several values of** r**. Left: Flamex measured. Right: simulated.**

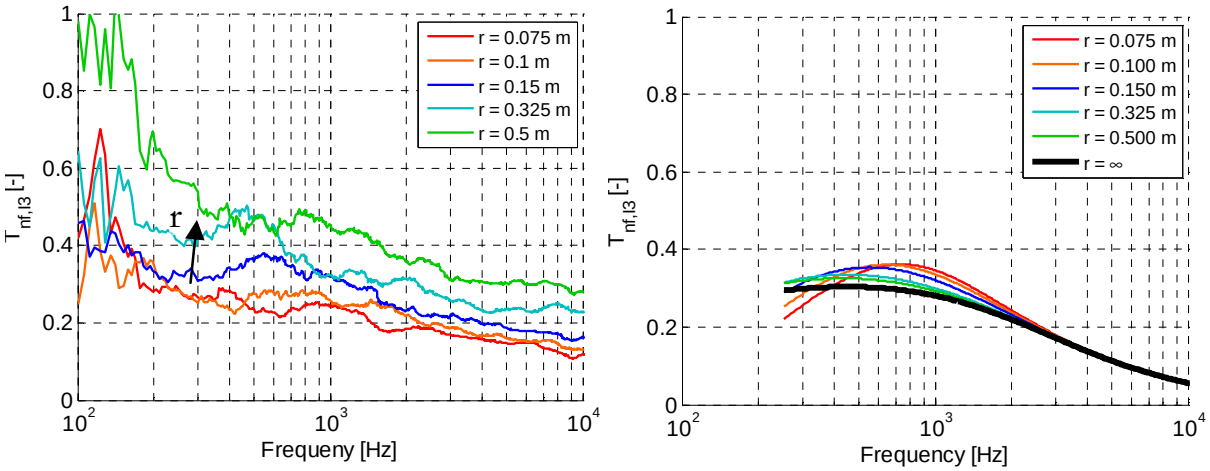

Fig. 6-10. Intensity 'transmission' $T_{\mathrm{nf},I3}$. Left: Flamex measured. Right: simulated.

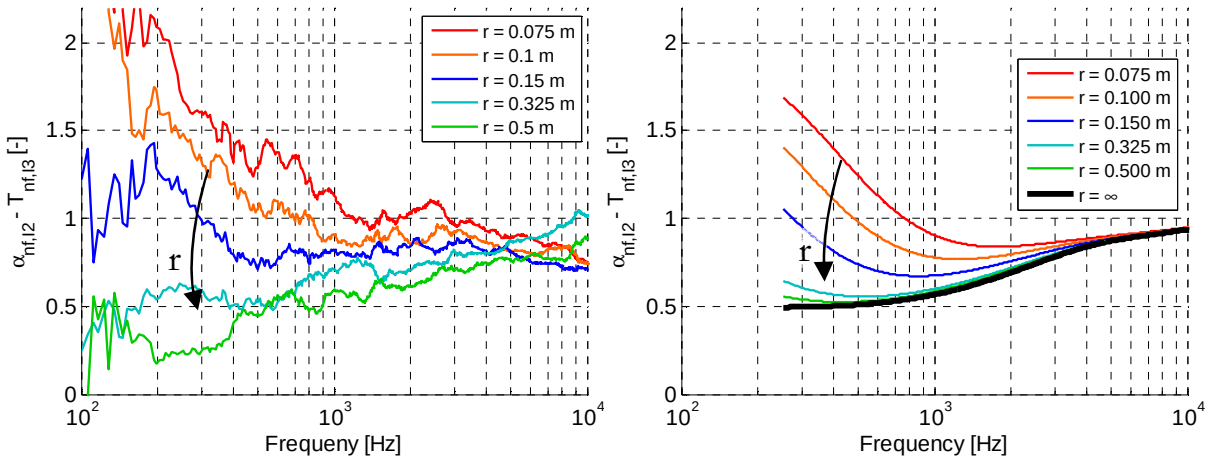

Fig. 6-11. 'Absorption' without a backplate $\alpha_{\mathrm{nf},\_I2}$ - $T_{\mathrm{nf},I3}$. Left: Flamex measured. Right: simulated.

Again intensity values larger than one are measured, especially with $\alpha_{\mathrm{nf},I2}$. Additionally, $\alpha_{\mathrm{nf},I2} - T_{\mathrm{nf},I3}$, which is related to the absorption, does not tend to go to zero at low frequencies as was the case for the sample with a backplate.

6.7. *Physical interpretation of the results*

6.7.1. a_{nf}: Reflected- exceeding the incoming intensity

The following example shows that the ratio of intensities above the sample can exceed one if there are near field effects. The intensity in the situation without reflections is calculated.

The ingoing sound pressure and normal particle velocity of the ingoing spherical sound wave are [4, p. 127]:

$$p_{\text{in}}(r) = p_0 \frac{e^{-ik_0 r}}{r} \qquad (6\text{-}24) \qquad \left| \qquad u_{\text{in}}(r) = p_{\text{in}}\left(1 + \frac{1}{ik_0 r}\right)/\rho c \qquad (6\text{-}25)$$

Hence, the complex time-averaged normal intensity of the ingoing sound wave can be written as:

$$I_{\text{in}}(r) = \frac{1}{2} p_{\text{in}} u_{\text{in}}^{*} = \frac{p_0^2}{2\rho c}\left\{\frac{e^{-ik_0 r}}{r}\right\}\left\{\frac{e^{ik_0 r}}{r}\left(1 + \frac{i}{k_0 r}\right)\right\} = \frac{p_0^2}{2\rho c r^2}\left(1 + \frac{i}{k_0 r}\right) \qquad (6\text{-}26)$$

The description of the sound field due to a monopole above a sample requires rather involved mathematics because interferences occur inside the sample. However, the reflected wave from a monopole above the surface can be approximated by a reflected monopole because only perpendicular reflection is of interest. When that the distance between the probe and the sample is small compared to r, the wavelength the complex time-averaged normal intensity above the sample can be written as:

$$I(r) = I_{\text{in}}(r)\left\{1 - R_{\text{s}}^2\right\} \qquad (6\text{-}27)$$

where R_{s} is the complex spherical reflection coefficient.

The total intensity cannot be higher than I_{in} if R_{s} is real. However, this is not necessarily the case if R_{s} is complex:

$$\begin{aligned} I(r) &= \frac{p_0^2}{2\rho c r^2}\left(1 + \frac{i}{k_0 r}\right)\left\{1 - \left(R_{\text{s,r}} + iR_{\text{s,i}}\right)^2\right\} \\ &= \frac{p_0^2}{2\rho c r^2}\left[\left(1 - {R_{\text{s,r}}}^2 + {R_{\text{s,i}}}^2 + \frac{2R_{\text{s,r}}R_{\text{s,i}}}{k_0 r}\right) + i\left(\frac{1 - {R_{\text{s,r}}}^2 + {R_{\text{s,i}}}^2}{k_0 r} - 2R_{\text{s,r}}R_{\text{s,i}}\right)\right] \end{aligned} \qquad (6\text{-}28)$$

The measured active intensity is the real part of equation 6-28:

$$\begin{aligned}\mathrm{Re}\{I(r)\} &= \frac{p_0^2}{2\rho c r^2}\left[1 - {R_{\mathrm{s,r}}}^2 + {R_{\mathrm{s,i}}}^2 + \frac{2R_{\mathrm{s,r}}R_{\mathrm{s,i}}}{k_0 r}\right] \\ &= \frac{p_0^2}{2\rho c r^2}\left[1 - |R_{\mathrm{s}}|^2\left\{2\cos^2(\phi_{\mathrm{Rs}}) - 1 - \frac{\sin(2\phi_{\mathrm{Rs}})}{k_0 r}\right\}\right]\end{aligned} \qquad (6\text{-}29)$$

where ϕ_{Rs} is the phase-angle of the complex reflection coefficient R_{s}. Note that $|R_{\mathrm{s}}| \leq 1$, and therefore, when $\phi_{\mathrm{Rs}} = 0$, R_{s} is real and the factor in square brackets is ≤ 1.

The ratio of absorbed to ingoing intensity α_{nf} is plotted in fig. 6-12 for several values of $|R_{\mathrm{s}}|$ and ϕ_{Rs}. The values of α_{nf} can be higher than one (and this does not correspond to negative absorption!).

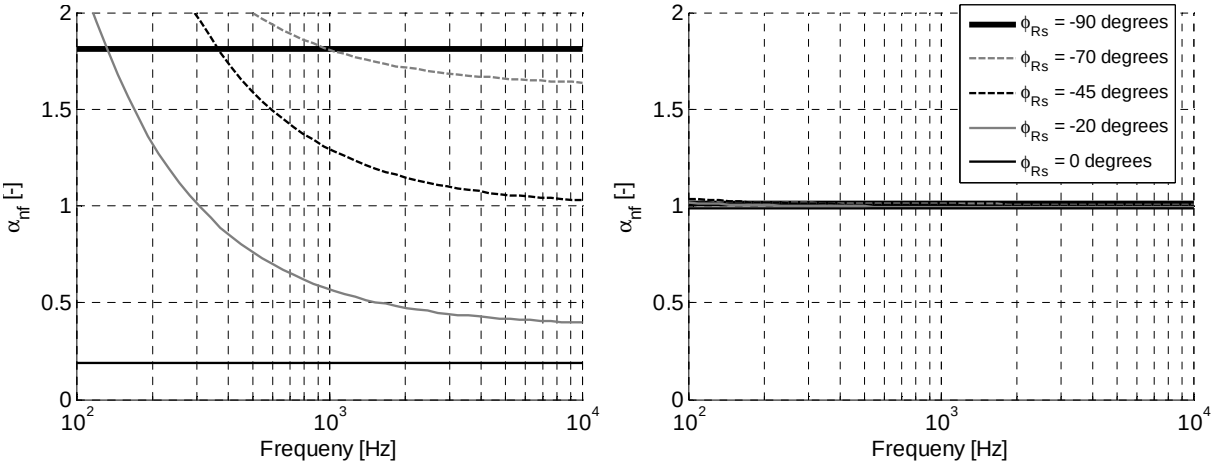

Fig. 6-12. α_{nf} for several phase angles.

6.7.2. High values of $a_{\mathrm{nf},I2}$-$T_{\mathrm{nf},I3}$ relative to $a_{\mathrm{nf},I1}$

At first sight, the high values of $\alpha_{\mathrm{nf},I2} - T_{\mathrm{nf},I3}$ without a backplate even at larger source-probe distances r might be a surprise. Such high 'absorption' values at low frequencies seemed counterintuitive for a thin sample without a backplate. These high values are caused by the interference of secondary reflections that went through the sample.

Let us consider a similar situation as in section 6.5 where the reflection from a sample was modelled by individual travelling waves of which some reflected at the top surface and some travelled through the sample several times. Fig. 6-13 shows a sketch of several successive travelling waves for a sample without a backplate. At each air-sample boundary there is a reflection. Expressions for the plane wave reflection and transmission at an impedance boundary for medium A and B can be found in most textbooks, see [4, p. 151]:

$$R = \frac{Z_A - Z_B}{Z_A + Z_B} \qquad (6\text{-}30) \qquad T = \frac{2Z_A}{Z_A + Z_B} \qquad (6\text{-}31)$$

Wave 2 is the portion of wave 1 that is reflected directly at the top surface. Typically the sample impedance is higher than that of the air, thus for a wave going from the air towards the sample the reflection is positive; $R = \left(Z_{\text{sample}} - Z_{\text{air}}\right)/\left(Z_{\text{sample}} + Z_{\text{air}}\right) \geq 0$. Since wave 2 travels in opposite direction from wave 1 it decreases the intensity above the surface. Wave 1 also partially penetrates through the top surface. This transmitted wave is damped to some degree, and is then partially reflected against the bottom of the sample because of the impedance transition. The crux is that for a sound wave travelling from inside the sample towards the air a *negative* reflection occurs; $R = \left(Z_{\text{air}} - Z_{\text{sample}}\right)/\left(Z_{\text{air}} + Z_{\text{sample}}\right) \leq 0$. This means that the phase between sound pressure and particle velocity of the reflected wave is shifted 180 degrees. Wave 6, which has travelled through the sample one time, instead of being destructive, increases the intensity above the surface because of the negative reflection. Other examples where a negative reflection is observed are the end of an open pipe, or a sound wave travelling from under water towards the air. Also, each successive wave (10, 14, 18, etc.) has a positive contribution to the intensity above the sample as the sound wave is always reflected at the sample-air interface at multiples of two (at the top and at the bottom of the sample). All the positive contributions elevate the intensity above the sample at the probe position and increase the 'absorption coefficient' that is measured.

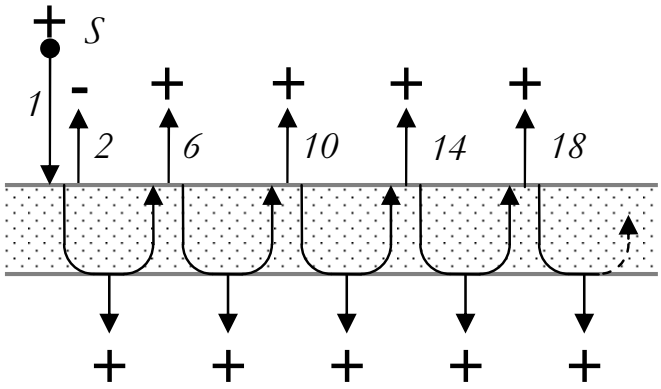

Fig. 6-13. Sample without plate: travelling waves from source *S* in vertical direction.

As there is no direct contribution of wave 1 only the virtual sources from wave 4, 8, 12, etc. contribute to the intensity behind the sample. Their virtual sources all have a positive sign (fig. 6-13) because there is always a negative reflection at multiples of two (at the top *and* at the bottom of the sample).

Now if a sample with a backplate would be studied a different pattern is observed. There is no negative reflection at the back of the sample because of the backplate. Waves that went through the sample are constructive and destructive in turn because there is only a negative reflection at the top surface and not at the bottom fig. 6-14. These positive and negative contributing travelling waves partially cancel each other. The impedance of the Flamex sample at lower frequencies is high and the damping low, which results in a lower absorption compared to the same sample without a backplate.

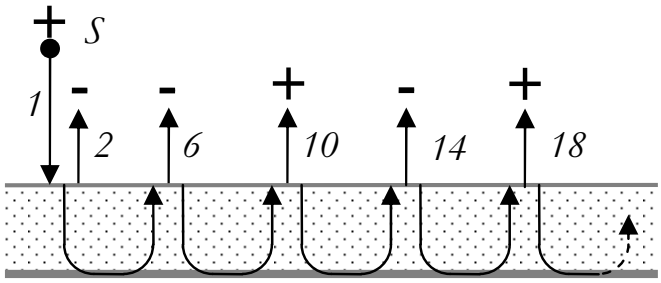

Fig. 6-14. Sample with a backplate: travelling waves from source *S* in vertical direction.

6.8. *Extrapolation of $a_{nf,I}$ at several distances*

6.8.1. Extrapolation principle

$\alpha_{\mathrm{nf},I}(r=\infty)$ should be available in order to predict the radiated sound energy in the far field. The reflection, transmission, and damping inside the sample have to be known to estimate this value from the individual tests ($r=0.1\,\mathrm{m}$, 0.2m, etc.), and a complex, detailed model should be worked out. This is complicated, whereas also a number of assumptions of the physical process have to be made.

An alternative procedure is to extrapolate the obtained values of $\alpha_{\mathrm{nf},I}(r)$ to the value $\alpha_{\mathrm{nf},I}(r=\infty)$. The basic idea of the extrapolation principle introduced here is that near field effects affect the measured ratio of absorbed to incoming intensities $\alpha_{\mathrm{nf},I}$ at a certain distance. The measured $\alpha_{\mathrm{nf},I}$ at a certain distance is expressed as the true absorption α plus a near field term.

An exact relation between $\alpha_{\mathrm{nf},I}$ and the height of the sound source is hard to find because of the complicated interactions of sound waves above and inside the sample. Several fitting functions that use a limited number of distances have therefore been investigated. The values of $\alpha_{\mathrm{nf},I}$ were simulated with the spherical model that was presented in section 6.5. The two functions of which the extrapolated results were in best agreement with the true values of $\alpha_{\mathrm{nf},I}$ are now introduced. The first function depends on the unknowns B and m:

$$\alpha_{\mathrm{nf},I}(r)=\frac{B}{r^m}+\alpha_{\mathrm{nf},I}(r\to\infty)=\frac{B}{r^m}+\alpha \qquad (6\text{-}32)$$

Measured values of $\alpha_{\mathrm{nf},I}$ from three distances r should be sufficient to solve the equation because there are three unknowns.

The reason for using this expression and not an exponential form (such as e^{-Br}) is that, apart from the wave propagation term e^{-ikr}, no exponential dependences on r are present. Equation 6-29 shows that the ratio of the intensity near the sample to the ingoing intensity strongly depends on $1/r$.

In addition, there are constants and other terms that depend on r in forms such as $1/(r+2d)$ and $1/r^2$. The total intensity contains a mixture of these terms, and therefore $B/r^m + a$ is used. The increase of I_1/I_0, such as in section 6.6, appears mainly at low frequencies where the damping of typical materials is weak, thus the virtual sources *M6*, *M10*,… become more important as there are strong near field effects.

The second extrapolation function consists of a summation of a number of C/r^n expressions:

$$\alpha_{\mathrm{nf},I}(r) = \frac{C_n}{r^n} + \ldots + \frac{C_2}{r^2} + \frac{C_1}{r} + \alpha_{\mathrm{nf},I}(r=\infty) \qquad (6\text{-}33)$$

where C is a constant and n is the expansion order of the function. Higher orders can be used as long as the number of measurement distances $\geq (n+1)$.

6.8.2. Fitting function evaluation

The previously introduced functions are used to fit $\alpha_{\mathrm{nf},I1}$. The performance of equation 6-32 and a second, third, and forth order expansion of equation 6-33 are evaluated. The values estimated with the fitting functions are compared to the values of $\alpha_{\mathrm{nf},I}$ simulated with the spherical model, which was introduced in section 6.5. The same complex impedance and wavenumber of the material are used for these simulations as in section 6.6. Fig. 6-15 shows an example of the decay of $\alpha_{\mathrm{nf},I1}$ versus r, and the curve fits for 200Hz, were strong near field effects occur, and for 1kHz. The five values of $\alpha_{\mathrm{nf},I1}$ used as input for the fitting functions are shown as black circles. It can be seen that in most cases the outcome of the fitting functions is similar to the simulated values of $\alpha_{\mathrm{nf},I}$ (black dotted line). The deviations are smallest for higher order functions. The same trend is visible in fig. 6-16 were the extrapolated values are compared to $\alpha_{\mathrm{nf},I}(r=\infty)$.

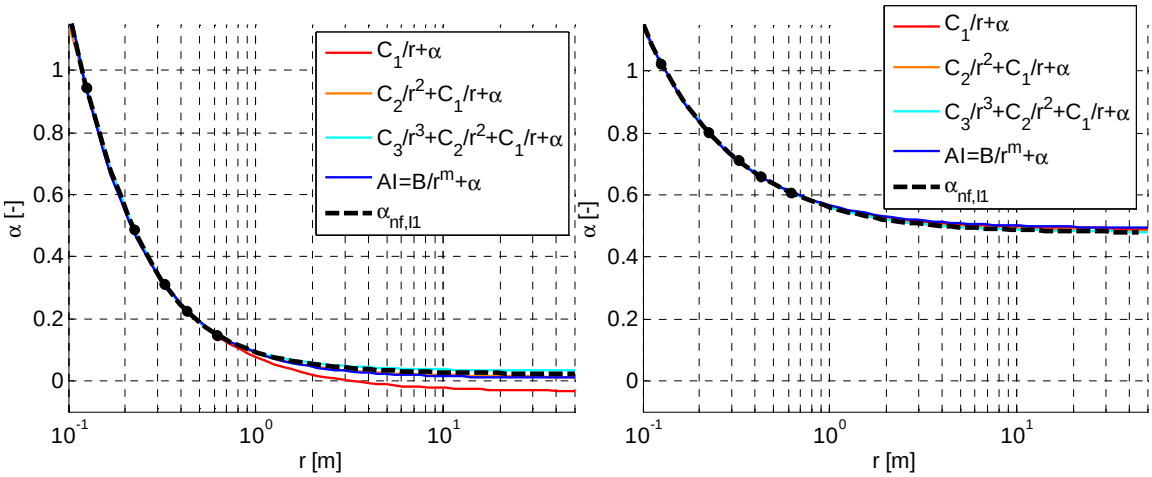

Fig. 6-15. Curve fit of simulated values of $\alpha_{\mathrm{nf},I1}$ for 200 Hz (left) and 1kHz (right).

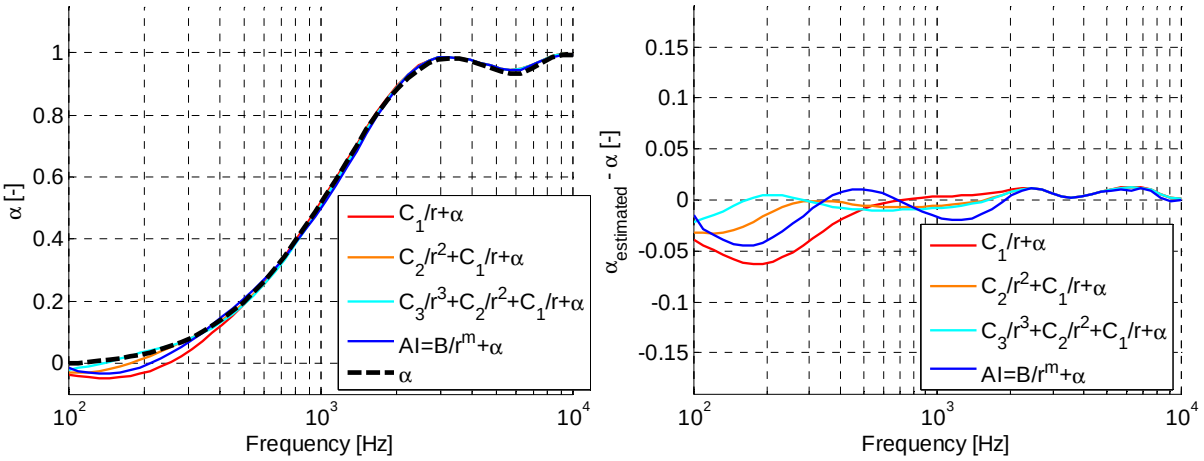

Fig. 6-16. Left: absorption α and estimated absorption. Right: difference between $\alpha_{\mathrm{estimated}}$ and α.

Real test data contains noise, which leads to errors. Noise is artificially combined with $\alpha_{\mathrm{nf},I1}$ to determine the effect on the fitting functions. Pseudo-randomly distributed values that do remain within ± 0.25 have been added to the five input values of $\alpha_{\mathrm{nf},I1}$, which are then fitted. Fig. 6-17 and 6-18 show that the fitting functions with fewer constants, i.e. $B/r^m + a$ and $C_2/r^2 + C_1/r + \alpha$, are more suitable for noisy measurement data. For extrapolating the measured $\alpha_{\mathrm{nf},I}$, best results were obtained with equation 6-32, which is therefore used in this thesis unless specifically mentioned.

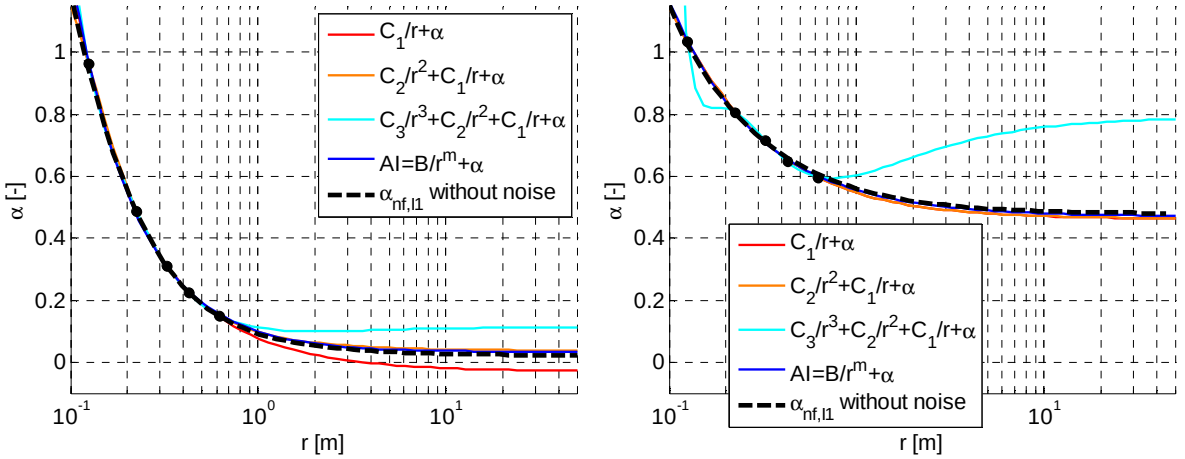

Fig. 6-17. Curve fit of simulated values of $\alpha_{\mathrm{nf},I1}$ with noise for 190 Hz (left) and 1 kHz (right).

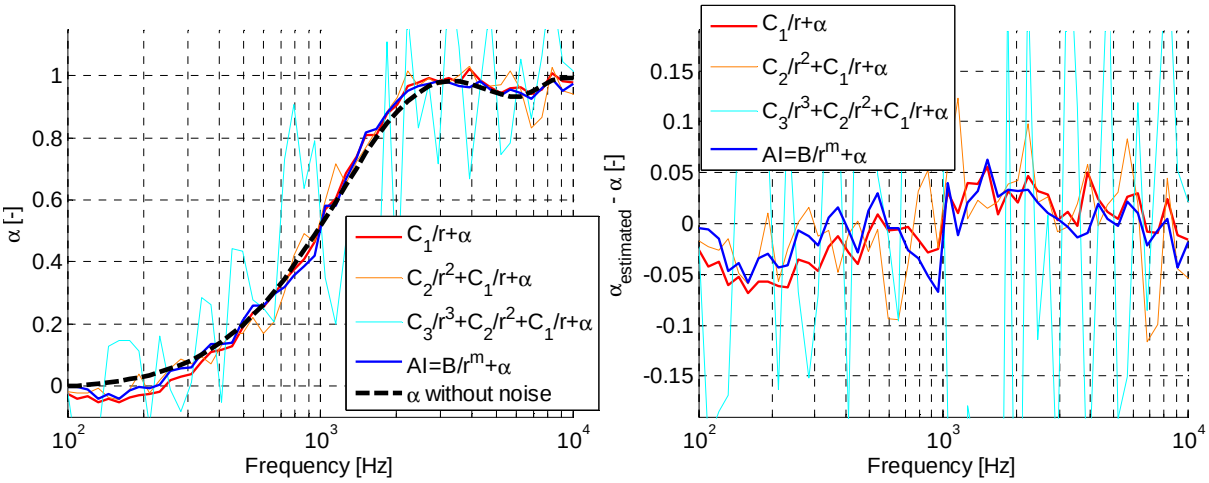

Fig. 6-18. Left: estimated absorption from $\alpha_{\mathrm{nf},I1}$ with noise. Right: difference between $\alpha_{\mathrm{estimated}}$ and α.

6.8.3. Optimisation method

To reduce noise from individual tests the $\alpha_{\mathrm{nf},I}$ at 25 positions are combined. The sound source distance r was varied from 25 mm up to 625 mm in 25 mm steps. The optimisation routine to calculate absorption consists of the following steps:

1. Values of $\alpha_{\mathrm{nf},I}$ were the phase exceeds ± 72 degrees are ignored to avoid inaccuracies in the intensity calculation.
2. $\alpha_{\mathrm{nf},I1}$ and $\alpha_{\mathrm{nf},I2}$ tend to decrease for larger distances of r (e.g. fig. 6-8 and 6-9). Values of $\alpha_{\mathrm{nf},I1}$ or $\alpha_{\mathrm{nf},I2}$ are therefore ignored if they are

smaller than those of a larger distance. The opposite is the case for $\alpha_{\mathrm{nf},I3}$; its values increase for larger values of r (e.g. fig. 6-10). Values of $\alpha_{\mathrm{nf},I3}$ are ignored if they exceed those of a larger distance.

3. A least mean square (LMS) fit of equation 6-32 or 6-33 is performed. Typical starting values are $B=0.05$, $m=1$ and $a=0.5$, for equation 6-32, and $C=0.5$ and $a=0.5$ for equation 6-33.
4. A method to remove outliers that proved successful for this set of test data was to perform a LMS fit for all possible pairs of three measurement distances. For equation 6-32 the constant m is usually a value near 1, and therefore only values between 0 and 2 are used. There were 25 distances, thus there were many calculations.
5. If the near field effects are small the values of $\alpha_{\mathrm{nf},I}$ are almost equal and similar to the absorption α. However, small measurement inaccuracies could cause unpredictable outcomes of the LMS fit. The outcome is conditioned because there is no need to extrapolate $\alpha_{\mathrm{nf},I}$ if the near field effects are small. The following function based on the standard deviation of $\alpha_{\mathrm{nf},I}$ and a constant c was used; $\alpha_{\mathrm{estimate}}=(1-X)\alpha_{\mathrm{LMS}}+X\overline{\alpha_{\mathrm{nf},I}}$, where $X=1/e^{\mathrm{std}(\alpha_{\mathrm{nf},I})c}$. If there are little near field effects the standard deviation of $\alpha_{\mathrm{nf},I}$ is small, thus $X\approx 1$ and $\alpha_{\mathrm{estimate}}\approx\overline{\alpha_{\mathrm{nf},I}}$. The constant c was 15 in this case.
6. Finally, to remove outliers, the median value of all valid $\alpha_{\mathrm{estimate}}$ solutions is taken.

Combining a large number of tests is impractical. The quality of the estimated absorption is studied if fewer tests (i.e. at fewer distances) are used. If r is large (about 0.4m or higher) the reactivity is high in a broad band for typical samples because of the high reflection at low frequencies. Measurements at these sound source positions generally contribute little to the final solution. Small distances of *r* should be avoided because of reflections against the sound source. In addition, $\alpha_{\mathrm{nf},I}$ values should be combined where *r* increases sufficiently. Fig. 6-19 shows an example of 2, 3, 4, and 5 measurement distances combined for the Flamex sample with a backplate.

As expected, the estimation improves if more measurement positions are included, but even with two positions the result is quite acceptable. In that situation m would be one and equation 6-32 becomes:

$$\alpha_{\mathrm{nf},I}(r \to \infty) = \frac{r_1 \alpha_{\mathrm{nf},r_1} - r_2 \alpha_{\mathrm{nf},r_2}}{r_1 - r_2} \qquad (6\text{-}34)$$

where α_{nf,r_1} and α_{nf,r_2} are the $\alpha_{\mathrm{nf},I1}$ (or $\alpha_{\mathrm{nf},I2} - \alpha_{\mathrm{nf},I3}$) at sound source heights r_1 and r_2.

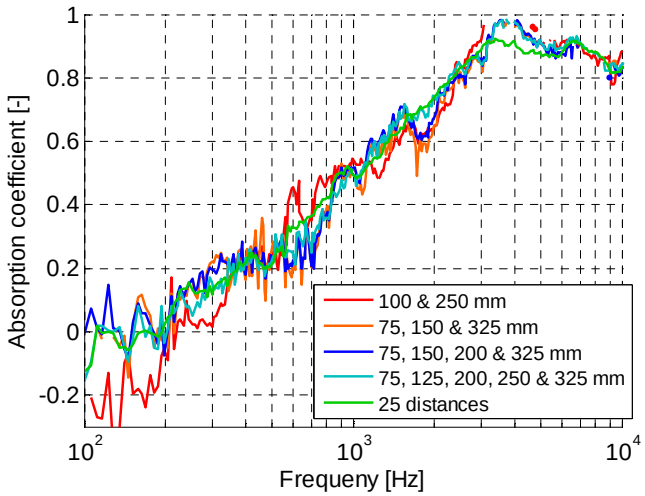

Fig. 6-19. Extrapolated absorption using a limited number of distances.

The outcome of the extrapolation procedure is validated in section 6.10.

6.9. *Extrapolation using impedance at several distances*

As is mentioned before, deviations can be found with the mirror source model or with the Q-term model when there are spherical waves inside the sample. An extrapolation method based on the intensity measured above the sample for several sound source heights has been investigated in the previous sections. Here, an extrapolation method that uses impedance-based absorption models is examined. Such a procedure based on the impedance rather than the intensity could be preferred if only the relative responsivity of the sensors is known, but not the absolute sound level during the reference measurement I_0 without a sample. This is for instance the case when the loudspeaker volume varies between the reference test without a sample and the test with a sample.

6.9.1. Extrapolation method

The impedance-based measurements principle resembles the intensity-based extrapolation procedure. First, the 'absorption' that is uncorrected for near field effects is measured for several sound source heights. For each sound source position the near field effect, and thus the outcome of the test, is different. Next, these results are extrapolated in order to obtain the plane wave absorption.

Earlier it was shown that the ratio of absorbed to incoming intensity always tends to be overestimated as the sample-probe distance *r* decreases. However, this is not the case for the outcome of the mirror source model or the Q-term model. Depending on frequency and on distance *r* the 'absorption' fluctuates. If the 'absorption' calculated with these models would also have followed a positive trend, extrapolation of the results would have been feasible. Such fluctuations are not found with the plane wave model, and therefore this model is used for extrapolation. As was the case for the intensity method, the 'absorption' values calculated with the plane wave model do increase gradually if distance *r* decreases. Especially at low frequencies, where there are stronger near field effects, the 'absorption' is overestimated. The plane wave reflection R_{plane} is calculated from the free field impedance measurement Z_{ff} without a sample and the impedance measurement Z_{m} with a sample:

$$R_{\text{plane}} = \frac{\frac{Z_{\text{m}}}{Z_{\text{ff}}}\frac{ik_0 r}{ik_0 r+1}-1}{\frac{Z_{\text{m}}}{Z_{\text{ff}}}\frac{ik_0 r}{ik_0 r+1}+1} \qquad (6\text{-}35)$$

Assuming that no sound transmits through the sample, the 'absorption' $\alpha_{\text{nf},Z}$ with near field effects is calculated by $\alpha_{\text{nf},Z} = 1 - R_{\text{plane}} \cdot R_{\text{plane}}^{*}$. A fitting function is subsequently used that combines multiple measurements of $\alpha_{\text{nf},Z}$ to obtain $\alpha_{\text{nf},Z}(r=\infty)$. Previously, equation 6-32 was used to fit the decay of the ratio of intensities $\alpha_{\text{nf},I}$ versus r. However, $\alpha_{\text{nf},Z}$ decays in a different way than the ratio of intensities $\alpha_{\text{nf},I}$. Simulations revealed that equation 6-33, rather than equation 6-32, is suitable for extrapolating $\alpha_{\text{nf},Z}$ to $r=\infty$.

6.9.2. $a_{nf,Z}$ at several distances

Fig. 6-20 shows the values of $\alpha_{nf,Z}$ for several values of r that were obtained using a sample with a backplate. The same test data and the same simulation conditions as in the previous sections were used.

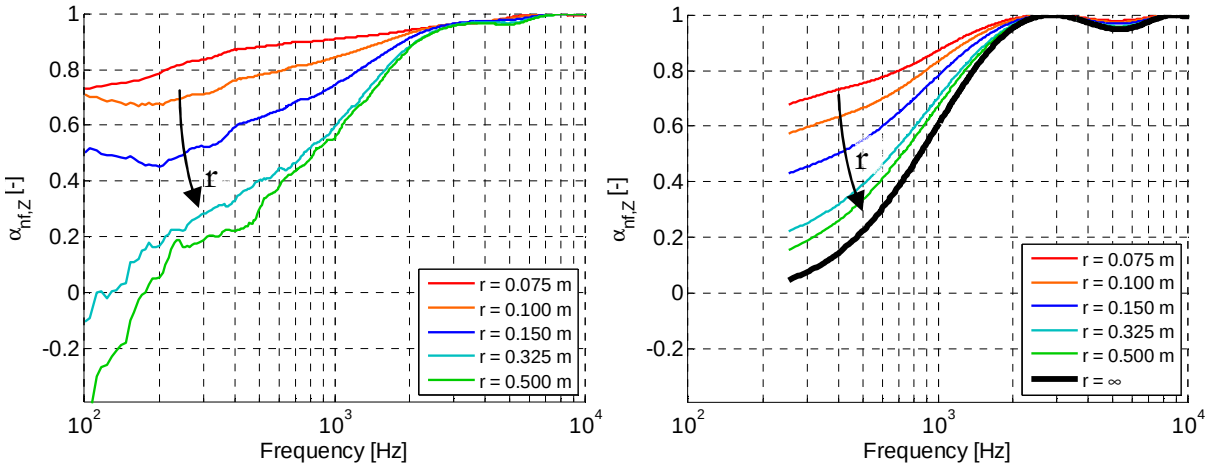

Fig. 6-20. 'absorption' obtained with equation 6-35 for several distances. Left: Flamex measured. Right: simulated (σ = 25 kPa·s/m², sample thickness 27 mm).

6.9.3. Using a limited order and number of distances

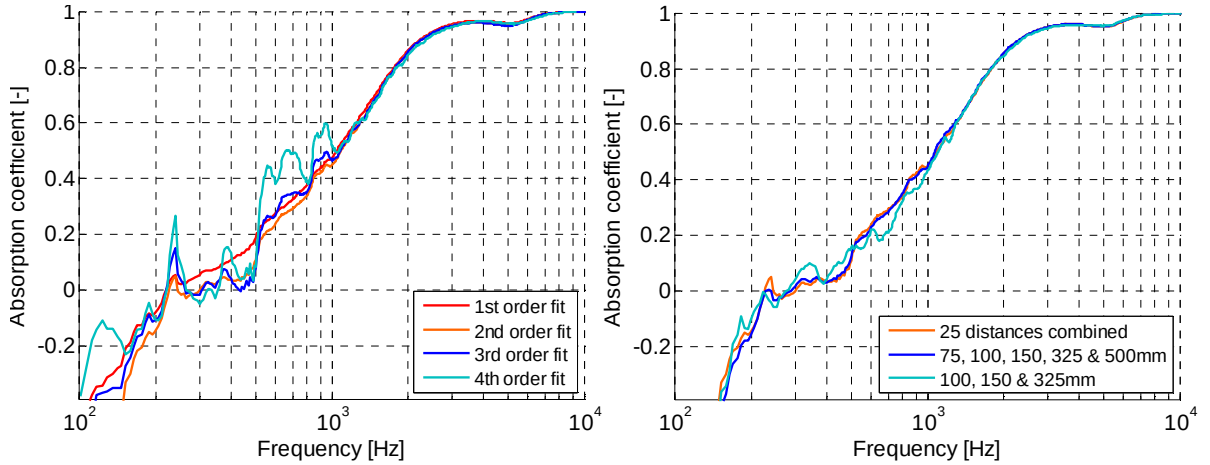

Fig. 6-21. Extrapolated absorption using a limited number of orders (left) or measurement distances (right).

Fig. 6-21 shows the plane wave absorption that is derived by extrapolating the values of $\alpha_{nf,Z}$. Negative absorption values are found below 200 Hz, which are most likely caused by measurement inaccuracies. When tests are performed at multiple sample-probe distances, the order of equation 6-33 can be increased to better approximate the measurement data. However, best results are obtained with a second order fit for the noisy measurement data (fig. 6-21 left).

Although similar values are occasionally found with only two tests and a first order fit, discrepancies can be found for some combinations of r. The absorption calculated through only a limited number of distances and a second order fit, is in good agreement with that of all 25 tests combined (fig. 6-21 right).

6.10. *Extrapolation results and comparison with the Kundt's tube*

The intensity and impedance based extrapolation principles have been applied to calculate the plane wave absorption of all three samples with a backplate. For comparison, the absorption is also calculated using the mirror source method ($r = 0.3$ m) and the samples are measured with a Kundt's tube. The latter method can be applied for these samples because they do not have a high flow resistivity and a low Young's modulus (see section 2.2.1). The upper frequency limit of the Kundt's tube is 3.6kHz in this case. The results of the four methods are shown in the next figures:

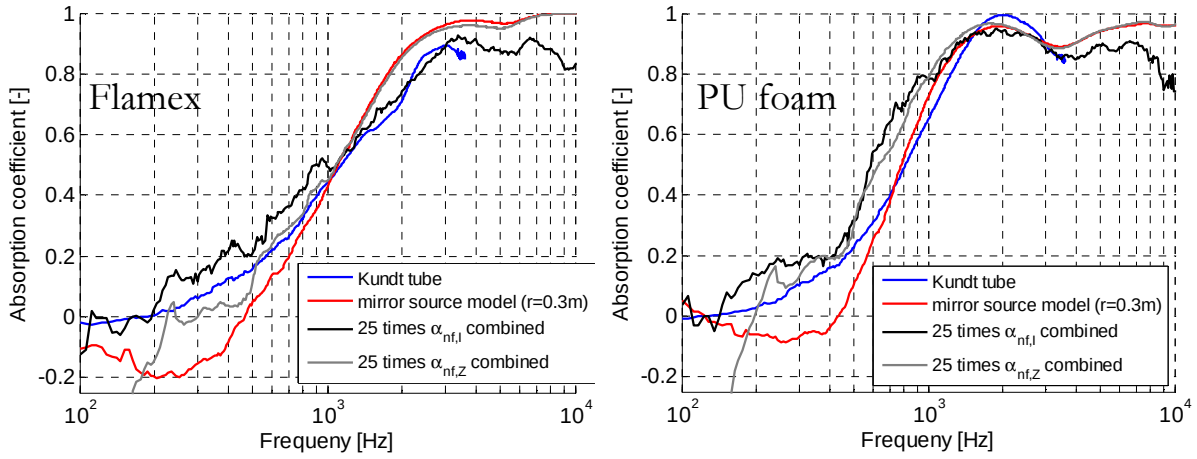

Fig. 6-22. Comparison of four absorption measurement methods.

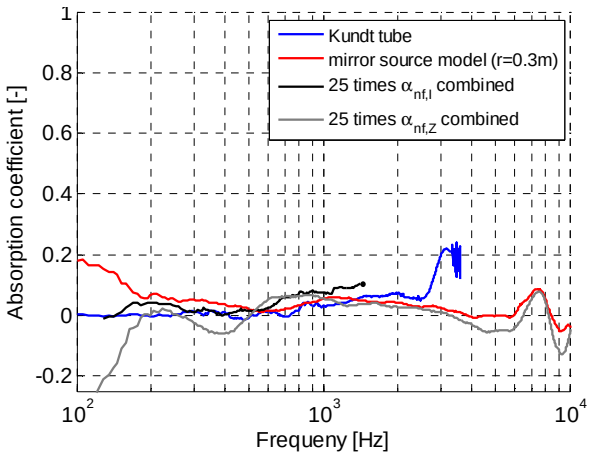

Fig. 6-23. Comparison of four absorption measurement methods: Linoleum.

Results from the intensity-based and the impedance-based extrapolation method are in good agreement with those of the Kundt's tube. However, there still are small differences and further validation would be required to determine which of the two methods is more accurate. At higher frequencies, the reactivity can increase if the reflection coefficient of the sample is high. Such conditions are complicated for the intensity method because there are fewer distances were the phase is within ± 72 degrees required for valid intensity calculations. In that case, it might be possible that no least mean square solutions for the extrapolation method are found. This is for instance the case for the linoleum sample above 1.5kHz (fig. 6-23, black line). However, at high frequencies the mirror source model or Q-term model can be used instead if the near field effects are small.

With the intensity extrapolation technique also the far field intensity reflection-, absorption- and transmission coefficients are calculated from the measured intensities in front and behind the Flamex sample without a backplate (fig. 6-24).

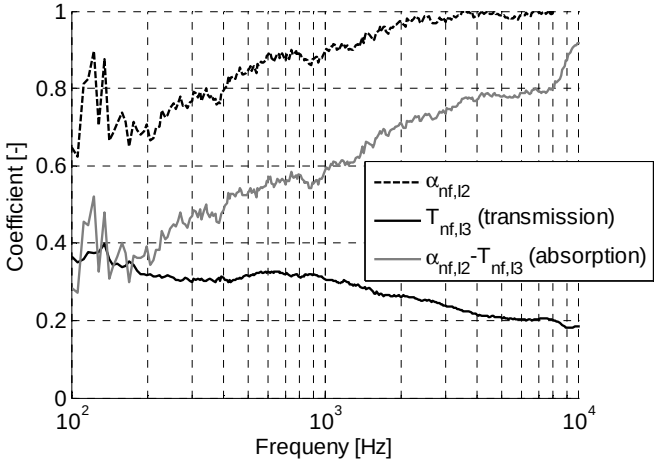

Fig. 6-24. Intensity reflection-, absorption- and transmission coefficients.

In addition, the simulated values of $\alpha_{\mathrm{nf},I}$ and $\alpha_{\mathrm{nf},Z}$ with near field effects can be used to extrapolate and obtain the far field absorption. Intensity-based absorption estimations of the direct solution for $\alpha_{\mathrm{nf},I}$ at two distances (equation 6-34), and the full LMS method for three distances, are shown in fig. 6-25 (solid and dotted black line, respectively). The extrapolation results of $\alpha_{\mathrm{nf},Z}$ using a limited number of distances are shown in fig. 6-26 for a sample with a backplate.

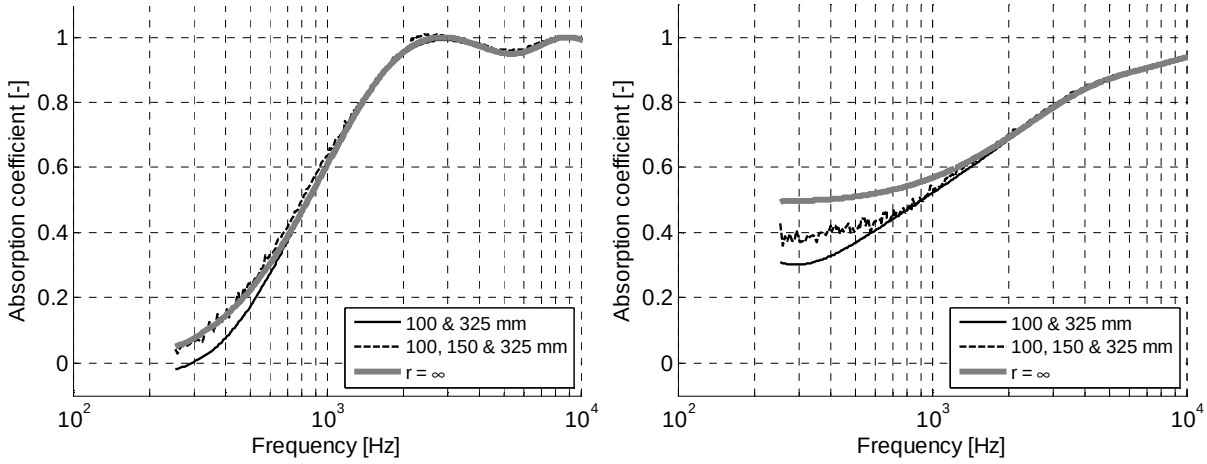

Fig. 6-25. Absorption extrapolated from $\alpha_{\mathrm{nf},I}$ simulated for a sample with (left) and without (right) a backplate.

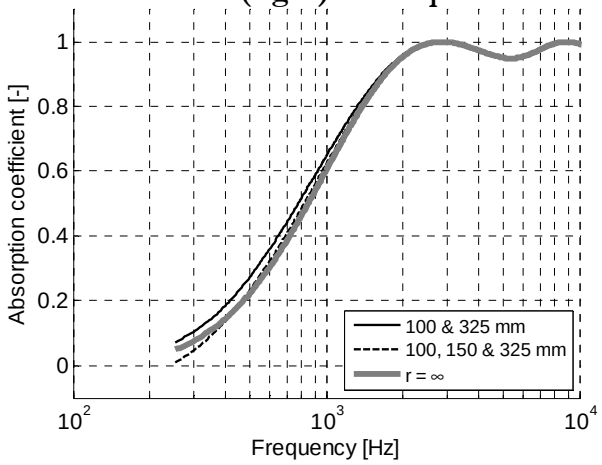

Fig. 6-26. Absorption extrapolated from $\alpha_{\mathrm{nf},Z}$ simulated for a sample with a backplate

6.11. *Simulated deviation of the mirror source and Q-term model*

As was mentioned before, similar errors are made with the mirror source model and the Q-term model because spherical waves inside the sample are disregarded. Simulations have been performed using a variety of material parameters to find out with which material properties errors can be expected. The impedance above the sample can be calculated with the spherical model and the complex material wavenumber and impedance obtained from the Delany and Bazley equations. The simulated impedance can be used to calculate the absorption with the mirror source model and compare it to the plane wave absorption for $r = \infty$. The next figure gives an indication of the error made for several probe-sample distances for a sample with a flow resistivity of 25 kPa·s/m^2 and a sample thickness of 27 mm.

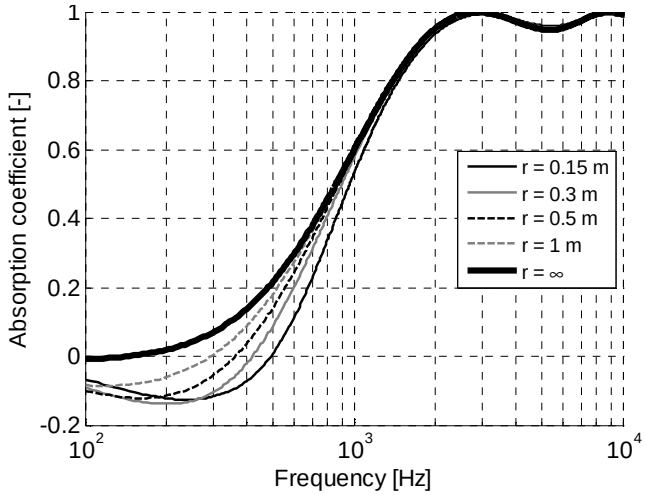

Fig. 6-27. Simulated absorption using the mirror source model for several distances r.

Fig. 6-27 shows that the results from the mirror source model are incorrect for small values of r. Negative absorption values are obtained as was also the case with the measurements (e.g. fig. 6-1) because of spherical standing waves inside the sample. The degree and frequency of deviation depends on the impedance and damping of the material. Such discrepancies are not found if:

- there are plane waves (i.e. large values of kr).
- the sample is infinitely thin because reflections can then be modelled by a single mirror source (which is the basic assumption for the mirror source model and the Q-term model).
- the sample is infinitely thick because then there is full damping of the first wave that travels through the sample and no contribution from waves that would have reflected against the back of the sample.

Any of the above conditions is rarely met in practice. The magnitude of the discrepancies obtained with the mirror source model if samples do have a certain thickness and if there are near field effects is further investigated. Although only simulations are used, which may not cover the wide range of existing samples, it gives a good impression of the degree of error expected for samples having certain properties and dimensions. Fig. 6-28 shows the maximum difference between the absorption calculated at distance $r = 0.3\,\text{mm}$ and at distance $r = \infty$ for a range of flow resistivity values and sample thicknesses. A 300 Hz -10 kHz frequency band is used and frequency values for which the Delany and Bazley model is invalid (section 2.4) are omitted. The maximum error is found for samples that have thicknesses in between 40 mm

to 100 mm and flow resistivity values in between 15 kPa·s/m^2 and 35 kPa·s/m^2. Weight is an issue for many applications such as the automotive or aerospace industry, and thinner samples of typically 5 mm to 30 mm are used, but even in this range, significant errors occur.

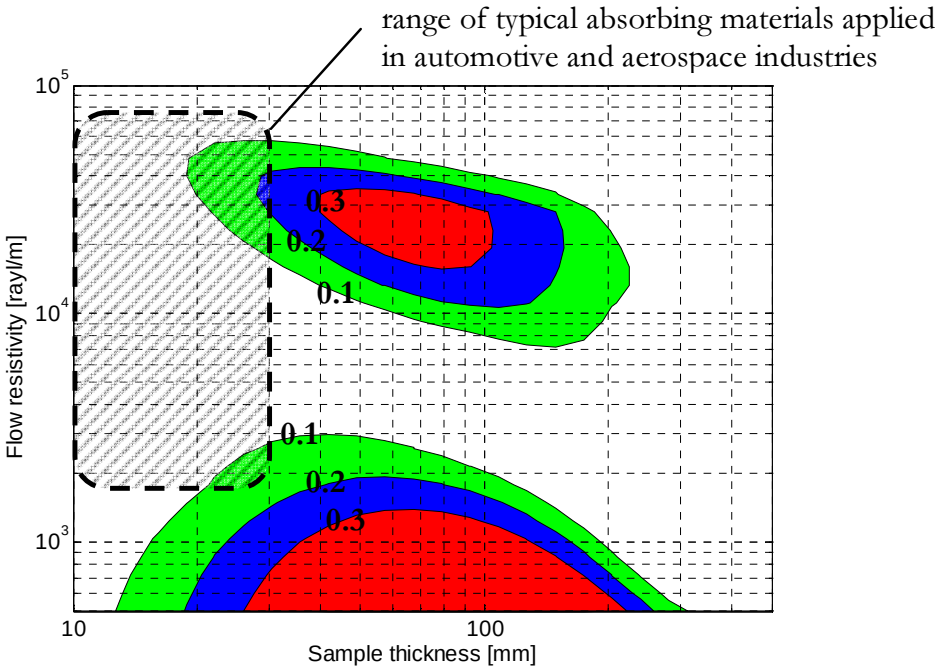

Fig. 6-28. Maximum deviation between the absorption at $r=0.3$ m and at $r=\infty$ (the axis are scaled logarithmically).

6.12. *Conclusion*

Models based on separate impedance tests, such as the mirror source model and the Q-term model, are frequently used. Although they correct for spherical waves from a monopole above the surface, they disregard spherical propagation of waves inside the sample. As a result, discrepancies occur, and even negative absorption coefficients are measured in some cases.

Therefore, a new interpretation of PU *in situ* measurements has been proposed. A sound source emitting spherical waves and a PU probe are placed near the surface of an absorbing sample. Instead of using one sound source position, measurements at several sample-probe distances are combined. Tests with three samples have been performed and conditions with and without a backplate have been analysed. Techniques have been introduced to extrapolate the plane wave absorption coefficient from the measured intensity or impedance above the surface using two or more source-probe distances.

The estimated absorption values are in good agreement with those of Kundt's tube tests (fig. 6-22 and 6-23). Furthermore, the extrapolation methods have been validated using a model that incorporates spherical waves inside the sample.

Different absorption models might be used for different situations because each model has its pro's and con's. The main properties of the models that have been introduced are summarised:

Model	Plane wave	Mirror source	Q-term	Multiple tests extrapolated
Bandwidth	-	+	+	+
Speed	+	+	+/-	-
Robustness	+	+	-	+/-
Accuracy	-	+/-	+/-	+
Main disadvantage	Low frequency errors	Negative absorption values are found because only plane sound waves inside the sample are considered		Requires multiple measurements with different sound source heights

If measurements can be performed with multiple source-probe distances, the extrapolation techniques are preferred because then proper corrections are applied for near field effects. If only a single sound source position can be used for practical reasons, the Q-term method or the mirror source method are most suitable, although errors can be expected if there are near field effects. The impedance at the probe position was simulated with a spherical sound field model, and the error made with the mirror source method could be calculated. For sample thicknesses to 30mm a maximum ± 0.2 discrepancy of the estimated absorption coefficient was found. Errors predominantly occur at low frequencies where samples absorb little sound. Although the Q-term method is more accurate than the mirror source method from a theoretical point of view because it accounts for spatial interferences, the outcome of both is often similar while the latter method is more robust.

7. Considerations of PU absorption measurements

7.1. *Introduction*

Several conditions that influence the outcome of PU *in situ* methods are investigated in this chapter. In section 7.2, two aspects limiting the measurement method itself are studied. Firstly, the influence of the spacing between the sample, the probe, and the sound source is discussed. For certain distances, interferences between the incoming and the reflected waves can cause measurement inaccuracies. The variation of the outcome of absorption models due to inaccurate determination of these distances is studied. Secondly, the stability of the measurement method over time is analysed. Several tests have been performed in a two-week period, and the results obtained are compared *[30]*.

Deviations are found with absorption measurements if samples are too small. Section 7.3 concerns the minimal sample size that is required for the results to agree with those of 'infinitely' large samples. It will be shown that, although other *in situ* methods usually require several square metres, smaller samples can be used for PU *in situ* methods.

In section 7.4, the spatial resolution of tests performed with a miniature PU probe is investigated. Measurements on a sample that contains a detailed logo revealed a resolution in the order of a millimetre *[121]*. Furthermore, by spatially integrating local measurements the effective absorption of the entire sample is obtained. Absorption values found for a quarter-lambda resonator sample and an aluminium foam sample are compared to those found with a Kundt's tube *[111]*.

When a sample is locally reacting, the surface impedance at any angle is related to the ratio of the normal surface impedance to the cosine of the angle. In that case, a measurement at a single angle of incidence is sufficient to calculate the random incidence absorption. However, all angles of incidence should be integrated in order to calculate the random incidence absorption coefficient of non-locally reacting samples. Even though the possibility of measuring

absorption at different angles of incidence has not been fully investigated here, the results of a preliminary study are presented in section 7.5 *[122]*. The impedance and the intensity have been measured at several points above the surface of a real sample. The variations of both quantities for different sound source orientations are studied.

Several aspects that affect the signal-to-noise ratio of absorption measurements are studied in section 7.6. Results from tests with and without a highly reflecting sample are used to illustrate under which conditions the quality of sound pressure and particle velocity measurements deteriorate *[77]*. Problems experienced at low and at high frequencies are considered.

In the last two sections, the effect of external influences is investigated. In section 7.7, the loudspeaker level that is required in order to exceed the background noise is determined. Tests have been carried out with and without a disturbing noise source. In section 7.8, practical wind caps for absorption measurements are briefly described. Such wind caps are useful for tests while an airflow is present above the sample. Measuring at different airflow speeds is desired because airflows might alter the performance of the sample. However, especially the signal from the Microflown sensor is affected by airflows. Small wind caps have been build and tests with flow have been performed, see for example *[34]* and *[123]*, respectively.

Different absorption models have been introduced in previous chapters, which either use intensity or impedance. The effect on both groups of methods is studied for the conditions investigated in this chapter. However, several tests have been performed in an early stage of this research. The extrapolation method had not been invented at that point in time and therefore only data of a single source-sample distance is acquired. Hence, results from the intensity method are not extrapolated and remain uncorrected for near field effects. For investigation of impedance-based models, the mirror source model is used because it is more robust than the Q-term model, and because no correction for the spherical sound field is made with plane wave models. Again, it must be noted that errors are found with the mirror source model because near field effects inside samples are disregarded.

7.2. *Limitations of PU in situ measurement methods*

7.2.1. Distance between sound source, probe, and sample

The probe-source distance r has an effect on the tests. Simple sound field models suffice to calculate the absorption coefficient if there would have been plane waves. However, in practice plane waves are difficult to generate, and for large sample-source distances there are signal to (background) noise issues and reflections from other objects. Sound sources are therefore often positioned closer to the sample. In that case, more complicated absorption models are required to correct for the spherical sound field. As was discussed already in the previous chapter, discrepancies are found with the mirror source model and the Q-term model because spherical wave effects inside the sample are disregarded. The outcome of the PU based intensity (extrapolation) method is only valid if the phase between sound pressure and particle velocity is small [11]. It should remain within ± 72 degrees in practice [13]. Therefore, kr should be large during the reference intensity measurement without a sample. For example, for the phase to remain below ± 72 degrees, r should be >0.18m for measurements in a 100Hz-10kHz band (eq. 3-4). On the other hand, large phase values are measured near strong reflecting samples for large values of r. By decreasing r, the phase can be lowered for most tests with a sample. However, small values of r should be used in order to avoid standing waves between the sound source and the sample. Typically, r should be kept within 0.2m to 0.5m.

Depending on the height of the source and on the damping properties of the sample, there can be interferences between incoming and reflected sound waves. For instance, if plane waves and a full reflective sample surface-air interface are assumed, the sound pressure is zero at the frequencies were probe-sample distance h is equal to a ¼ wavelength (or its odd multiples), and the particle velocity is zero at frequencies where h is equal to ½ a wavelength (or its multiples). The measurement quality is poor at those frequencies because there is always additive noise in the measured signal (for example self-noise from the sensor and background noise). Therefore, the probe-sample distance should be smaller than a quarter wavelength. On the other hand, h should not be too small because then the signal-to-noise ratio of particle velocity tends to be low at the probe position. However, in most

situations these interferences are weakened by damping of the material and by near field effects, which is illustrated with the following example. A monopole is situated at distance r above a probe that is positioned at distance h from a reflecting boundary. The reflected wave is represented as a mirror source at a distance $r+2h$ below the probe. The sound pressure and particle velocity of the incoming and of the reflected sound waves can be calculated with equation 6-24 and 6-25 (or with equation 7-2 and 7-3), where the sound pressure and particle velocity are attenuated with the spherical reflection coefficient R_s. The sound pressure and particle velocity are obtained by adding the contributions of the incoming and the reflected waves; $p = p_{in} + p_r$ and $u = u_{in} + u_r$, where it must be noted that u_r has a negative sign because this wave is travelling in opposite direction. Depending on frequency, there can be strong fluctuations in the impedance because the sound pressure decreases and the particle velocity increases (or visa versa) due to interferences of the incoming sound and the reflected sound.

Fig. 7-1 shows the simulated impedance for $r=10\,\text{m}$ and $h=50\,\text{mm}$ (black curves); a situation that is limiting to plane waves. The first sound pressure minimum occurs at $\frac{1}{4}\lambda = \frac{1}{4}\frac{c}{h} = 1715\,\text{Hz}$, and the first particle velocity minimum at $\frac{1}{2}\lambda = \frac{1}{2}\frac{c}{h} = 3430\,\text{Hz}$. However, in reality not all sound is reflected. On the assuming a reflection of $R_s=0.7$, the impedance is damped at the frequencies of the modes (fig. 7-1, red lines). Due to near field effects, a similar weakening of the modes is found if the sound source is positioned closer to the material (fig. 7-1 blue lines, for $r=0.27\,\text{m}$ and $R_s=1$).

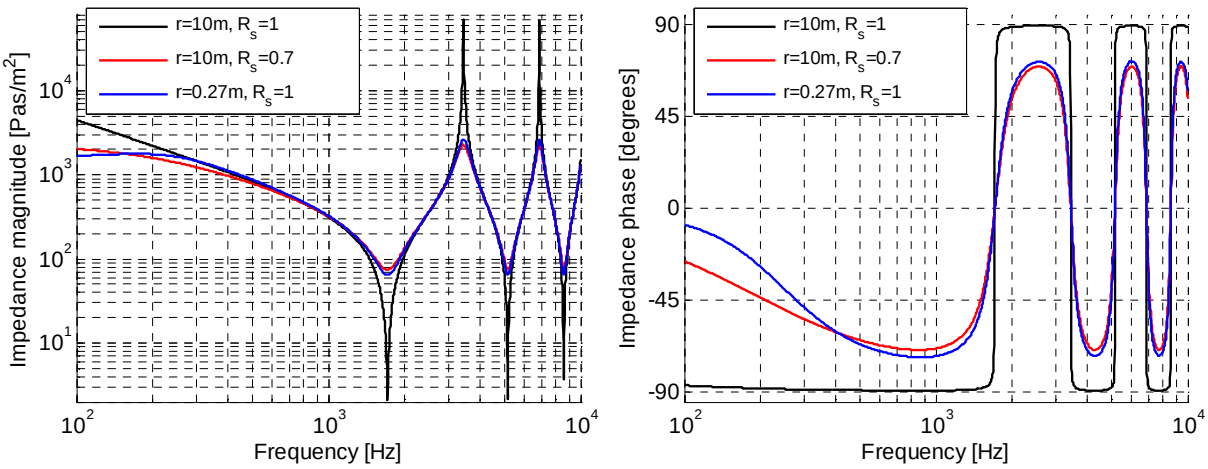

Fig. 7-1. Impedance with and without reflection by the sample or near field effects.

In order to determine which values of h can be used for measurements on real samples, tests were performed in a quiet room for several values of h while r was kept 27 cm. The sample was large and it consisted of a material called Flamex, which was backed by a full reflecting plate. The absorption was not calculated with the intensity model because measurements were performed at one position only. The mirror source model is used instead. Fig. 7-2 shows a similar trend of the absorption coefficient for all values of h. However, depending on h, discrepancies occur at low frequencies because near field effects of waves inside the sample are disregarded with the mirror source model. In addition, at high frequencies small discrepancies are found for larger values of h because of interferences of incoming and reflected sound waves. In practical situations, tests with probe-sample distances larger than 50 mm are difficult to perform because the sound that is reflected from the sample is weak compared to the incoming sound [30, 76]. For that reason, there are difficulties with background noise and reflections from other objects. Usually, best results are obtained if $h \leq 30$ mm.

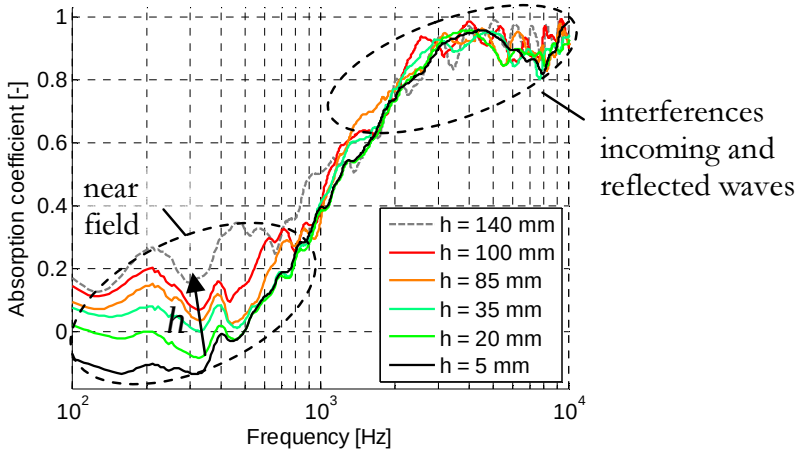

Fig. 7-2. Measurement results for several values of *h* (probe-source distance 27 cm).

Distance h can be hard to determine. An offset of ± 5 mm has been added to h for the measurement at $h = 5$ mm in order to study the effect of erroneous estimates (fig. 7-3). At low frequencies discrepancies are found with the mirror source model because the reflection of the sample is high (fig. 7-3 left). Similar deviations are found throughout the frequency range with samples that have a high reflection. The results of the mirror source model and the Q-term model are in good agreement. However, it was impossible to find a solution for all frequencies with the latter model because the involved iterative algorithm could not converge properly to a minimum (fig. 7-3 right).

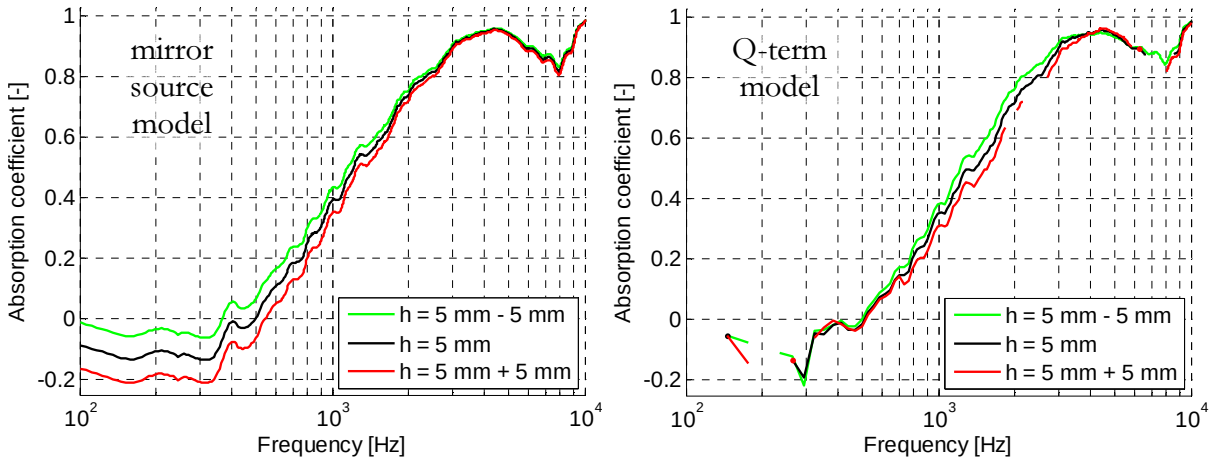

Fig. 7-3. Misestimating the probe-sample distance: $h = 5\ \text{mm} \pm 5\ \text{mm}$.

7.2.2. Stability over time

Many factors can cause deviations over time. For instance, the characteristic impedance of air may change because it depends on temperature, and the sensors are susceptible to variations of temperature, humidity, and ambient pressure. Errors might occur because the reference test without a sample and the test with a sample are sometimes performed in different periods. To study the effect, the absorption of a polystyrene foam sample called Foamex was measured on eight days during a two-week period by Nosko et al. *[30]*. Each time a reference measurement without a sample and a measurement with a sample were performed. The absorption was calculated for each day. Fig. 7-4 shows the mean absorption value over time calculated by the mirror source model (black line) and by the ratio of absorbed to ingoing intensity (red line), and their standard deviations indicated by the coloured areas.

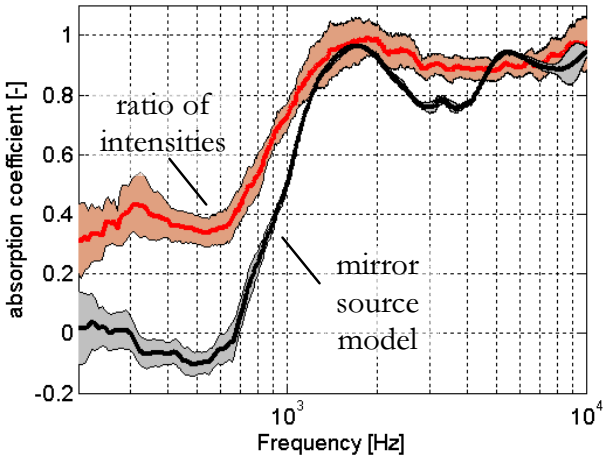

Fig. 7-4. Dispersion of absorption in a two-week period (standard deviation coloured).

The tests with and without a sample are sometimes performed on different days. Reference measurements of several days were therefore combined with a sample measurement of a single day, and visa versa. Fig. 7-4 and 7-5 show that the absorption varies little in a two-week period in the mid frequency range (800Hz–8kHz). Slightly higher discrepancies are found for the intensity method than with the mirror source model because the sound source level was not kept constant during all tests. In all, the mean standard deviation from 100Hz to 10kHz was 0.03 for the mirror source model, and 0.05 for intensity. Apart from errors caused by human mistakes, a main cause for these discrepancies might be the change in the humidity of air that changes the sensitivity of the microphone inside the PU probe; its sensitivity dependence is 0.05dB per percent humidity change [14]. Although the humidity was not monitored, a variation of 20% amongst the measurements cannot be ruled out, which would result in a sensitivity variation of 1dB. The sensitivity of the particle velocity sensor remains rather constant under the same conditions; its humidity dependence is only 0.003dB per percent humidity change. Changes in ambient pressure and temperature might have also contributed slightly to the discrepancies. The pressure and temperature dependencies of both sensors are respectively 1.7dB/bar and 0.03dB/°C for the sound pressure sensor, and 4dB/bar (at 300Hz) and 0.02dB/°C for the particle velocity sensor [14]. Most likely, the ambient pressure varied by less than 20mbar, whilst the temperature, varied by less than 5°C. This would result in a maximum 0.19dB sensitivity variation for the sound pressure sensor, and a 0.18dB for the particle velocity sensor. Further research is required to determine the exact cause of the discrepancies.

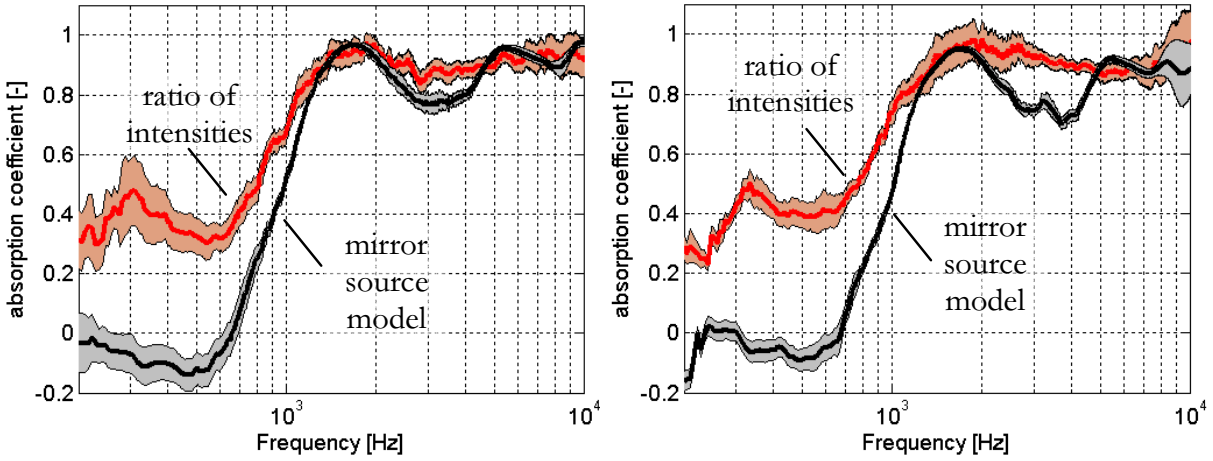

Fig. 7-5. Dispersion of absorption in a two-week period (standard deviation coloured). Left: one reference test and different sample tests. Right: different reference tests and one sample test.

7.3. *Sample size*

Although samples are mostly assumed infinitely large in theory, their size is limited in reality. Strictly spoken one single minimum sample size cannot be defined for all applications because the absorption depends on the sample area (and on the position of the observer and the sound field present). However, the absorption coefficient of infinitely large samples is considered to compare different materials in a convenient manner. In that context, the minimal sample size is the sample area required for the measurement results to be sufficiently consistent with those of an infinitely large sample. With the set-up used here, the sample size required is smaller than for many other *in situ* methods because the probe and sound source are positioned close to the surface. The effect of a decreasing sample area on the test results obtained by the PU method is studied here.

7.3.1. Limited sample size; simulations and measurements

In the past, several authors have simulated the effect of finite sample size for *in situ* absorption measurements with PU probes at normal incidence using Boundary Element Methods. Otsuru et al. [69] used a sound source at 500m from the sample, and they found absorption deviations in the mid frequency range as high as 0.05 with a 16m^2 sample already, and 0.2 with a 1m^2 sample. Hirosawa et al. [62] used a 1m source-sample distance and they found deviations smaller than 0.05 for samples larger than 0.25m^2. In addition, they found higher deviations for the PP *in situ* impedance method, mainly because one of the microphones is positioned further from the sample than the other. Brandão et al. [124] found similar values of about 0.36m^2. Here, simulations are performed to indicate for which conditions sample size errors can be expected, and tests are performed with several sample types to indicate which sample sizes are required in reality.

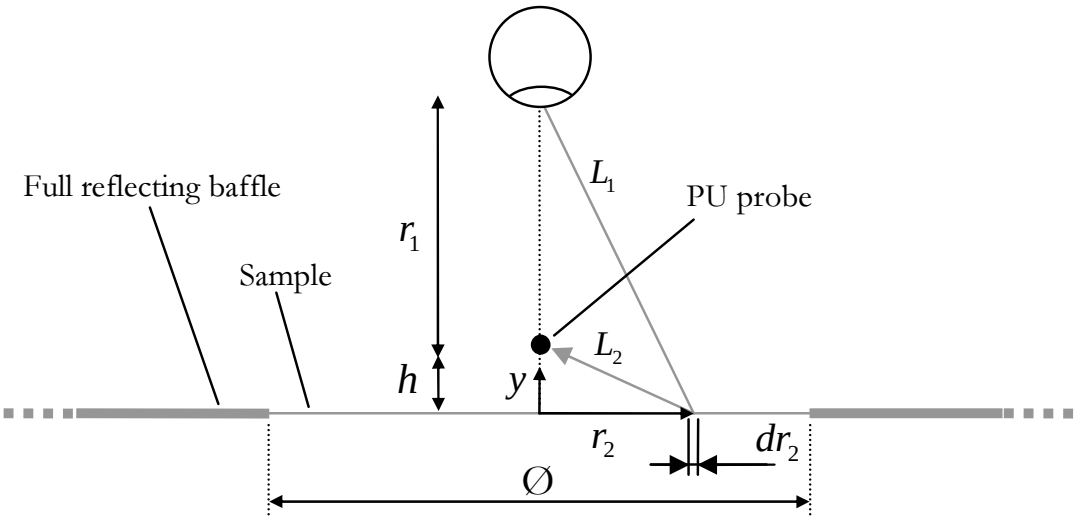

Fig. 7-6. A probe and a spherical sound source above a sample in a baffle.

The simulations involve a circular sample in a flat, infinitely large full reflecting baffle (fig. 7-6). The absorption for samples with a restricted size is calculated for several values of probe-sample distance h, source-probe distance r_1, sample thickness d, and flow resistivity σ. The absorption models that were introduced in earlier chapters use either the intensity or the specific impedance above the sample, which require the sound pressure p_{m} and particle velocity u_{m} above the sample. This involves addition of incoming and reflected sound pressures ($p_{\mathrm{m}} = p_{\mathrm{in}} + p_{\mathrm{R}}$), and the incoming and reflected particle velocities ($u_{\mathrm{m}} = u_{\mathrm{in}} + u_{\mathrm{R}}$).

The reflection from each section of the reflective boundary is assumed as a separate source. By adding the sound pressure and particle velocity contributions of each section, p_{R} and u_{R} are obtained. These contributions are obtained using the Rayleigh integral for circular segments. The sound pressure and particle velocity reflected from each sample section depend on the reflection coefficient of each particular segment. The reflection coefficient of the baffle is one. The reflection coefficient of the sample is more complicated to calculate. If the sample is locally reacting and if there are plane waves propagating inside it, the reflection of each sample segment is calculated here with an approximate model.

The reflection coefficient R_{sample} of the sample can be obtained from the surface impedance Z_{surface} of the sample. The surface impedance of a sample with a backplate can be obtained if the complex characteristic impedance Z_1 and wavenumber k_1 are known [18], [4, p. 151 and 273]:

$$R_{\text{sample}} = \frac{Z_{\text{surface}} - \rho c}{Z_{\text{surface}} + \rho c}, \text{ where } \quad Z_{\text{surface}} = -iZ_1 \cot(k_1 d) \tag{7-1}$$

here, Z_1 and k_1 were obtained from the Delany and Bazley model (section 2.4). The ingoing sound pressure and normal particle velocity for a monopole are [4, p. 127], [72, p. 36]:

$$p_{\text{in}} = p_0 \frac{e^{-ik_0 r_1}}{r_1} \tag{7-2}$$

$$u_{\text{in},\perp} = p_{\text{in}} \left(1 + \frac{1}{ik_0 r_1}\right) / \rho c \tag{7-3}$$

where p_0 is the amplitude related to the strength of the monopole, ρ is the density of air and c is the speed of sound in air. The reflected sound pressure and particle velocity are obtained by integrating the sound pressure and particle velocity from each sample section. The procedure involves the following steps. First, the normal velocity $u_{\text{s},\perp}$ of a sound wave that arrives at each particular circular sample segment with radius r_2 is calculated. $u_{\text{s},\perp}$ is obtained by combining equation 7-2 and 7-3, and by accounting for the angle of arrival of the incoming sound wave:

$$u_{\text{s},\perp}(r_2) = \frac{p_0}{\rho c} \frac{e^{-ikL_1}}{L_1} \left(1 + \frac{1}{ikL_1}\right) \frac{r_1 + h}{L_1} \tag{7-4}$$

where $L_1 = \sqrt{(h + r_2)^2 + r_2^2}$. Next, by treating each sample segment as a baffled source the resulting contribution to the sound pressure at position $(0, h)$ is calculated by [4, p. 179]:

$$p_{\text{r}_2} = i\rho c k R(r_2) u_{\text{s},\perp}(r_2) \frac{e^{-ikL_2}}{L_2} r_2 dr_2 \tag{7-5}$$

where $L_2 = \sqrt{h^2 + r_2^2}$, and, depending on r_2, $R(r_2)$ is either the reflection coefficient of the sample or the baffle. Then, by combing equation 7-5 and Euler's linear equation [4, p. 119], and by accounting for the oblique angle at which sound is reflected, the associated normal particle velocity at position $(0, h)$ can be calculated by:

$$u_{r_2,\perp} = R(r_2) u_{s,\perp}(r_2) \frac{e^{-ikL_2}}{L_2} \left(ik + \frac{1}{L_2} \right) \frac{h}{L_2} r_2 dr_2 \qquad (7\text{-}6)$$

Subsequently, the reflected sound pressure p_R and normal particle velocity u_R can be calculated by numerically integrating the sound pressure and particle velocity contributions from $r_2 (0 \rightarrow \infty)$. The impedance at the probe position is obtained from p_m and u_m, and the absorption is then determined with the mirror source model (see section 2.8.1). Fig. 7-7 shows the calculated absorption for several combinations of h, r_1, d, and σ. As can be seen in the left figure, higher deviations are found if h increases (grey versus red line), or if r increases (grey versus blue line). For $r = 1\,\text{m}$, the sample diameter should be larger than 3m for the discrepancy to be below 0.1. Largest discrepancies are found for a flow resistivity in the range of 5kPa·s/m^2 to 10kPa·s/m^2 (fig. 7-7 right), which are typical values for open porous materials.

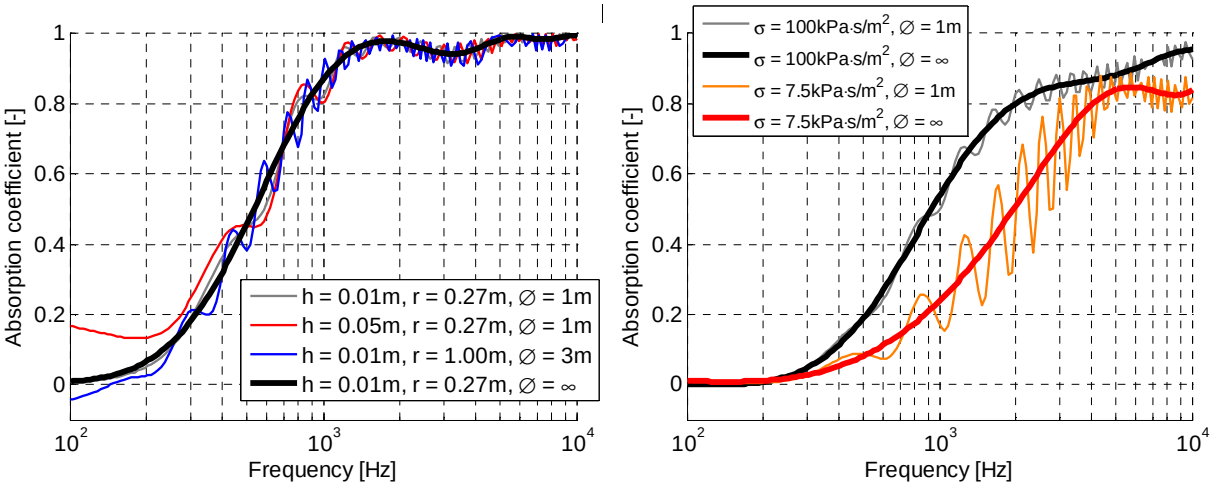

Fig. 7-7. Simulated influence of limited sample size. Left: variation of h and r_1 (d = 0.04 m, σ = 25 kPa·s/m²). Right: variation of σ (d = 0.02 m, h = 0.01 m, r = 0.27 m).

The sample size that is required is determined experimentally for five sample types. Tests have been performed with a sample area of 8m^2 or larger, and, due to practical limitations, only with several smaller diameters. The probe and the sound source were positioned 0.01m and 0.27m above the centre of the sample, respectively. Fig. 7-8 to 7-12 show the calculated ratio of absorbed to incoming intensities $\alpha_{\mathrm{nf},I}$ and the absorption coefficient calculated by the mirror source model. In the legend of the figures also the mean standard deviation (std.) compared to the large sample is displayed, which is calculated from all 1690 linearly distributed FFT points in the plotted frequency range. There are near field effects because the sound source is positioned only 0.27m above the sample. Therefore, $\alpha_{\mathrm{nf},I}$ increases at low frequencies and discrepancies with the mirror source model are found. The first sample that was measured consists of a 24mm thick material called Flamex, which is a type of melamine foam. As can be seen in fig. 7-8, the results are similar to those of a large sample if the diameter of the sample is 33cm or larger.

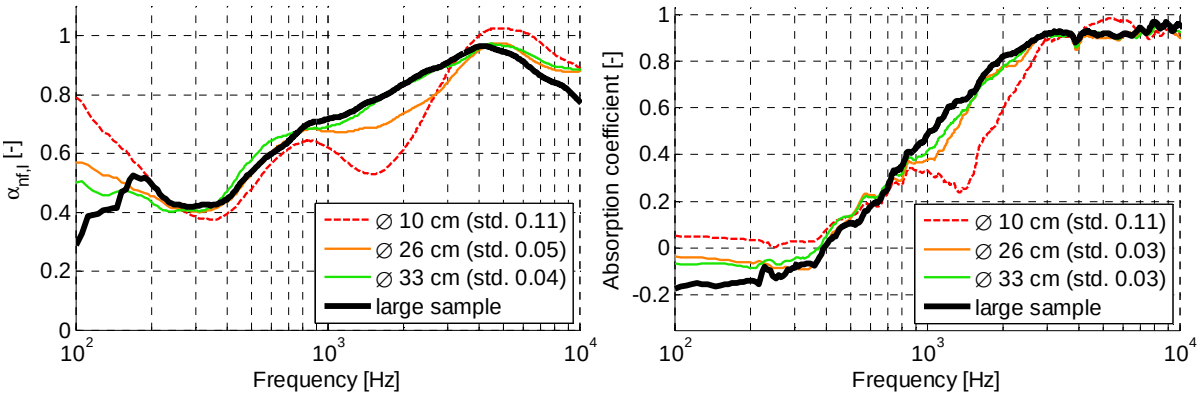

Fig. 7-8. Variation of sample size; Flamex.

The second sample is 28mm thick and consists of shredded pieces of recycled low-density polyurethane foam, which are bonded together. In the frequency band around 2kHz (around the frequency of the first material mode) discrepancies are found for $\alpha_{\mathrm{nf,I}}$, even for a 60cm diameter sample (fig. 7-9).

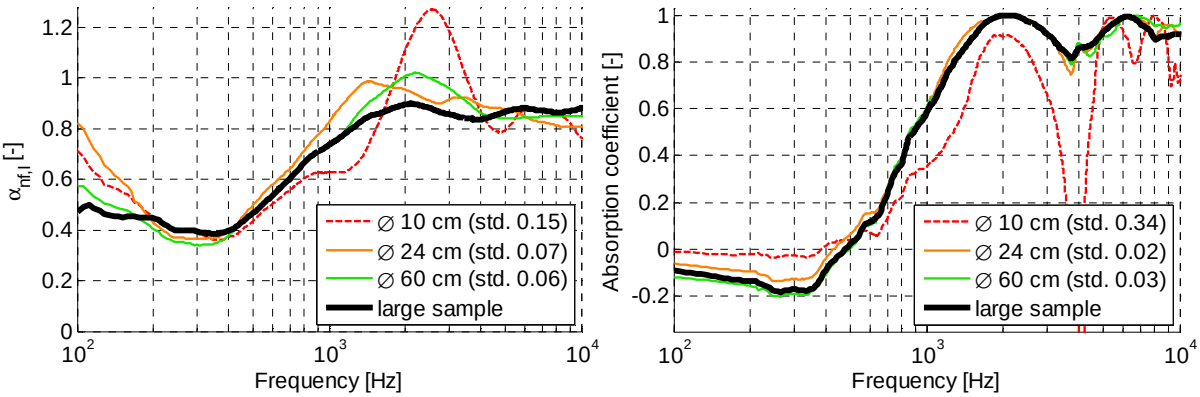

Fig. 7-9. Variation of sample size; recycled polyurethane foam.

Next, a sample consisting of a homogeneous 20mm layer of polyurethane is investigated (fig. 7-10). For $\alpha_{nf,I}$, the near field effects are strong compared to the recycled polyurethane sample, and again the sample should be large; at least 70cm in diameter at the frequency of the first absorption maximum (i.e. 2kHz).

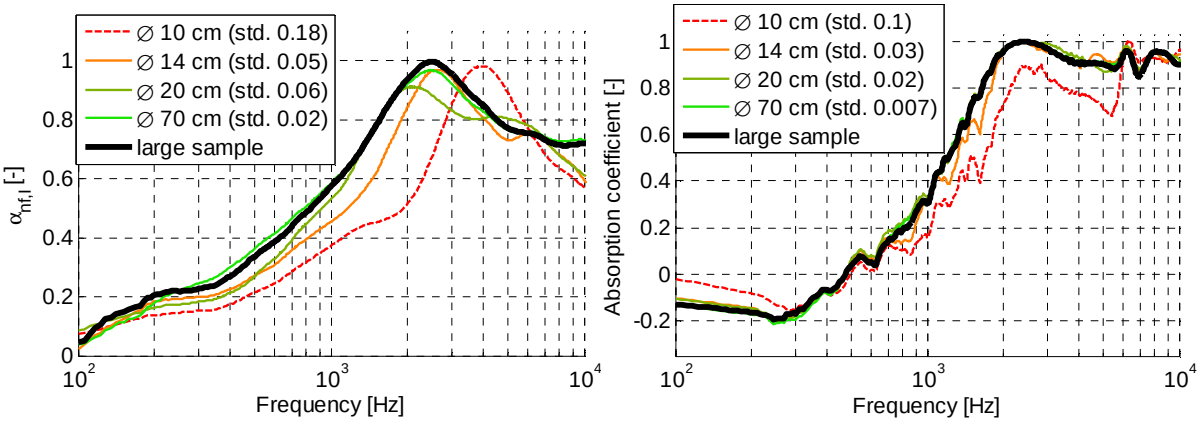

Fig. 7-10. Variation of sample size; polyurethane foam.

The fourth sample is a 30mm layer of stone wool, which consists of small fibres of molten rock. Fig. 7-11 shows the minimum allowed size is 30cm for this type of sample. The coherence was poor below 200Hz because the loudspeaker volume was not properly adjusted during the measurements of this sample, so these values are omitted.

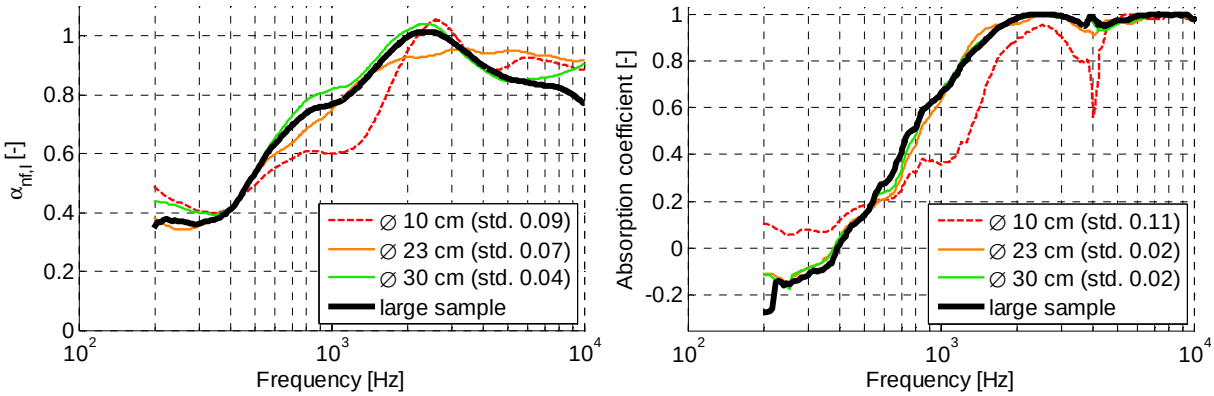

Fig. 7-11. Variation of sample size; stone wool.

Fig. 7-12 shows the results from the last sample that was tested; a 60 mm thick slab of open polyester wool material called Akotherm. At low frequencies, high values are measured because of near field effects; $\alpha_{\mathrm{nf,I}}$ even exceeds one. The results of a 48 cm diameter sample are similar to those of the large sample.

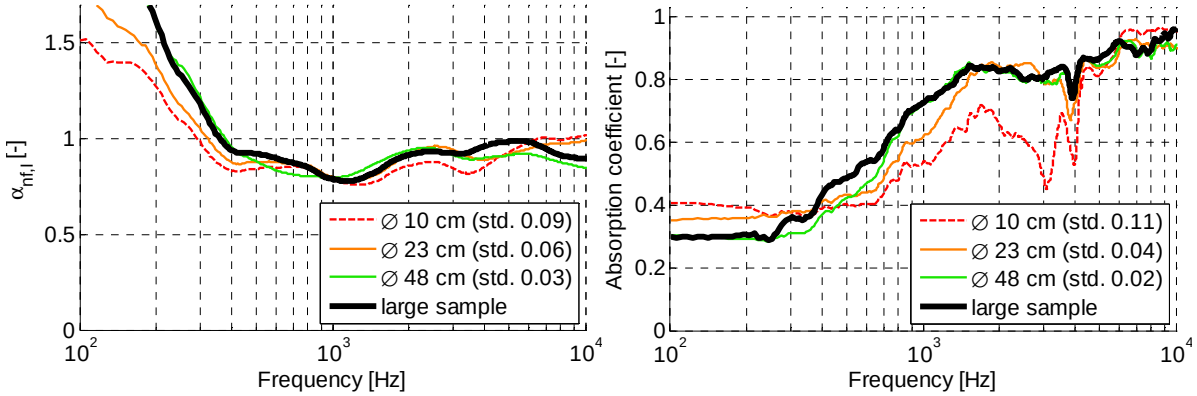

Fig. 7-12. Variation of sample size; Akotherm.

For the five sample types that have been measured, the sample diameter required varies from 30 cm to 70 cm for $\alpha_{\mathrm{nf,I}}$, and from 24 cm to 48 cm for the absorption calculated by the mirror source model. This corresponds to a sample area of 0.07 m^2 to 0.38 m^2, and 0.03 m^2 to 0.18 m^2, respectively. Deviations are found throughout the measurement bandwidth for samples that are too small. Although the absorption values found for the Flamex sample, the polyurethane samples and the stone wool sample are similar, the minimum sample size found for these materials is different. Further research would be required to determine the cause of the difference.

7.3.2. Sample properties as determined by a Kundt's tube

To validate *in situ* methods, the results are sometimes compared with those obtained with Kundt's tubes. In some cases, similar values are found [27, 110, 115], [125]. However, discrepancies are found in other cases that cannot be explained by near field effects only. An interesting observation was made by de Bree et al. with a type of polyurethane foam called Foamex [77]. A sample was cut from this material, and measured in a Kundt's tube that has an inner cross-section of 45mmx45mm. Next, a 600mmx600mm large sample with a rigid backplate was measured *in situ*. The absorption was calculated using the mirror source model. Fig. 7-13 right shows that the results are different (black and green line, respectively). There are low values with the mirror source model at low frequencies because of near field effects, but also the first absorption peak is measured at 2.7kHz with the Kundt's tube while the first peak is measured at 1.6kHz with the *in situ* method. The 45mmx45mm sample was also measured *in situ* using the same mounting conditions to determine why the frequency of the first absorption peak is different (red line). These results are unclear because of leakage through the sides of the sample. Therefore another test was performed with the same 45mmx45mm sample, which did not only have a backplate but also steel borders to contain the sample on the sides (fig. 7-13 bottom left). The results from this test (fig. 7-13 right, orange curve) are in better agreement with those of the Kundt's tube measurement. The frequency of the first absorption maximum is comparable for both methods. The sample properties appear to vary depending on the sample size.

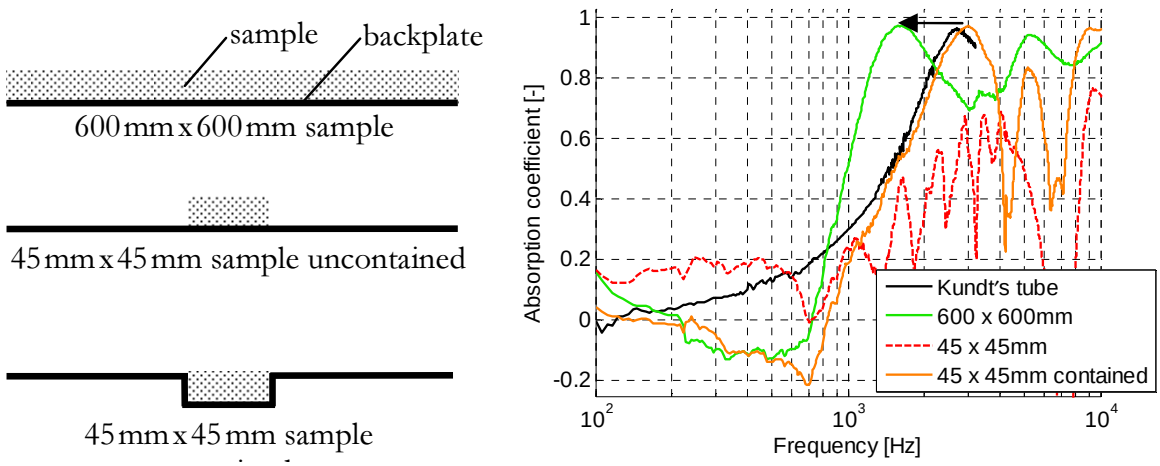

Fig. 7-13. Kundt's tube error because of the limited sample size.

In *[77]* the influence of the size of this type of sample was studied further. These results (not shown here) demonstrated that the first absorption peak shifted gradually to lower frequencies as the sample size increased until the sample is sufficiently large (in this case 300mmx300mm or larger). Similar distortions were found with the Kundt's tube for other sample types due to the limited sample size, but not for all. Highest discrepancies have been observed for materials that have a high flow resistivity and a low Young's modulus. Many double layer materials have such characteristics. An explanation for the difference in absorption properties as measured for different sample sizes is that the top surface might be seen as a kind of membrane if such samples are clamped at the sides. Its properties are altered because the sample size is limited, and thus the behaviour of the material is modified. Similar conclusions were also reported in [28, 29].

7.4. *Resolution and spatial integration*

The properties of many sound-absorbing samples are not uniform. In addition, nearby surfaces might influence the overall acoustic behaviour. To better understand the absorption mechanisms it can be helpful to study small sections rather than one overall value of the entire sample. PU probes are small and can be positioned close to the sample. The acoustic centre of the smallest probe used in this research, called the PU match probe, can be placed as close as 2mm from the sample surface. Many points above the surface of four samples have been measured to demonstrate the spatial resolution. Subsequently, the effective absorption of the entire sample is calculated, and these results are compared to those obtained with a Kundt's tube.

7.4.1. Sample #1: a single quarter-lambda resonator

The behaviour of resonator samples such as Helmholtz or quarter-lambda resonators are known from literature, see [4, 125, 126]. Sound energy is partly converted into heat due to viscous losses, mainly at the frequency of resonance. In addition, a portion of the reflected intensity becomes reactive due to interferences. Both effects are measured simultaneously, but because no energy is converted into heat by interferences, the 'absorption' between quotes is used here.

The first sample studied is a quarter-lambda resonator, which consists of a tube that is closed at one end and has a flange at the other end (fig. 7-14 left). If there is no damping, the impedance Z of the pipe with a cross-sectional area S at the entrance (0,0) is given by [4, p. 273]:

$$Z = -i\cot(kL)\rho cS \qquad (7\text{-}7)$$

Equation 7-7 implies that the incident sound pressure amplitude is in anti-phase with that of the reflected wave if L is equal to a quarter wavelength, or an odd multiple of that. The sound pressure at the tube entrance is therefore zero at this resonance frequency and the particle velocity would be high. In reality, viscous damping occurs at the opening and at the walls of the tube. The sound pressure at the tube entrance is therefore not zero, and it depends on the incoming sound field. The particle velocity magnitude at the same position is high. Due to inlet effects the acoustic length of the tube is longer than the geometrical length and therefore a correction a should be applied; $L = L_{\text{geometric}} + a$ [125, 126]. The value of a depends on the size and shape of the opening, and on the length of the tube, and it lies between $\frac{1}{4}\pi r$ and $8r/3\pi$ for a cylindrical opening [126, p. 198].

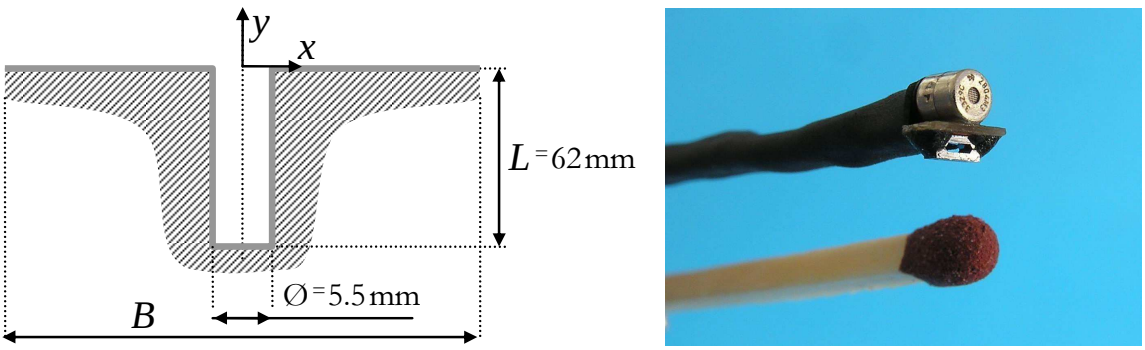

Fig. 7-14. Left: A single quarter-lambda resonator with flange. Right: PU match probe.

The sample that is studied consists of a rigid 115mmx115mm steel plate and one quarter-lambda tube with length $L = 62$mm and a diameter of 5.5mm, Tijs et al. *[111]*. Such a sample is expected to 'absorb' at the resonance frequency [126]. A PU match probe (fig. 7-14 right) is positioned at $y = 3$mm above the plate, and is moved from the entrance of the tube along the x-axis of the plate. The measurement results are plotted in fig. 7-15 to 7-19. Fig. 7-17 also shows the theoretical impedance of a system without damping (i.e. equation 7-7), which is similar to the impedance measured at the tube entrance.

The auto-spectra in fig. 7-15 are normalised with the reference test without a sample. A value of zero dB represents free field conditions. The impedance variations above the plate are mainly determined by particle velocity variations, while sound pressure remains nearly constant. This can also be seen in fig. 7-16 where the normalised sound pressure and particle velocity at the first resonance frequency of the tube (i.e. 1330 Hz) are plotted.

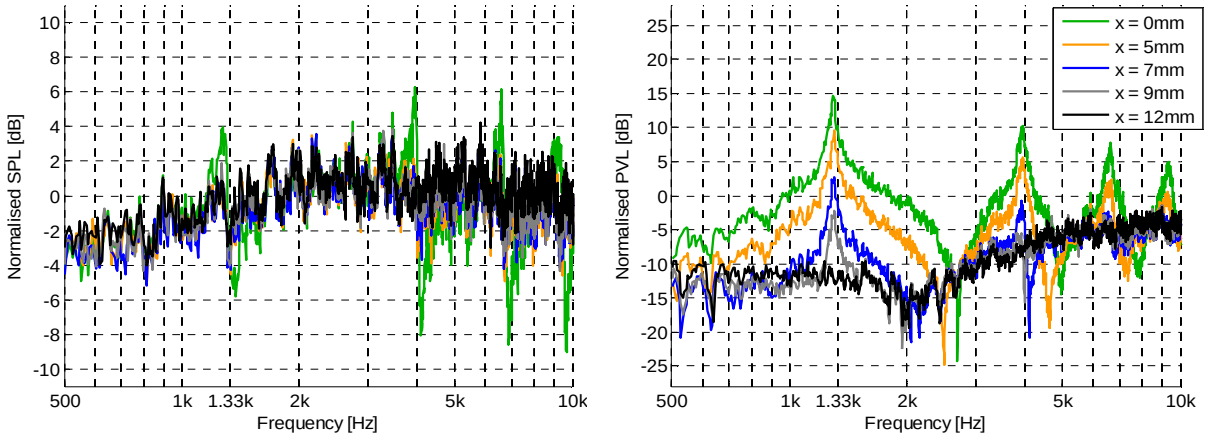

Fig. 7-15. Normalised sound pressure (left) and particle velocity (right).

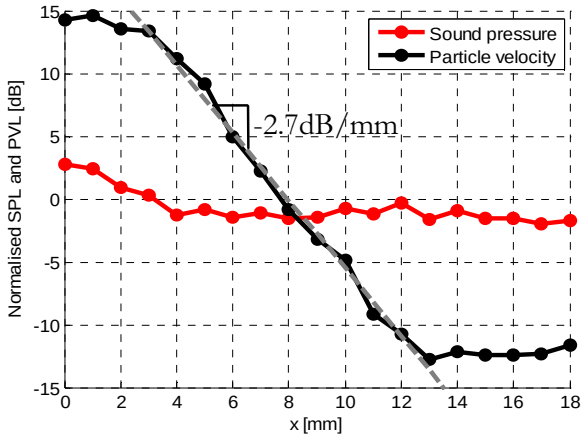

Fig. 7-16. Normalised sound pressure and particle velocity at 1330 Hz.

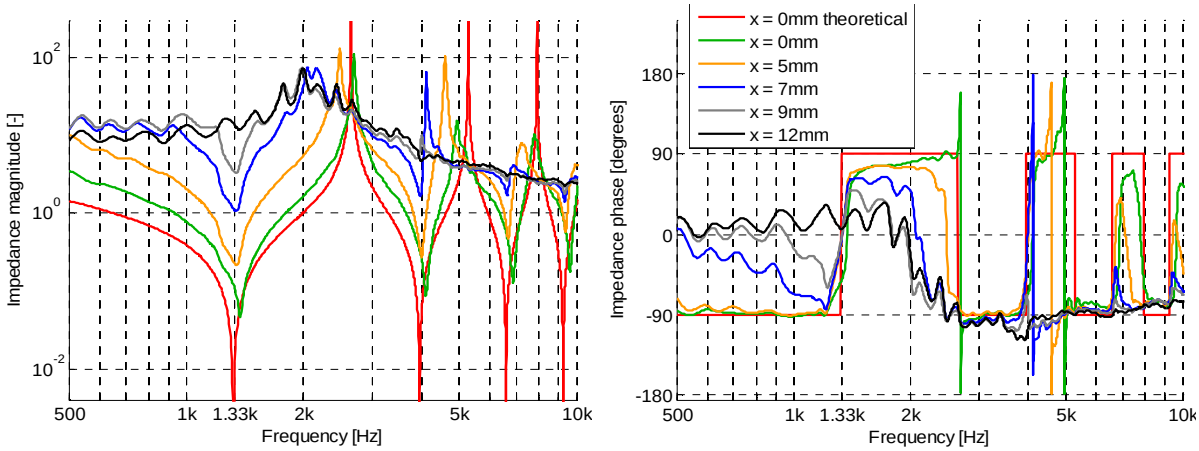

Fig. 7-17. Impedance magnitude (left) and phase (right).

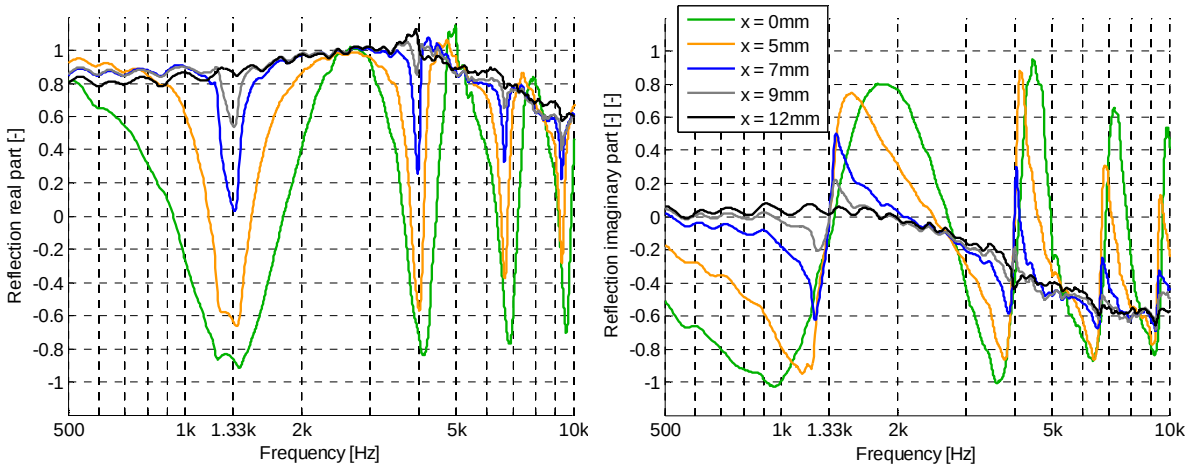

Fig. 7-18. Real part (left) and imaginary part (right) of the reflection (Z-1/Z+1).

From the figures above it can be seen that the resolution is in the order of a millimetre. Although it has no direct meaning for a listener in the far field, the reflection and the 'absorption' can be calculated at each specific measurement position using the impedance ($R = \frac{Z-1}{Z+1}$, and $\alpha = 1 - R \cdot R^*$). An interesting phenomenon is observed at 1330 Hz. The absorption (fig. 7-19) is one near the tube ($x = 7$mm), but is zero directly above it. The real part is considered only because the imaginary part is zero at this frequency. The real part of the reflection is -1 because the phase is flipped. If a larger area would be covered, a more averaged value unequal to -1 would have been measured.

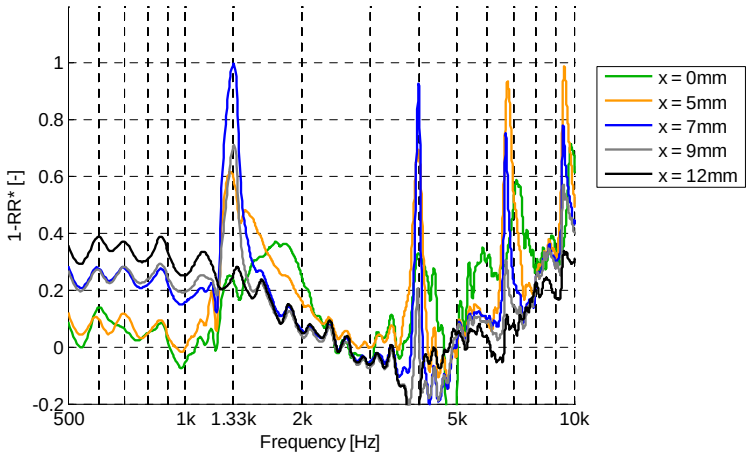

Fig. 7-19. Local absorption derived from impedance.

7.4.2. Sample #2: three quarter-lambda resonators

The acoustic properties of the entire surface of the same sample, in which now three quarter-lambda tubes with different lengths are placed, has been measured in a grid consisting of 5 mm x 5 mm sections (fig. 7-20). The results for the first resonant frequencies of each tube (1330 Hz, 1841 Hz and 2218 Hz) are shown in fig. 7-21 to 7-23. Similar results as in the previous section are found. The impedance and the local 'absorption' of the individual tubes can be obtained for this geometry. For example, such high-resolution impedance measurements near the opening of separate resonator cavities might be used to optimise their characteristics.

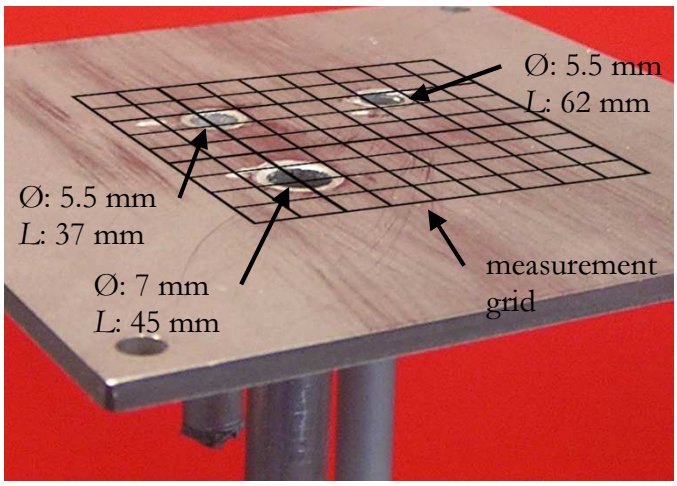

Fig. 7-20. Sample consisting of a steel flange and three tubes of different lengths.

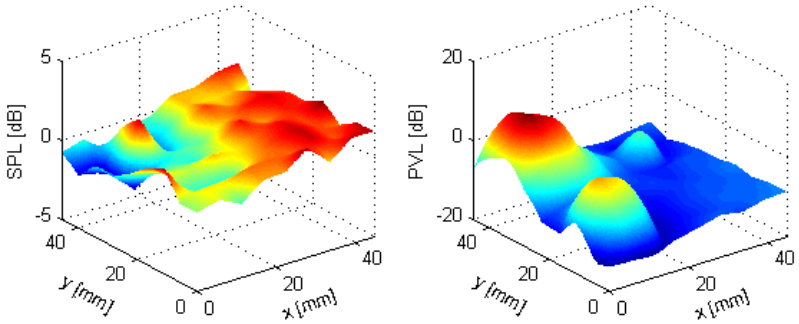

Fig. 7-21. Normalised sound pressure (left) and particle velocity (right) at 2218 Hz.

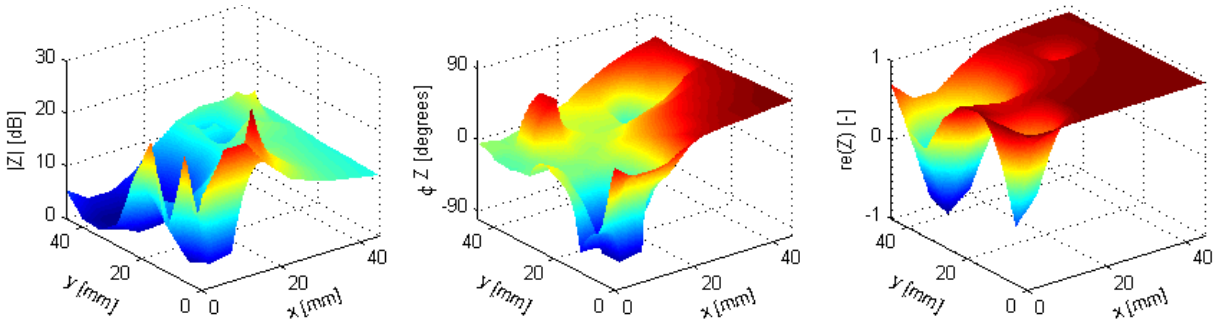

Fig. 7-22. Normalised impedance magnitude (left), impedance phase (middle), and real part of the reflection (right) at 2218 Hz.

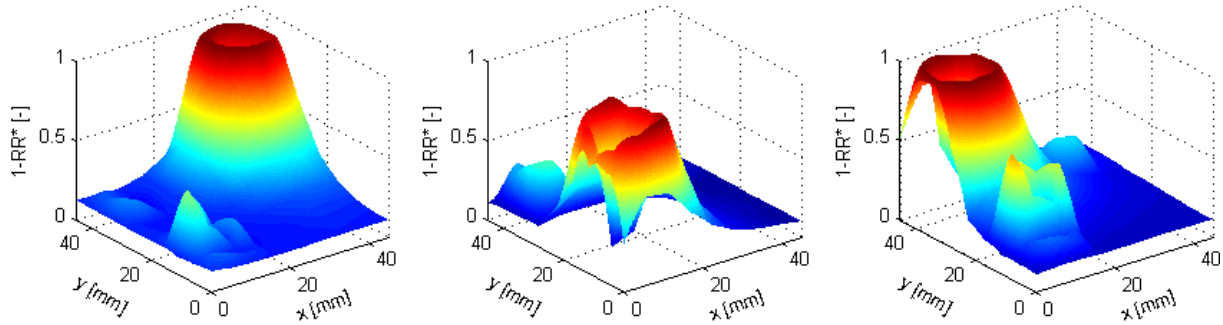

Fig. 7-23. 'Absorption' at 1330 Hz, 1841 Hz and 2218 Hz.

These tests demonstrate that the absorption properties of individual tubes can be characterised. Similar as in the case for a single quarter-lambda tube, the local absorption is one around the tube because the real part of the reflection is zero, but approaches zero directly above the tube because the real part of the reflection approaches minus one.

7.4.3. Integration over the surface

Often, the overall absorption of the whole sample surface is of interest, rather than the absorption at a specific point. The overall absorption is not obtained by summing the local impedance or absorption values, but by integrating the intensity over the surface of the sample. When there are plane waves, this can be achieved by integrating the normal ingoing intensity I_0, which is measured if the sample is not present, and the normal intensity above the sample I_1 (equation 2-23 and 6-1):

$$\alpha = \frac{\mathrm{Re}\int_S I_1 dS}{\mathrm{Re}\int_S I_0 dS} \qquad (7\text{-}8)$$

The intensity integral may be approximated by measuring multiple points or by scanning the surface. The latter procedure resembles surface scans, which are frequently performed for sound power measurements. For light samples, the sample can sometimes better be moved rather than the test set-up because then the probe-surface distance is kept constant. However, sound generation induced by this movement should be avoided.

Fig. 7-24 shows the 'absorption' coefficient of the quarter-lambda sample measured with a Kundt's tube compared to 'absorption' obtained using equation 7-8. The frequency where the 'absorption' is highest is equal for both methods, but the value estimated with the Kundt's tube is higher. An explanation for the differences between the two methods could be that the measured sample area with the Kundt's tube was smaller than with the *in situ* method. The 'absorption' of such samples depends on the surface area of the flat plate versus the total surface area of all tubes. The area of the flat plate is restricted by the inner dimensions of the Kundt's tube, which were 46mmx46mm.

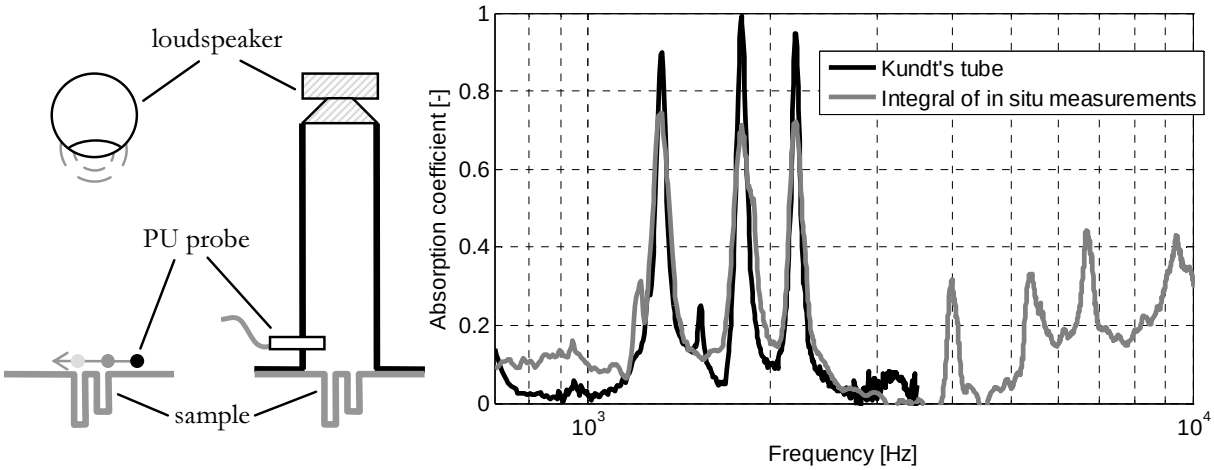

Fig. 7-24. Left: quarter-lambda sample measured *in situ* with a probe at multiple positions and with the Kundt's tube. Right: measured 'absorption' coefficients.

7.4.4. Sample #3: Open aluminium foam

The third example is a 10mm thick light aluminium foam filled with cavities, which is used in aerospace applications (fig. 7-25 left). The same grid and measurement conditions as in the previous example are used and the absorption is calculated with equation 7-8. Fig. 7-25 right shows a high spatial variation of the local absorption at 3kHz. Again the effective absorption is calculated, which shows the same trend as the absorption obtained with a Kundt's tube (fig. 7-26).

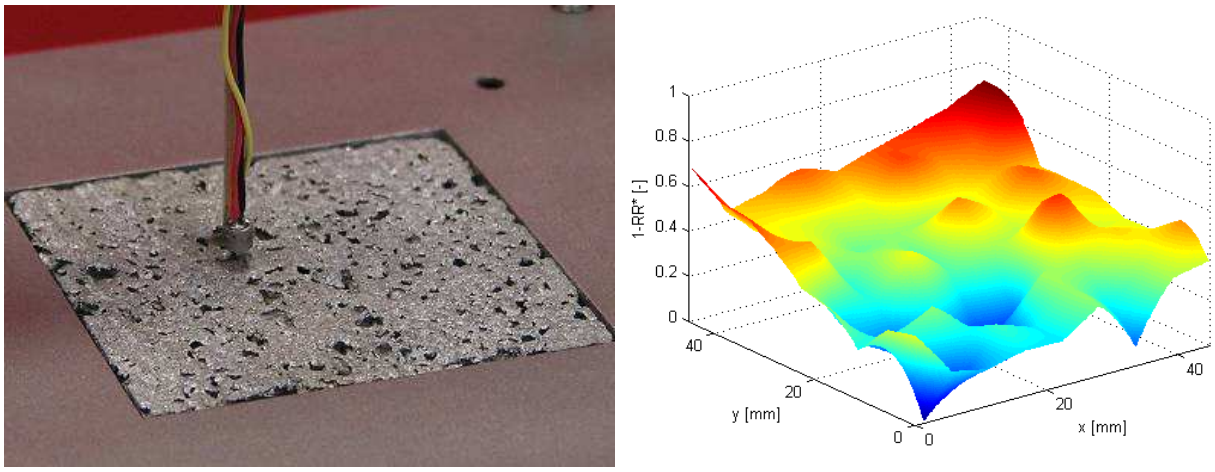

Fig. 7-25. Aluminium foam sample. Left: PU match probe scanning the surface. Right: spatial distribution of absorption at 3kHz.

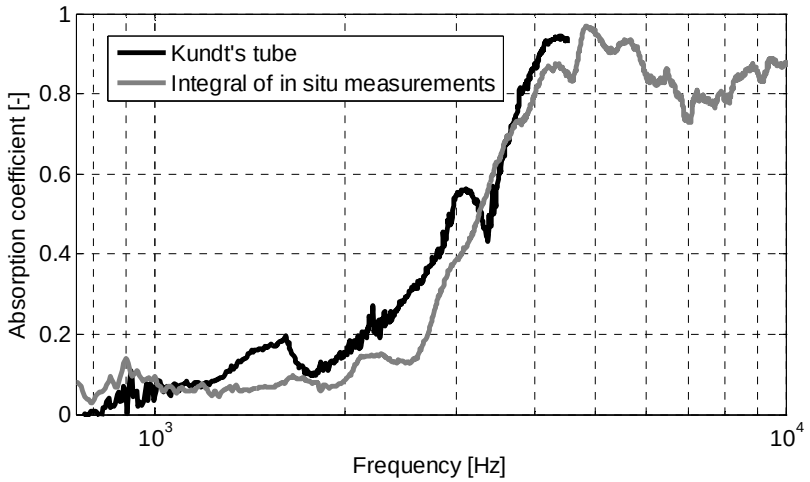

Fig. 7-26. Absorption coefficient of the aluminium foam sample determined by combining multiple measurements using equation 7-8.

7.4.5. Sample #4: μ-logo

The next example also demonstrates that the resolution is in the order of a millimetre *[121]*. The sample that is measured consists of a sheet metal layer with a refined μ-logo (fig. 7-27 left). A layer of acoustically damping melamine foam is present behind the logo. Instead of moving the measurement set-up, the sample itself is moved with an X-Y table (fig. 7-27 right). The tests are performed with a miniature probe approximately 1.5mm above the sample surface. The X-Y table is moved in both directions in small steps of 0.67mm. The sound pressure and particle velocity are measured at 2754 positions in a 12.3cm^{2}area.

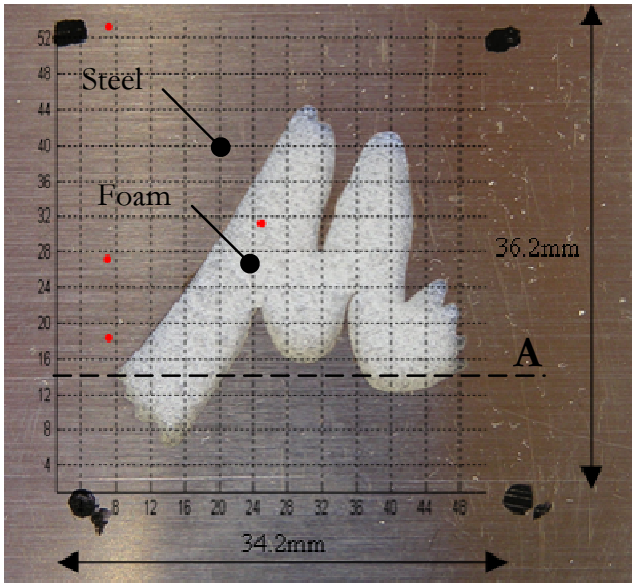

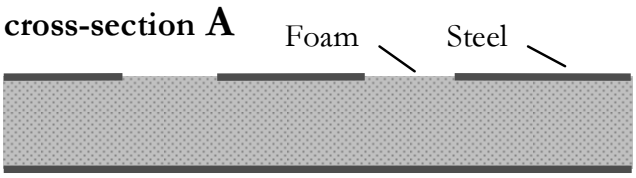

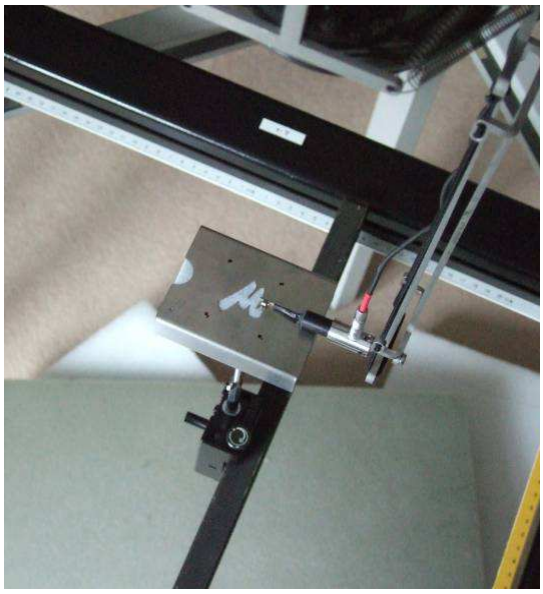

Fig. 7-27. Left top: Sample and the measurement grid. Left bottom: cross-section A as was indicated in the top figure. Right: sample is moved with an X-Y table.

Again, a higher spatial variation is measured with particle velocity (maximum 30 dB) than with sound pressure (maximum 10 dB) and the contour of the logo is better recognisable with particle velocity (fig. 7-28). For example, at cross-section A ($y = 7$ mm), the particle velocity changes 6.1 dB per millimetre over x, while the sound pressure hardly varies (fig. 7-29).

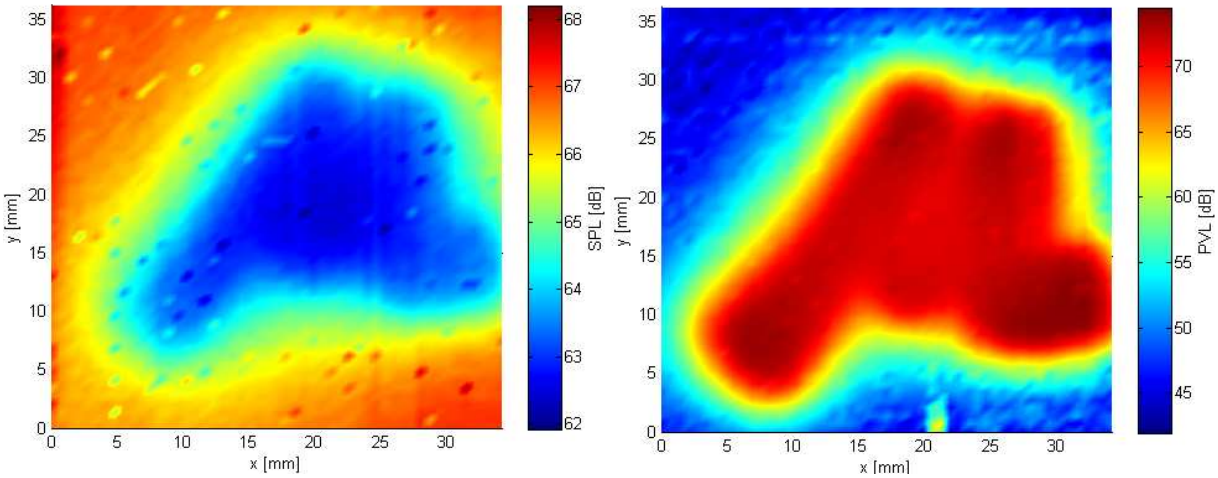

Fig. 7-28. Spatial distribution. Left: sound pressure at 2733 Hz in dB (re. 20 µPa). Right: particle velocity at 1857 Hz in dB (re. 50 nm/s).

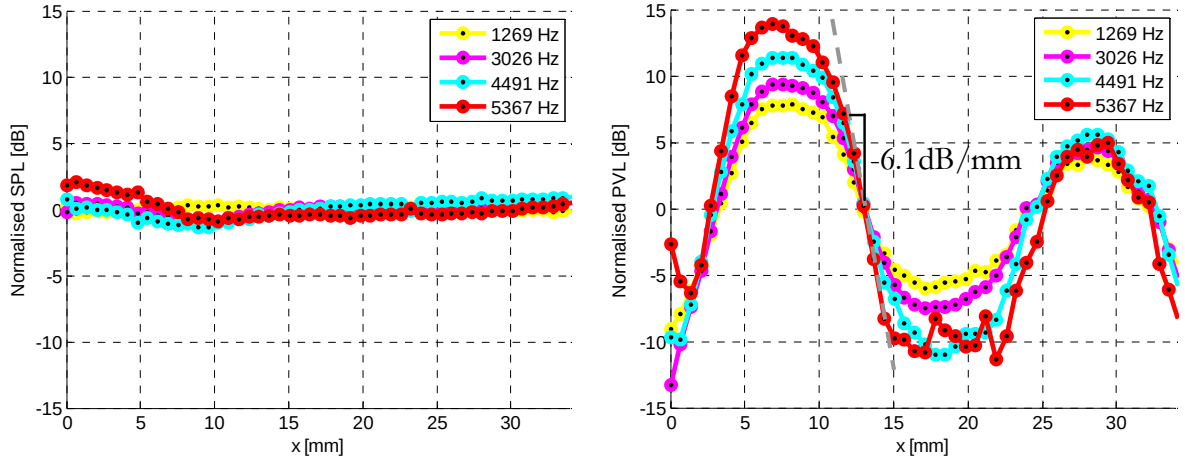

Fig. 7-29. Variation of sound pressure (left) and particle velocity (right) over x at cross-section A (y = 7 mm).

Fig. 7-30 shows the local reflection and absorption. The contours of the logo are best visible in between 1.5 kHz to 5 kHz. Further investigation is required to reveal if the resolution of the measurement method is frequency dependent, or if the variations found over frequency are caused by the damping properties and the geometry of the sample.

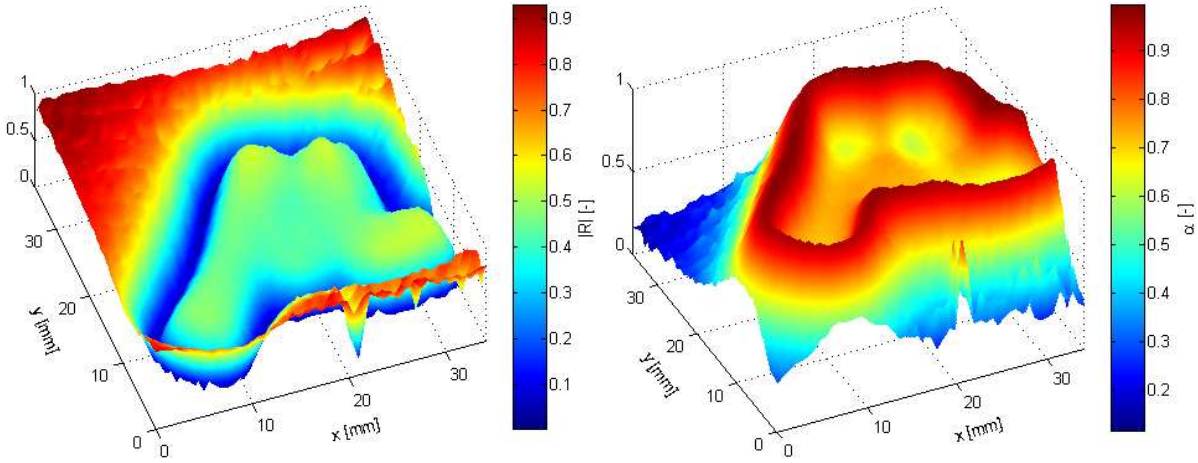

Fig. 7-30. Left: local reflection at 1878 Hz. Right: local absorption at 2133 Hz.

7.5. *Variation of intensity and impedance versus angles of incidence*

The surface impedance of a sample may vary for different angles of incidence. In that case, the random incidence absorption coefficient should be calculated by integrating tests for all angles of incidence. Here, the possibility of measuring absorption at oblique angles of incidence has not been investigated, and this remains a topic of interest. However, in a preliminary study the variations of the impedance and the intensity above the surface of a real

sample have been measured for different angles of incidence *[122]*. The test procedure and the results obtained are presented.

A sound source was positioned 265mm above a Flamex sample, while the probe was moved in horizontal direction (fig. 7-31). The particle velocity normal to the surface and the sound pressure were measured. In direction x, measurements were done in 10mm steps from $x=0$mm up to $x=560$mm. The probe-surface distance was kept 5mm.

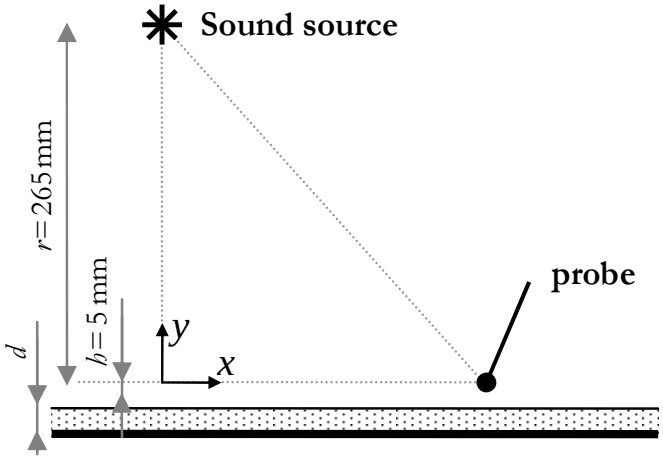

Fig. 7-31. PU probe moved in direction *x* in 1cm steps across the sample surface.

Fig. 7-32 shows the measured intensity and impedance at each position for several frequencies. These values are normalised with the test at position $x=0$. Intensity declines gradually with angle of incidence and no strong spatial variations occur (fig. 7-32 left). However, an interesting observation is made at for example 250 Hz and 325 Hz; the normalised intensity is negative between $x=0.22$m and $x=0.36$m, which means the reflected intensity exceeds the ingoing intensity. A possible cause could be that the probe is positioned above the sample and that the reflection against the sample does not occur below the probe, but slightly to the side, and that the absorption is low at those frequencies. In that case, the angle of incidence of the direct and the reflected wave are different. Supposing that all sound reflects at the surface of the sample, the reflections can be represented as a mirror source at $-r$. Intensity I_1 of the reflected wave is lower than intensity I_0 of the incoming wave due to the slightly longer path length. However, the intensity normal to the surface is measured here, which is $I_0 r/\sqrt{r^2+x^2}$. The angle of incidence of I_1 is smaller because the mirror source is positioned at $-(r+2h)$ instead of r.

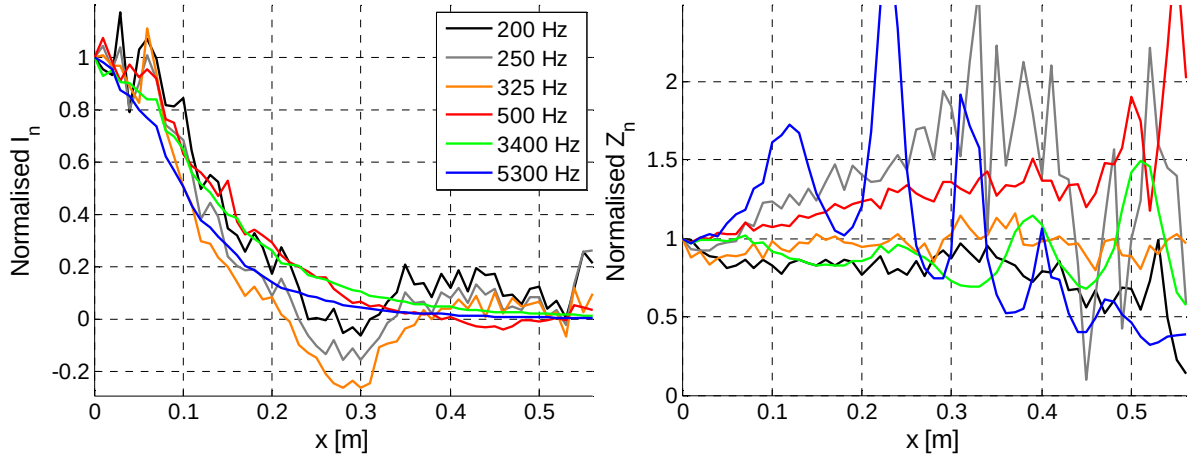

Fig. 7-32. Normalised intensity (left) and impedance (right).

The impedance (fig. 7-32 right) shows larger spatial variations than the intensity. At high frequencies (>800Hz), but also at for example 250Hz, strong interferences occur between the incoming and reflected waves. Although there are impedance-based absorption models that correct for these spatial interferences, they seem more sensitive for measurement and modelling errors. Absorption methods based on intensity rather than impedance are therefore potentially more robust for measurements at oblique angles and fewer tests might be required to calculate the random incidence absorption. An explanation for the more gradual decay of intensity is that there are spatial interferences depending on frequency and position, which causes the sound pressure to decrease while the particle velocity increases (or visa versa). The variation of the product of these quantities, which is used for intensity, is lower than that of the ratio of these quantities, which is used for impedance.

7.6. *Dynamic range of PU absorption measurements*

The signal-to-noise ratio (SNR) is an important figure. The measurement is invalid if the self-noise of the sensor or background noise is too high. In order to get an impression of the SNR during typical absorption measurements the sound pressure and the particle velocity signals are measured under different conditions; i.e. under free field conditions, close to a full reflective plate, and with the sound source switched off *[77]*. The distance between the probe and the sound source was 17cm, and the distance between the probe and the plate was 4.5mm. The sound source was driven with 1W pink noise. Fig. 7-33 shows the measured responses. The SNR of sound pressure signal is smaller than 10dB in the free field below 100Hz. As expected, the sound pressure response

increases about 6 dB if there is a reflective plate. The free field particle velocity SNR is higher than that of the sound pressure, especially at low frequencies. However, near the plate the particle velocity SNR is smaller than 15 dB because the particle velocity decreases due to reflections.

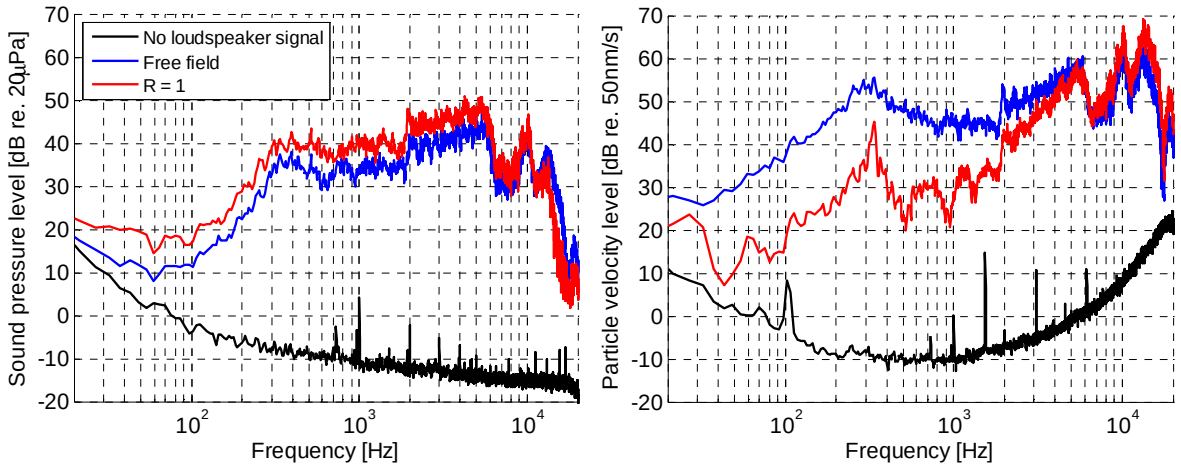

Fig. 7-33. Measured sound pressure and particle velocity in front of a sound source.

Two main factors limit the SNR at low frequencies. Firstly, there are restrictions to the size and type of the sound source because of the close proximity of the sound source. Compared to the far field, sound pressure increases less than particle velocity during the reference test without a sample because of near field effects (fig. 7-33, blue lines, below 100 Hz). Sound pressure is therefore earlier affected by background noise than the particle velocity. Secondly, the particle velocity, and thus the SNR, can be low if the reflection from a sample is strong (fig. 7-33 right, red line). The SNR of particle velocity often increases when the probe is moved further from the sample. With the current set-up, tests are difficult to perform below 100 Hz to 300 Hz because of SNR issues. Lower frequencies might be accessed with different geometries and sound sources.

Problems are also experienced at high frequencies. Firstly, for smaller wavelengths the probe becomes an obstacle because of its size. For instance, the maximum frequency of a regular half-inch PU probe is 10 kHz. Smaller probes should be used above that frequency. In addition, there can be interferences between the incoming and the reflected sound wave depending on the probe-sample distance h. If there would be plane waves and a single full reflective surface such interferences occur if h is equal to an odd multiple

of a quarter wavelength for sound pressure, or a multiple of half a wavelength for particle velocity. These interferences occur at higher frequencies by decreasing h. However, in most cases there are spherical waves and some sound has travelled through the sample. The frequency at which, and the degree to which, these interferences occur therefore change, see section 7.2.1. Furthermore, at high frequencies the self-noise of a Microflown sensor is higher than that of typical microphones. This is not a problem for absorption measurements in front of the sample, but the SNR is sometimes low for transmission loss tests behind the sample because sound waves that have travelled through the sample are usually strongly attenuated. Finally, small surface irregularities may become important because the probe is positioned near the surface, and sometimes even reflections from small objects near the set-up can cause discrepancies.

Validation of the results at very high frequencies is problematic because there are no other suitable measurement techniques beyond 10kHz, and because a comparison with absorption models only is not necessarily convincing. With miniature PU probes, credible results have been measured up to at least 20kHz; i.e. the measured absorption continues in an oscillating manner for a foam sample and is low for a steel plate, as would be expected from theory.

The coherence function is suitable for identifying if two inputs are linearly related, and is often used to check if the SNR is high enough. It can be calculated by the squared cross-spectrum of two signals divided by the auto-spectra of both signals. However, this quantity is not necessarily predictive for the quality of absorption measurements. In *[61]* the coherence of a PP probe and a PU probe were compared in a situation without a sample. The distance between the probe and the sound source was 23cm. Fig. 7-34 shows the results. The left figure shows the coherence between the sensors of both probes. The right figure shows the coherence of a sound pressure- and a particle velocity sensor relative to the input signal of the sound source (the 'perfect' reference).

The coherence between the two microphone signals of the PP probe is high, even at low frequencies (left figure, grey line). However, as is previously mentioned the sound pressure may be dominated by background noise rather than the loudspeaker-signal at low frequencies. The coherence between a

sound pressure microphone and the loudspeaker input signal is therefore also calculated (right figure, grey line). It can be seen that the coherence is low below 100Hz, which means that the sound pressure signal and the loudspeaker-signal are weakly related. Therefore, the coherence between the two sound pressure microphones of a PP probe is an inadequate indicator for the quality of the absorption measurement.

The coherence between the particle velocity signal and the loudspeaker signal is still high down to 70Hz (right figure, black line). However, also the coherence between the two sensors of the PU probe is sometimes a poor indicator for the quality of the absorption measurement. For example, if the reflection from the sample is strong the coherence can drop because the particle velocity level near the sample is low, but this does not necessarily mean that the measurement quality is poor. The coherence is only an appropriate quality indicator if the loudspeaker signal sufficiently exceeds the signal of other noise sources.

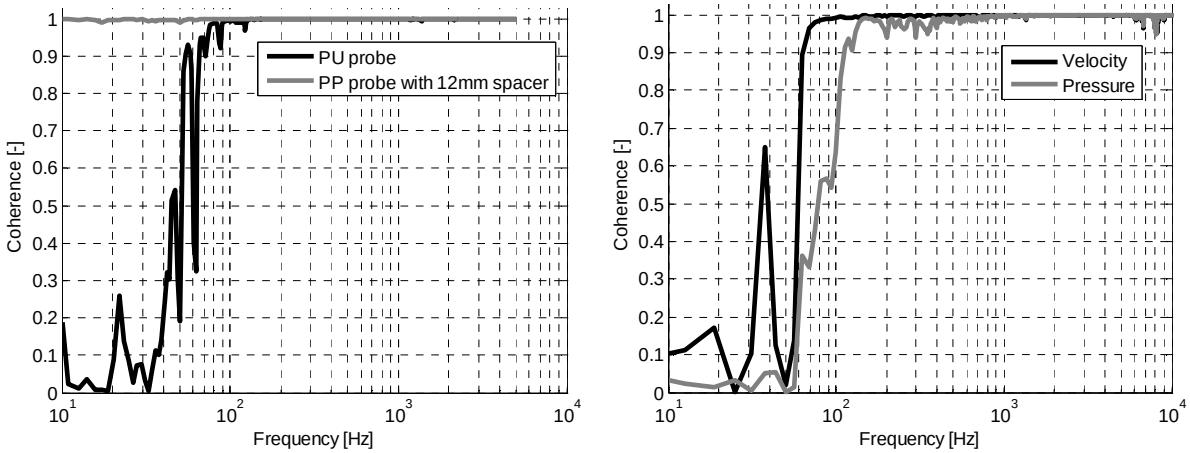

Fig. 7-34. Left: Coherence between each probe's associated sensors. Right: Coherence of sound pressure and particle velocity to the loudspeaker input signal.

7.7. *Influence of background noise*

Background noise can be a source of error for any *in situ* measurement. The effect on the measurement results depends on the distance, the angle of incidence, and the strength of external sound sources relative to the sound source of the set-up itself. The absorption model used, the characteristics of the absorbing sample, and the probe-sample distance are also of influence. The effect on impedance- and intensity-based methods is determined using the sample arrangements shown in fig. 7-35.

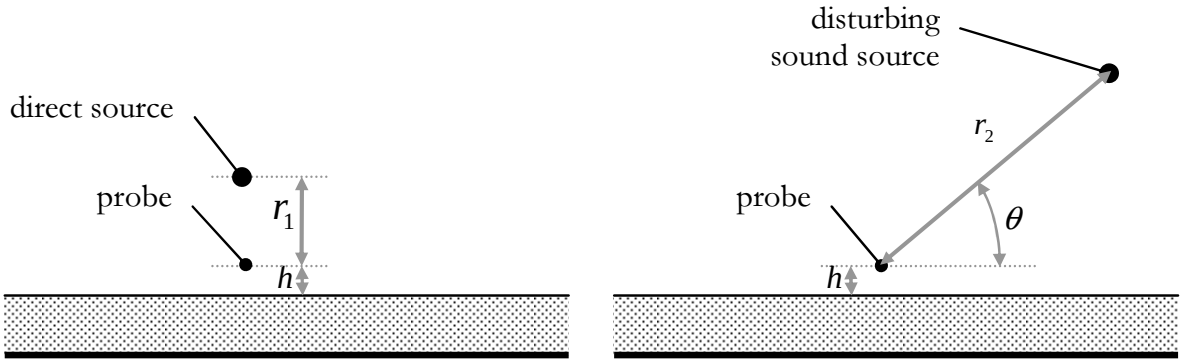

Fig. 7-35. Background noise tests. Left: configuration B with the direct source only. Right: configuration C with the disturbing sound source at an oblique angle.

In order to compare the results with and without background noise the tests with the direct source and with the disturbing sound source are performed separately to allow their relative strength to be varied artificially afterward. The following measurement configurations were used:

Config. A. A reference measurement without a sample to characterise the responsivities of the sensors (no background noise source).

Config. B. Normal incidence absorption measurements above a sample with a backplate (fig. 7-35 left). In this configuration four tests were performed, i.e. with the Flamex sample for $h = 5\,\text{mm}$ and 30 mm, and with the Linoleum sample for the same distances.

Config. C. The same sound source is positioned further from the probe at an angle θ to mimic a disturbing source (fig. 7-35 right). In total 80 tests were performed for different values of θ (varying from 0 degrees up to 90 degrees in 10 degrees steps), for $h = 5\,\text{mm}$ and 30 mm, for the Flamex sample and the Linoleum sample, and for $r_2 = 0.5\,\text{m}$ and 1 m.

The absorption without background noise can be obtained by combining measurements from configurations A and B. The distance between the probe and the sound source was $r_1 = 300\,\text{mm}$ in both configurations. The noise of the sound source in configuration B is uncorrelated to that of configuration C, just as would be the case in reality. The absorption with background noise can be obtained using the measured sensor signals from configuration B and C.

The absorption is calculated for the situation without background noise (the reference absorption measurement), and for the situation with a disturbing source that has a three times higher intensity than the direct source. Fig. 7-36 and 7-37 show the results for both absorption models ($h = 5\,\text{mm}$ and $r_2 = 1\,\text{m}$).

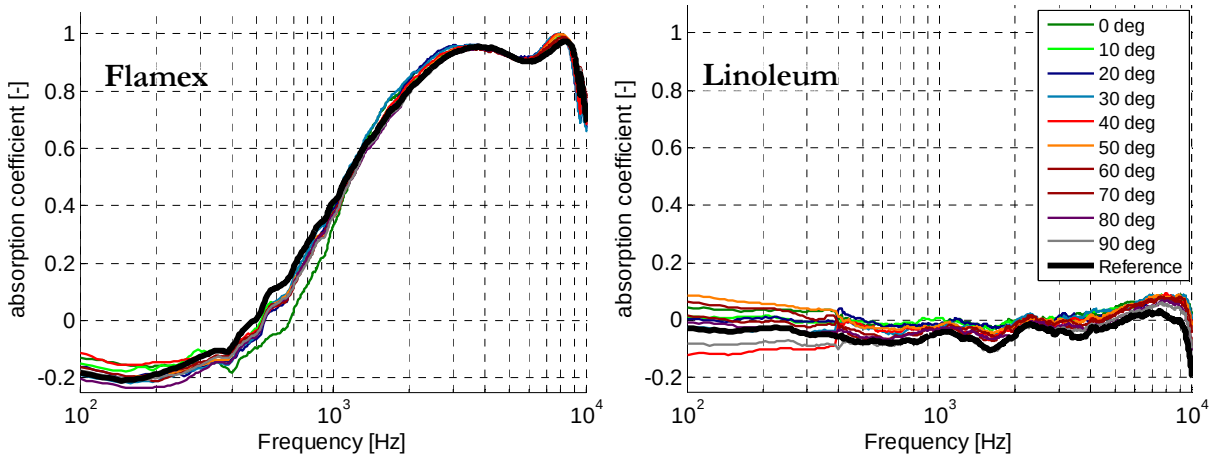

Fig. 7-36. The 'absorption' that is calculated by the mirror source model with a disturbing sound source that has a three times higher intensity than the direct source.

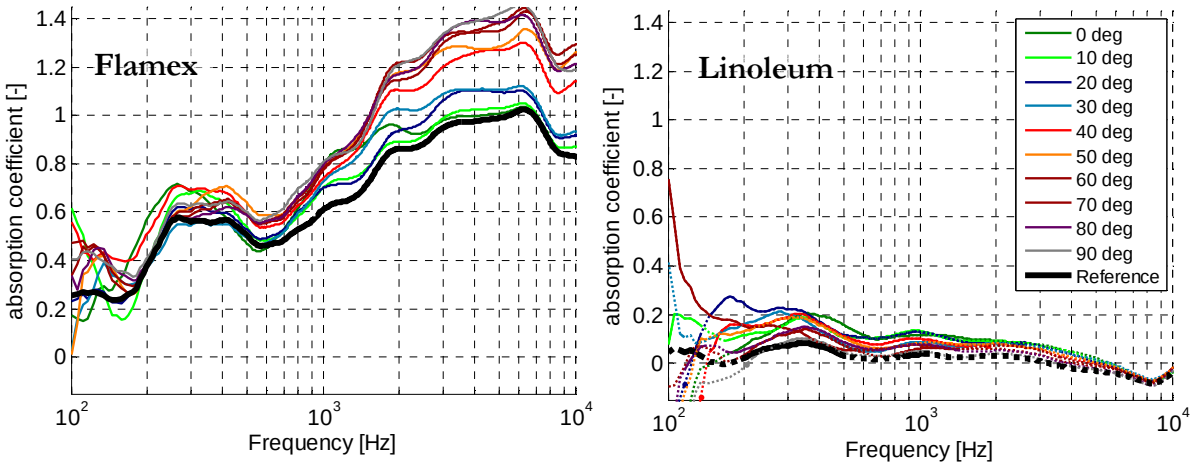

Fig. 7-37. The 'absorption' that is calculated with intensity with a disturbing sound source that has a three times higher intensity than the direct source.

As was mentioned before, absorption values of the Flamex sample are underestimated at low frequencies with the mirror source model due to near field effects, and overestimated by the ratio of intensities because it is not extrapolated to $r = \infty$. For $h = 5\,\text{mm}$, the absorption is hardly affected by background noise, except with the intensity method for the Flamex sample at high frequencies. In this case, the absorption is overestimated because the sound level is elevated by the external sound source during intensity measurement I_1

with a sample, and not during measurement I_0 without a sample. In actual applications, the ingoing intensity of the background noise is sometimes impossible to determine. The background noise causes an increase of I_1 if the reflection coefficient of the sample is low. If the reflection coefficient is high, which is the case for the Flamex sample at low frequencies and for the Linoleum sample, the strength of the reflected sound waves is considerable compared to the ingoing sound waves, thus the net intensity contribution of background noise is low. The discrepancies of the mirror source model are smaller for low reflecting samples than those of the intensity model. This is because the mirror source model uses the impedance rather than the intensity; although the sound levels are increased by the background noise, the impedance, which is the ratio of sound pressure to particle velocity, is affected little because both quantities are increased in a similar way.

The required loudness of the direct source relative to the disturbing sound source was determined for the maximum absorption deviation of 0.1. Fig. 7-38 and 7-39 show the dynamic range in dB that is required when using the mirror source model and the intensity model, respectively. For example, a value of -10 dB means that the intensity of the direct source is allowed to be 10 dB lower than the disturbing sound source. As expected, the required dynamic range is higher if the disturbing sound source is positioned closer to the probe; apart from small variations due to spatial interferences, the required range increases roughly 6 dB (grey versus black curves, and blue versus red curves).

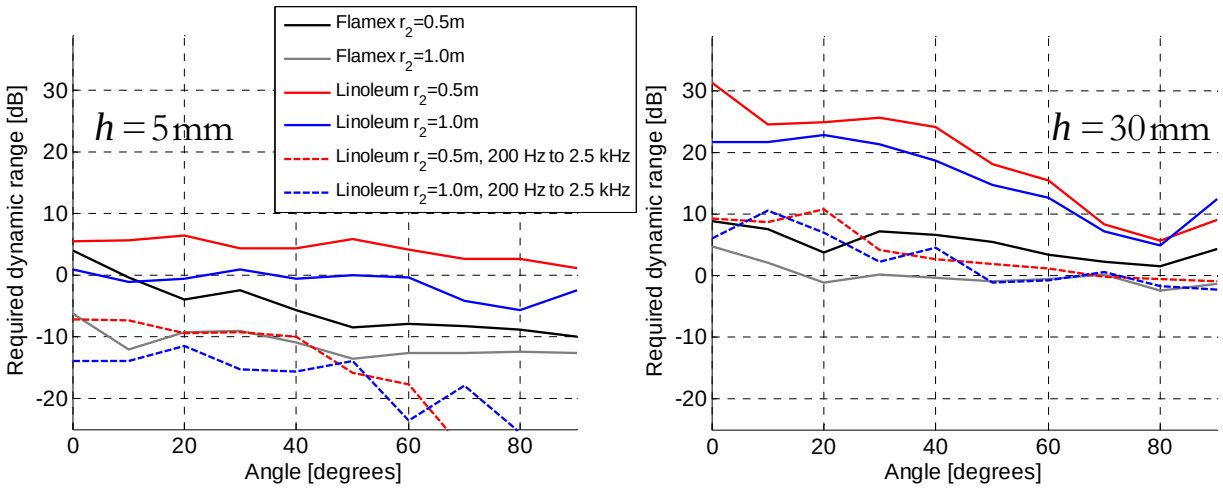

Fig. 7-38. Required dynamic range for the mirror source model for a maximum error of 0.1 for two probe-sample distances.

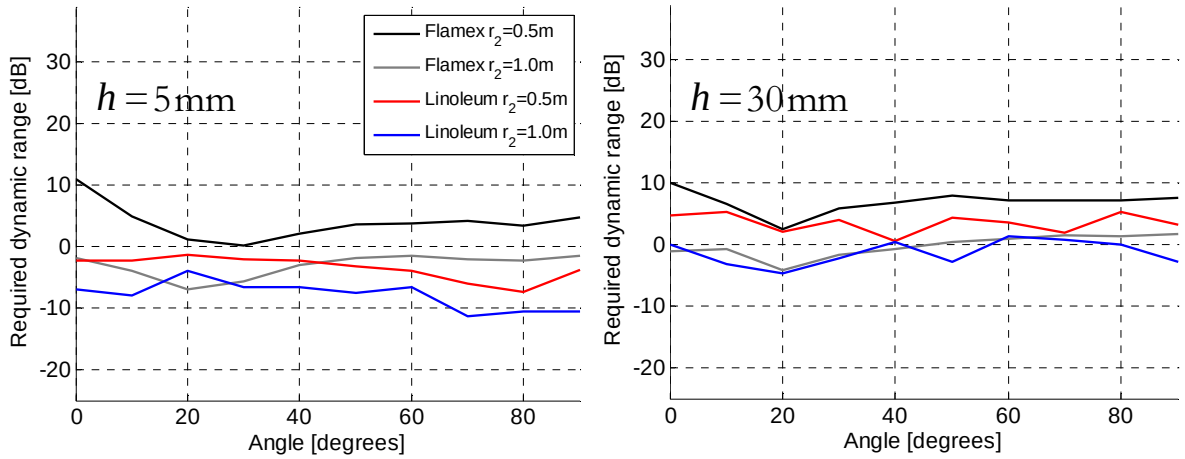

Fig. 7-39. Required dynamic range for absorption obtained with intensity for a maximum error of 0.1 for two probe-sample distances.

The disturbing sound source mostly affect the results calculated with the mirror source model for the linoleum sample and $h = 30\,\text{mm}$. The required dynamic range is highest in that case (fig. 7-38 right, solid red and blue line). Although a different loudspeaker was used to generate the background noise, similar deviations were found in [128] where a dynamic range was found in between 23 dB (at $\theta = 70$ degrees) and 30 dB (at $\theta = 0$ degrees) for $r_2 = 1\,\text{m}$.

The tests described here revealed that high errors mainly occur when the particle velocity without background noise is low. Fig. 7-40 left shows the absorption calculated by the mirror source model for $h = 30\,\text{mm}$ and $r_2 = 1\,\text{m}$ for a disturbing sound source that is equally loud as the direct source. It can be seen that the highest discrepancies are found around 2.8 kHz (indicated by the dashed oval), because the sound waves from the direct source and its reflections interfere. The sound pressure or particle velocity level due to the direct source is low around the frequency of interference, and then the effect of small measurement inaccuracies is profound. Therefore, the required dynamic range was also calculated for a limited frequency band of 200 Hz to 2.5 kHz (fig. 7-38 right, dashed red and blue lines). These values are lower than the broadband values.

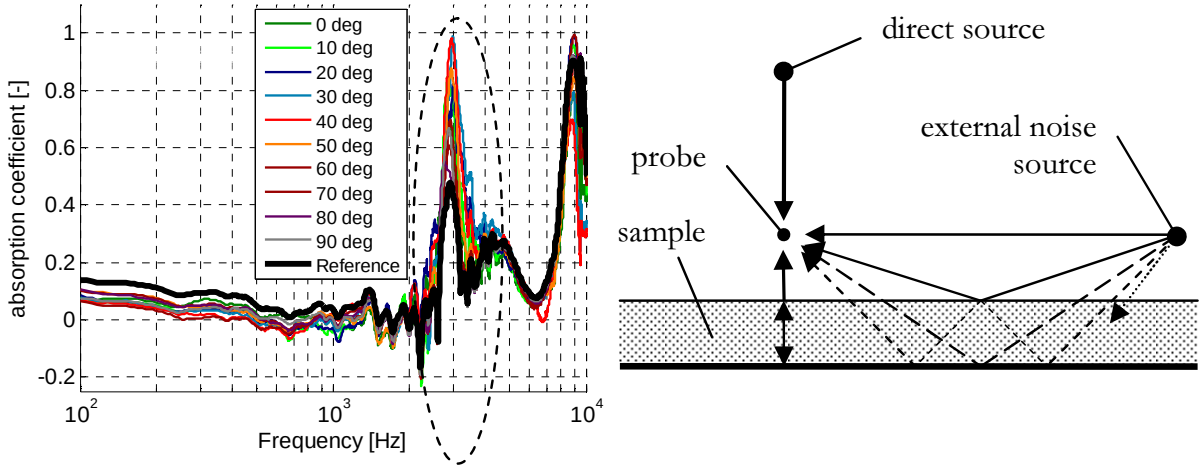

Fig. 7-40. Left: The 'absorption' that is calculated by the mirror source model for a disturbing sound source that has an intensity three times higher than the direct source. Right: contributions of reflections from the external sound source for $\theta = 0$ degrees.

Another observation from fig. 7-38 and 7-39 is that the required dynamic range depends less on the angle of incidence as might be expected. Although at $\theta = 0$ degrees the direct contribution from the disturbing sound source to the normal particle velocity is zero, there is a contribution from sound that has reflected at the top or that has travelled through the sample (several times). The matter is illustrated in fig. 7-40 (right).

It can be concluded that the influence of background noise is rather low. The intensity of a disturbing sound source at 1m distance is allowed to be 10dB higher than the intensity of the sound source of the set-up for these two samples. Noise sources are usually positioned further from the probe. However, in reality the shape of the background noise spectrum may be different from that of the direct source.

7.8. *Measurements with airflows*

Airflows can considerably affect the signal of a Microflown sensor. Regular PU probes already overload at an airflow level of ~0.5m/s, mainly because the sensor wires are cooled down too much, and because of airflow instabilities [14]. The microphone signal is usually less affected by mean airflows and flow instabilities. Apart from (flow-induced) sound, much of the particle velocity signal and sound pressure signal is uncorrelated, and the cross-spectrum of both signals is therefore less affected by airflows than the particle velocity auto-spectrum alone.

Several wind caps have been developed throughout the years in order to cope with higher airflow levels. Larger wind caps generally perform better, but for absorption measurements this would mean that the distance to the sample surface would need to increase as well. Three existing wind caps that have smaller diameters are shown in fig. 7-41 [14], *[123]*. The maximum wind speed ratings displayed are valid for free field conditions, but not for absorption measurements. Additional turbulences are introduced by the sample, which affects the sensor signals. For instance, tests with the nose cone have been done 2cm from the surface of a flat sample. The measured impedance was already at 7m/s severely affected below 400Hz, instead of 70m/s in the free field situation *[34]*. This is sufficient for most outdoor tests, but there is a desire to measure up to 30 m/s or higher for e.g. jet engines. Depending on the application, different measures to protect against airflows might be applied. For example, in the next chapter a dedicated wind cap is presented which is intended for absorption measurements whilst driving.

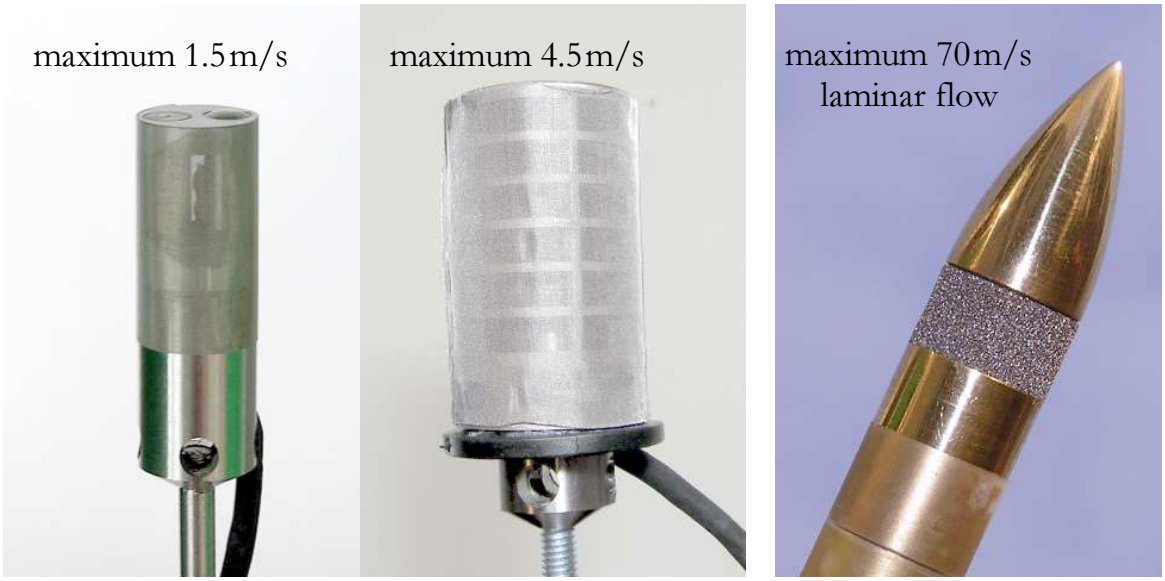

Fig. 7-41. Small wind caps. Left: half-inch single metal mesh. Middle: one-inch double metal mesh. Right: half-inch nose cone.

7.9. Conclusion

Several conditions that influence *in situ* absorption measurements with PU probes have been investigated in this chapter. Tests were performed with small samples and with high spatial resolution relative to other (*in situ*) methods, while little being affected by background noise. Two limitations of the absorption measurements themselves have been examined; i.e. the effect of the distance between the sample, the probe, and the sound source, and the stability over time. With the handheld measurement set-up, best results are obtained for source-probe distances in between 0.2m and 0.5m, and for probe-sample distances smaller than 30mm. In addition, the stabilities of the test set-up and test method were investigated with measurements performed over a two-week period. The mean standard deviation of the absorption coefficient found was below 0.05 in a 100Hz to 10kHz frequency range.

Furthermore, it was investigated which sample size is required. Certain trends were identified with simulations; i.e. higher deviations are found for larger values of h and r, and for open porous materials. The required size was determined experimentally for five sample types. Small sizes can be allowed compared to other *in situ* techniques that require several square metres. For these samples, the size should minimally be 0.07m^2 to 0.38m^2 in order for the results of the intensity method to be equal to those of large samples. For the mirror source model even smaller samples are allowed; i.e. 0.03m^2 to 0.18m^2. Furthermore, it was demonstrated that the results of the PU *in situ* method and the Kundt's tube can differ, depending on the sample type, but that similar values can be obtained if the sample mounting conditions are the same. Also, the results of the Kundt's tube can differ from those of large samples.

Tests with a miniature probe near the surface of non-homogeneous samples revealed that the resolution is in the order of a millimetre. This allows measurement of separate sections of acoustic absorbing samples. For example, the impedance of individual resonators and irregularities of non-homogeneous samples can be determined. By integrating the intensity across the surface, the effective absorption of the sample can be obtained.

The variation of impedance and intensity has been measured for oblique angles of incidence using a real sample. Tests were performed at several points just above the sample while keeping a sound source at a fixed position. Although the intensity decreases gradually with angle of incidence, the impedance varies strongly. It has not been attempted to determine the random incidence absorption coefficient that involves integration over all angles of incidence. Such results would allow a comparison to those of the frequently used reverberant room method. Yet, these tests show that, in order to approximate the random incidence absorption coefficient, fewer measurements might be required for methods based on intensity than on impedance.

The signal-to-noise ratio during absorption measurements is affected by a number of factors. For example, a low sound pressure level is emitted by the sound source at low frequencies, and the particle velocity level near a reflecting sample can also be low. Tests below 100 Hz to 300 Hz are therefore difficult to perform. Lower frequencies might be assessed with a more powerful sound source, although inevitably there are compromises regarding the set-up size and thus the influence of external disturbances. There are difficulties at high frequencies, because the incoming and reflected sound waves interfere, because of sample irregularities, and because the probe becomes an obstruction. Above 10 kHz, validation of absorption measurements is difficult because of a lack of appropriate techniques to compare with.

High levels of background noise can be tolerated, which could for example enable measurements in noisy production environments. For a source-probe distance of 30 cm, and probe-sample distances of 5 mm and 30 mm, the intensity of the uncorrelated disturbing sound source at 1 m from the probe is allowed to be 10 dB higher than the intensity of the sound source of the set-up.

In the last section of this chapter, several wind caps that can be used for measurements in airflows have been presented. The development of even smaller wind caps that can be used at higher airflow speeds remains a topic of interest for e.g. wind tunnel and outdoor tests.

8. New applications of PU *in situ* absorption methods

8.1. *Introduction*

Absorption measurements with PU probes might be used to complement or replace existing techniques, but also to enable new applications. In this chapter, some applications are explored for which other measurement methods where failing before. The objective of the investigations described was not to analyse specific acoustic problems in detail, but to demonstrate the potential of this new type of *in situ* measurement technique.

Examples of tests that were done in reverberant conditions are presented. It will be shown that the absorption coefficient of a sample that is measured while mounted at various positions inside a car is similar to the absorption measured under laboratory conditions *[77]*. The headliner (i.e. the car's inner ceiling) and passenger seat of several cars were measured to investigate if methods based on PU probes can be used consistently *[*91, 92*]*. Tests have also been performed in two concert halls *[*112, 128*]*. Up to now, there are few techniques to measure acoustic properties of separate structures in such rooms. *In situ* absorption measurements might be used for this purpose.

Sound-absorbing liners are used frequently to attenuate the noise of jet engines. Their absorption characteristics are usually determined with an open Kundt's tube. In *[34]* the outcome of tests with the PU *in situ* method and the Kundt's tube were compared, and large differences were found. Shortcomings of the latter method could be identified by adapting the test conditions for both methods.

Road need to be closed down for traffic for existing absorption measurement techniques. A dedicated set-up was build to explore the possibility of measuring the absorption with PU probes whilst driving, thus leaving traffic undisturbed *[130]*. Although improvements can be made, realistic results were obtained with the current set-up at regular driving speeds.

A quick high-resolution visualisation technique called 'Scan and Paint' will be introduced. Dedicated software that has been developed by Microflown Technologies is applied for the first time to measure radiation of sound sources *[*130-132*]* and absorption *[134]*.

Most results shown in this chapter are calculated with the mirror source model because the intensity-based extrapolation method was developed after many of the tests were performed.

8.2. *Measurements in non-anechoic conditions*

Up to date there are no generally applicable methods to determine the quality of acoustic absorbing samples properly during or after they are manufactured. If the consistency of samples over time is monitored at all, producers mostly perform random checks in a laboratory only, which requires samples to be cut out. Other existing *in situ* methods are affected by background noise and reflections from surrounding objects. PU *in situ* methods are less affected, mainly because the distances between the sound source, the probe, and the sample are kept small. Possible applications might be the assessment of for example rooms or industrial products during or after they are built.

Two applications with reverberant conditions are studied here, i.e. the possibility of measuring inside a car and inside a concert hall. Tests on a homogeneous sample have been performed on several locations inside a car, and the results are compared to those measured in the laboratory. Furthermore, the repeatability of the measurement method and the consistency of acoustic packages inside cars are investigated. Large inconsistencies of these sound-absorbing packages have been found. In addition, tests have been performed successfully on objects inside concert halls such as seats, walls, and carpets.

8.2.1. Measurements inside cars

The design of acoustic trim packages is an ongoing trade off between reducing noise levels, saving weight, and saving costs. Laboratory tests sometimes poorly represent samples as they are installed, and their consistency cannot be guaranteed. Therefore, accurate assessment of their absorbing properties *in situ* is a desirable matter.

A 15cmx15cm Foamex melamine foam sample with a strong reflecting and rigid backplate was first measured in laboratory conditions; i.e. a silent room with few reflections from surrounding surfaces. The sample was then placed at several positions in a car by de Bree et al. *[77]* with the doors open and closed to test the influence of different acoustic environments (fig. 8-1).

Fig. 8-1. Some positions that have been measured in the car.

Fig. 8-2 shows that the results obtained at several locations in the car are similar to those obtained in the laboratory. It hardly seems to matter whether the car door is open or closed. The foot area is a complicated place to measure; deviations are found below 800Hz, probably because there are reflecting surfaces at most sides close to the set-up. These tests demonstrate that the absorption can be determined under the reverberant conditions present in a car.

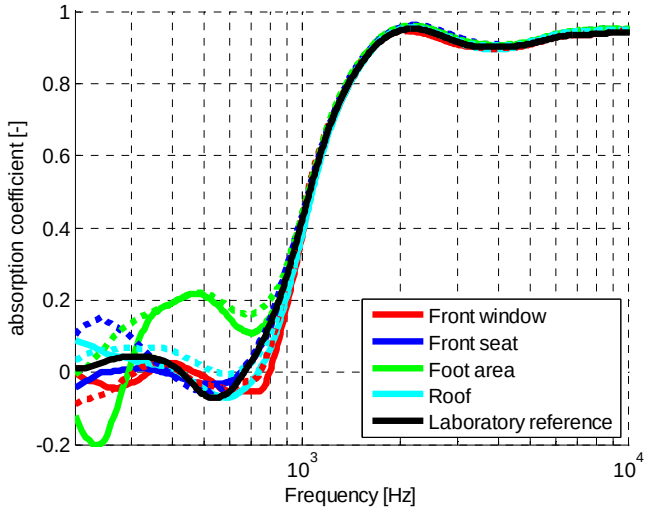

Fig. 8-2. Measured absorption of a test sample at several positions in a car. Solid lines: car door closed. Dotted lines: car door open.

In another test series, the headliner and the front passenger seat of 25 cars of the same make were measured to investigate if their acoustic properties are consistent [91, 92]. The reference car was measured each time before each of the 25 other cars was measured to demonstrate the reproducibility of the measurement method. The measured location on the headliner and seat was kept rather constant (fig. 8-3).

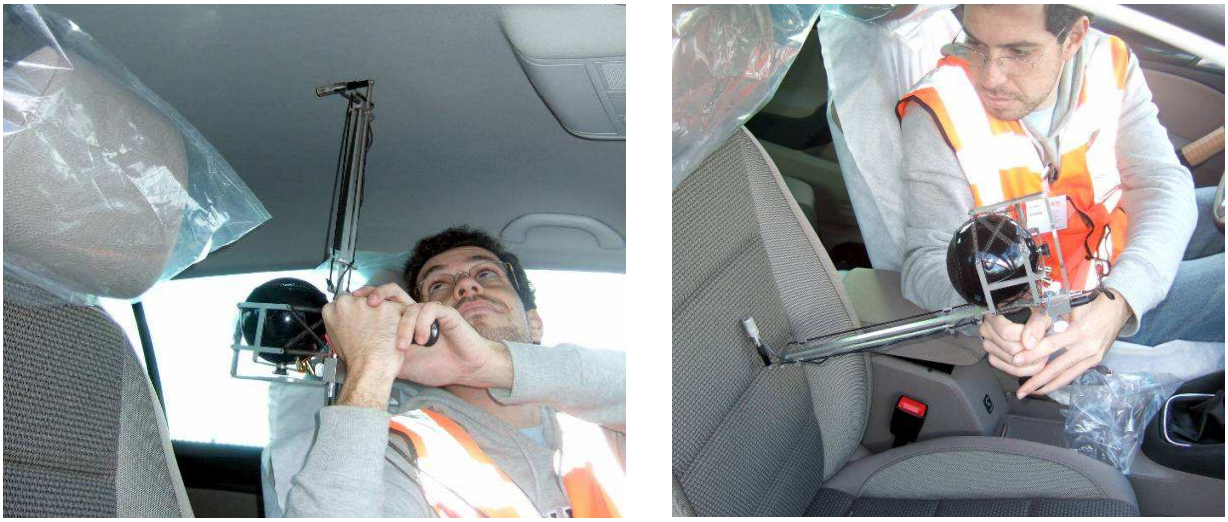

Fig. 8-3. Measurements on a headliner and a passenger seat.

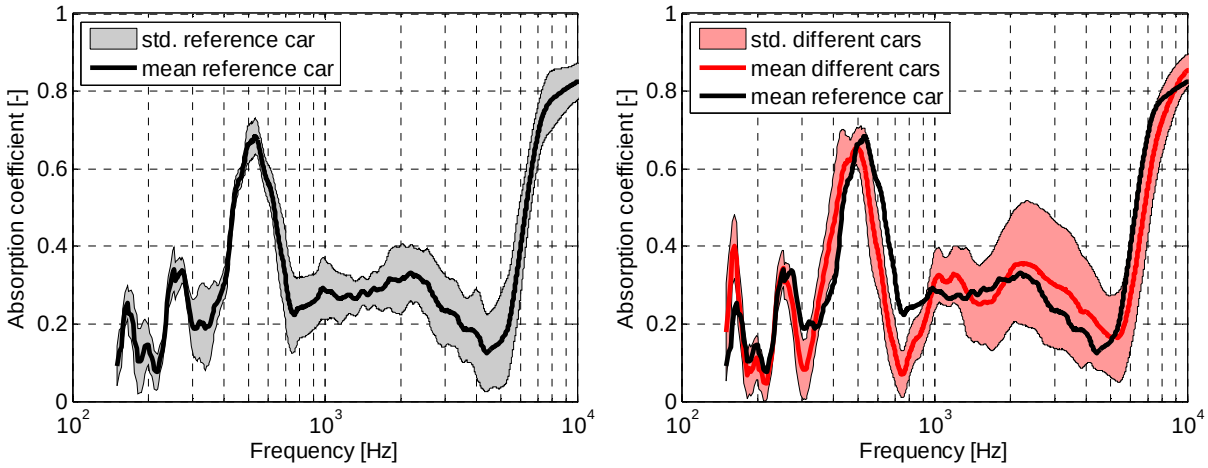

Fig. 8-4. 25 headliner measurements of the reference car and 25 measurements of different cars. Standard deviation is indicated by the coloured area.

Fig. 8-4 shows the mean value and the standard deviation of the 25 absorption measurements of the headliner in the reference car and 25 measurements of the headliner in different cars. Although more research is required to validate if the obtained absorption values are correct, it is possible to study the variations amongst the tests. Slightly higher discrepancies are found for the 25 different

cars than for the reference car, which might be caused by positioning errors and by variations amongst cars (fig. 8-4). However, the standard deviations of the tests in the reference car and the different cars were larger than expected originally. Several positions on a typical felt headliner sample were measured in order to determine the cause of the discrepancies for the reference car. The results from these tests were similar (fig. 8-5 left). Next, 25 tests were done across a larger area of an actual headliner in a car. Now even higher discrepancies were found than was the case with the reference car (fig. 8-5 right). It can therefore be assumed that these discrepancies are most likely caused by spatial variations of the headliner. The location varied during the 25 measurements of the reference car because no spot was marked on the headliner. These spatial variations could be caused by the air gap inside the headliner or by variations in the way the headliner is mounted with adhesives.

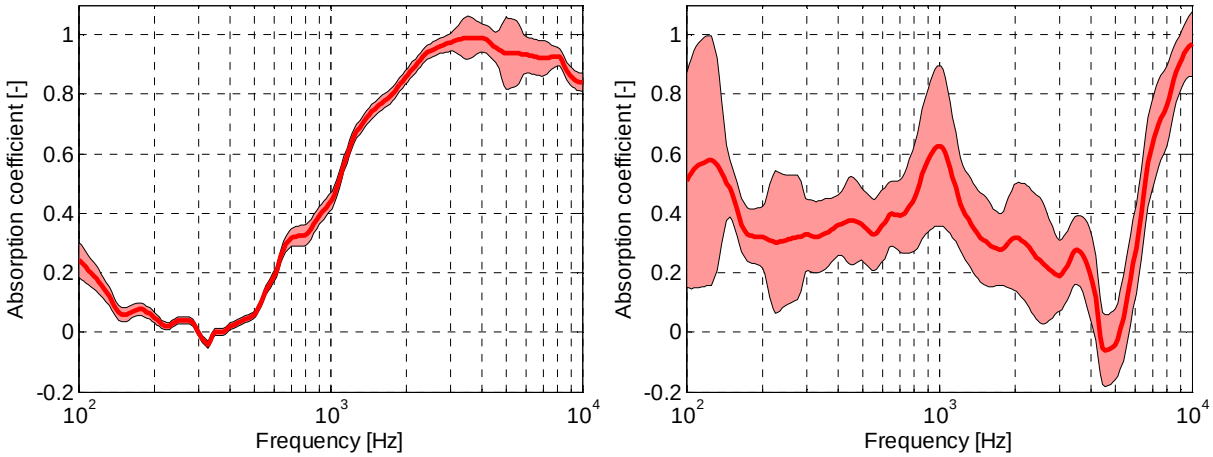

Fig. 8-5. 25 positions on a typical headliner sample: before mounting (left) and after installation inside a car (right). Standard deviation is indicated by the coloured area.

The results obtained from the tests of the left passenger seats are shown in fig. 8-6. The variations are low for the reference car (left figure). Surprisingly, the situation differs for the 25 different cars (right figure); the acoustic properties for different seats of the same type vary much. For car manufacturers who want consistent acoustic performance, this variation is problematic because due to weight savings there are few locations inside a car other than the seats were thick layers of damping material can be used. An acoustic quality check of car seats in particular is therefore recommendable.

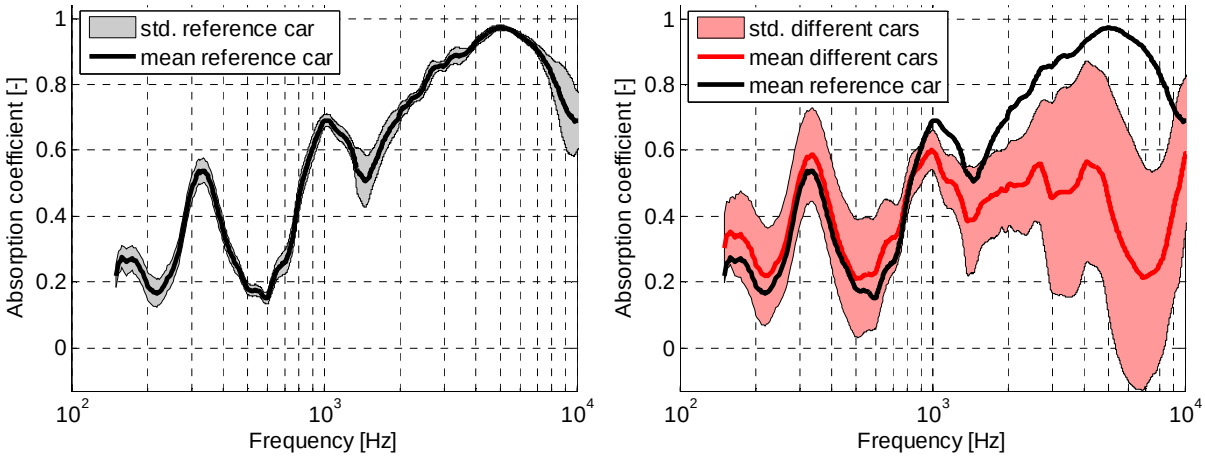

Fig. 8-6. Seat measurements: 25 times the reference car and 25 different cars. Standard deviation is indicated by the coloured area.

8.2.2. Measurements in concert halls

There is an interest to measure the acoustic performance of buildings like concert halls. Room acoustic parameters such as early decay time, clarity index, or definition are determined to characterise rooms by measuring the decay of sound pressure over time. However, such tests only provide a value of the entire room, while a suitable method for measuring individual structures *in situ* is lacking. Several wall panels, seats, and floor sections have been measured in the Musis Sacrum concert hall in Arnhem *[113]* and the concert hall of the Music Academy in Budapest *[129]*. Although these absorption measurements provide interesting results, their outcome should be interpreted with caution because real samples can be more complex than flat homogeneous samples, which have been considered up to now. For instance, all sound that is not reflected from a thin seat is not only absorbed by it, but is also partly transmitted through it. The absolute part of the reflection coefficient is shown in the following examples instead of the absorption coefficient because only tests in front of the test article have been performed. The transmission through the seat might have been considered as well with a method such as presented in chapter 6, but this method was not available yet at the time that the measurements were performed.

Fig. 8-7 shows the measured reflection of several seats in the Music Academy in Budapest. Reflection values slightly higher than one are measured below 150Hz and around 800Hz. Possible explanations for these errors are measurement inaccuracies, and that the applied mirror source model disregards the propagation of spherical waves inside samples (see chapter six).

Several thicker seats that reflect less at lower frequencies were measured in the Musis Sacrum concert hall (fig. 8-8).

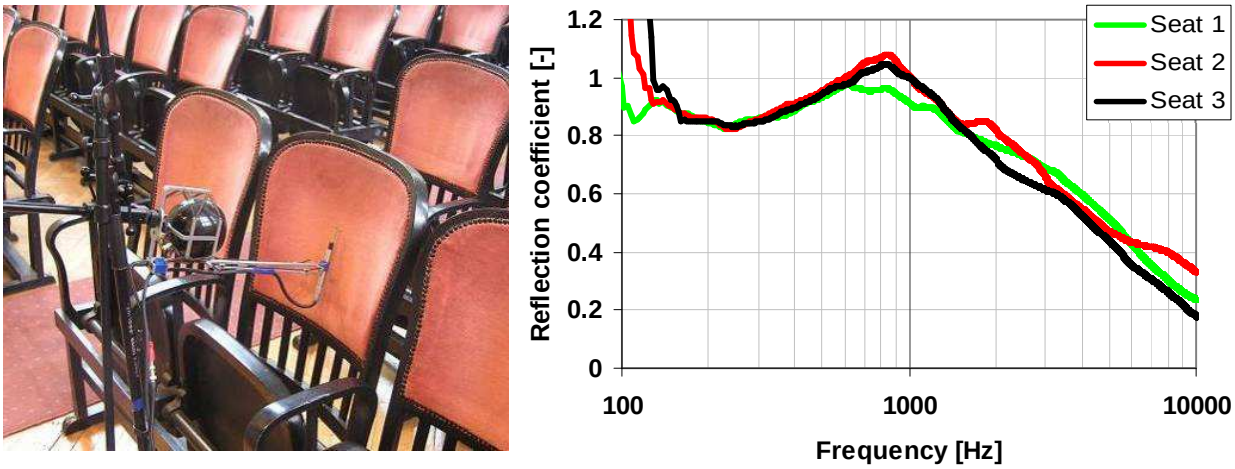

Fig. 8-7. PU reflection measurements on seats in the Music Academy in Budapest.

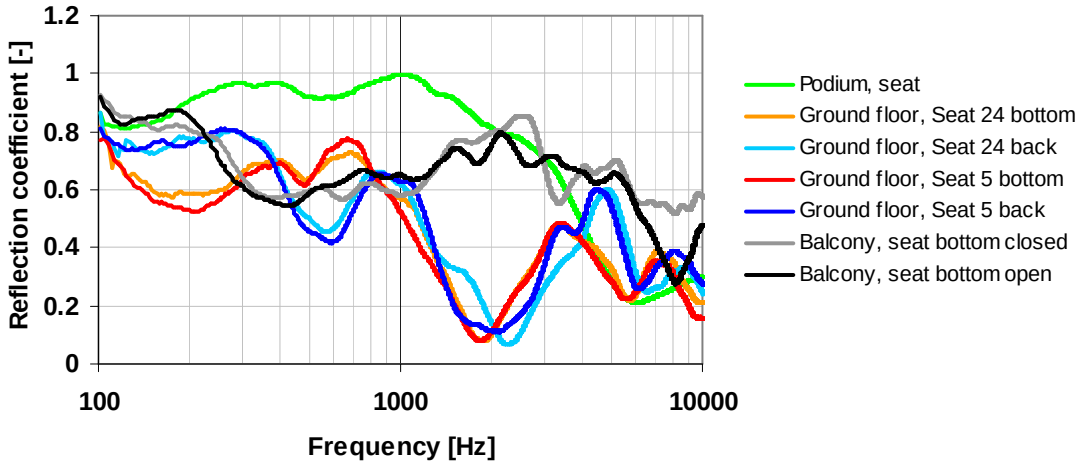

Fig. 8-8. PU reflection measurements on seats in the Musis Sacrum in Arnhem.

The reflection coefficients of the balcony floor and the deflector panels at the side of the stage are shown in fig. 8-9. The deflector panels were measured by scanning a small portion of their surface because they exhibit irregularities. Around 5kHz, the reflection coefficient of the deflector panel and the deflector panel with slots is slightly higher than one, which is probably related to measurement inaccuracies (fig. 8-9 red and blue line). Low reflection coefficients are measured at low frequencies on panels with slots because these are connected to the ventilation system. The frequency response of these samples mainly depends on the length of the ventilation shaft. The influence of such ventilation systems is often disregarded during the design of the room. However, these tests demonstrate their significance.

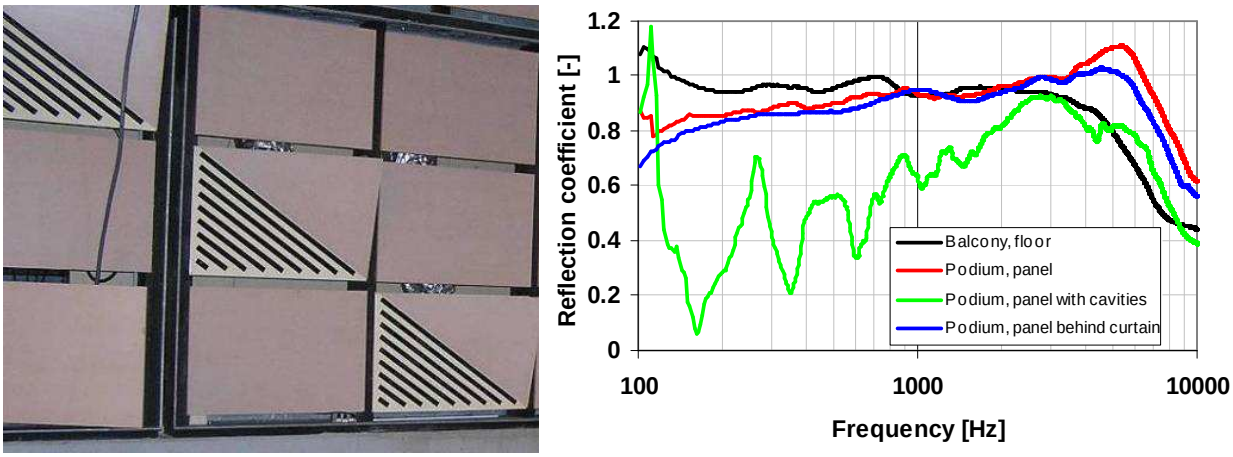

Fig. 8-9. Left: Panels at the sides of the podium.
Right: Measured reflection of the panels and the balcony floor.

8.3. *Measurements on jet engine intake liners*

Perforated liner samples are frequently used to attenuate the acoustic emission of aircraft jet engines. These liners are made from metals instead of fabric or plastics because large temperature variations and high mechanical stresses are experienced during flights. They consists of (a sandwich of) honeycomb structure(s) with a perforated top layer that is a light but strong (fig. 8-10). Various methods are used to determine their acoustic performance such as open Kundt's tubes, simulations, and insertion loss measurements. The open Kundt's tube is most frequently used. *In situ* measurement methods are not applied because such samples are too small. Tests on liners with the PU *in situ* method have been attempted for the first time *[34]*. Large discrepancies between the results of the Kundt's tube and the PU *in situ* method were found. By varying the sample mounting conditions for both methods, it could be shown that errors can be made with the Kundt's tube.

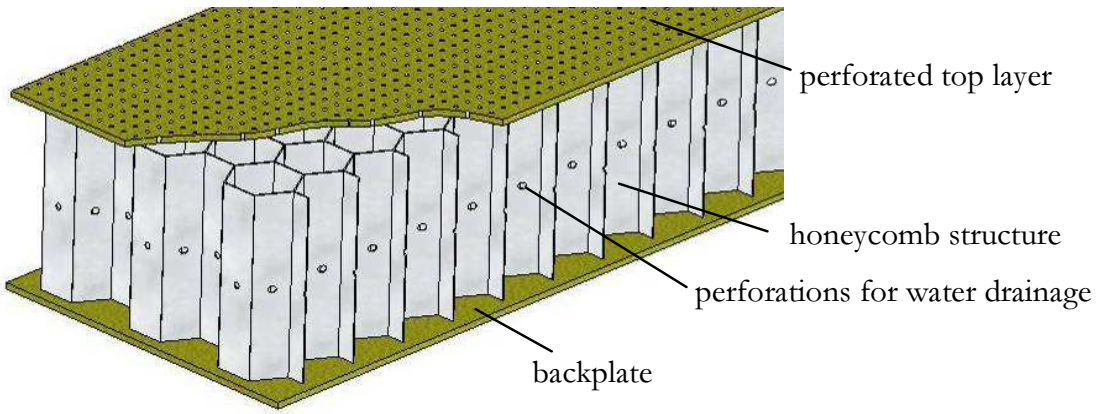

Fig. 8-10. Jet engine liner with interconnected honeycomb cavities.

A liner sample comprising perforated honeycomb cells was measured with an open Kundt's tube and the PU *in situ* technique. With the *in situ* method a small surface area was measured, thus the effective 'absorption' of it could be calculated. The perforations connect all cavities, and allow water to drain towards the bottom of the engine. The results of both methods were compared, but interesting observations were made. There were discrepancies between the results of both methods. To investigate the matter further, a special Kundt's tube was made onto which flanges with different sizes could be mounted. Three tests were performed with this Kundt's tube: i.e. one without a flange, one with a flange of 115mmx115mm (the standard size), and one with a large flange that covered a large part of the sample. With the PU *in situ* method, an additional measurement with a flange was performed in order to investigate the effect.

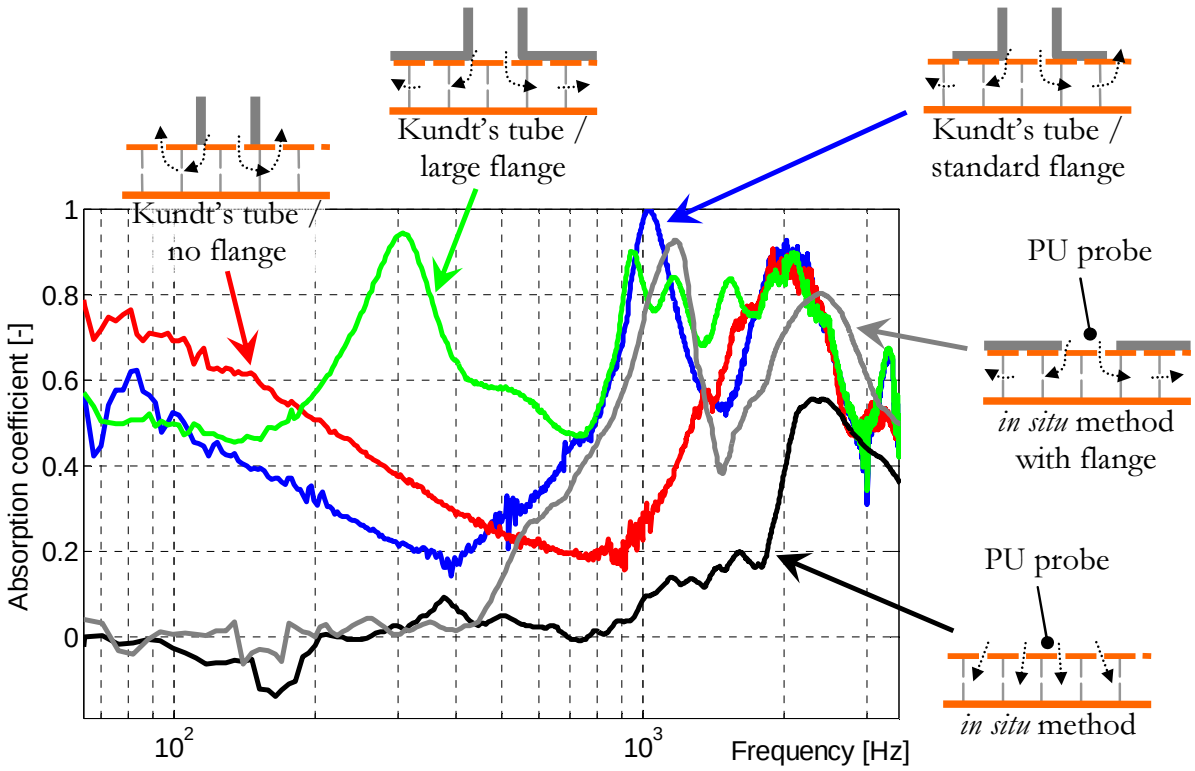

Fig. 8-11. Variation of flange size. Jet engine liner 'absorption' measured *in situ* and with the Kundt's tube.

The results of these tests are shown in fig. 8-11. The values of the *in situ* method (black line) are not only lower than the values of the Kundt's tube with standard flange (blue line), but the first peak around 1kHz that appears with the Kundt's tube is even absent. The second peak is also different and is

positioned at 2.5kHz instead of 2kHz. It is unlikely that these discrepancies are caused by the type of sensors used because the principles of measuring the impedance in a Kundt's tube and *in situ* are similar. In addition, the absorption models used are similar in both cases, except that the *in situ* method involves a correction for spherical waves.

The results of the Kundt's tube with different flange sizes are analysed in order to find the cause of these discrepancies. The outcome of the Kundt's tube is questionable, as it is varying depending on the size of the flange. On one hand, the flange size needs to be large to prevent sound leakage that occurs because all cavities are connected. The absorption is overestimated due to such a leakage, mainly at low frequencies. A value of 0.7 is measured at 100Hz in this case, which is unrealistic for such thin samples. On the other hand, the flange size should be small to prevent that additional standing waves occur inside the sample. The 1kHz peak is not measured without flange (red line). Additional modes are measured for larger flanges (for example the green line).

Next, the *in situ* measurement with flange is examined (black versus grey line). Higher 'absorption' values are measured, which are similar to those obtained using the Kundt's tube with a standard flange (grey versus blue line, >400Hz). It can therefore be concluded that errors are made when a flange is used.

The tests revealed that more accurate results can be obtained with *in situ* measurements for liners with interconnected honeycomb cells. In the future, such measurements might be performed under more realistic conditions for the application; i.e. at high sound levels (up to about 150dB), high temperatures (up to about 200ºC), and high airflows (up to about 30m/s). A set-up to measure liner samples with PU probes up to 150dB OASPL is currently developed by Microflown Technologies.

8.4. *Measurements on asphalt, whilst driving*

Sound-absorbing porous road surfaces can attenuate tyre-road noise by 6 dB or more [135]. In the Netherlands, porous asphalt concrete is now the standard surface on motorways. Porous road surfaces actually absorb little sound, but mainly reduce the so-called 'horn effect' [136]. A pressure is build-up between the tyre and the road, and the radiation efficiency of the horn like shape between the tyre and road is high. The pressure build-up and the radiation efficiency diminish through porous surfaces. Although there is no direct relation, the sound absorption coefficient and the sound reduction that is finally achieved are strongly correlated. The largest reduction of tyre-road noise is achieved with roads that absorb sound in the middle frequency range; around 1 kHz for passenger cars, and around 800 Hz for truck tyres that have larger diameters. The rate and the frequency of absorption are mainly determined by the number of cavities, the air resistance and the thickness of the porous layer.

Three methods are mainly used to measure absorption of road surfaces; i.e. Kundt's tubes, the spot method (ISO 13472-2), and the extended surface method (ISO 13472-1). However, these methods have their disadvantages. The cut out of asphalt and concrete samples for the Kundt's tube is destructive and a complicated task. Often, the best results are obtained by casting the asphalt sample directly in a Kundt's tube fixture. The usage of closed Kundt's tubes is questionable because there is sound leakage and because the sample cavity size is limited by the dimensions of the tube. Results of the spot method (an open Kundt's tube) and the results of the extended surface method (*in situ* microphone method) are often in conflict even though they are both standardised and used for normal incidence measurements.

Pollution or degradation of the road surface can affect absorption properties over time. Fixed set-ups are unsuitable for periodic inspections because then the road needs to be closed down for traffic. Even then, the results of the extended surface method are often affected by background noise. At a test speeds of 80 km/h or higher, the road can remain open and traffic would hardly be disturbed. For these reasons, the principle of measuring road absorption with PU probes whilst driving has been investigated *[130]*.

A dedicated measurement set-up has been constructed (fig. 8-12). The main disturbances that can be expected are noise from other sound sources and flow induced by the movement of the car. Therefore, a powerful loudspeaker has been used, and the probe is packaged in open porous foam that has a low acoustic damping to shield it from the wind. The foam is thicker in the driving direction, which allows the sensor-road distance to be kept as small as possible. The measurement probe is suspended in elastic bands to reduce vibrations from the car and the loudspeaker, and to ensure that the probe can bounce back if the road surface is accidentally hit. To reduce vibrations further, the sensor inside the wind shielding is also suspended in a low frequency spring system, which has a high damping above 50Hz.

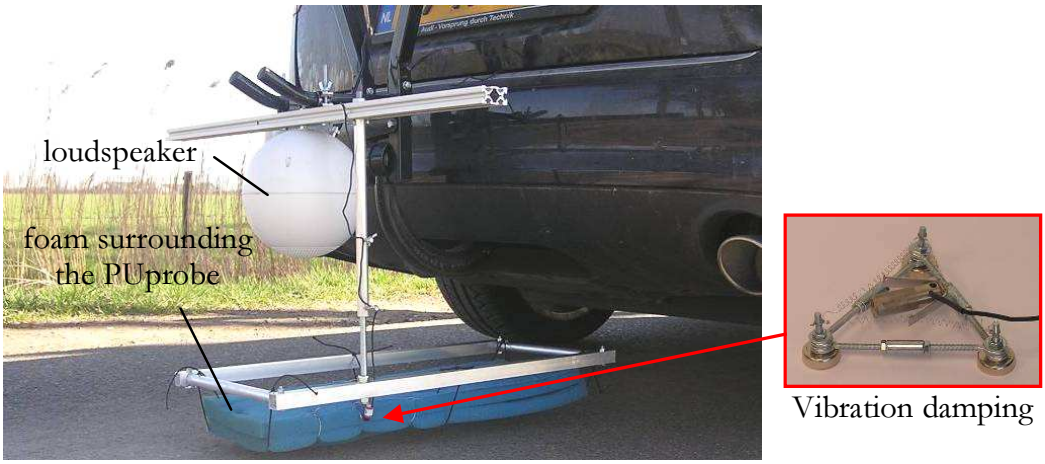

Fig. 8-12. PU absorption measurement set-up mounted behind a car.

With this set-up, measurements have been performed at several speeds on a quiet countryside road. The results obtained are shown in fig. 8-13. The normalised specific impedance is plotted instead of the absorption coefficient because little sound is absorbed for most frequencies by this particular road. Interferences of the direct and reflected sound waves occur because the reflection coefficient of the road is high. They occur at multiples of 1.9kHz because the distance between the sensor and the road surface was 44mm. Up to a driving speed of 40km/h the impedance is similar to the impedance in still standing situation for frequencies higher than 300Hz. At higher speeds, deviations are found at low frequencies. For frequencies above 800Hz similar results are found even up to 80km/h. Already at 40km/h some time sections of the particle velocity signal were dominated by external noise sources such as airflow, background noise, and vibrations of the car. Yet, still parts of the signals were undistorted at 80km/h.

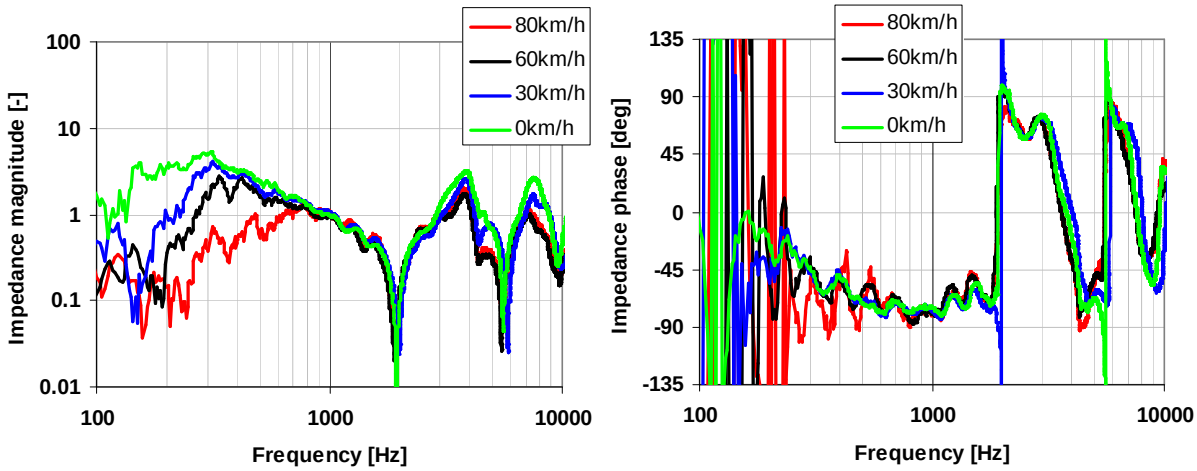

Fig. 8-13. Normalised specific impedance at several speeds.

The response of the sensors is also measured for several speeds without loudspeaker excitation. That way only external noise sources are measured. The next figure shows the measured auto-spectrum which is normalised by the measurement at 0km/h with loudspeaker excitation. The external noise exceeds that of the loudspeaker if this value exceeds 0dB. The signal of external noise sources is dominant at low frequencies, and in a small band around 2kHz for sound pressure for speeds beyond 30km/h.

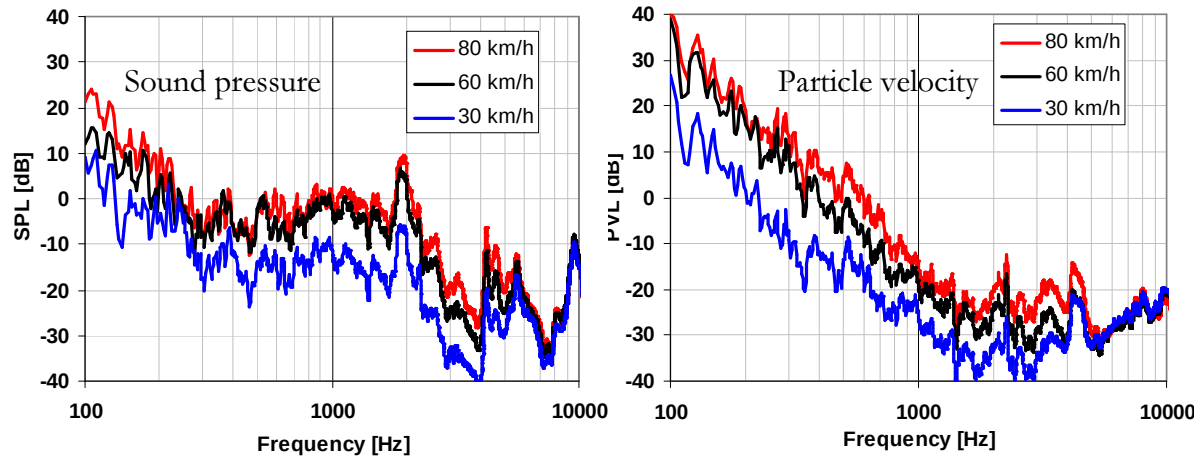

Fig. 8-14. Spectrum without loudspeaker minus the spectrum with loudspeaker.

The road absorption measurement set-up might be developed further. Since the tests were carried out, improved wind caps [14], *[123]* and less sensitive particle velocity sensors that overload less quick have become available *[137]*. It is the author's belief that proper measurements in a 300Hz-10kHz frequency range at 80km/h are feasible.

8.5. *Scan and Paint*

The 'Scan and Paint' method is used to visualise the sound field in a surface quickly and with high resolution [130-133]. The method involves a PU probe that is swept across the surface of interest. While the sensor signals are recorded, a video is captured at the same time with a webcam that is placed at a certain distance. The position of the probe is determined from the video using an automatic tracking algorithm that detects a colour marking on the probe. The sound properties are then calculated for each position from a short period just before and after each particular measurement point is acquired. An adequately long time signal is required for proper frequency analysis. Typically, ten Fourier transforms or more are averaged in order to reduce noise, which means that for a frequency of 100Hz the time signal should at least be 0.1 seconds long. The results are therefore smeared out, depending on the length of the time segment and the speed with which the probe is moved [59, p. 119]. An alternative method has been introduced in [138]. The measurement area is divided into a number of grid sections. If the probe is located in a grid section for two successive movie frames the piece of time data in between is assigned to that section. More time data is attributed each time a certain grid section is scanned, thus statistically improving the results.

A precursor to the Scan and Paint method was developed by W. Kock in 1965 [139]. In this method, the brightness of a light bulb that was attached to a microphone was varied proportionally to the microphone signal. To determine the sound pressure distribution, the brightness of the light bulb is captured at each position with a camera that was set to a long exposure of about 30 seconds. Although the current Scan and Paint method is relatively new (2009), it is now frequently used to visualise the particle velocity or intensity radiation from stationary sound sources (see appendix A1). The advantage of using PU probes is that particle velocity is directly measured, and that intensity measurements are less susceptible to background noise compared to tests performed with PP probes (see appendix A2). The Scan and Paint routine is quick, cost effective, and accurate compared to microphone-based beamforming or holography techniques described in [46-48].

Here, the method is also used to visualise local absorption effects. The surface is scanned with the handheld *in situ* absorption device, instead of using a PU probe only. Examples of several tests that have been performed are shown in this section. The first example is a hedge; see Tijs et al. *[134]*. The handheld set-up is moved across the hedge, and the local absorption coefficient values are calculated. Effectively the absorption plus the transmission is measured because most sound goes through the hedge. A wooden board and garden gnome have been placed in front of the hedge to discriminate between high and low reflective surfaces. Fig. 8-15 shows the test set-up and the estimated position of the probe at the time a movie frame was taken. Fig. 8-16 shows the absorption that is calculated with the mirror source model for 2.9kHz. The set-up time was around ten minutes and the measurement time was approximately one minute. Although the wooden board and the gnome are small, the higher reflection from them is revealed. The colour map has a slight offset in negative x and positive y direction because the video frames were captured under an angle and the probe was positioned about five centimetres from the surface.

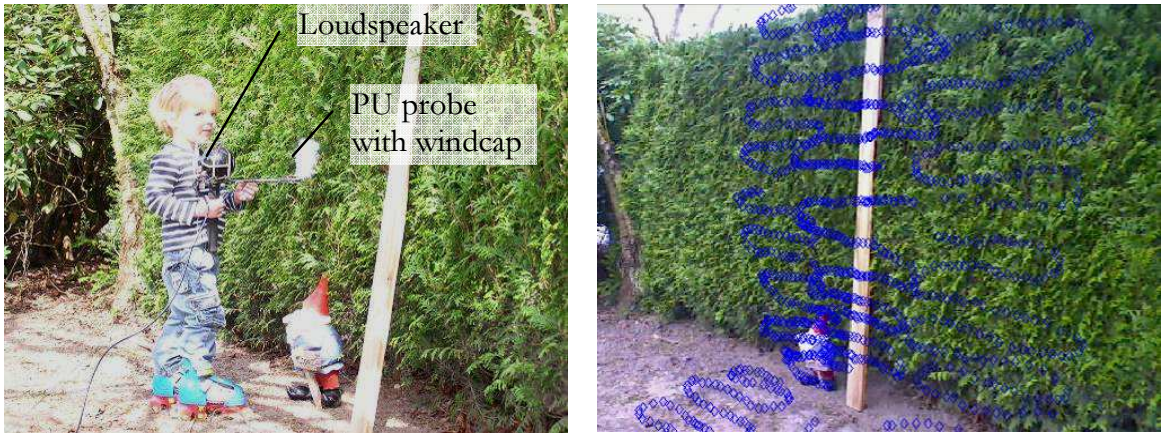

Fig. 8-15. Left: measurement set-up. Right: Measurement points distribution.

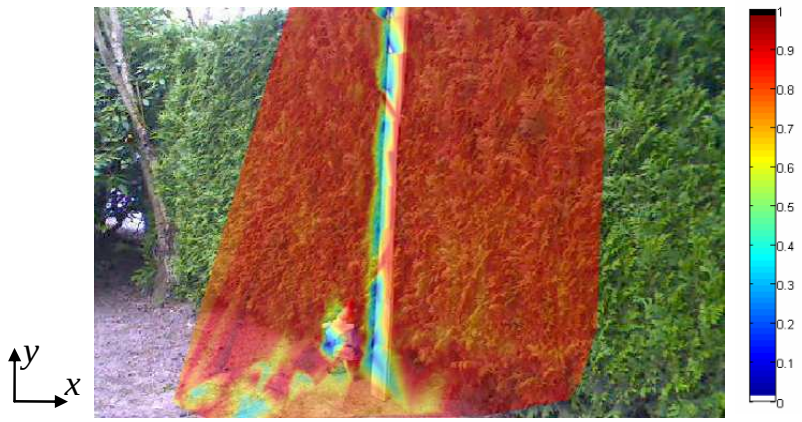

Fig. 8-16. $1-R\cdot R^*$ at 2.9kHz (absorption plus transmission).

The next figures show examples of Scan and Paint measurements performed on the seat of an aircraft, on the seat of a car, and a door of a car. The measurement time was approximately three minutes in these cases. These tests are not fully conclusive, and further investigation of their absorbing behaviour is necessary. For example, in some situations a narrow frequency band may be of interest, rather than the wide frequency band, which is shown in these figures. These examples are merely intended to demonstrate that spatial variations can be visualised quickly and easily.

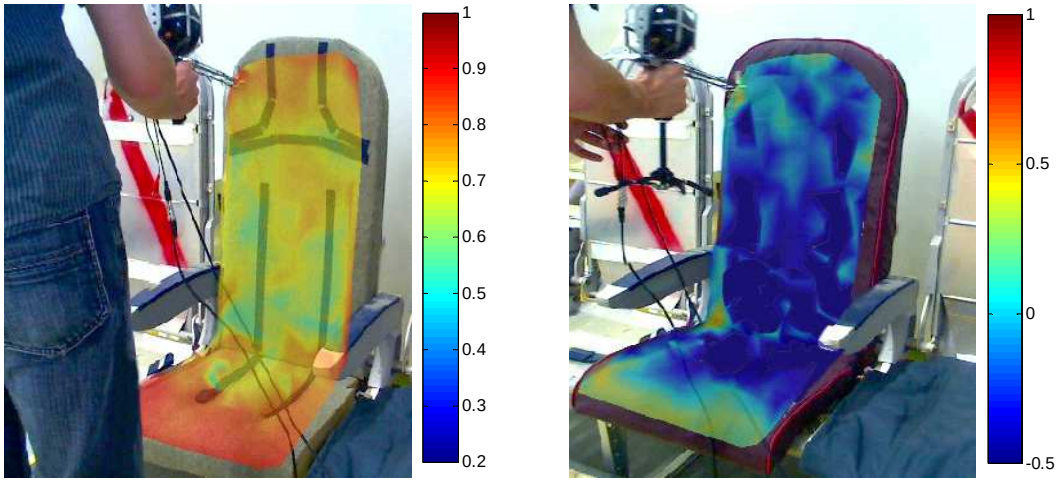

Fig. 8-17. Local absorption of an aircraft seat without (left), and with cover (right). Mean value of a 215 Hz to 7.1 kHz band.

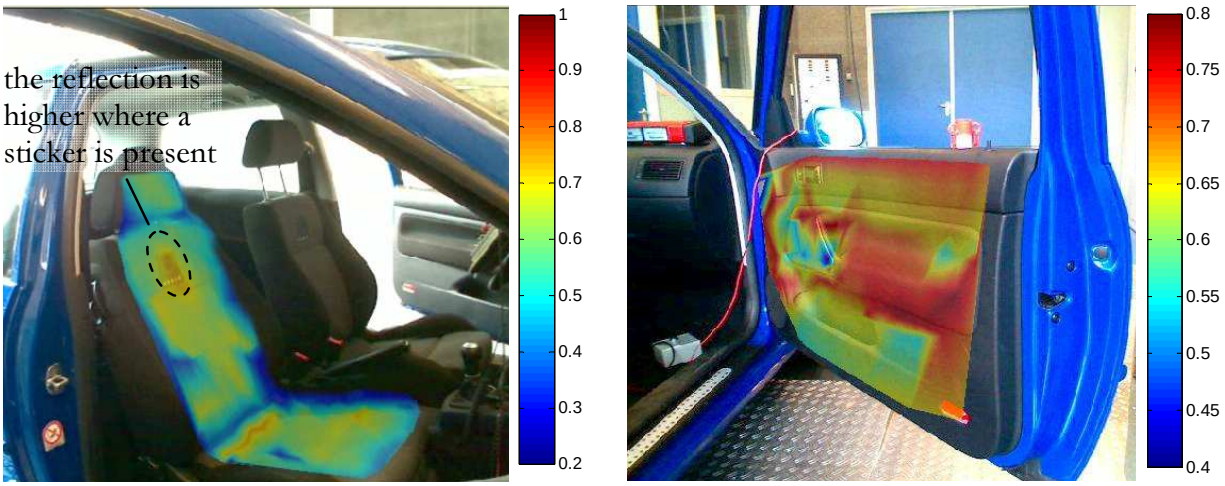

Fig. 8-18. Left: local reflection of a car seat (mean value of 100 Hz to 3350 Hz). Right: local aborption of a car door (mean value of 110 Hz to 4 kHz).

Although the capabilities and limitations of such Scan and Paint absorption measurements have to be explored further, the examples in this section demonstrate the potential for characterising the local absorption properties of sound-absorbing samples. Applications are e.g. the development of samples, troubleshooting in situations with noise problems, and identification of local inconsistencies after manufacturing. Depending on the application of interest, different conditions may be used for future tests. For example, while the existing test set-up allows for straightforward comparison of different sections, a measurement with a fixed sound source may allow studying the absorbing properties for different angles of incidence. In addition, other sound fields may be used such as reverberant fields or the sound field that is normally present.

8.6. *Conclusion*

Several new applications of *in situ* measurements with PU probes have been described in this chapter. It has been demonstrated that PU probes can be used to measure absorption in situations where other methods cannot be applied or are inconvenient to use.

PU probes enable testing under reverberant conditions. Examples have been shown of measurements performed successfully inside concert halls and cars. Such tests are useful for R&D because absorption can be determined under the conditions in which the sample is used in practice. Suitable methods to determine the absorption characteristics of individual structures are currently lacking, and such *in situ* measurements are a valuable addition. Also, such tests can be used for assessing the quality of products during or after manufacturing. Currently, their absorption characteristics are only measured periodically, or not at all, because existing methodologies are time-consuming and sometimes even destructive. With *in situ* measurements, dispersions of the absorbing properties of parts were found amongst different cars of the same type.

Another quality control application is the monitoring of road surfaces whilst driving. There is a desire to measure the acoustic performance of roads after they are produced and over time. Existing absorption measurement systems cannot be used whilst driving at 80km/h or faster, which means traffic is severally hindered. A dedicated has set-up been build, which is mounted behind a car. The impedance was measured at several speeds.

Distortions of the particle velocity signal were already found at 40km/h, yet even up to 80km/h some parts of the signal were usable. Recently, less sensitive particle velocity sensors and improved wind caps have become available. If the method would be developed further, it would be feasible to assess speeds of 80km/h or higher to the authors belief, thus leaving traffic undisturbed. With such a method also holes and other mechanical damages may be detected in the road surface. A future measurement system might be combined with other measurement systems that monitor road surfaces whilst driving.

Several test with jet engine liners revealed shortcomings of the open Kundt's method, which is frequently used. Tests have been performed on a typical liner with interconnected honeycomb cells. Unrealistic high absorption values were found at low frequencies because of sound leakage, and in the middle frequency range because of resonances inside the sample caused by the flange of the tube. These tests revealed that more accurate results can be obtained for such samples with *in situ* measurements. The applications and limitations of such *in situ* measurements on jet engine lines have to be explored further, especially because it could allow measuring under more realistic conditions for the application; i.e. high sound levels, high temperatures, and high airflows.

Lastly, the Scan and Paint technique has been presented. With this method, sound fields can be visualised quickly and with high resolution. A PU probe is scanned across the surface of interest while its position is tracked by camera that is placed at some distance. The technique is frequently used to map the particle velocity and intensity near surfaces to determine the location and strength of sound sources. Here, it was applied to measure the spatial distribution of absorption and reflection. Several examples have been presented that demonstrate the capabilities of the technique. The high-resolution absorption measurement technique can be used as a fast troubleshooting tool to characterise local absorption mechanisms and to check the consistency of sound-absorbing samples.

9. Alternative principles to characterise absorption with PU probes

9.1. *Introduction*

The sound pressure that is perceived at a particular position not only depends on the position and characteristics of the sound source, but also on the arrangement and the properties of all surrounding surfaces. In previous chapters, methods have been described to determine absorption properties of individual samples. In this chapter, two techniques that can be used to characterise the effect of the entire arrangement are investigated.

With the first method investigated, the diffusion at the particular point of interest is determined. The diffusion changes due to an absorbing/reflecting sample, and the influence on the sound field can be measured. In [140] a metric was developed relating the degree of diffuseness to the ratio of time-averaged intensity to energy density. In *[*128, 139*]* the diffuseness was measured by Tijs et al. in several sound fields. The principles of the method and preliminary test results are presented.

The second method investigated uses a high number of three-dimensional sound intensity measurements. Vector and streamline plots are used to visualise the distribution of sound intensity around structures. Although such results are sometimes difficult to interpret, the complexity of the sound field and the interaction of different objects can be demonstrated. Results from measurements performed by Tijs et al. in a car *[142]* and around a theatre seat *[129]* are discussed.

Both methods use a three-dimensional acoustic vector sensor called the USP probe, which comprises one microphone and three orthogonally orientated Microflowns. With this probe, the sound pressure and the three particle velocity components are measured. Hence, quantities such as impedance, energy and intensity can be obtained in 3D.

The measurements are performed under normal, i.e. non-anechoic, conditions. Three-dimensional PP intensity probes are seldom employed under such

conditions because complicated hardware is involved, and because the pressure-intensity index (i.e. the ratio of sound pressure squared to active intensity) is high, which causes measurement inaccuracies. With PP probes, the pressure-intensity index might be estimated incorrectly because the calculated intensity might be incorrect. The intensity measurements of by means of PU probes can also be complicated in reverberant conditions because the reactivity, which is the ratio of reactive to active intensity in logarithmic form, can be high. Yet, this reactivity depends on the phase of the sound field, which is measured properly. Intensity values can therefore be omitted if the phase exceeds a certain value. The matter was discussed earlier in section 1.4.

9.2. *Measurement of sound diffusion*

Sound diffusion can be defined as the randomness of sound wave arrival directions [5]. A method for measuring the scattering of sound from separate samples is described in ISO standard 17497-2. It involves the calculation of a surface diffusion index, which is a measure for the uniformity of the reflected sound due to a sound source that is positioned at different angles of incidence [141, 142]. In [145] and [146] a method was introduced with which the free field particle velocity measured by Microflown sensors can be distinguished from the particle velocity due to the reverberant sound. The ratio of both values provides a measure for the degree of diffusion at arbitrary positions in a room. Here, a different approach is investigated to quantify diffusion at arbitrary points in a room, which is based on energy flow and energy density. It can e.g. be used to assess the performance of rooms such as reverberant and anechoic rooms. The underlying principle is that the amount of diffusion in a room is depending on the net active intensity. E.g., in a diffuse field the active intensity approaches zero because the energy flow is randomly orientated.

9.2.1. Field index *F*

In [140] a metric called the field index F was proposed, which is defined as the ratio of the modulus of the active intensity $\boldsymbol{I}$ to the scaled energy density w. The energy density is defined as [5, 8]:

$$w = w_{\text{pot}} + w_{\text{kin}} = \frac{\langle p^2 \rangle}{2\rho c^2} + \rho \frac{\langle |\boldsymbol{u}^2| \rangle}{2} \quad \left[\frac{J}{m^3}\right] \tag{9-1}$$

where $\langle\ \rangle$ indicates a time average, ρ is the density of air, c is the speed of sound, and $\boldsymbol{u} = u_{\text{dir}} \cdot \hat{\boldsymbol{e}}$ with $\boldsymbol{u}$ being the full particle velocity vector and $\hat{\boldsymbol{e}}$ a unit vector in the direction of interest. Traditionally, the energy density is determined with a microphone only. The potential energy density is obtained, which is then multiplied by 2 in order to approximate the energy density ($w \approx 2w_{\text{pot}}$). With PU probes also the kinetic energy density w_{kin} can be measured. By measuring sound pressure and particle velocity in three orthogonal directions, the energy density w can be calculated. The energy density and, for harmonic signals, the active intensity can be written as a function of pressure p and impedance Z, [4, p. 124]:

$$w = \frac{\langle p^2 \rangle}{2}\left(\frac{1}{\rho c^2} + \frac{\rho}{Z^2}\right) \qquad \left[\frac{J}{m^3}\right] \tag{9-2}$$

$$\boldsymbol{I} = re\{pu^*\} \cdot \hat{\boldsymbol{e}} = re\left\{\frac{|p|^2}{Z}\right\} \cdot \hat{\boldsymbol{e}} \qquad \left[W/m^2\right] \tag{9-3}$$

For a single sound source in the far field the impedance Z is equal to ρc, thus $\boldsymbol{I} = cw \cdot \hat{\boldsymbol{e}}$.

F is defined as the ratio of the active intensity to the speed of sound and the energy density, where in some situations the energy density may be approximated using the potential energy density only:

$$F_w = \left|\frac{\boldsymbol{I}}{cw}\right| \tag{9-4}$$

$$F_{w,\text{pot}} = \left|\frac{\boldsymbol{I}}{2cw_{pot}}\right| \tag{9-5}$$

F is a metric for diffusion, ranging from zero to one. In anechoic conditions, intensity would be high and this ratio would ultimately approach unity. In perfect reverberant conditions the active intensity would be zero. Diffusion is also expected to be lower in the proximity of sound-absorbing samples.

The potential and kinetic energy densities vary depending on the position in the room due to interferences of sound waves. Usually, the potential energy is low at positions were the kinetic energy is high, and visa versa. Conventional microphone-based measurements are therefore position dependent, while the sum of the potential and kinetic energy density is more spatially uniform [147]. On the other hand, usage of the potential energy might be preferred in the near field of sound sources because it decays with $1/r^2$ in the same way as the active intensity does. Compared to the far field, the kinetic energy increases more towards the near field than the potential energy. Therefore, F will not become one if both energy densities are used.

9.2.2. Diffusion measurements

Sound intensity and energy density measurements have been performed with a three-dimensional PU probe, and the field index F has been calculated. Results are presented of measurements performed in a silent room with a sound source at 1 meter from the probe, and in a reverberant room. Fig. 9-1 shows the measured energy densities for both situations. The total kinetic energy density (cyan line) and the potential energy density (grey line) are similar in the silent room because there are no strong reflections, thus the variation of the potential energy density is low. Both energy densities are also similar in the reverberant room. In the situation with the single sound source, the kinetic energy density in direction x (fig. 9-1 left, blue line) is much higher than the intensity in the directions y and z, whereas the kinetic energies in each direction are nearly equal in the reverberant room. By summing the potential and the kinetic energy densities the energy density is obtained (black lines).

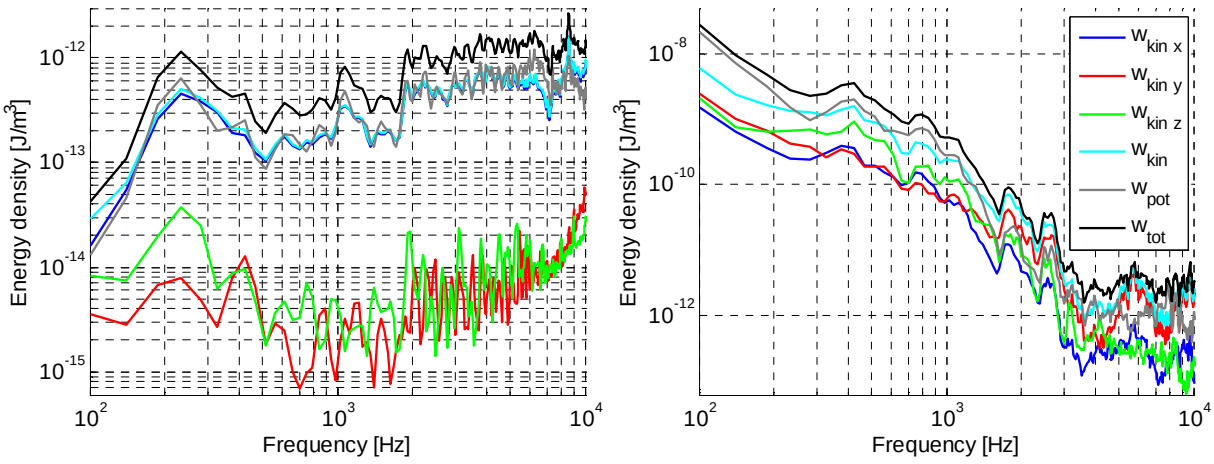

Fig. 9-1. Energy density for a single sound source (left) and a reverberant room (right).

The active intensity in each direction was also calculated. In order to compare these values the potential energy density is multiplied with $2c$ and the energy density is multiplied with c. As can be seen in fig. 9-2 the intensity is similar to the scaled energy density for a single sound source, thus F approaches one. In the reverberant room the intensity is low compared to cw.

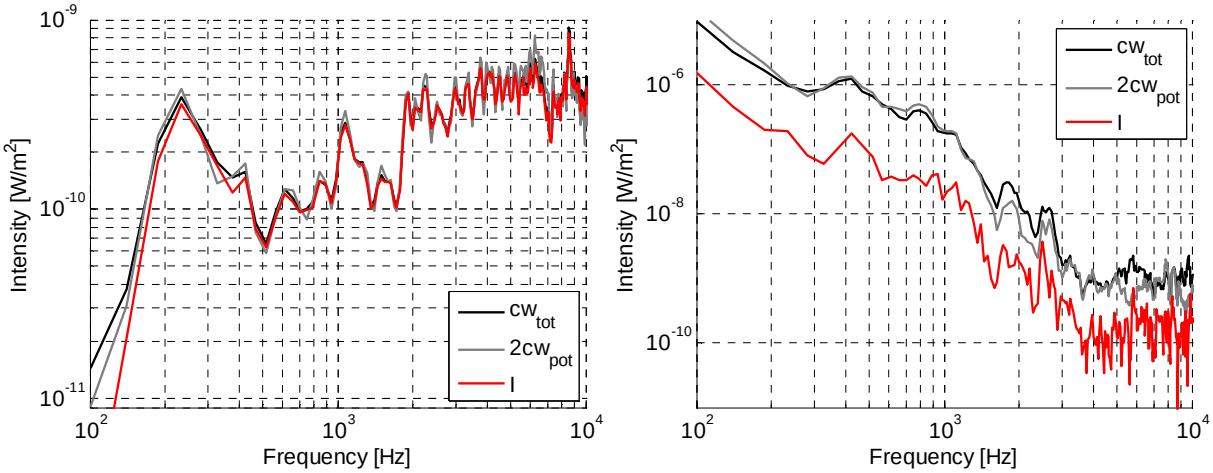

Fig. 9-2. Scaled active intensity compared to scaled energy density for a single sound source (left) and a reverberant room (right).

The diffusion metric F was calculated for the silent room and for two positions in the reverberant room (fig. 9-3). F approaches unity for the situation with a single sound source because the intensity and scaled energy density are nearly equal. Small energy and intensity measurement inaccuracies can have a larger effect under such conditions. F varies more using w_{pot} than using w (red versus blue line), which may be the results of reflections. There are measurement inaccuracies below 200 Hz because the sound source volume is low. In addition, discrepancies occur above approximately 5 kHz because the responsivities of the sensors are not matched exactly by the calibration curves. The height of the resulting error of the calculated energy densities is equal to difference between the actual and the estimated amplitude responsivities of the corresponding sensors. The height of the error of the calculated intensity can be higher because then also the phase responsivities are involved. Because the intensity is low in the reverberant room, also F is. During the test there were test articles present in the reverberant room, which may be the reason why F does not approach zero. By comparing the two tests in the reverberant room it can be seen that, depending on position, $F_{w,\mathrm{pot}}$ calculated with potential energy only can be different than F_w (grey versus black line).

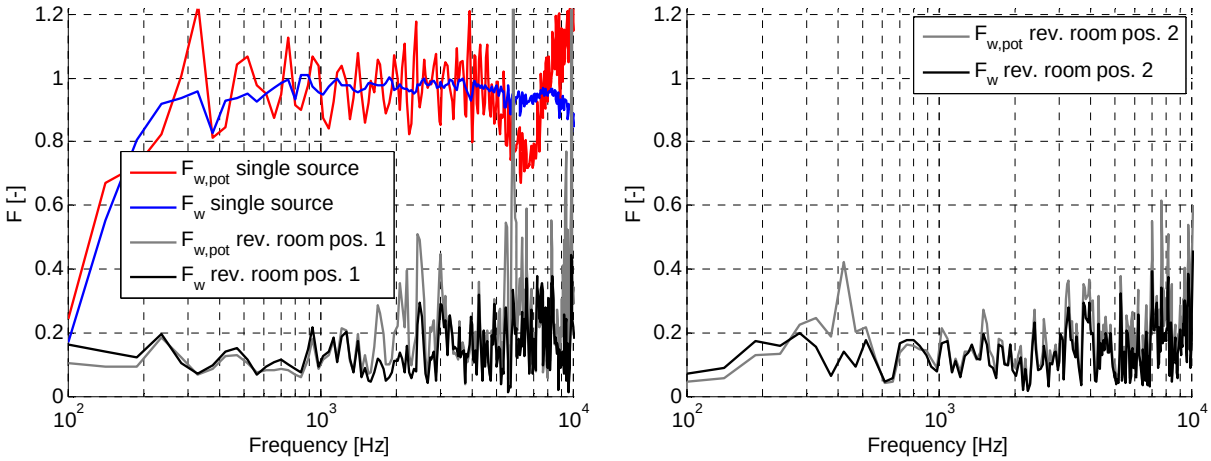

Fig. 9-3. Diffusion for a single sound source in a silent room, and for two positions in the reverberant room.

It has been shown that the three-dimensional intensity and energy density can be determined even in reverberant environments where traditional intensity probes cannot be used. These preliminary measurements demonstrated that the field index F provides a different measure, which is easy to interpret and is used to characterise the performance of rooms at distinct points.

9.3. *Sound energy flow around structures*

The flow of sound energy is often unknown because it is influenced by all sound sources and reflecting surfaces present. Simulations require much calculation power and small details existing in reality are usually disregarded. In [146, 147] a method was applied to visualise sound intensity vector fields. It was shown that complicated sound intensity fields exist even around the simplest structures. Tests were performed inside a semi-anechoic room with set-ups that often only involved a loudspeaker and an ordinary object like a square box. Depending on frequency, the straight propagation or the more complicated interaction of sound waves was visualised. Sometimes even vortices were encountered; similar to those visualised with smoke around aircraft wings in a wind tunnel.

The method was further investigated with measurements that were performed inside a car and around a theatre seat, *[142]* and *[129],* respectively. The results from these studies are analysed. Such measurements give more insight in the sound path from the source to the listener, and could help finding the optimal location of additional sound absorbing samples. However, interpretation of the results can be complicated.

9.3.1. Description of the method

The flow of sound energy (i.e. the intensity) can be measured with intensity probes. By measuring at multiple positions, the energy flow throughout space can be determined. Depending on the resolution and size of the volume of interest many measurements may be required. For example, in a single case study in [150] at up to 6647 positions intensity readings were acquired.

Energy flows around structures can be visualised with for example colour-maps, vector fields and streamline plots. Streamlines are curves fitted tangentially to intensity vectors [8]. They originate from a defined set of starting points and follow the direction of the intensity vectors. The spatial resolution of the measurement points should be sufficiently high for the constructed streamlines to follow the direction of the energy flow accurately. A high resolution is required if the energy field contains fine details. Errors inherent to the streamline algorithm also have to be considered such as user settings and crossing of streamlines over an area with zero intensity instead of ending it. Furthermore, the number of seeding points (starting points of the streamlines) is limited to reduce computation time.

9.3.2. Example 1: Energy flow inside a car

In *[142]* the 3D intensity was acquired at 900 positions inside a car for several loudspeaker arrangements (fig. 9-4). The positions are evenly distributed throughout space in a 3D grid with 10 cm spacing. The test engineer was located on the right back seat during the tests, which limited the measurement area and which may have influenced the sound field. The inner dimensions of the car were measured with a geometric digitiser. All tests were performed in a single day.

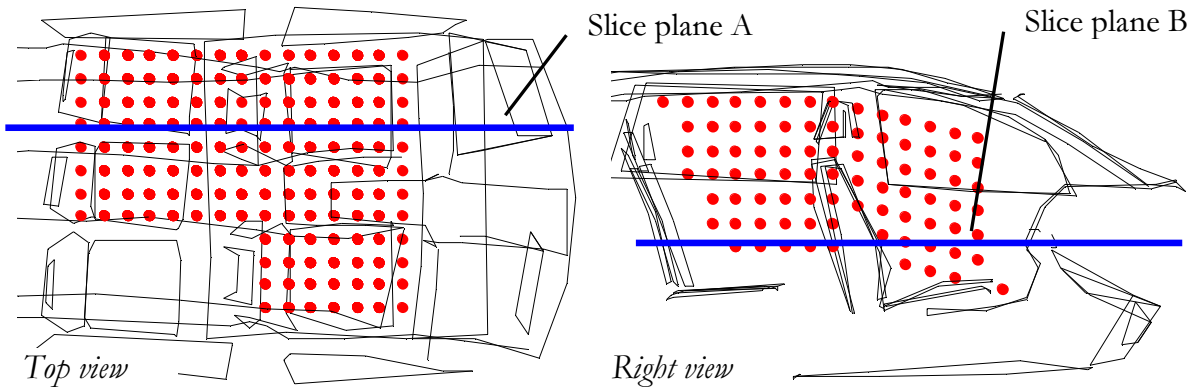

Fig. 9-4. Distribution of measurement points throughout the car.

Fig. 9-5 shows the three-dimensional intensity field that is visualised with vectors (left) and streamlines (right). Two loudspeakers on the dashboard were excited in this case. Their positions are displayed as blue spheres in the figure. The results are calculated for a 300Hz-450Hz frequency band. All outer measurement points are used as starting lines for the streamline algorithm, but not the points inside the volume. The colour of the streamline is a measure for the intensity level of the nearest point (although 3D interpolation could also have been used). High intensity values are red, low values blue. It can be seen that the intensity often does not point away from the loudspeakers, which is the result of interferences of the direct sound waves and their reflections.

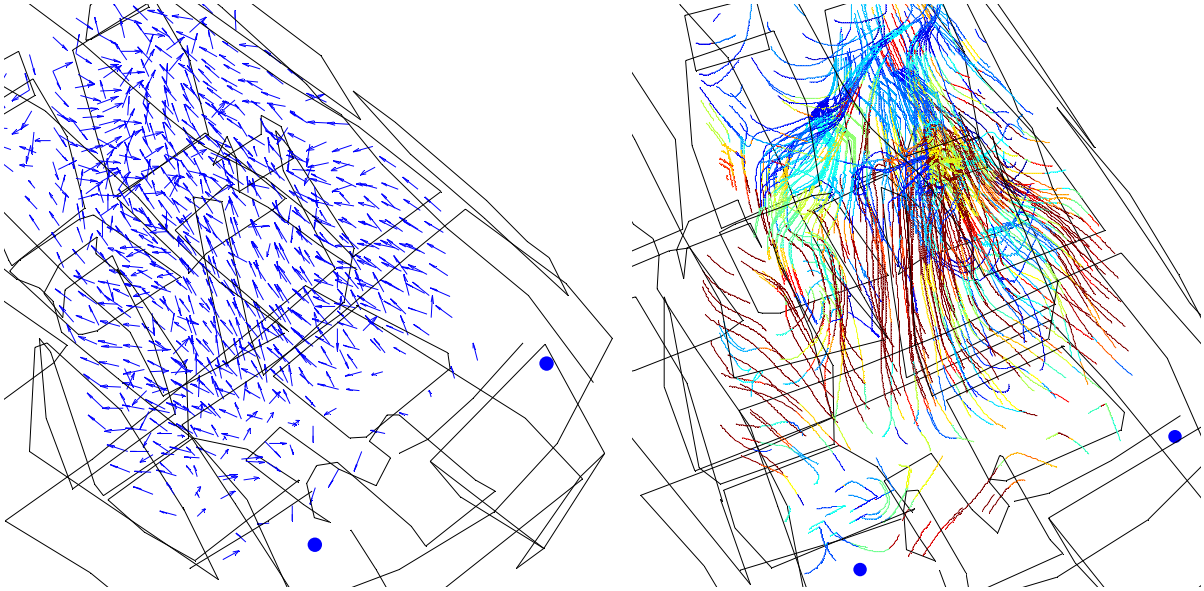

Fig. 9-5. 3D intensity field with dashboard loudspeakers excited (Bandwidth 300Hz-450Hz. Left: Normalised intensity vectors. Right: intensity streamlines.

Pictures like fig. 9-5 depict much information, which can also be confusing. Results visualised in one plane are usually easier to interpret. The next two figures show the intensity streamlines of the slice planes indicated in fig. 9-4. The level of intensity is displayed as a colour-map. The estimated intensity streamlines are strongly bending and do not always point away from the source. Their direction depends on for example the position of the loudspeakers, the geometry of the car, and on frequency. The sound appears to go into or through the seats in some cases.

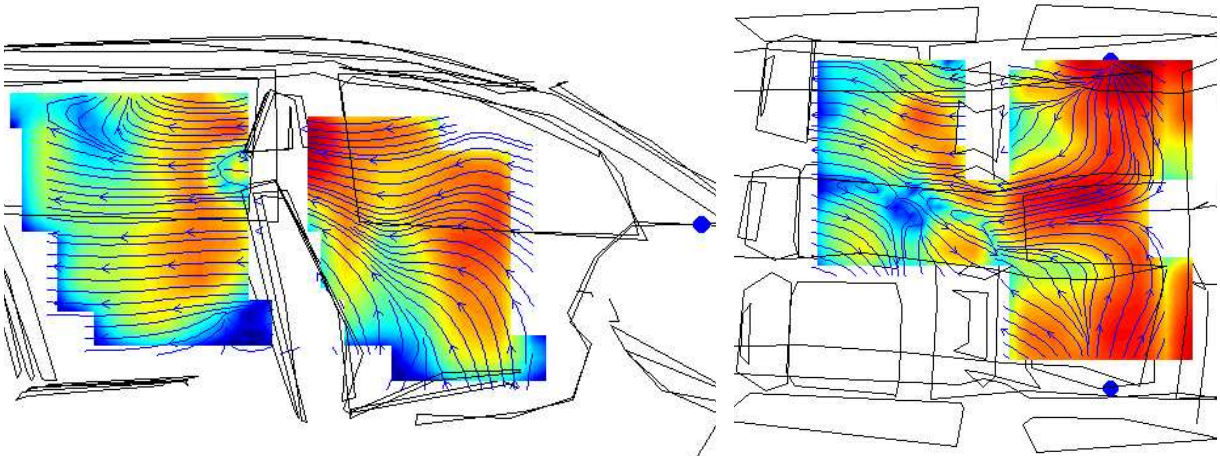

Fig. 9-6. Streamlines plot in a 300 Hz - 450 Hz band. Left: slice plane A with dashboard loudspeakers. Right: slice plane B with loudspeakers in the front doors.

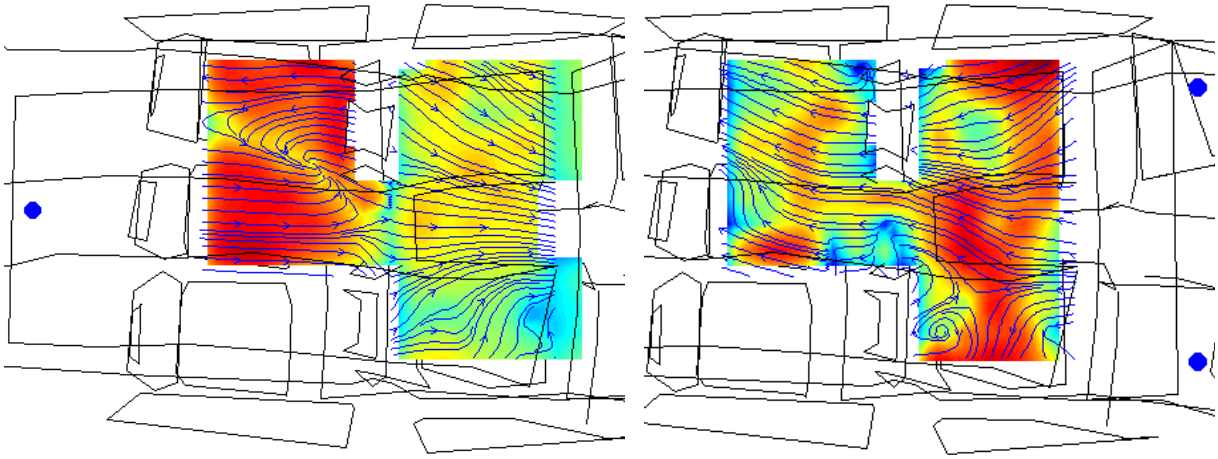

Fig. 9-7. Streamlines plot of slice plane B in a 300 Hz - 450 Hz band. Left: loudspeaker in the trunk. Right: Two loudspeakers on the dashboard.

9.3.3. Example 2: Energy flow around a seat

A theatre seat is positioned in a non-anechoic room to mimic a situation where there are reflections *[129]*. Tests were performed in two situations; i.e. with the seat down, and with the seat up. The distance between two measurement points was 2cm. Only a small area in one plane is measured because the resolution is high (fig. 9-8).

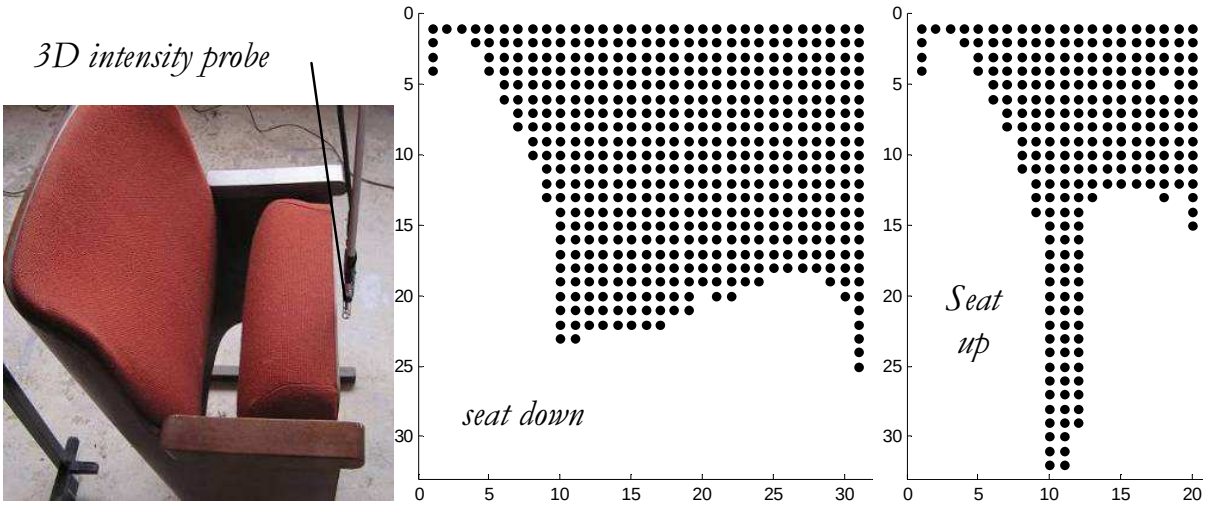

Fig. 9-8. Distribution measurement points around the theatre seat.

The intensity field is visualised by combining a colour-map, streamlines and a vector plot. Results of two frequency ranges are shown in fig. 9-9 and 9-10. It can be seen that the complexity of the intensity field increases at higher frequencies. At some positions the intensity level increases near the surface of the seat (indicated by the yellow and red areas). In addition, due to interference of incoming and reflected sound waves there are local minima and maxima (see for example between the back and the bottom of the upright seat (fig. 9-9 and 9-10, right figures).

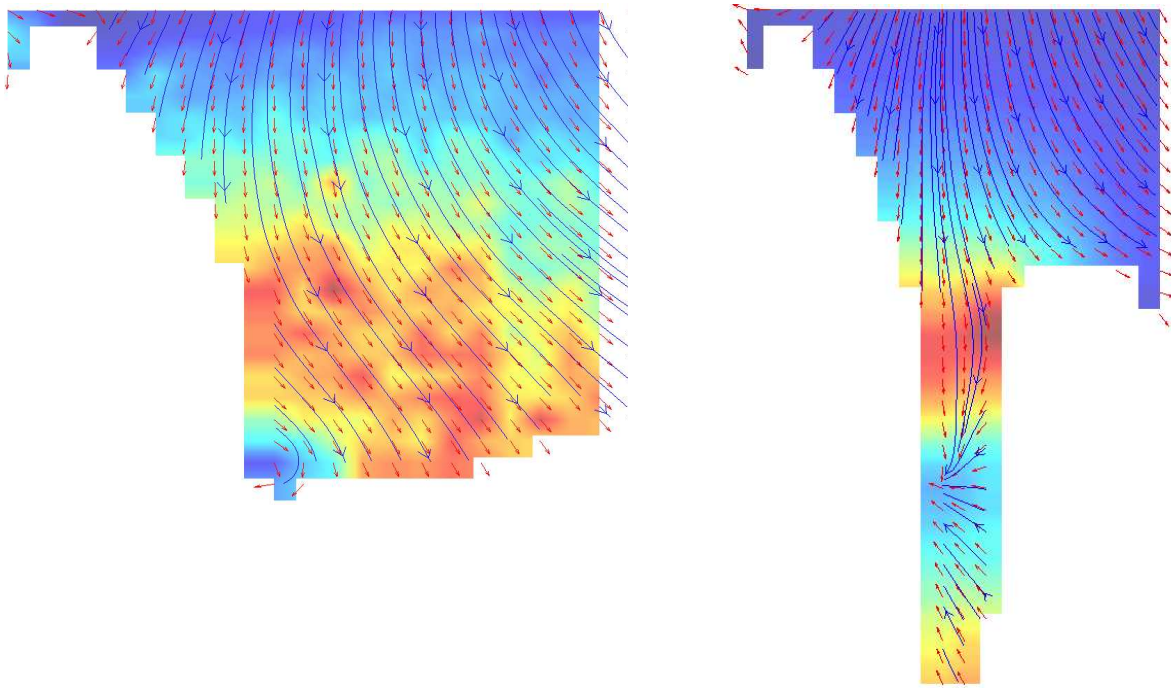

Fig. 9-9. Intensity streamlines at 250 Hz with the seat down (left), and up (right).

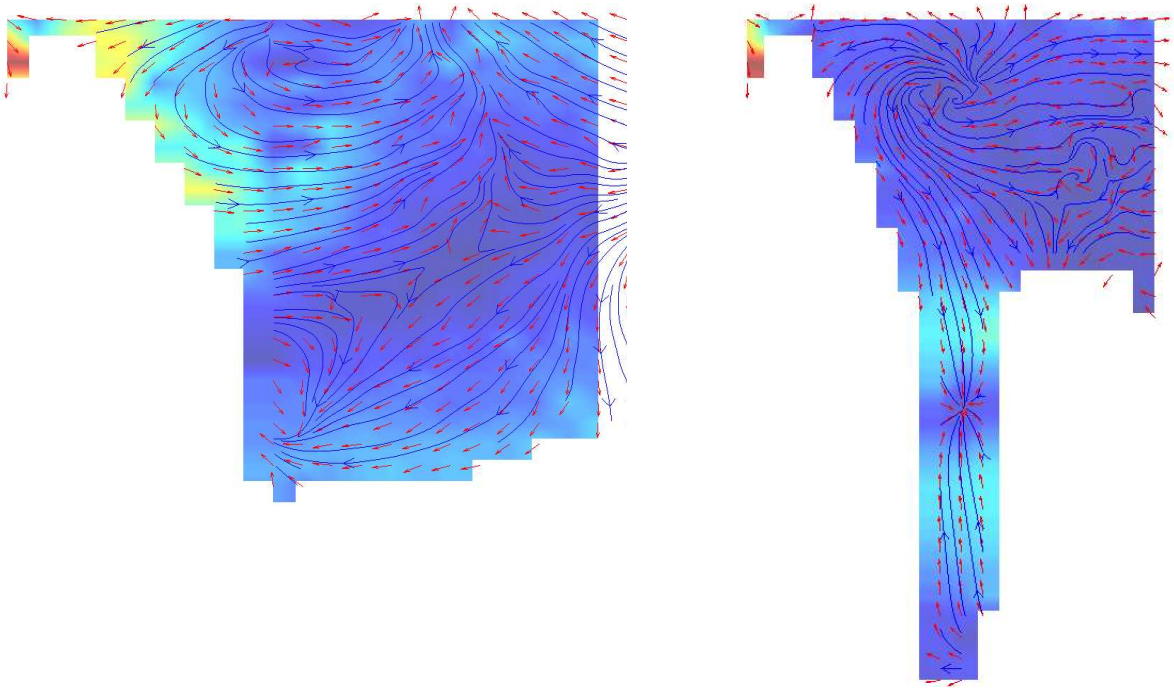

Fig. 9-10. Intensity streamlines at 500 Hz with the seat down (left), and up (right).

9.3.4. Other potential applications of visualised intensity fields

Sound pressure is sometimes predicted with simulated energy flows. Results from real tests, like those presented in the previous sections, could be used as input for such simulations or to validate their outcome. The test procedure might be accelerated with the Scan and Paint method, which has been introduced in section 8.5. At least two cameras would be required for measurements in 3D space. Such tests would for example enable the study of the energy flow around absorbing samples inside a reverberant room [148]. Following ISO 354 and ASTM C423 standards, absorption values higher than one are sometimes measured. The effect of finite sized samples and edge effects on the measurement results have not been explained indisputably [37], and 3D sound intensity measurements might be used to visualise these effects. Another application could be the measurement of energy flows around (the top of) road noise barriers. Simulations are frequently used, but their outcome is sometimes unconvincing.

9.4. *Conclusion*

In this chapter, two usable techniques have been investigated to characterise the effect of the entire arrangement, rather than the performance of separate samples. Both techniques use 3D sound intensity and/or energy density measurements. Such tests could not have been performed with PP probes because, unlike with PU probes, problems are experiences in environments where sound pressure is high compared to net intensity. With PU probes, the energy density can also be obtained. Energy density has the advantage of being more spatially uniform than potential energy density only, which is captured with microphones [147].

A method to measure diffusion at an arbitrary position in a room, which uses the scaled ratio of intensity to energy density, has been investigated. The values of field index metric F range between zero and one, where zero corresponds to perfect reverberant conditions (the net intensity vanishes), and one stands for a perfect anechoic condition. It has been shown that tests can be performed successfully in several environments; i.e. an anechoic room, a reverberant room, and an office. However, F then tends to approach zero if there are near field effects because the kinetic energy is high but little intensity is propagating, and if there are strong standing waves in one direction because then the intensity is low even though the direction of arrival of sound waves is not random.

The second method investigated uses a high number of measurement points, which are used to chart energy flows around structures. The intensity fields inside a car and around a theatre seat have been measured, and they were visualised by vector and streamline plots. Complex sound fields were shown in which the intensity vectors do not always point away from the sound source at each measurement position because sound waves from multiple source and their reflections interact. Although interesting results can be obtained with this method, the interpretation can be difficult. The procedure is rather labour intensive currently, but could be accelerated with the Scan and Paint method introduced in section 8.5.

10. Summary

Determining the absorbing properties of sound-absorbing samples can be impossible with existing measurement methods. While some methods are limited in frequency, others cannot be used *in situ*, for certain sample types, or for the as-mounted samples. The possibilities of PU absorption measurements have not fully been explored, and therefore several *in situ* methods that use PU probes have been investigated in this research. This thesis covers some of the major achievements.

A PU probe comprises a sound pressure sensor and a particle velocity sensor, and with it, quantities required for absorption measurements such as impedance, energy density and intensity can be easily obtained. Compared to regular PP (intensity) probes they can be small, they allow for frequency independent execution, show low susceptibility to background noise, and they can be extended easily to full 3D probes. A handheld set-up developed in this research contains a loudspeaker box and a PU probe. It enables performing absorption measurements *in situ*, in a broad frequency range (typically from 300Hz to 10kHz), on small samples (typically $0.03\mathrm{m}^2$ to $0.38\mathrm{m}^2$ or larger), while hardly being affected by background noise and reflections. The relative responsivities of the sensors can be determined in a convenient manner with the same set-up by performing a reference test without a sample. The normal incidence absorption is measured with the probe positioned near the sample while the sound source is placed above it. Several known models that consider spherical waves above the sample have been examined, as well as a new model that also considers spherical waves inside the sample. The characteristics of the measurement methods have been investigated and their feasibility has been explored with respect to several applications that were impossible before.

The sensor responsivities need to be determined for absorption measurements. In the past, PU probes were calibrated with methods that are limited in frequency range. Here, a broadband calibration procedure is explored which uses a piston-on-a-sphere. The radiation characteristics of this type of sound source are similar to that of a monopole when on or near the acoustic axis of the source. The procedure involves a broadband calibration method and a low frequency calibration method that, when both methods are combined, can

typically be used from 20Hz to 20kHz. It is shown that even frequencies as low as 4Hz can be assessed under favourable conditions. For most absorption measurements only the relative responsivity of the sound pressure sensor to the particle velocity sensor needs to be known. The broadband piston-on-a-sphere calibration method can also be used for this purpose. A relative test is usually easier and faster to perform than a full calibration.

Several existing and new absorption models have been analysed. There are spherical waves because the sound source is positioned near the sample. Evidently, errors are therefore found with plane wave absorption models. Two existing models that do consider spherical waves were investigated; i.e. the mirror source model and the Q-term model. The mirror source model involves near field corrections for sound waves above the sample. The Q-term model also considers the spatial interferences of spherical sound waves above the sample. Surprisingly, similar results are often obtained with both models for this type of measurements, although the latter model appeared to be less robust. However, these models only account for the spherical propagation of sound waves above the sample, while erroneously assuming plane propagation of the sound waves inside the sample. Discrepancies, and even negative absorption values, are therefore found. A procedure that does consider spherical waves inside samples has been developed. It either involves the ratio of active absorbed to ingoing intensity or the impedance normal to the sample. Near field effects become stronger as the source-sample distance decreases. By extrapolated results from tests at several source distances, the plane wave absorption coefficient is obtained. The matter has been examined and verified with tests on several sample types, and with simulations.

Some of the main factors affecting the absorption measurements have been investigated. For probe-loudspeaker separations in between 0.2m and 0.5m, and probe-sample separations smaller than 30mm, tests can be performed on small samples, while the influence of reflections from surrounding surfaces and background noise is usually low. For five different sample types, the minimum sample size required was found to be 0.03m^2 to 0.38m^2, depending on the type of sample that is tested and on the absorption model used. A comparative study showed that errors can occur with the Kundt's tube because of its sample size restrictions. Measurements have been performed successfully *in situ*

under anechoic and non-anechoic conditions. However, the error increases if the reflections from surrounding surfaces strongly interfere with the direct sound waves. In most cases, reflections can be removed with several techniques such as impulse windowing, moving averages in the frequency domain, and spatial averaging. With several tests it was demonstrated that the influence of external sound sources is rather low. The intensity of a disturbing (background) noise source that was positioned 1m from the set-up is allowed to be 10dB higher than the intensity of the sound source of the set-up. Usually a lower sound source signal can be tolerated because disturbing sound sources are normally positioned further from the set-up. Tests are difficult to perform below 300Hz because the efficiency of the piston-on-a-sphere decreases at low frequencies. Yet, even frequencies of 100Hz and lower have been assessed under favourable conditions. Plausible results were obtained for frequencies as high as 20kHz, although it remains hard to validate the results beyond 10kHz because of a lack of suitable measurement techniques to compare with. Furthermore, it was shown that the resolution of *in situ* measurements can be in the order of a millimetre if a miniature PU probe is used. This allows for detailed examination of non-homogeneous samples.

Tests can be performed under conditions that were inaccessible before because of the unique properties of the PU *in situ* method. This may be advantageous for R&D in the automotive and aerospace industry, building acoustics, environmental noise, end-of-line control, etc. Several applications have been investigated to demonstrate the capabilities of the method. Firstly, it was shown that performance of products can be checked while they are installed. Measurements were performed successfully in concert halls and inside cars. During these tests large inconsistencies were found amongst cars of the same type. The second application investigated was the measurement of jet engine liners. Such samples often consist of interconnected cavities. It has been demonstrated that large errors can occur if an open Kundt's tube is used; i.e. at low frequencies there is sound leakage, and at high frequencies there are standing waves in between the flange of the tube and the backside of the sample. The tests revealed that more accurate results can be obtained with *in situ* measurements. In the future, such tests might be performed under more realistic conditions for the application (i.e. high sound levels, temperatures, and airflows). A set-up to measure liner samples with PU probes up to

150 dB OASPL is currently under development. The third application was the measurement of the absorption of roads whilst driving. Tests were performed at several speeds with a dedicated set-up. Although improvements can be made, measurements at speeds of 80 km/h or higher seem feasible. At such speeds the tests could be performed while the traffic remains nearly undisturbed. Finally, the Scan and Paint method has been introduced, which is frequently used to quickly localise and quantify sound sources. Here, the same method has been applied for the first time to map the spatial distribution of absorbing parameters. It has been demonstrated that the sound field above the sample can be visualised in high-resolution.

In the last chapter, two techniques to characterise the effect of the entire measurement arrangement have been presented. Both techniques use three-dimensional intensity measurements. With PU probes, such tests can be performed even in non-anechoic conditions. The first technique also uses the energy density. Contrary to microphones that measure potential energy density only, the kinetic energy density can also be obtained with PU probes. With the technique the diffusion at an arbitrary point is determined, which could be useful for determining the acoustic performance of rooms. It involves the measurement of a field index F, which is defined as the scaled ratio of the real part of intensity to the energy density. F ranges from zero (for a perfect diffuse field) to one (for a perfect anechoic condition). The functionality of the method has been demonstrated through tests that were performed in several environments. The second method that was investigated involved measurements at many positions, which are used to visualise the propagation of sound intensity throughout space. Complicated energy flows inside a car and around a theatre seat were visualised with vector plots, streamline plots and colour-maps. Such tests could be used in addition to-, or as replacement of simulations.

11. Samenvatting

De absorptie-eigenschappen van geluidsabsorberende samples kunnen niet in alle gevallen worden bepaald. Sommige meetmethoden kunnen niet *in situ* gebruikt worden; andere meetmethoden hebben een beperkt frequentiebereik of kunnen niet worden gebruikt voor bepaalde samples of voor geïnstalleerde samples. De mogelijkheden van de PU absorptiemetingen zijn nog niet volledig onderzocht. In dit onderzoek zijn verschillende *in situ* methoden die gebruik maken van PU probes geanalyseerd. De belangrijkste bevindingen zijn in dit proefschrift opgenomen.

Een PU probe bevat een geluidsdruksensor en een deeltjessnelheidsensor. Met deze probe kunnen benodigde grootheden voor absorptiemetingen, zoals impedantie, energiedichtheid en intensiteit, gemakkelijk worden gemeten. Vergeleken met PP intensiteit probes zijn PU probes klein. Ze kunnen in een frequentie-onafhankelijke configuratie uitgevoerd worden en ze zijn ongevoelig voor achtergrondlawaai. Tevens kunnen ze eenvoudig worden uitgevoerd als 3D probes. De handheld opstelling die is ontwikkeld in dit onderzoek bevat een luidspreker en een PU probe. Hiermee is het mogelijk om relatief kleine samples *in situ* te meten (gewoonlijk $0.03\,\mathrm{m}^2$ tot $0.38\,\mathrm{m}^2$ of groter), terwijl er nauwelijks verstoring is door achtergrondlawaai of reflecties. De relatieve gevoeligheden van de sensoren kunnen eenvoudig bepaald worden met een referentiemeting zonder sample. De absorptie wordt gemeten door de probe dicht bij het sample te plaatsen en de geluidsbron loodrecht erboven te zetten. Een aantal bekende modellen die rekening houden met bolvormige golven boven het sample en een nieuw model dat ook rekening houdt met bolvormige golven in het sample zijn geanalyseerd. De eigenschappen van de meetmethodes zijn onderzocht en mogelijkheden van nieuwe applicaties, die tot dusver niet mogelijk waren, zijn verkend.

Voor het meten van de absorptie moeten de gevoeligheden van de sensoren bepaald worden. Tot dusver werden PU probes gekalibreerd met in frequentie beperkte methoden. In dit onderzoek is een breedbandige kalibratie procedure onderzocht die gebruik maakt van een bolvormige luidspreker. Deze geluidsbron heeft soortgelijke afstraalkarakteristieken op de akoestische as als een monopool. De procedure bestaat uit een breedbandige en een

laagfrequente kalibratiemethode die, wanneer beide methoden worden gecombineerd, gewoonlijk van 20Hz tot 20kHz gebruikt kan worden. Het is aangetoond dat zelfs lage frequenties van 4Hz bereikt kunnen worden onder gunstige omstandigheden. Voor de meeste absorptiemetingen is alleen de relatieve gevoeligheid van de geluidsdruksensor ten opzichte van de deeltjessnelheidsensor van belang. Ook hiervoor kan de kalibratiemethode met de bolvormige luidspreker worden toegepast. Vaak is een relatieve test makkelijker en sneller uit te voeren dan een volledige kalibratie.

Verschillende bestaande en nieuwe absorptiemodellen zijn geanalyseerd. Doordat de geluidsbron dicht bij het sample geplaatst wordt zijn er bolvormige geluidsgolven. Daardoor worden er onjuiste resultaten verkregen met vlakke-golf absorptiemodellen. Twee bestaande modellen waarbij bolvormige golven worden beschouwd zijn onderzocht; namelijk het spiegelbron model en het Q-term model. Met het spiegelbron model worden nabije-veld correcties toegepast voor geluidsgolven boven het sample. Het Q-term model houdt tevens rekening met ruimtelijke interferenties van de geluidsgolven boven het sample. Verrassend genoeg is de uitkomst van beide modellen vaak gelijk voor dit type metingen, hoewel het laatstgenoemde model minder robuust is. Deze modellen houden alleen rekening met de bolvormige voortplanting van geluidsgolven boven het sample, terwijl er onterecht wordt aangenomen dat er vlakke golven zijn in het materiaal. Hierdoor worden afwijkingen en zelfs negatieve absorptiewaarden gemeten. Er is een procedure ontwikkeld waarmee ook bolvormige golven in het sample worden beschouwd. Hierbij wordt gebruik gemaakt van de ratio van de actieve geabsorbeerde en de ingaande intensiteit, of van de impedantie loodrecht op het sample. Voor kleinere bron-sample afstanden zijn de nabije-veld effecten sterker. Door de resultaten van metingen bij verschillende afstanden te extrapoleren, kan de vlakke-golf absorptiecoëfficiënt worden berekend. De procedure is onderzocht en geverifiëerd met metingen van verschillende sample types en met simulaties.

Een aantal belangrijke factoren die de absorptiemetingen beïnvloeden zijn onderzocht. Met een probe-luidspreker afstand tussen de 0.2m en de 0.5m en met een probe-sample afstand kleiner dan 30mm, kunnen metingen worden verricht op samples die klein zijn, terwijl er weinig invloed is van achtergrondlawaai en reflecties van andere oppervlakken. De minimale

samplegrootte varieert tussen de $0.03\,m^2$ en de $0.38\,m^2$ voor vijf sample types. In een vergelijkend onderzoek is aangetoond dat er onjuiste resultaten kunnen worden verkregen met de Kundt's buis, omdat de grootte van het sample hierdoor begrensd wordt. *In situ* metingen zijn met succes uitgevoerd in anechoïsche en niet-anechoïsche condities. Echter, de fout neemt substantieel toe als er een sterke interferentie is van reflecterende en directe geluidsgolven. In de meeste gevallen kunnen reflecties worden verwijderd met verschillende technieken, zoals impulsfilters, voortschrijdende gemiddeldes in het frequentiedomein en middelen over plaats. Met verschillende tests is aangetoond dat de invloed van externe geluidsbronnen tamelijk klein is. De geluidsintensiteit van een verstorende geluidsbron op 1m afstand van de meetopstelling mag 10dB hoger zijn dan de intensiteit van de luidspreker van de meetopstelling. Gewoonlijk kunnen zelfs lagere luidsprekerniveaus worden gebruikt omdat externe geluidsbronnen normaliter verder van de meetopstelling verwijderd zijn. Het is moeilijk om metingen uit te voeren onder de 300Hz omdat de efficiëntie van de luidspreker verminderd bij lage frequenties. Echter, er zijn frequenties van 100Hz en lager bereikt onder gunstige omstandigheden. Plausibele resultaten zijn verkregen bij frequenties zo hoog als 20kHz, al blijft het moeilijk om de resultaten boven 10kHz te valideren vanwege een gebrek aan geschikte meettechnieken om mee te vergelijken. Ook is aangetoond dat een resolutie van ongeveer één millimeter kan worden behaald met een miniatuur PU probe, wat het mogelijk maakt om inhomogene materialen in detail te bestuderen.

Door de unieke eigenschappen van de PU *in situ* methode is het mogelijk om testen onder condities uit te voeren die tot dusver ontoegankelijk waren. Dit bied onder andere voordelen voor R&D in de auto- en luchtvaartindustrie, bouwakoestiek, omgevingslawaai en productiecontrole. Een aantal toepassingen zijn onderzocht om de mogelijkheden van deze methode te demonstreren. Ten eerste is met metingen in concerthallen en auto's aangetoond dat het mogelijk is om de eigenschappen van producten te controleren, terwijl deze zijn geïnstalleerd. Bij deze tests zijn grote inconsistenties tussen verschillende auto's van hetzelfde type vastgesteld. De tweede applicatie is het meten van geluidsabsorberende panelen die in vliegtuigmotoren worden gebruikt. Deze samples bestaan meestal uit onderling verbonden holtes. Het is aangetoond dat grote fouten kunnen optreden met

een open Kundt's buis, want bij lage frequenties is er geluidslekkage en bij hoge frequenties onstaan er staande golven tussen de flens van de buis en de achterplaat van het sample. De uitkomst van deze test was dat nauwkeurigere resultaten worden verkregen met *in situ* metingen. De potentie is om zulke metingen uit te voeren onder condities die realistisch zijn voor de applicatie (hoge geluidsniveaus, temperaturen en luchtsnelheden). Op dit moment wordt een set-up ontwikkeld waarmee tot 150 dB OASPL kan worden gemeten. De derde applicatie is het rijdend meten van de geluidsabsorptie van wegdekken. Met een speciale opstelling zijn metingen uitgevoerd bij verschillende snelheden. Hoewel er verbeteringen mogelijk zijn, lijkt het haalbaar om bij snelheden van 80 km/u of hoger te meten. Bij zulke snelheden zou er gemeten kunnen worden met minimale verstoring van het verkeer. Als laatste is de "Scan and Paint" methode geïntroduceerd, welke vaak gebruikt wordt om geluidsbronnen snel te lokaliseren en te kwantificeren. Deze methode is voor het eerst toegepast om de ruimtelijke distributie van absorberende grootheden te bepalen. Aangetoond is dat het geluidsveld boven het sample kan worden gevisualiseerd met een hoge resolutie.

In het laatste hoofdstuk zijn twee technieken gepresenteerd waarmee het effect van de totale meetomgeving kan worden gekarakteriseerd. Beide technieken maken gebruik van driedimensionale intensiteitsmetingen. Met PU probes kunnen zulke metingen zelfs worden uitgevoerd in niet-anechoïsche condities. De eerste techniek maakt ook gebruik van de energiedichtheid. In tegenstelling tot microfoons, kan met PU probes niet alleen de potentiële, maar ook de kinetische energiedichtheid worden gemeten. Met deze techniek wordt de diffusie op arbitraire punten bepaald. Dit kan bijvoorbeeld nuttig zijn bij het bepalen van de akoestische prestaties van ruimtes. De methode maakt gebruik van een meting van de veld index F, welke gedefinieerd is als de geschaalde verhouding van het reële deel van de intensiteit en de energiedichtheid. F varieert van nul (voor een perfect diffuus veld) tot één (voor een perfect anechoïsch veld). De werking van de methode is aangetoond met metingen in een aantal omgevingen. De tweede methode die onderzocht is, maakt gebruik van metingen op veel posities, waarmee de propagatie van de geluidsintensiteit door de ruimte kan worden weergegeven. Gecompliceerde energiestromen zijn weergegeven in een auto en rond een theaterstoel. Zulke metingen kunnen een aanvulling zijn op simulaties of een vervanging ervan.

12. Conclusion and discussion

The accuracy and applicability of the PU *in situ* absorption method may be further investigated. Future research might be focussed on investigating the possibility of measuring more complicated material packages and measuring at low frequencies. The existing set-up may also be adapted to enable tests at multiple probe or sound source distances. Other sound field types may be considered; i.e. other angles of incidence, reverberant fields, or even the sound field present in the application. In addition, the transmission loss of a sample without a backplate might be determined. Existing techniques require large reverberant rooms, and the installation of samples is problematic. PU probes might allow (*in situ*) testing without such facilities and installation problems.

Before the invention of the Microflown sensor in 1994 it was impossible to measure acoustic particle velocity directly in a convenient manner [14, 15]. Since then, the usage of this sensor type has increased rapidly because it has been shown for numerous applications that directly determination of the particle velocity is advantageous or essential. Some of these applications have been described in this thesis. However, the application of the directly obtained particle velocity could be highly increased if it were supported by international standards, currently lacking.

Firstly, the development of standards for near field sound source localisation and quantification should be considered. Compared to existing methods, a broad frequency range can be accessed with high resolution while there is little influence from background noise and reflections (see appendix A). A separate standard should involve such near field tests as well as the measurement of the acoustic transfer path. The sound pressure contribution of each separate measurement section to the listener's position can be obtained by combining both measurements (see appendix A4 the "panel noise contribution application"). In addition, existing standards to measure intensity and sound power should be extended with direct sound pressure - particle velocity tests because it allows for frequency independent execution and is unaffected by the height of the pressure-intensity index.

Furthermore, the lack of an involved standard also limits the widespread usage of the PU *in situ* absorption method that has been investigated in this thesis because most customers of sound absorbing material suppliers the products to be tested with standardised methods. Conditions can be accessed with the *in situ* method under which existing measurement methods cannot be used, and the incorporation in a standard could benefit many industries.

Finally, there are several other applications involving the directly obtained particle velocity that, although more investigation is required, may be applicable for standardisation like the improved method to measure energy density, which also incorporates the kinetic energy density (see section 9.2).

Strikingly, the outcomes of many (standardised) absorption measurement and simulation methods are often conflicting. Consequently, erroneous judgements are made and noise issues are improperly treated. Even the usage of existing techniques for relative comparison of samples is questionable. The truly suitable absorption measurement methods should be identified with extensive round-robin tests that involve many methods and different samples. If an *in situ* method like the one described in this thesis would be found suitable, other absorption measurement techniques would be redundant for most cases.

Although much effort is put in designing the optimal material package, the consistency of the acoustic performance of products after they are manufactured is hardly checked because of a lack of appropriate measurement techniques. PU probes enable such tests because it has been shown that sound source radiation measurements and absorption measurements can be performed with high resolution, and in non-anechoic environments (see appendix A and chapter seven, respectively).

A sound field model that considers the spherical propagation of sound waves above and inside the sample was introduced in this thesis. Now the propagation of spherical waves inside samples is better understood, other absorption measurement methods can also be investigated. A method that is introduced in *[151]* involves determining bulk absorption properties of the sample. It uses several tests of different configurations, which are combined, because only then enough information is available to determine the complex

characteristic impedance and wavenumber. A second method that might be feasible is the so-called mirror source method *[76]*. It uses a miniature set-up consisting of a particle velocity sensor and a small omni-directional sound source. The orientation of the sensor is adjusted in such a way that only reflections are measured, and not the direct sound. The strength of the incoming sound waves is known because the sound source is characterised beforehand, and the relative strength of the reflected wave can be calculated. In the past, it has been shown that broadband absorption tests can be done on samples as small as $1\,\mathrm{cm}^2$ because the distance to the sample can be kept small, while there hardly is influence from background noise and reflections. Previously, deviations were found because near field effect inside the sample were neglected. The procedure might now be improved by extrapolating the results from multiple distances in a similar way as was done in this thesis.

There are many opportunities to develop and exploit existing and new applications. For example, the signal-to-noise ratio of PP probes is currently slightly higher than that of Microflown PU probes above approximately 3kHz [14]. However, if the high frequency performance of PU probes would be improved, PP probes would become superfluous for most applications. In addition, there might be methodologies that only have been investigated briefly or not at all that use for example far field tests, infra- and ultrasonic tests, and measurements in other media such as water. Although sound pressure microphones exist for a long time already and they are used in many applications, the widespread usage of particle velocity sensors and the development of involved applications has only just commenced.

Nomenclature

Roman symbols

a	Sphere radius	[m]
a	Correction for acoustic length	[m]
A	Equivalent sound absorption	[-]
b	Piston radius	[m]
c	Speed of sound	[m/s]
d	Diameter or (sample) thickness	[m]
d	Decay rate	[dB/s]
f	Frequency	[Hz]
F	Field index	[s/m^3]
G	Complex cross-spectral density	[-]
G_{corr}	Amplitude correction	[-]
h	Probe-sample distance	[m]
h	Spherical Hankel function of the second kind	[-]
H	Complex transfer function	[-]
$\boldsymbol{I}$	Active time averaged sound intensity	[W/m^2]
$\boldsymbol{J}$	Reactive time averaged sound intensity	[W/m^2]
k	Wavenumber	[1/m]
k_0, k_1	Wavenumber of air and the sample, respectively	[1/m]
l	Window length	[samples]
L	Length	[s]
m	Power attenuation coefficient	[1/m]
p	Sound pressure	[Pa]
p_{static}	Static ambient pressure	[Pa]
P	Sound power	[W]
P	Legendre function	[-]
r	Distance	[m]
Q	Volume velocity	[m^3/s]
R	Complex reflection coefficient	[-]
S	Surface area	[m^2]
S_{u}	Amplitude responsivity	[V·s/m]
t	Time	[s]
T	Reverberation time	[s]

T	Transmission loss	[dB]
T	Intensity transmission coefficient	[-]
$\boldsymbol{u}$	Acoustic particle velocity	[m/s]
V	Volume	[m^3]
w	Acoustic energy density	[J/m^3]
x, y, z	Cartesian coordinates	[m]
Z	Impedance	[Pa·s/m]
Z_n	Normalised characteristic impedance	[Pa·s/m]
Z_s	Surface impedance	[Pa·s/m]
Z_0, Z_1	Characteristic impedance of air and the sample, resp.	[Pa·s/m]

Greek symbols

α	Absorption coefficient	[-]
γ	Specific heat ratio	[-]
θ	Angle of incidence	[degrees]
λ	Wavelength	[m]
ρ	Density	[kg/m^3]
σ	Flow resistivity	[Pa·s/m^2]
φ	Phase	[degrees]
φ_{Su}	Phase responsivity	[degrees]
ω	Angular frequency ($2\pi f$)	[rad/s]
ξ	Ratio of specific to characteristic impedance	[-]

Abbreviations

FFT	Fast Fourier Transform
IFFT	Inverse Fast Fourier Transform
MLS	Maximum Length Sequence
PVL	Particle velocity Level (dB re. $50 \cdot 10^{-9}$ m/s)
SDI	Surface Diffusion Index
SIL	Sound Intensity Level (dB re. 10^{-12} W/m^2)
SNR	Signal-to-noise ratio
Std	Standard Deviation
SPL	Sound pressure Level (dB re. $20 \cdot 10^{-6}$ Pa)
TL	Transmission Loss

References

[1] Oldfield, R. (2006) *Improved membrane absorbers*. PhD dissertation. University of Salford. United Kingdom.

[2] Lanoye, R. (2007) *Assessment of the absorption performance of sound absorbing materials*. PhD dissertation. Katholieke Universiteit Leuven. Belgium. ISBN 978-90-5682-795-3.

[3] Kruse, R. (2008) *In situ measurement of ground impedance*. PhD dissertation. University of Oldenburg. Germany.

[4] Kinsler, L.E. and Frey, A.F. and Coppens, A.B. and Sanders, J.V. (2000) *Fundamentals of acoustics*. Forth edition. John Wiley & Sons Inc. New York. United States of America. ISBN 0-471-84789-5.

[5] Morfey, C.L. (2001) *Dictionary of Acoustics*. Academic press. London. England. ISBN 0-12-506940-5.

[6] Blackstock, D.T. (2000) *Fundamentals of physical acoustics*. John Wiley & Sons. New York. United States of America. ISBN 0-471-31979-1.

[7] Pierce, A. (1991) *Acoustics. An introduction to its principles and applications*. Second printing. Acoustical Society of America. New York. United States of America. ISBN 0-88318-612-8.

[8] Fahy, F.J. (2005) *Sound intensity*, 2nd edition. E & FN Spon, Chapman & Hall. London. England. ISBN 0-419-19810-5.

[9] Wind, J.W. (2009) *Acoustic source localization exploring theory and practice*. PhD dissertation. University of Twente. The Netherlands.

[10] Jacobsen, F. (2011) *Sound intensity and its measurement and applications*. Note no. 31262. Technical University of Denmark.

[11] Jacobsen, F. and de Bree, H-E (2005) *A comparison of two different sound intensity measurement principles*. Journal of the Acoustical Society of America. 118 (3). pp. 1510-1517. ISSN 0001-4966.

[12] Druyvesteyn, W.F. and de Bree, H-E. (2000) *A new sound intensity probe: comparison to the "pair of pressure microphone" intensity probe*. Journal of Audio Engineering Society, 48 (1/2).

[13] Jacobsen, F. and de Bree, H-E. (2005) *Measurement of sound intensity: P-U probes versus P-P probes*. Novem, Noise and Vibration: Emerging Methods. Saint-Raphael. France.

[14] de Bree, H-E. (2011) *E-book, The Microflown*. www.microflown.com.

[15] de Bree, H-E. and Leussink, P. and Korthorst, T. and Jansen, H. and Lammerink, T. and Elwenspoek, M. (1996) *The Microflown; a novel device measuring acoustic flows*. Sensors and Actuators, 54 (1-3). pp. 552-557. ISSN 0924-4247.

[16] Iwase, T. and Yoshihisa, K. (2003) *Measuring Method of Sound Reflection and Absorption Characteristics Based on the Particle velocity and its Applications to Measurements on Such as Drainage Pavement of Road Surface*. Internoise 206, International Congress and Exposition on Noise Control Engineering. pp. 697-704. ISSN 0736-2935.

[17] Lanoye, R. and de Bree, H-E. and Lauriks, W. and Vermeir, G. (2004) *A practical device to determine the reflection coefficient of acoustic materials in-situ based on a Microflown and microphone method*. ISMA International Conference on Noise Vibration Engineering. Leuven. Belgium.

[18] Allard, J.F. (1994) *Propagation of sound in porous media, Modelling sound absorbing materials*. Elsevier Applied Science. Andover. England.

[19] Chung, J.Y. and Blaser, D.A. (1980) *Transfer function method of measuring in a duct system with flow*. Journal of the Acoustical Society of America. 68 (6). pp. 1570-1577. ISSN 0001-4966.

[20] Yunseon, R. (2002) *The acoustic impedance measurement system using two microphones*. Forum Acusticum conference. Sevilla. Spain.

[21] (2006) *PULSE acoustic material testing in a tube - type 7758*. Product data sheet. Brüel & Kjær.

[22] (2009) *Impedance tube kit – type 4206, Impedance tube kit type - 4206A, Transmission loss kit – type 4206-T*. Product data sheet BP1039-17. Brüel & Kjær

[23] Lanoye, R. and Boeckx, L. and De Geetere, and L. Vermeir, G. and Lauriks, W. (2004) *Experience with different free field techniques to evaluate the surface impedance*. ICA, 18th International Conference on Acoustics. pp. 1983-1986. Kyoto. Japan. ISBN 4-9901915-3-6.

[24] Liu, Y. and Jacobsen, F. (2005) *Measurement of absorption with a p-u sound intensity probe in an impedance tube*. Journal of the Acoustical Society of America. 118 (4). pp. 2117-2120. ISSN 0001-4966.

[25] Dalmont, J.P. (2000) *Acoustic impedance measurement*. Journal of Sound and Vibration, 243 (3). pp. 427-459. ISSN 0022-460X.

[26] Bonfiglio, P. and Prodi, N. and Pompoli, F. and Farina, A. (2006) *On the use of a P-U sound intensity probe for the qualification of complex surface properties*. ICSV 13, congress on sound and vibration. Vienna. Austria.

[27] de Bree, H-E. and Tijs, E.H.G. and Basten, T. (2006) *Two complementary Microflown based methods to determine the reflection coefficient in situ*. ISMA International Conference on Noise Vibration Engineering. Leuven. Belgium.

[28] Allard, J.F. and Henry, M. and Boeckx, L. and Leclaire, P. and Lauriks, W. (2005) *Acoustical measurement of the shear modulus for thin porous layers*. Journal of the Acoustical Society of America. 117 (4). pp. 1737-1743. ISSN 0001-4966.

[29] Vigran, T.E and Kelders, L. and Lauriks, W. and Leclaire, P. and Johansen, T.F (1997) *Predictions and measurements of the influence of boundary conditions in a standing wave tube*. Acta Acustica united with Acustica, 83 (1). pp. 419-423. ISSN 1610-1928.

[30] Nosko, M. and Tijs, E.H.G. and de Bree, H-E. (2008) *A study of influences of the in situ surface impedance measurement technique*. DAGA, 34th German Annual Conference on Acoustics. Dresden. Germany.

[31] Horoshenkov, K.V and Khan, A. and Bécot, F-X. and Jaouen, L. and Sgard, F. and Renault, A. and Amirouche, N. and Pompoli, F. and Prodi, N. and Bonfiglio, P. and Pispola, G. and Asdrubali, F. and Hübelt, J. and Attala, N. and Amédin, C.K. and Lauriks, W. and Boeckx, L. (2007) *Reproducibility experiments on measuring acoustical properties of rigid-frame porous media* (*round robin test*). Journal of the Acoustical Society of America. 122 (1). pp. 345-353. ISSN 0001-4966.

[32] Miranda, L. and Alvarez, J. and Jacobsen, F. (2007) *In-situ measurements of the complex acoustic impedance of materials in vehicle interiors*. ICA, 19th International Conference on Acoustics. Madrid. Spain.

[33] Seybert, A. and Han, J. (2008) Meas*urement of pavement absorption using ISO 13472-2*. Acoustics'08. Paris. France.

[34] Tijs, E.H.G. and de Bree, H-E. and Ferrante, P. and Scofano, A. (2008) *PU surface impedance measurements on curved liner materials in the presence of a grazing flow*. 12th CEAS workshop. Bilbao. Spain.

[35] www.spectronics.net.

[36] www.silentroads.nl.

[37] Bischel, M. and Roy, K. and Greenslade, J. (2008) *Comparison of ASTM and ISO sound absorption test methods*. Acoustics'08. Paris. France.

[38] (2008) *Standard Test Method for Sound Absorption and Sound Absorption Coefficients by the Reverberant Room Method*. ASTM C423-08. ASTM International.

[39] (2003) *Measurement of sound absorption in a reverberant room*. ISO 354, 2nd edition. International Organization for Standardization.

[40] www.rieter.com.

[41] Jacobsen, F. (2011) *The sound field in a reverberant room*. Note no. 31261. Technical University of Denmark.

[42] D'Alessandro, F. and Pispola, G. (2005) *Sound absorption properties of sustainable fibrous materials in an enhanced reverberation room*. Internoise 208, International Congress and Exposition on Noise Control Engineering. pp. 2209-2218. ISSN 0736-2935.

[43] Attenborough, and K. Bashir, I. and Taherzadeh, S. (2010) *Review of ground impedance models for propagation modelling*. Internoise 221, International Congress and Exposition on Noise Control Engineering. pp. 3151-3159. ISSN 0736-2935.

[44] Boeckx, L. (2005) *Study of the sound field in and above porous materials-application to characterization of sound absorbing materials*. PhD dissertation. Katholieke University Leuven. Belgium.

[45] Boeckx, L. and Leclaire, P. and Khurana, P. and Glorieux, C. and Lauriks, W. and Allard, J.F. (2004) *Investigation of the phase velocities of guided acoustic waves in soft porous layers*. Journal of the Acoustical Society of America. 117 (2). pp. 545-554. ISSN 0001-4966.

[46] Komatsu, T. (2008) *Improvement of the Delany-Bazley and Miki models for fibrous sound-absorbing materials*. Acoustic society & Technology, 29 (2). pp. 121-129. The acoustical society of Japan.

[47] Visser, R. (2004) *A boundary element approach to acoustic radiation and source identification*. PhD dissertation. University of Twente. The Netherlands. ISBN 90-365-2051-7.

[48] Hald, J. (2005) *An integrated NAH/Beamforming solution for efficient broad-band noise source localization*. SAE Noise and Vibration conference. Num.: 2005-01-2537.

[49] Williams, E. (1999) *Fourier Acoustics, Sound Radiation and Nearfield Acoustical Holography*. Academic Press. London. England. ISBN 0-12-753960-3.

[50] Bérengier, M. and Garai, M. (2002) *In situ sound absorption coefficient measurement of various surfaces*. Forum Acousticum. Sevilla. Spain.

[51] Suhanek, M. and Jambrosic, K. and Milicevic, A. (2009) *A comparison of two procedures for in-situ measurements of sound absorption coefficient*. Proceeding in 51st international Elmar 2009 symposium. Zadar. Croatia. pp. 213-216.

[52] Asdrubali, F. and Pispola, G. and Baldinelli, G. (2004) *Optimization of in situ noise barrier intrinsic characteristics measurements*. ICSV 11, congress on sound and vibration. St. Petersburg. Russia.

[53] http://acustica.ing.unibo.it/Researches/barriers/adrienne.html.

[54] Smal, L. and den Hertog, M. and Laureijssen, B. and Ruiter, B. (2007) *De 'SteamCleaner' eindrapport*, Dura Vermeer Infrastructuur, rapport DWW-2007-024.

[55] Guidorzi, P. and Garai, M. (2008) *Signal analysis in the sound absorption measurement procedure: The importance of time subtraction and reference surface corrections*. Acoustics '08. Paris. France.

[56] Kruse, R. (2007) *Application of the Two-Microphone method for In-Situ Ground Impedance Measurements*. Acta Acustica united with Acustica, 93 (5). pp. 837-842. ISSN 1610-1928.

[57] Kruse, R. and Mellert, V. (2008) *Effect and minimization of errors in in situ ground impedance measurements*. Applied Acoustics, 69 (10), pp. 884-890. ISSN 0003-628X.

[58] Kruse, R. and Sauerzapf, S. (2009) *Reducing the influence of microphone errors on in-situ ground impedance measurements*. Acta Acustica united with Acustica, 95 (1). pp. 151-155. ISSN 1610-1928.

[59] Allard, J. and Champoux, Y. (1989) *In situ, Two-Microphone Technique for the Measurement of the Acoustic Surface Impedance of Materials*. Noise Control Engineering Journal, 32(1). pp. 15-23. ISSN 0736-2501.

[60] Havelock, D. and Kuwano, S. and Vorländer, M. (2008) *Handbook in signal processing in acoustics*. Vol. 1. Springer science + business media. New York. United states of America. ISBN 978-0-387-77698-9.

[61] Tijs, E.H.G. and Nejade, A. and de Bree, H-E. (2009) *Verification of PU intensity calculation*. Novem, Noise and Vibration: Emerging Methods. Oxford. England.

[62] Hirosawa, K. and Nakagawa, H. and Kon, M. and Yamamoto, A. (2009) *Comparison of three measurement techniques for the normal absorption coefficient in the free field*. ICSV 16, congress on sound and vibration. Krakóv. Poland.

[63] van Honschoten, J. and Svetovoy, V. and Krijnen, G. and Elwenspoek, M. (2005) *Optimization of a thermal flow sensor for acoustic particle velocity measurements*. Journal of Microelectromechanical Systems, 14 (3), ISSN 1057-7157.

[64] Svetovoy, V. and Winter, I. (2000) *Model of the μ-flown microphone*. Sensors and Actuators A: Physical, 86 (3). pp. 171-181.

[65] van Honschoten, J. (2004) *Modelling and optimization of the Microflown*. PhD dissertation. University of Twente. The Netherlands. ISBN 90-365-2030-4.

[66] de Bree, H-E. and W. Druyvesteyn, W. (2005) *A particle velocity sensor to measure the sound from a structure in the presence of background noise*. Forum Acusticum conference. Budapest. Hungary.

[67] Schurer, H. and Annema, P. and de Bree, H-E. and Slump, C.H. and Herman, O. (1996) *Comparison of two methods for measurements of horn input impedance*. Journal of the Audio Engineering Society. 44. p. 649.

[68] Takahashi, Y. and Otsuru, T. and Tomiku, R. (2005) *In situ measurements of surface impedance and absorption coefficients of porous materials using two microphones and ambient noise*. Applied Acoustics, 66 (7). pp. 845-865. ISSN 0003-628X.

[69] Otsuru, T. and Tomiku, R. and Okamoto, N. and Murakami, M. and Kutsukake, F. and Che Din, N. (2008) *In-situ measurement of ensemble averaged impedance and absorption characteristics of materials at field incidence using p-v or p-p sensors*. Internoise 210, International Congress and Exposition on Noise Control Engineering. pp. 3200-3211. ISSN 0736-2935.

[70] Otsuru, T. and Okuzono, T. and Akamoto, N. and Tomiku, R. Takahashi, Y. (2006) *Impedance measurement of materials by use of ambient noise for computational acoustics*. Internoise. International Congress and Exposition on Noise Control Engineering. Honolulu. United States of America.

[71] bin Che Din, N. and Otsuru, T. and Tomiku, R. and Okamoto, N. and Kusno, A. (2010) *An in-situ technique for extensive field measurements of absorption characteristics of materials using ensemble averaging*, ICA, 20th International Conference on Acoustics. Sydney. Australia.

[72] Brandão, E. (2011) *Análise teorica e experimental al do processo de medição in situ da impedância acústica*. PhD dissertation. Universidade Federal de Santa Catarina. Brazil.

[73] Beranek, L. (1996) *Acoustics*. Acoustical Society of America. New York. The United States of America. ISBN 0-88318-494-X.

[74] Alvarez, J. and Jacobsen, F. (2008) *An Iterative Method for Determining the Surface Impedance of Acoustic Materials In Situ*. Internoise 210, International Congress and Exposition on Noise Control Engineering. pp. 4055-4065. ISSN 0736-2935.

[75] Lanoye, R. and Vermeir, G. and Lauriks, W. and Kruse, R. and Mellert, V. (2006) *Measuring the free field acoustic impedance and absorption coefficient of sound absorbing materials with a combined particle velocity-pressure sensor*. Journal of the Acoustical Society of America, 119 (5). pp. 2826-2831. ISSN 0001-4966.

[76] de Bree, H-E. and Tijs, E.H.G. and Basten, T. (2007) *An ultra miniature measurement tool to measure the reflection coefficient of acoustic damping materials in situ*. SAE Noise and Vibration conference. Num.: 2007-01-2212.

[77] de Bree, H-E. and Nosko, M. and Tijs, E.H.G. (2008) *A handheld device to measure the acoustic absorption in situ*. SNVH, 5th International Styrian Noise Vibration & Harshness conference. Graz. Austria.

[78] Filippi, P. (1983) *Extended sources radiation and Laplace type integral representation: Application to wave propagation above and within layered media*. Journal of Sound and Vibration, 91 (1). pp. 65-84. ISSN 0022-460X.

[79] Ingard, U. (1951) *On the reflection of a spherical sound wave from infinite plane*. Journal of the Acoustical Society of America. 23 (3). pp. 329-335. ISSN 0001-4966.

[80] Taraldsen, G. (2005) *The complex image method*. Wave motion 43. pp. 91-97. Elsevier.

[81] Nobile, M.A. and Hayek, S.I. (1985) *Acoustic propagation over an impedance plane*. Journal of the Acoustical Society of America. 78 (4). pp. 1325-1336. ISSN 0001-4966.

[82] Alvarez, J. (2006) *In-situ measurements of the Complex Acoustic Impedance of materials for automobile interiors*. Master thesis. Technical University of Denmark.

[83] Sidi, A. (2008) *Generalization of the secant method for nonlinear equations*. Applied Mathematics E-notes. 8. pp. 115-123.

[84] (2009) *Primary method for pressure calibration of laboratory standard microphones by the reciprocity technique*. Second edition. IEC 61094-2 international standard.

[85] (2011) *G.R.A.S Pistonphone Type 42AP datasheet*, product data and specifications.

[86] (2001) *Methods for pressure calibration of working standard microphones by comparison*. First edition. IEC 61094-5 international standard.

[87] de Bree, H-E. and Svetovoy, V. and Raangs, R. and Visser, R. (2004) *The very near field, theory, simulations and measurements, of sound pressure and particle velocity in the very near field*. ICSV 11, International Congress on Sound and Vibration. St. Petersburg. Russia.

[88] Raangs, R. and Schlicke, T. and Barham, R. (2005) *Calibration of a microflown in a standing wave tube using an LDA photon-correlation technique*. Measurement Science and Technology, 16 (5). ISSN 1361-6501.

[89] Jacobsen, F. and Jaud, V. (2006) *A note on the calibration of pressure-velocity sound intensity probes*. Journal of the Acoustical Society of America. 120 (2). pp. 830-837. ISSN 0001-4966.

[90] van Honschoten, J. and de Bree, H-E. and van Eerden, F. and Krijnen, G. (2000) *The influence of viscothermal effects on calibration measurements in a tube*. Audio Engineering Society, 109th conference. Los Angeles. United States of America. ISSN 1071-6947.

[91] Bree, H-E. and Basten, T. (2008) *Microflown based monopole sound sources for reciprocal measurements*. SAE Noise and Vibration conference. Num.: 2008-36-0503.

[92] Tijs, E.H.G. and Brandão, E. and de Bree, H-E. (2008) *In situ tubeless impedance measurements in a car interior*. SIA, 5th symposium on Automobile and Railroad Comfort. Le Mans. France.

[93] Tijs, E. and Brandão, E. and de Bree, H-E (2009) *In situ PU surface impedance measurements for quality control at the end of an assembly line*. SAE Noise and Vibration conference. Num.: 2009-01-2142.

[94] Raangs, R. and Druyvesteyn, W.F. and de Bree, H-E. (2001) *A low cost Intensity Probe*. Audio Engineering Society, 111th conference. New York. United States of America. ISSN 1071-6947.

[95] Tijs, E.H.G. (2012) *Sound source characterization for PU based in situ absorption measurements*. Euronoise, the 9th European Conference on Noise Control. Prague. Czech republic.

[96] Basten, T. and de Bree, H-E. (2009) *Full bandwidth calibration procedure for acoustic probes containing a pressure and particle velocity sensor*. Journal of the Acoustical Society of America. 127 (1). pp. 264-270. ISSN 0001-4966.

[97] (2011) *Mid-High frequency monopole*. Datasheet, V1.2. Microflown Technologies. www.microflown.com.

[98] Jacobsen, F. and Poulsen, T. and Rindel, J.H. and Gade, A.C. and Ohlrich, M. (2011) *Fundamentals of acoustics and noise control*. Note 31200. Technical University of Denmark.

[99] Vigran, T.E (2008) *Building Acoustics*. p. 166. Taylor & Francis e-Library. ISBN 0-203-931-31-9.

[100] de Bree, H-E. and Lanoye, R. and de Cock, S. and van Heck, J. (2005) *In situ, broad band method to determine the normal and oblique reflection coefficient of acoustic materials*. SAE Noise and Vibration conference. Num.: 2005-01-2443.

[101] Tijs, E. and de Bree, H-E. (2008) *Recent developments free field PU impedance technique*. Sapem. Bradford. England.

[102] Boreman, G.D. (1998) *Basic Electro-Optics for Electrical Engineers*, p. 55. SPIE - the national society for optical engineering. Washington. United States of America. ISBN 0-8194-2806-X.

[103] Hänsler, E. and Schmidt, G. (2004) *Acoustic echo and noise control – a practical approach*. John Wiley & Sons. New Jersey. United states of America. ISBN 0-471-45346-3.

[104] Smith, S.W. (1997) *The Scientist and Engineer's Guide to Digital Signal Processing*. E-book. www.dspguide.com.

[105] Cobo, P. and Fernández, A. and Palacios, R. and Colina, C. and Siguero, M. (2004) *In situ absorption measurement of antinoise devices using pre-determined pulse waveforms*. Acústica. Guimarães. Portugal.

[106] Shin, K. and Hammond, J.K. (2008) *Fundamentals of signal processing for sound and vibration engineers*. John Wiley & Sons Ltd. West Sussex. England ISBN-13 978-0470-51188-6.

[107] Press, W.H. and Flannery, B.P. and Teulkolsky, S.A. and Vlettering, W.T. (1992) *Numerical recipes in Fortran 77*: *the art of scientific computing*. Second edition. Press syndicate of the University of Cambridge. Cambridge. England. ISBN-13 978-0521-43064-7.

[108] Struck, C.J. and Temme, S.F. (1994) *Simulated Free Field Measurements*. Journal of the Acoustical Society of America. 42 (6). pp. 256-263. ISSN 0001-4966.

[109] Montgomery, D.C. and Runger, G.C. (1999) *Applied Statistics and Probability for Engineers*. Second edition, p. 158. John Wiley & Sons, Inc. New York. United States of America. ISBN 0-471-17027-5.

[110] Jacobsen, F. and Molares, A. (2009) *The ensemble variance of pure-tone measurements in reverberation rooms*. ICSV 16, congress on sound and vibration. Krakóv. Poland.

[111] Tijs, E.H.G. and de Bree, H-E. and Basten, T. and Nosko, M. (2007) *Non destructive and in situ acoustic testing of inhomogeneous materials*. ERF33, 33rd European Rotorcraft Forum. Kazan. Russia.

[112] Knutzen, J. (2008) *Untersuchung der akustischen Eigenschaften von typischen Materialien für den Fahrzeuginnenraum*. Master thesis. RWTH Aachen. Aachen. Germany.

[113] Tijs, E.H.G. and de Bree, H-E. and Brandão, E. (2009) *Large scale in situ acoustic absorption measurements in a theatre*. DAGA, 35th German Annual Conference on Acoustics. Rotterdam. The Netherlands.

[114] Tijs, E.H.G. and de Bree, H-E. (2008) *Acoustic absorption measurements of moving structures and under influence of flow*. ISMA International Conference on Noise Vibration Engineering. Leuven. Belgium.

[115] Brandão, E. and Tijs, E.H.G. and Lenzi, A. and de Bree, H-E (2011) *A comparison of three methods to calculate the surface impedance and absorption coefficient from measurements under free field or in situ conditions*. Acta Acustica united with Acustica, 97 (6). pp. 1025-1033. ISSN 1610-1928.

[116] Tijs, E.H.G and Druyvesteyn, W.F (2012) *An intensity method for measuring absorption properties in situ*. Acta Acustica united with Acustica, 98 (1). pp. 342-353. ISSN 1610-1928.

[117] Tijs, E.H.G. and Druyvesteyn, W.F. and de Bree, H-E. (2011) *A Handheld Intensity Device for Measuring Absorption Properties in situ*. Forum Acusticum conference. Aalborg. Denmark.

[118] Tandon, N. (1999) *Sound intensity technique and its applications in noise control*. PINSA, 65 (1). pp. 51-60.

[119] Prascevic, R.M. and Milosevic, A.M. and Cvetkovic, S.D. (1994) *Determination of absorption characteristic of materials on basis of sound intensity measurement*. Journal de Physique IV, C5-149.

[120] Farina, A. and Torelli, A. (1997) *Measurement of the sound absorption coefficient of materials with a new sound intensity technique*. Audio Engineering Society, 102th convention. Munich. Germany.

[121] Tijs, E.H.G. and de Bree, H-E. and Brandão, E. (2010) *High resolution absorption mapping with a pu surface impedance method*. ASA-INCE NoiseCon. Baltimore. United States of America.

[122] Tijs, E.H.G. and Druyvesteyn, W.F. (2011) *Spatial variation of impedance and intensity measured close to a sample in the near field of a spherical sound source*. Sapem. Ferrara. Italy.

[123] de Bree, H-E. and Tijs, E.H.G. (2009) *PU nosecone intensity measurements in a wind tunnel*. DAGA, 35th German Annual Conference on Acoustics. Rotterdam. The Netherlands.

[124] Brandão, E. and Lenzi, A. and Cordioli, J. (2012) *Estimation and minimization of errors caused by sample size effect in the measurement of the normal absorption coefficient of a locally reacting surface*. Applied Acoustics, 73 (6-7). pp. 543-556. ISSN 0003-628X.

[125] Sandier, C. and Peteul, C. and Guyader, E. and Guyader, J-L. (2006) *In situ measurements of acoustic impedance for car applications: influence of forming effect*. Euronoise, the sixth European Conference on Noise Control. Tampere. Finland.

[126] van der Eerden, F. (2000) *Noise reduction with coupled prismatic tubes. PhD dissertation*. University of Twente. The Netherlands. ISBN 90-36515211.

[127] Rayleigh, J.W.S. (1945) *The theory of sound*, volume 2, Second edition. Dover Publications. New York. United States of America. ISBN 0486602931.

[128] Kühnert, C. and Figula, U. and Hübelt, J. (2009) *Acoustical method for the non-destructive determination of the porosity of asphalts*. Euronoise, the 8th European Conference on Noise Control. Edinburgh. Scotland.

[129] Tijs, E. and Botts, J. and de Bree, H-E. and Arato, E. (2009) *Acoustic particle velocity enabled methods to assess room acoustics*. Euronoise, the 8th European Conference on Noise Control. Edinburgh. Scotland.

[130] Tijs, E.H.G. and de Bree, H-E. (2009) *An in situ method to measurement the acoustic absorption of roads whilst driving*. DAGA, 35th German Annual Conference on Acoustics. Rotterdam. The Netherlands.

[131] Grosso, A. and de Bree, H-E. and Steltenpool, S. and Tijs, E.H.G. (2011) *Scan* & *paint for acoustic leakage inside the car*. SAE Noise and Vibration conference. Num.: 2011-01-1673.

[132] Tijs, E.H.G. and de Bree, H-E. and Steltenpool, S. (2009) *A novel acoustic pressure-velocity based method to access acoustic leakages of an acoustic enclosure in non anechoic conditions*. Euronoise, the 8th European Conference on Noise Control. Edinburgh. Scotland.

[133] de Bree, H-E. and Grosso, A. and Wind, J.W. and Tijs, E.H.G. (2010) *Scan*&*Paint*, *a new fast tool for sound source localization and quantification of machinery in reverberant conditions*. VDI conference, Schwingungsanalyse und Identifikation. Leonberg. Germany.

[134] Tijs, E.H.G. and de Bree, H-E. and Steltenpool, S. (2010) *Scan* & *Paint*: *a novel sound visualization technique*. Internoise 221, International Congress and Exposition on Noise Control Engineering. pp. 6232-6237. ISSN 0736-2935.

[135] Peeters, B. and Ammerlaan, I. and Kuijpers, A. and van Blokland, G. (2010) *Reduction of the horn effect for car and truck tyres by sound absorbing road surfaces*. Internoise 221, International Congress and Exposition on Noise Control Engineering. pp. 830-839. ISSN 0736-2935.

[136] Bernhard, R. and Wayson, R.L. (2005) *An Introduction to Tire/Pavement Noise of Asphalt Pavement*. Final research report. Purdue University, and University of central Florida. quietpavement.com.

[137] de Bree, H-E. and Tijs, E.H.G. (2009) *A PU sound probe for high sound levels*. DAGA, 35th German Annual Conference on Acoustics. Rotterdam. The Netherlands.

[138] Fernández, D. and Wind, J.W. and de Bree, H-E (2011) *A scanning method for source visualization and transfer path analysis using a single probe*. SAE Noise and Vibration conference. Num.: 2011-01-1664.

[139] Kock, W.E. (1965) *Sound Waves and Light Waves, the Fundamentals of Wave Motion*. Anchor Books. pp. 7-33. ISBN 978-0385027748.

[140] Vigran, T.E. (1988) *Acoustic intensity – energy density ratio: An index for detecting deviations from ideal field conditions*. Journal of Sound and Vibration, 127 (2). pp. 343-351. ISSN 0022-460X.

[141] Tijs, E.H.G. and Wijker, J. and Grillenbeck, A. (2011) *Benefit of Acoustic Particle velocity Based Reverberant Room Testing of Spacecraft*. IMAC XXXI, A Conference and Exposition on Structural Dynamics. Jacksonville. United States of America.

[142] Tijs, E.H.G. and de Bree, H-E. (2009) *Mapping 3D sound intensity streamlines in a car interior*. SAE Noise and Vibration conference. Num.: 2009-01-2175.

[143] d'Antonio, P. and Rife, B. (2011) *The state of the art in measurement of acoustical coefficients*. 161st meeting of the Acoustical Society of America, 12. Seattle. United States of America. ISSN 1939-800X.

[144] Cox, T.J. and d'Antonio, P. (2009) *Acoustic Absorbers and Diffusers*, 2nd edition. Taylor & Francis. Abingdon. United Kingdom. ISBN10 0-415-47174-5.

[145] Raangs, R. and Druyvesteyn, W.F. and de Bree, H-E (2001) *A novel two-dimensional sound particle velocity probe for source localization and free field measurements in a diffuse field*. Internoise. International Congress and Exposition on Noise Control Engineering. The Hague. The Netherlands.

[146] Yntema, D.R. and Druyvesteyn, W.F. and Elwenspoek, M. (2006) *A four particle velocity sensor device*. Journal of the Acoustical Society of America. 119 (2). pp. 943-951. ISSN 0001-4966.

[147] Nutter, D.B. and Leishman, T.W. and Sommerfeldt, S.D. and Blotter, J.D. (2007) *Measurement of sound power and absorption in reverberation chambers using energy density*. Journal of the Acoustical Society of America. 121 (5). pp. 2700-2710. ISSN 0001-4966.

[148] Cats, P. and Tijs, E.H.G. and Fernandez, D.C. (pending; to be presented at the ICA conference 2013) *Exploration of the differences between a pressure-velocity based in situ absorption method and the standardized reverberant room method*. ASA ICA. Montreal. Canada.

[149] Weyna, S. (2004) *Experimental 3D visualization of power flow around obstacles in real acoustic fields*. ICSV 11, congress on sound and vibration. St. Petersburg. Russia.

[150] Weyna, S. (2007) *Acoustic energy distribution in space around the pipe outlet*. Noise Control Engineering National Conference. Reno. United States of America.

[151] Tijs, E.H.G and Druyvesteyn, W.F (pending) *Direct measurement of the bulk properties of acoustic absorbing samples*. Acta Acustica united with Acustica

[152] de Bree, H-E. and Druyvesteyn, W.F. and Tijs, E.H.G. (2009) *Broad banded acoustic vector sensors for passive monitoring of aircraft*. DGLR, Deutscher Luft- und Raumfahrtkongress. Aachen. Germany.

[153] Wolff, O. and Tijs, E.H.G. and de Bree, H-E (2009) *In-flight panel noise contribution analysis on a helicopter cabin interior*. SAE Aerospace.

[154] de Bree, H-E. and Basten, T. and Tijs, E. (2008) *Source path contribution breakdown of a sound pressure based compliance test*. SNVH, 5th International Styrian Noise Vibration & Harshness conference. Graz. Austria.

[155] de Bree, H-E. and Basten, T. and Tijs, E.H.G. and Voogdt, J. (2007) *Fast in-flight cabin interior sound source localization*. ERF33, 33rd European Rotorcraft Forum. Kazan. Russia.

[156] Tijs, E. and de Bree, H-E. and Bussow, R. (2009) *PU sound power measurements on large turbo machinery*. ICSV 16, congress on sound and vibration. Krakóv. Poland

[157] Wolff, O. and Sottek, R. (2005) *Panel Contribution Analysis - An Alternative Window Method*. SAE Noise and Vibration conference. Num.: 2005-01-2274.

[158] Grosso, A. and Comesana, D. F. and de Bree, H-E (2012) *Further Development of the PNCA: New Panel Noise Contribution Reference-Related (PNCAR)*. Num.: 2012-01-1539.

[159] Wolff, O. and Tijs, E. and de Bree, H-E. (2009) *A PU probe array based panel noise contribution analysis whilst driving*. SAE Noise and Vibration conference. Num.: 2009-01-2123.

[160] Tijs, E.H.G. and Wind, J.W. and Fernández, D.F. and de Bree, H-E. (2011) *Fast, high resolution panel noise contribution method*. SAE Noise and Vibration conference. Num.: 2011-01-1594.

[161] de Bree, H-E. and Wind, J.W. and Tijs, E.H.G. (2010) *Environmental noise monitoring with acoustic vector sensors*. Internoise 221, International Congress and Exposition on Noise Control Engineering. pp. 6225-6231. ISSN 0736-2935.

[162] Escribano, D. and Tijs, E.H.G. (2011) *Measurement of the acoustic noise map of a city using acoustic vector sensors*. Internoise 232, International Congress and Exposition on Noise Control Engineering. pp. 2391-2396. ISSN 0736-2935.

[163] Basten, T. and de Bree, H-E. and Tijs, E. (2007) *Localization and tracking of aircraft with ground based 3D sound probes*. ERF33, 33rd European Rotorcraft Forum. Kazan. Russia.

[164] Wind, J.W. and de Bree, H-E. and Tijs, E. and Yntema, D. (2009) *Acoustic vector sensors for aeroacoustics*. CEAS European Air and Space Conference. Manchester. England.

[165] Wind, J.W. and de Bree, H-E. and Tijs, E. (2009) *Source localization using acoustic vector sensors, a MUSIC approach*. Novem, Noise and Vibration: Emerging Methods. Oxford. England.

[166] Tijs, E.H.G. and de Croon, G. and Wind, J.W. and Remes, B. and De Wagter, C. and de Bree, H-E. and Ruijsink, R. (2010) *Hear-and-Avoid for Micro Air Vehicles*. IMAV, International Micro Air Vehicle Conference. Braunschweig. Germany.

[167] de Bree, H-E and Akal, T and Tijs, E.H.G. (2010) *The Hydroflown: MEMS-Based Underwater Acoustical Particle Velocity Sensor. Results of lab tests and sea trials*. ECUA 2010. 10th European Conference on Underwater Acoustics. Istanbul. Turkey.

List of publications

Journal papers:

Brandão, E. and Tijs, E. H.G. and Lenzi, A. and de Bree, H E (2011) *A comparison of three methods to calculate the surface impedance and absorption coefficient from measurements under free field or in situ conditions*. Acta Acustica united with Acustica, 97 (6). pp. 1025-1033. ISSN 1610-1928.

Tijs, E.H.G and Druyvesteyn, W.F (2012) *An intensity method for measuring absorption properties in situ*. Acta Acustica united with Acustica, 98 (1). pp. 342-353. ISSN 1610-1928.

Tijs, E.H.G and Druyvesteyn, W.F (pending) *Direct measurement of the bulk properties of acoustic absorbing samples*. Acta Acustica united with Acustica.

Conference papers:

de Bree, H E. and Tijs, E.H.G. and Basten, T. (2006) *Two complementary Microflown based methods to determine the reflection coefficient in situ*. ISMA International Conference on Noise Vibration Engineering. Leuven. Belgium.

de Bree, H-E. and Basten, T. and Tijs, E.H.G. and Voogdt, J. (2007) *Fast in-flight cabin interior sound source localization*. ERF33, 33rd European Rotorcraft Forum. Kazan. Russia.

Basten, T. and de Bree, H-E. and Tijs, E. (2007) *Localization and tracking of aircraft with ground based 3D sound probes*. ERF33, 33rd European Rotorcraft Forum. Kazan. Russia

de Bree, H-E. and Yntema, D. and Tijs, E.H.G. (2007) *A PU sound intensity probe designed for high temperature use*. SAE Noise and Vibration conference. Num.: 2007-01-2336.

de Bree, H E. and Tijs, E.H.G. and Basten, T. (2007) *An ultra miniature measurement tool to measure the reflection coefficient of acoustic damping materials in situ*. SAE Noise and Vibration conference. Num.: 2007-01-2212.

Tijs, E.H.G. and de Bree, H-E. and Basten, T. and Nosko, M. (2007) *Non destructive and in situ acoustic testing of inhomogeneous materials*. ERF33, 33rd European Rotorcraft Forum. Kazan. Russia.

Tijs, E.H.G. and Brandão, E. and de Bree, H E. (2008) *In situ tubeless impedance measurements in a car interior*. SIA, fifth symposium on Automobile and Railroad Comfort. Le Mans. France.

Schedlinski, C. and Tijs, E.H.G. (2008) *Computational Model Updating of Structural Damping and Acoustic Absorption for Coupled Fluid-Structure-Analyses of Passenger Cars*. ISMA International Conference on Noise Vibration Engineering. Leuven. Belgium.

Tijs, E. and de Bree, H-E. (2008) *Recent developments free field PU impedance technique*. Sapem. Bradford. England.

Tijs, E.H.G. and de Bree, H-E. and Ferrante, P. and Scofano, A. (2008) *PU surface impedance measurements on curved liner materials in the presence of a grazing flow*. 12th CEAS workshop. Bilbao. Spain.

Tijs, E.H.G. and de Bree, H-E. (2008) *Acoustic absorption measurements of moving structures and under influence of flow*. ISMA International Conference on Noise Vibration Engineering. Leuven. Belgium.

de Bree, H-E. and Nosko, M. and Tijs, E.H.G. (2008) *A handheld device to measure the acoustic absorption in situ*. SNVH, 5th International Styrian Noise Vibration & Harshness conference. Graz. Austria.

Nosko, M. and Tijs, E. and de Bree, H-E. (2008) *A study of influences of the in situ surface impedance measurement technique*. DAGA, 34th German Annual Conference on Acoustics. Dresden. Germany.

de Bree, H E. and Basten, T. and Tijs, E. (2008) *Source path contribution breakdown of a sound pressure based compliance test*. SNVH, 5th International Styrian Noise Vibration & Harshness conference. Graz. Austria.

de Bree, H-E. and Tijs, E. (2008) *Calibration of a particle velocity sensor for high noise levels*, DAGA, 34th German Annual Conference on Acoustics. Dresden. Germany.

de Bree, H-E. and Tijs and E.H.G. and Basten, T. (2008) *Real time sound field visualization in the near field, far field and at absorbing surfaces*, Acoustics '08. Paris. France.

Tijs, E.H.G. and de Bree, H E. (2009) *Mapping 3D sound intensity streamlines in a car interior*. SAE Noise and Vibration conference. Num.: 2009-01-2175.

Tijs, E. and Brandão, E. and de Bree, H-E (2009) *In situ PU surface impedance measurements for quality control at the end of an assembly line*. SAE Noise and Vibration conference. Num.: 2009-01-2142.

Wolff, O. and Tijs, E. and de Bree, H E. (2009) *A PU probe array based panel noise contribution analysis whilst driving*. SAE Noise and Vibration conference. Num.: 2009-01-2123.

Wolff, O. and Tijs, E.H.G. and de Bree, H-E (2009) *In-flight panel noise contribution analysis on a helicopter cabin interior*. SAE Aerospace conference.

Tijs, E.H.G. and de Bree, H-E. and Steltenpool, S. (2009) *A novel acoustic pressure-velocity based method to access acoustic leakages of an acoustic enclosure in non anechoic conditions*. Euronoise, the eighth European Conference on Noise Control. Edinburgh. Scotland.

Tijs, E.H.G. and de Bree, H-E. (2009) *An in situ method to measurement the acoustic absorption of roads whilst driving*. DAGA, 35th German Annual Conference on Acoustics. Rotterdam. The Netherlands.

Tijs, E.H.G. and de Bree, H-E. and Brandão, E. (2009) *Large scale in situ acoustic absorption measurements in a theatre*. DAGA, 35th German Annual Conference on Acoustics. Rotterdam. The Netherlands.

Tijs, E.H.G. and Nejade, A. and de Bree, H-E. (2009) *Verification of PU intensity calculation*. Novem, Noise and Vibration: Emerging Methods. Oxford. England.

de Bree, H-E. and Tijs, E.H.G. (2009) *PU nosecone intensity measurements in a wind tunnel*. DAGA, 35th German Annual Conference on Acoustics. Rotterdam. The Netherlands.

de Bree, H-E. and Tijs, E.H.G. (2009) *A PU sound probe for high sound levels*. DAGA, 35th German Annual Conference on Acoustics. Rotterdam. The Netherlands.

Tijs, E.H.G. and Botts, J. and de Bree, H-E. and Arato, E. (2009) *Acoustic particle velocity enabled methods to assess room acoustics*. Euronoise, the 8th European Conference on Noise Control. Edinburgh. Scotland.

Wind, J.W. and de Bree, H-E. and Tijs, E.H.G. and Yntema, D. (2009) *Acoustic vector sensors for aeroacoustics*. CEAS European Air and Space Conference. Manchester. England.

Wind, J.W. and de Bree, H-E. and Tijs, E. (2009) *Source localization using acoustic vector sensors, a MUSIC approach*. Novem, Noise and Vibration: Emerging Methods. Oxford. England.

Tijs, E. and de Bree, H-E. and Bussow, R. (2009) *PU sound power measurements on large turbo machinery*. ICSV 16, congress on sound and vibration. Krakóv. Poland.

de Bree, H.E. and Druyvesteyn, W.F. and Tijs, E.H.G. (2009) *Broad banded acoustic vector sensors for passive monitoring of aircraft*. DGLR, Deutscher Luft- und Raumfahrtkongress. Aachen. Germany.

Brandão, E. and Tijs, E. and de Bree, H-E. (2009) *PU probe based in situ impedance measurements of a slotted panel absorber*. ICSV 16, congress on sound and vibration. Krakóv. Poland.

Wolff, O. and Tijs, E.H.G. (2009) *In-flight panel noise contribution analysis on a helicopter*. DGLR, Deutscher Luft- und Raumfahrtkongress. Aachen. Germany.

Tijs, E.H.G. and de Bree, H-E. and Steltenpool, S. (2010) *Scan & Paint: a novel sound visualization technique*. Internoise 221, International Congress and Exposition on Noise Control Engineering. pp. 6232-6237. ISSN 0736-2935.

de Bree, H E. and Wind, J.W. and Tijs, E.H.G. (2010) *Environmental noise monitoring with acoustic vector sensors*. Internoise 221, International Congress and Exposition on Noise Control Engineering. pp. 6225-6231. ISSN 0736-2935.

Schedlinski, C. and Arzul, C. and Bohnert, K. and Clasen, D. and Glandier, C.C. and Kropp, A. and Tijs, E.H.G. (2010) *Untersuchungen zur Erfassung von Absorption bei gekoppelten Fluid/Struktur-Analysen von Gesamtkraftfahrzeugmodellen*. VDI conference, Schwingungsanalyse und Identifikation. Leonberg. Germany.

Tijs, E.H.G. and de Bree, H-E. and Brandão, E. (2010) *High resolution absorption mapping with a pu surface impedance method*. ASA-INCE NoiseCon. Baltimore. United States of America.

Tijs, E.H.G. and de Croon, G. and Wind, J.W. and Remes, B. and de Wagter, C. and de Bree, H-E. and Ruijsink, R. (2010) *Hear-and-Avoid for Micro Air Vehicles*. IMAV, International Micro Air Vehicle Conference. Braunschweig. Germany.

de Bree, H-E. and Grosso, A. and Wind, J.W. and Tijs, E.H.G. (2010) *Scan&Paint, a new fast tool for sound source localization and quantification of machinery in reverberant conditions*. VDI conference, Schwingungsanalyse und Identifikation. Leonberg. Germany.

de Bree, H-E and Akal, T and Tijs, E.H.G. (2010) *The Hydroflown: MEMS-Based Underwater Acoustical Particle Velocity Sensor. Results of lab tests and sea trials*. ECUA 2010. 10th European Conference on Underwater Acoustics. Istanbul. Turkey.

Tijs , E.H.G. and Wijker, J. and Grillenbeck, A. (2011) *Benefit of Acoustic Particle velocity Based Reverberant Room Testing of Spacecraft*. IMAC XXXI, A Conference and Exposition on Structural Dynamics. Jacksonville. United States of America.

Grosso, A. and de Bree, H E. and Steltenpool, S. and Tijs, E.H.G. (2011) *Scan & paint for acoustic leakage inside the car*. SAE Noise and Vibration conference. Num.: 2011-01-1673.

Tijs, E.H.G. and Wind, J.W. and Fernández, D.F. and de Bree, H-E. (2011) *Fast, high resolution panel noise contribution method*. SAE Noise and Vibration conference. Num.: 2011-01-1594.

Escribano, D. and Tijs, E.H.G. (2011) *Measurement of the acoustic noise map of a city using acoustic vector sensors*. Internoise 232, International Congress and Exposition on Noise Control Engineering. pp. 2391-2396. ISSN 0736-2935.

Tijs, E.H.G. and Druyvesteyn, W.F. and de Bree, H E. (2011) *A Handheld Intensity Device for Measuring Absorption Properties in situ*. Forum Acusticum conference. Aalborg. Denmark.

Tijs, E.H.G. and Druyvesteyn, W.F. (2011) *Spatial variation of impedance and intensity measured close to a sample in the near field of a spherical sound source*. Sapem. Ferrara. Italy.

Tijs, E.H.G. (2012) *Sound source characterization for PU based in situ absorption measurements*. Euronoise, the 9th European Conference on Noise Control. Prague. Czech republic.

Zajamšek, B. and Tijs, E.H.G. and Wagner, M. and Grillenbeck, A. (2012) *MEVAT: Microflown Enabled Vibro Acoustic Testing*. The 12th European Conference on Spacecraft Structures, Materials & Environmental Testing. Noordwijk. The Netherlands.

Grosso, A. and Tijs, E.H.G. and Zajamšek, B (pending; to be presented at the AMA conference 2013) *An in situ impedance measurement set-up for high sound pressure levels*. AMA Sensor and Test Fair. Nürnberg. Germany.

Cats, P. and Tijs, E.H.G. and Fernandez, D.C. (pending; to be presented at the ICA conference 2013) *Exploration of the differences between a pressure-velocity based in situ absorption method and the standardized reverberant room method*. ASA ICA. Montreal. Canada.

Appendix A. Main applications of PU probes

Several unique applications of PU probes emerged in the past decade. This appendix contains a brief introduction to the main applications for which they are used currently. The most important features of PU probes are:

- Their small size
- They allow for frequency independent execution [11].
- The high dynamic range of particle velocity measurements in the near field, which are usually less affected by background noise or reflections than sound pressure measurements [66].
- The intensity can be determined in sound fields with a high pressure-intensity index [11]. The error of traditional pressure-gradient based sound intensity probes is high under such conditions.
- They can easily be extended to full 3D probes.

Further details on other applications can be found on www.microflown.com.

A.1. Scan and Paint

First applied in 2009, the Scan and Paint method is now a primary application of PU probes *[*130-133*]*. With this method, sound fields can be mapped quickly and with high resolution. It involves a probe that is swept across a surface while a video is captured of the measurement set-up. The position of the probe is obtained from the video with dedicated software. The tracking procedure is automated, which speeds up the post-process procedure. Several software versions for different applications exist:

- Scan and Paint (regular): mainly used for sound source localisation based on the visualisation of particle velocity and intensity. Fig. A-1 and A-2 show some examples of tests that have been performed.
- Scan and Paint Absorption: used for visualisating the spatial distribution of absorption properties (see section 8.5).
- Scan and Paint Transfer Path Analysis: similar to the regular Scan and Paint software but it also includes a phase reference, which is used to determine the contribution of separate sources.

The Scan and Paint method is suitable for sufficiently stationary sound fields. Contrary to array-based methods that require a large amount of probes, Scan and Paint only requires one PU probe and, in some cases, a reference sensor. Currently the usage of Scan and Paint for far field sound source localisation and for measuring 3D sound intensity streamlines is investigated.

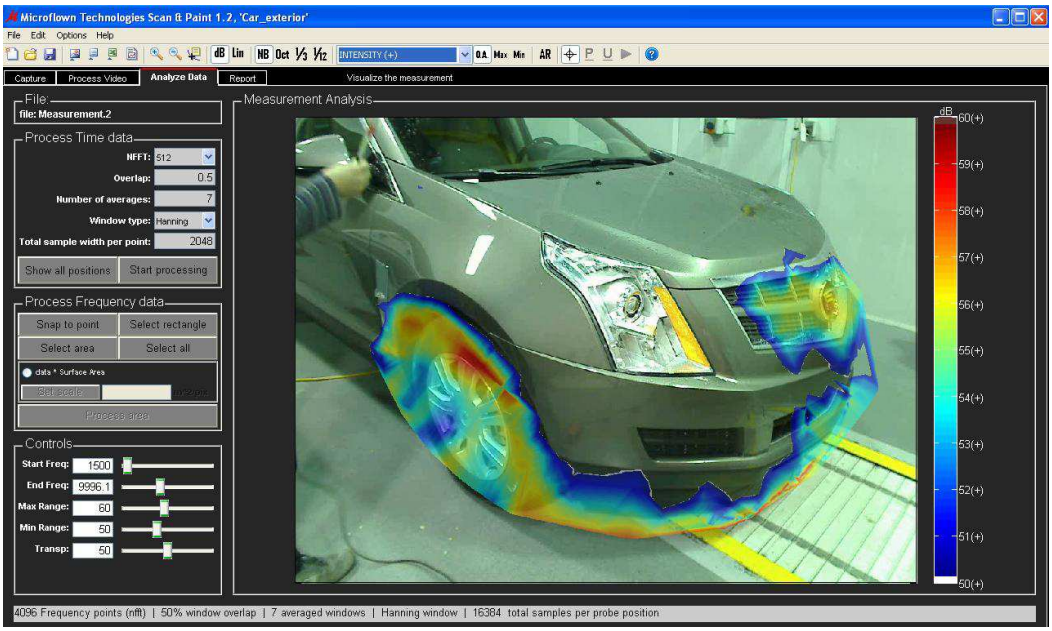

Fig. A-1. A car tested with Scan and Paint. Mean intensity from 1.5 kHz to 10 kHz.

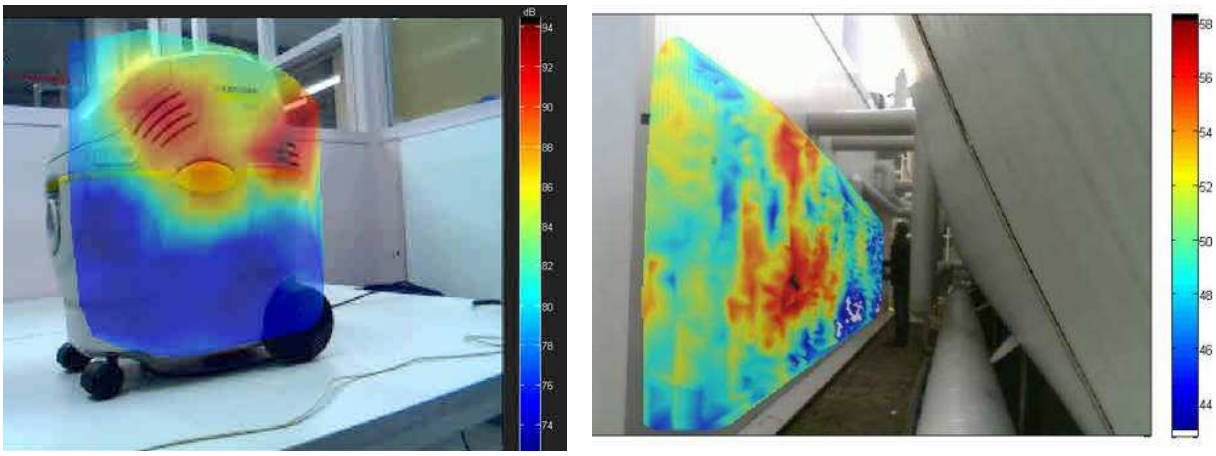

Fig. A-2. A vacuum cleaner and a gas turbine enclosure tested with Scan and Paint. Mean particle velocity from 2.4 kHz to 14 kHz and 124 Hz to 129 Hz, respectively.

A.2. Particle velocity and intensity near objects

PU probes can be used for sound source localisation near objects. A wide frequency range can be covered with two methods that use the same measurement; i.e. the velocity method is used for low frequencies, and the intensity method is used for high frequencies.

In the very near field, the normal component of the structural velocity is similar to the normal particle velocity, see [87], /149-152/. Particle velocity sensors can therefore be used to measure structural vibrations in the vicinity of objects. Such vibration tests have a high signal-to-noise ratio because [66]:

- The particle velocity level, due to the vibration of the surface itself, is high because of near field effects.
- The particle velocity level, due to background noise, usually is low because many objects have a high impedance. The incoming and reflected sound waves are nearly equal of strength but opposite in phase thus they destructively interfere.
- Particle velocity sensors are directional, and can be pointed towards the vibrating surface.

Very near field assumptions apply if two conditions are met; i.e. distance h to the surface should be much smaller its typical size L, and wavelength λ should be much larger than the size of the vibrating surface L; $h << \frac{L}{2\pi} << \frac{\lambda}{2\pi}$ [87].

Although the error of the velocity method increases for high frequencies and large probe-surface distances, intensity can usually be used instead [11], /60, 153/. PU intensity probes are small compared to PP intensity probes, have no spacing problems, and can be used in environments with high levels of background noise. However, the error of intensity obtained with PU probes increases in reactive fields, which sometimes means that low frequencies cannot be assessed. Usually, there is an overlapping frequency range where the velocity method and the intensity method both can be used. The frequency range of the velocity method is typically 20Hz to 1kHz, and 1Hz to 5kHz under favourable conditions. The frequency range of the intensity method is typically 30Hz to 10kHz, and 100Hz to 20kHz under favourable conditions.

A.3. Near field acoustic camera

Fig. A-3. Acoustic camera hardware and software.

Non-stationary sound sources can be localised and quantified with the near field acoustic camera. The particle velocity and intensity are measured at multiple positions. The signals are acquired and visualised with dedicated multichannel hardware and software. Optionally, a reference sensor can be used, like an rpm sensor. Various probe mountings are available. Fig. A-3 shows a handheld acoustic camera grid for twelve probes.

A.4. Panel noise contribution

Whereas the acousic camera is used to map the radiated sound, the panel noise contribution (PNC) method also involves a measurement of the transfer path from the sound source to a defined reference position (usually the listeners position) [150, 152, 156, 157], [154, 155]. With the PNC method the contribution of each radiating section to the sound pressure at the reference position is determined. Up to now, the method is mostly applied inside cars where it has demonstrated to be accurate and fast compared to existing methods. The PNC method consists of two steps. First the object is devided into sections, and the radiation of it, is measured with a probe. Fig. A-4 shows a special suspension has been developed to de-couple the probe body from the vibrating surface. Due its low resonance frequency (appoximately 15Hz) vibrations are highly damped above 40Hz.

The second step involves measuring the transfer path from the panel to the reference position. The object (e.g. a car) is turned off, and an omni-directional sound source is placed at the reference position. The principle of reciprocity is used which states that the sound path from the panel to an arbitrary position is the same as from that position to the panels. A reciprocal measurent is convenient because, when the omni-directional sound source is excited, all transfer paths to the panels can be measured at once. The position of the probe remains constant between step one and two, which saves handling. The synthesised sound pressure at the reference position is finally obtained by summing all sound pressure contributions. This synthesised sound pressure should be equal to the sound pressure measured at the reference position by a regular microphone during step one. The measurement quality can be checked by comparing both values.

Fig. A-4. Left: probe suspension. Right: Panel noise array mounted in a car.

A.5. Far field source localisation

Three-dimensional PU probes also can be used to determine the direction and the location of sound sources in the far field. Some applications that have been investigated by the author are the:

- localisation of low frequency sources in urban environments *[*158, 159*]*.
- tracking of a helicopter from the ground *[163]*.
- simultaneous measurement of multiple sound sources *[*161, 162*]*.
- measurement of direction of sound sources with a sensor that is mounted on a small radio controlled aeroplane *[166]*.
- measurement of direction of sound sources under water [167].

Acknowledgements

Although this research continues, this thesis is a milestone after several years of work. I wish to acknowledge my gratitude to various persons who have worked with me in the past years. First, I would like to thank my promoters Erik Druyvesteyn and Gijs Krijnen for your efforts, patience, and contributions to this work. Erik; thank you for your encouragements and all the time you invested in me. I especially admire your dedication and your ability to come up with innovative and radically different solutions. Gijs; thank you in particular for your thoroughness and attention to detail, and for improving the readability of this thesis. I learned much from your suggestions. I also want to thank the members of the jury for their careful reading and assessment of this manuscript.

I would like to mention Hans-Elias de Bree and Alex Koers for your inspiration, humour, never-ending enthusiasm, and for enabling this research. I much enjoy the open-minded and creative working atmosphere that you establish, where a broad experience can be gained through, for example, the wide range of activities and frequent trips abroad.

Microflown was small when I started at the company, but it has grown substantially. I want to thank all of my current and previous colleagues who helped making the work exciting over the years. Microflown attracts interesting and somewhat peculiar persons, which makes the work all the more fun. I am particularly grateful for the persons who contributed to this research; i.e. Andrea, Branko, Dani, Els, Jelmer, Jeroen, Jin, Jhonny, Jordy, Lola, Martin, Olga, Peter, Paul, Roald, Sergey, Steven, Tim, Tom, Erik, and anybody else that I may have forgotten to mention, and to Rien (daank veur oe mooie vertealsels).

Als laatste wil ik graag mijn familie vrienden en vooral mijn moeder Ada, mijn vader Gerard en uiteraard mijn vrouw Karin bedanken voor jullie interesse, ondersteuning en gezelligheid.

Emiel, Arnhem 2013

Propositions accompanying the PhD thesis:

Study and Development of an In Situ Acoustic Absorption Measurement Method

by Emiel Tijs

1. More energy is spend while determining the behavior of a sound absorbing sample than the sample will ever absorb.
2. We can land on the moon and build complex computers, yet the determination of the actual sound absorption of most samples cannot be determined indisputable with current measurement methods.
3. If the high frequency performance of PU probes is improved, PP intensity probes are superfluous for most applications.
4. In most applications, it cannot be proven that the targeted absorption of samples is reached within 50% accuracy.
5. Due to advancements of simulation methods, few people are being taught to do fundamental research on measurement techniques. Development of suitable measurement methods can be easier and more feasible than the development of robust and sufficiently detailed simulation methods.
6. The consistency of acoustic properties of products is checked insufficiently.
7. In most acoustic measurements, the inaccuracies of the measurement system are insignificant compared to human errors and errors related to mounting of test items and sensors.
8. Standards complicate the deployment of adequate measurement methods.
9. Too many food scandals will reduce the variety of food intake.